

Summer 7-28-2018

From olfaction to immunity: Characterization of nasal immunity in bony fish

Ali Sepahi

Follow this and additional works at: https://digitalrepository.unm.edu/biol_etds



Part of the [Biology Commons](#), and the [Immunity Commons](#)

Recommended Citation

Sepahi, Ali. "From olfaction to immunity: Characterization of nasal immunity in bony fish." (2018).
https://digitalrepository.unm.edu/biol_etds/277

This Dissertation is brought to you for free and open access by the Electronic Theses and Dissertations at UNM Digital Repository. It has been accepted for inclusion in Biology ETDs by an authorized administrator of UNM Digital Repository. For more information, please contact disc@unm.edu.

Ali Sepahi

Candidate

Biology

Department

This dissertation is approved, and it is acceptable in quality and form for publication:

Approved by the Dissertation Committee:

Dr. Irene Salinas , Chairperson

Dr. Dr. Coenraad Adema

Dr. Judy Cannon

Dr. Jacques Robert

**From olfaction to immunity:
Characterization of nasal immunity in bony fish**

by

Ali Sepahi

B.S. Fisheries, Gorgan University (Iran), 2008

M.Sc. Aquaculture, University of Tehran (Iran), 2012

M.Sc. Biology, University of New Mexico (US), 2016

Ph.D Dissertation

Submitted in Partial Fulfillment of the
Requirements for the Degree of
Doctor of Philosophy in Biology

The University of New Mexico

Albuquerque, New Mexico

July 2018

Ph.D. committee members:

1. **Dr. Irene Salinas**, Associate professor at biology department, University of New Mexico (advisor and mentor)
2. **Dr. Coenraad Adema**, Professor at biology department, University of New Mexico (internal committee member)
3. **Dr. Judy Cannon**, Associate professor at pathology department, University of New Mexico (internal committee member)
4. **Dr. Jacques Robert**, Professor of Microbiology and Immunology department, University of Rochester (external committee member)

گجان ممبرکہ بہ پیمان رسید کار مغان

ہزار بادہ ناخوردہ درک تاک است

اقبال لاہوری

Acknowledgement

It was a long journey!

I would like to thank Dr. Irene Salinas for her support and for giving me the opportunity to fulfill my dreams as a researcher in her lab. Irene taught me how to do research and be passionate about science. She is a great scientist, very hard working and very reliable. Thank you Irene!

I was lucky to be a part of a great team in Salinas's lab with wonderful lab mates, Luca T, Elisa C, Susana M, Ryan B, Erin L, Mariah S, Alejandra D, Aurora K and Ryan H. Thank you all!

I am very grateful to my PhD committee members, Dr. Coenraad Adema and Dr. Judy Cannon for their guidance through the long path of my PhD. Coen helped me from the first semester in his class and all the way up until my defense day and supported me for my postdoc position. Judy supported me from the first day that we met in the committee meeting. Judy is indeed very kind, understanding, and supportive. She supported me through my entire PhD and post-doc and even my immigration status as an international student. Thank you both!

I would like to thank my external PhD committee member, Dr. Jacques Robert for his feedback on the dissertation and defense.

I would like to express my appreciation to UNM biology department and CETI members particularly Dr. Eric Sam Loker for supporting me through my PhD and my post-doctoral position. I was very lucky to have your support, Sam. Thank you!

I would like to thank my family, particularly my mother, Parvin. She has been always with me in all stages of my life and supported me. Finally, I would like to thank my lovely wife, Bani for standing by me during this long journey. None of this would have been possible without you. Thank you **Bani**.

**From olfaction to immunity:
Characterization of nasal immunity in bony fish
by
Ali Sepahi**

B.S., Fisheries, Gorgan University (Iran), 2008

M.Sc., Aquaculture, University of Tehran (Iran), 2012

M.Sc., Biology, University of New Mexico (US), 2016

Ph.D., Biology, University of New Mexico (US), 2018

Abstract:

The olfactory system is a common route pathogen entry in vertebrates. As a consequence, the nasopharynx-associated lymphoid tissue (NALT) needs to rapidly clear infections without compromising the sense of olfaction. NALT is present in teleost fish but its cellular and molecular mechanisms of action have not been investigated to this date. This dissertation focuses on three aims: 1. investigating the role of CCL19-like as a primordial chemokine in vertebrate nasal immunity, 2. determining the presence of tissue microenvironments within the olfactory organ (OO) of rainbow trout, and 3. understanding the immune contributions of olfactory sensory neurons (OSNs) in teleosts against viruses. In aim 1, we report six isoforms of CCL19-like chemokine in salmonids such as CK12. CK12 is mainly expressed in mucosal tissues and plays an important role in antiviral immunity. Although recombinant protein CK12 is not chemotactic *in vitro*, it induces infiltration of APCs and CD8⁺ T cells into OO of rainbow trout *in vivo*. In aim 2,

we demonstrate the presence of two different microenvironments (mucosal tip and neuroepithelial) in the OO of rainbow trout. The tip of the epithelium harbors clusters of CD8 α ⁺ cells whereas few numbers are found in the neuroepithelium. CD8 α ⁺ cell localization corresponds with a higher expression of chemokine and chemokine receptors in the tip versus the neuroepithelial side. We report that cell proliferation in response to viral nasal delivery occurs mainly at the tip. In aim 3, we unravel for the first time a new function for OSNs by which nasal rhabdoviruses induce apoptosis in crypt neurons, a type of OSN, in rainbow trout via the interaction of viral G glycoprotein and the neuron TrkA receptor. CD8 α ⁺ T cells infiltrate to the OO within minutes of nasal viral delivery and this response was abrogated when TrkA was blocked. Infiltrating CD8 α ⁺ T cells originated from the microvasculature surrounding the olfactory bulb (OB) and not the periphery. In conclusion, this dissertation provides the first tissue, cellular and molecular characterization of teleost NALT and reveals a novel function of vertebrate OSNs in eliciting rapid nasal anti-viral immune responses in the OO and OB.

TABLE OF CONTENTS

I. Introduction

1. The innate and adaptive immunity in vertebrates.....	1
1.1. <i>Innate immune molecules: chemokines</i>	2
1.2. <i>Innate vs adaptive immunity in teleost fish</i>	2
1.3. <i>Chemokines in teleost</i>	3
2. Mucosal immunity in vertebrates.....	4
2.1. <i>Nasal immunity in vertebrates</i>	5
2.2. <i>Nasal immunity in teleost</i>	6
3. The olfactory system of vertebrates.....	7
3.1. <i>General organization of olfactory systems in vertebrates</i>	8
3.2. <i>Teleost olfactory system</i>	8
4. Neuro-immune interaction in mucosal surfaces in vertebrates.....	9

II. Significance.....10

III. Chapter 1.....12

Sepahi, Ali, and Irene Salinas. "The evolution of nasal immune systems in vertebrates." Molecular immunology (2016). <https://doi.org/10.1016/j.molimm.2015.09.008>

Article pages131-138 (8 pages)

IV. Chapter 2.....21

Sepahi, Ali, Luca Tacchi, Elisa Casadei, Fumio Takizawa, Scott E. LaPatra, and Irene Salinas. "CK12a, a CCL19-like chemokine that orchestrates both nasal and systemic antiviral immune responses in rainbow trout." The Journal of Immunology 11 (2017). DOI: <https://doi.org/10.4049/jimmunol.1700757>

Article pages3900–3913 (18 pages with supplementary data)

V. Chapter 3.....39

*Sepahi, Ali, Elisa Casadei, Luca Tacchi, Pilar Muñoz, Scott E. LaPatra, and Irene Salinas. "Tissue microenvironments in the nasal epithelium of rainbow trout (*Oncorhynchus mykiss*) define two distinct CD8 α + cell populations and establish regional immunity." The Journal of Immunology (2016). DOI: <https://doi.org/10.4049/jimmunol.1600678>*

Article pages 4453–4463 (14 pages with supplementary data)

VI. Chapter 4.....53

Sepahi, Ali, Aurora, Kraus, Chris Johnston., Jorge Galindo-Villegas., Cecilia Kelly., Diana Garcia-Moreno., Pilar Muñoz., Victoriano Mulero., Mar Huertas and Irene Salinas. "Olfactory sensory neurons mediate ultra-rapid antiviral immune responses in teleosts in a TrkA-dependent manner". Immunity. Under review

Manuscript pages(42 pages with supplementary data)

VII. Summary of findings.....96

VIII. Conclusion.....97

IX. References.....98

Appendices

Appendix A.....102

Sepahi, Ali, Héctor Cordero, Howard Goldfine, Maria Ángeles Esteban, and Irene Salinas. "Symbiont-derived sphingolipids modulate mucosal homeostasis and B cells in teleost fish." Scientific Reports 6 (2016). doi:10.1038/srep39054

Article pages 1-13 (21 pages with supplementary data)

Appendix B.....124

*Sanchez, Mariah, Ali Sepahi, Elisa Casadei, and Irene Salinas. "Symbiont-derived sphingolipids regulate inflammatory responses in rainbow trout (*Oncorhynchus mykiss*)." Aquaculture (2018).<https://doi.org/10.1016/j.aquaculture.2018.05.051>*

Article pages 932-939 (8 pages with supplementary data)

Appendix C.....133

Authors' contributions

Appendix D.....135

Copyright permissions for papers that are not open access

I. Introduction

1. The innate and adaptive immunity in vertebrates

The immune system is able to differentiate between self and non-self and protect hosts against infection. The immune system is traditionally divided into innate and adaptive immunity. Innate immunity is the first line of defense against pathogens, exerts rapid effector functions but is unable to recognize specific pathogens and therefore does not provide specific protection that avoids reinfection. In contrast, adaptive immunity, present in agnathans and gnathostomes, is characterized by the presence of two types of lymphocytes, B and T cells that bear highly diverse antigen-specific receptors that recognize antigens specifically (**Table 1**).

Evolutionary speaking, the innate immune system appeared before the adaptive immune system, and some form of innate immunity probably exists in most of multicellular organisms ranging from small antimicrobial peptides to large phagocytic cells. Traditionally speaking, innate immune recognition is mediated by germ-line–encoded receptors and the specificity of each receptor is genetically predetermined and the innate immune system cannot have immunological memory (1, 2). However, new studies on the innate immune system show that this concept is no longer accurate and innate immunity can also show some immune memory (3-5). In contrast with the innate immune system, during the development of lymphocytes, B and T cells receptors (BCR, TCR) are generated somatically in a way that endows each lymphocyte with a structurally unique receptor (1, 6) (**Table 1**).

**Table 1. Distinctive features of innate versus adaptive immunity*

	<i>Innate immunity</i>	<i>Adaptive immunity</i>
<i>Receptors</i>	Germline-encoded and none germline-encoded	Antigen receptors are products of site-specific somatic recombination
<i>Distribution</i>	Subset-specific but non-clonal	Antigen receptors are clonally-distributed
<i>Repertoire</i>	Limited	Immense
<i>Memory response</i>	some	Yes
<i>Response time</i>	Minutes/hours	Days
<i>Major cell types</i>	Phagocytes NK cells, dendritic cells	T cells and B cells, antigen presenting cells

*The table is adapted from (7)

The crosstalk between the innate and adaptive immune systems is essential for the adequate onset of adaptive immunity. This crosstalk is regulated by cells as well as soluble factors, including cytokines and chemokines (8, 9). Chemokines play key roles in the immune system and orchestrate the precise movement of leukocytes that is necessary to generate and deliver immune and inflammatory responses to specific anatomic sites (10).

1.1. Innate immune molecules: chemokines

Chemokines (chemotactic cytokines) are small proteins that direct the movement of circulating leukocytes to sites of inflammation or injury and induce activation of cells, especially phagocytic cells and lymphocytes (11). Around fifty chemokines have been identified in human and mice (12).

In mammals, homeostatic chemokines such as CCL19 and CCL21, are known to play an important role in cell migration and secondary lymphoid organ's organization and development (13, 14). Homeostatic chemokines are also important during microbial infection, for example studies showed that chemokine CCL19 expression is induced by viral infection and caused inflammatory responses (15).

1.2. Innate vs adaptive immunity in teleost fish

The innate immune system of teleost fish is very similar to that of mammals (16, 17). In fish, the innate response is considered an essential component in combating pathogens due to the limitations of their adaptive immune system (18). The innate immune system of teleosts includes the epithelial/mucosal barrier, humoral parameters and cellular components (19). Evolutionary speaking, after cartilaginous fish, teleost are the earliest organisms with an adaptive immune system based on B and T cells (20). Teleost adaptive immune system is similar to that of mammals, as they have immunoglobulins, BCRs, TCRs, the major histocompatibility complex (MHC) class I and II, as well as a spleen and a thymus (20, 21). In spite of many similarities, the immune system of teleosts is different from that of mammals in a number of ways such as absence of lymph nodes, lack of germinal center formation, lack of class switch recombination and absence of a bone marrow (21, 22) (**Table 2**).

*Table 2. Fundamental features of adaptive immune systems of teleost fish and mammals

	<i>Teleost</i>	<i>Mammals</i>
<i>Immunoglobulin</i>	IgM, IgD and IgT (or IgZ)	IgM, IgG, IgA, IgD and IgE
<i>Activation-induced cytidine deaminase (AID)</i>	Yes	Yes
<i>Class-switch recombination</i>	No	Yes
<i>Somatic hypermutation</i>	+++	+++
<i>Affinity maturation</i>	+	+++
<i>Memory responses</i>	+	+++
<i>TCR, CD4, CD8</i>	Yes	Yes
<i>MHC class I and II</i>	Yes	Yes
<i>CD28, CD40, CD80, CD86, ICOS</i>	Yes	Yes
<i>TH1, TH2 and TH17 cytokines</i>	Yes	Yes
<i>Spleen, thymus and bone marrow</i>	Spleen and thymus but no true bone marrow	Yes
<i>Mucosa-associated lymphoid tissue (MALT)</i>	Yes	Yes
<i>Germinal centers and lymph nodes</i>	No	Yes

*The table is adapted from (21)

1.3. Chemokines in teleost

Teleosts have the highest number of chemokine genes in vertebrates, for example more than 100 chemokine genes have been reported in zebrafish (23) a much larger number than in human with 44 chemokine genes. Chemokines play a central role in the immune response in all vertebrates including teleost fish through the coordination of immune cell localization and function (24). CC and CXC chemokines are the main chemokine families in teleost fish (24). Chemokine CCL19 molecules have not been reported in amphibians but they are present in teleost fish. In zebrafish, for instance, three copies of CCL19 genes were reported (25). Previous studies reported three CCL19 genes in salmonids, CK10, CK12a, and CK12b (26, 27). However, little information is available regarding the functionality of CCL19 chemokines in rainbow trout. In the Chapter two of this dissertation, we reported three new CCL19-like genes in salmonids: CK10b, CK13a and CK13b. Moreover, we showed the role of chemokine CCL19 in nasal and systemic immune responses in rainbow trout (Published in The Journal of Immunology 2017) (28).

2. Mucosal immunity in vertebrates

Mucosal surfaces are the first line of defense against pathogen entry and are equipped with mucosa-associated lymphoid tissues (MALT). In endotherms, MALT includes secondary lymphoid tissues that contain both well-organized lymphoid structures (organized MALT, O-MALT) as well as scattered or disseminated lymphoid cells (diffuse MALT, D-MALT) (29). According to their anatomical location, MALT is subdivided into the gut-associated lymphoid tissue (GALT), bronchus-associated lymphoid tissue (BALT), nasal lymphoid tissue (NALT), among others. **Table 3** summarizes the presence of different MALT in vertebrates.

**Table 3. Presence of different mucosal lymphoid tissues in vertebrates*

<i>Mucosal area</i>	<i>Present in</i>
MALT	All vertebrates
GALT	All vertebrates
Peyer's patch	Birds, mammals
Mesenteric lymph node	Birds, mammals
Lamina propria leucocytes in gut	All vertebrates
Intraepithelial lymphocytes in gut	All vertebrates

NALT	Birds, mammals, teleost fish, lungfish
BALT	Birds, mammals
Skin-associated lymphoid tissue (SALT)	Fish, amphibians
Gill-associated lymphoid tissue (GALT)	Fish

*The table is adapted from (30)

D-MALT such as lamina propria in gut is present in all vertebrates from agnathans to mammals whereas O-MALT such as peyer's patch in gut is mainly reported in birds and mammals (30). Similarly, D-NALT is present in all vertebrates from teleost to mammals whereas primitive O-NALT structured first appeared in lungfish and are composed of lymphocytic aggregates of both B and T cells. These structures may have evolved into more organized structures such as the tonsils of mammals (**Figure 1**) (31). However, Most of the mucosal immunity studies focus on GALT and that the biology of NALT is poorly understood, even in mammals.

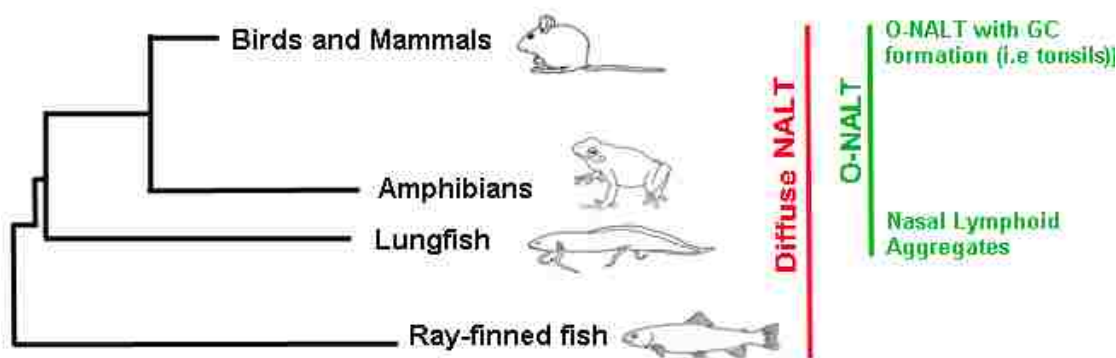


Figure 1: Phylogenetic tree showing the presence of NALT (organized and diffuse) in vertebrates.

2.1. Nasal immunity in vertebrates

NALT has been traditionally thought to protect terrestrial vertebrates against inhaled antigens. NALT is strategically located in the upper part of the respiratory tract of terrestrial vertebrates. For

instance, murine NALT consists of a pair of O-NALT structures located on the palate at the entrance to the nasopharyngeal duct and the less well organized diffuse lymphoid tissue lining the nasal passages (D-NALT) (32, 33).

In mammals, the type of immune response that takes place in NALT as a result of infection or vaccination usually depends on the type of antigen. For example, immunization with cholera toxin in mice elicits IgA responses as well as a T cell response (34, 35). On the other hand, immunization with protein-containing microparticles, elicits primarily IgG responses (36). However, cellular responses such as IFN γ -producing CD4⁺ and CD8⁺ T cells are often observed in NALT following nasal infection or vaccination. For instance, viruses such as influenza (37-39), reovirus (40) and Sendai virus (41), promote CD8⁺ T cell responses supporting the idea that CD8 T cells play an important role in removing virally infected cells in NALT. The first chapter of this dissertation is a review paper on the evolution of NALT in vertebrates (Published in Molecular Immunology 2016)(31).

2.2. Nasal immunity in teleost

Until recently, three MALT have been characterized in teleost fish: GALT, SALT and GIALT (30). Recently, histological examination of the olfactory organ of four different families of teleost fish showed that fish olfactory organs have an associated lymphoid tissue. This study included a preliminary characterization NALT at the cellular and molecular level in rainbow trout with a focus on B cells and immunoglobulins and demonstrated that NALT is conserved in vertebrates (42). However, very little was known about the cells and molecules that are implicated in the nasal immune response against different types of antigen in teleost fish.

Similar to other teleost MALT, teleost NALT harbors diffuse lymphoid cells only, lacking an O-NALT (42). However, the histological regionalization present in teleosts and mammals led us to hypothesize that regional immunity may exist in different portions of the vertebrate nasal cavity. **Chapter 3 of this dissertation demonstrates the presence of two different microenvironments (mucosal and neuroepithelial) in the olfactory organ of rainbow trout (published in The Journal of Immunology, 2016) (43).**

3. The olfactory system of vertebrates

3.1. General organization of olfactory systems in vertebrates

Olfactory systems are one of the most ancient and conserved sensory systems in vertebrates (44). Strikingly, the molecular and neurological arrangements of zebrafish and mouse olfactory systems are highly conserved (45). Most terrestrial vertebrates possess two distinct olfactory systems, the main olfactory system and the vomeronasal system. The surface of the nasal cavity is comprised of squamous epithelium, respiratory epithelium, and olfactory epithelial types in the main olfactory system (46). The olfactory epithelium of vertebrates has been examined extensively (47). It consists of three basic cell types, olfactory receptor cells, supporting cells and basal cells (47). The human olfactory epithelium has similar cellular characteristics to that of other vertebrates (47).

The vomeronasal organ, on the other hand, is not present in fish, birds, old world monkeys, apes, or humans (48-50). The vomeronasal organ is located at the base of the nasal septum or in the roof of the mouth in most amphibians, reptiles and mammals and its main function is pheromone detection (51, 52).

In the main olfactory system, the receptor cells project their axons to the main olfactory bulb. However, in the vomeronasal system the receptor cells project their axons to the accessory

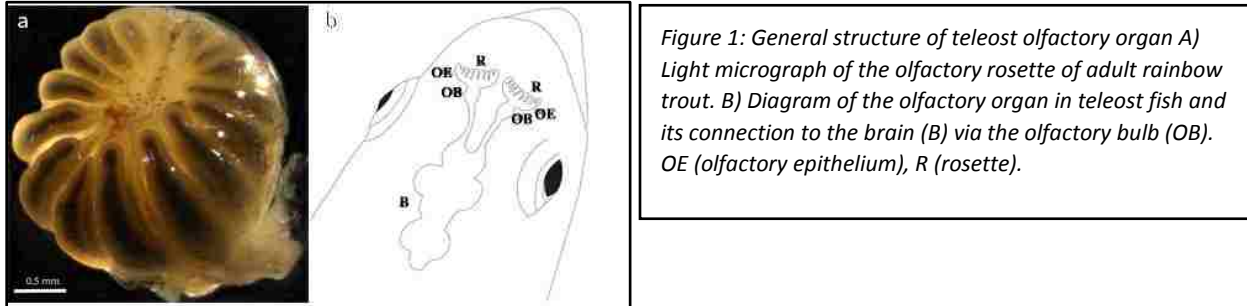
olfactory bulb (53-55). The olfactory epithelium and vomeronasal organ are also different with respect to their G-protein-coupled receptors and types of olfactory receptors. In other words, the olfactory epithelium expresses olfactory receptor (OR) genes or trace amine-associated receptors (TAARs) genes whereas the vomeronasal organ expresses vomeronasal receptors, V1R or V2R genes (53, 56, 57). Ciliated neurons express ORs and TAARs and they are coupled to G α olf. However, in microvillus neurons V1Rs and V2Rs are coupled to G α i and G α o in mammals (53) and G α q in teleost (50).

3.2. Teleost olfactory system

In vertebrates, the main olfactory sensory neurons (OSNs) are located in the sensory epithelium, which in fish is called the olfactory rosette due to the leaf-like structures of the lamellae resembling a miniature rose (**Figure 1**) (58). The olfactory system of teleost fish consists of two paired nasal cavities located at the dorsal part of the head. Unlike terrestrial vertebrates, there is no contact between the olfactory and respiratory systems including the oral cavity. The fish olfactory organ is comprised of a single olfactory system and lacks the vomeronasal organ and the accessory olfactory bulbs (59, 60). Although fish do not show anatomic segregation in two olfactory subsystems, the teleost single olfactory epithelium contains different types of OSNs. The main OSNs are ciliated and microvillous neurons. Interestingly, fish feature a third OSN type within their olfactory epithelium, the crypt neuron (61, 62).

Crypt neurons were originally identified at the electron microscopy level, they are oval to egg-shaped neurons that are completely surrounded by one or two supporting cells (62). Crypt neurons are present in cartilaginous fish, primitive bony fish, and also many modern fish species (63). They are located in the upper third of the olfactory epithelium and their axons travel towards the basal lamina and join the axon bundles of other OSNs (63). Thus, although not grouped in one organ,

the scattered crypt cells present in teleost olfactory organ are the functional equivalent to the vomeronasal organ of other vertebrates.



Crypt neurons appear to express the G-proteins G_{i1b} , G_{ao} and $G_{\alpha q}$ as well as adenylyate cyclase type-III and the glial marker protein S100 (49, 50, 64-66). Importantly, crypt neurons only express one type of olfactory receptor, the vomeronasal receptor 1-like Ora4. Additionally, crypt neurons can be identified by their tropomyosin-related kinase A receptor (TrkA) immunoreactivity (65, 67, 68). The specific odors recognized by crypt neurons and their function are still enigmatic although recent evidence suggests that these neurons are responsible for kin recognition in zebrafish (69).

4. Neuro-immune interaction in mucosal surfaces in vertebrates

The interactions between immune system and nervous system are complex and multidirectional. The neurons can sense immune signals and immune cells express neurotransmitters and their receptors (70). The similarity between these two systems suggests that they may have the common ancestors through evolution (71). Neurons at mucosal surfaces such as nose are in direct contact to environmental antigens. A growing body of evidence indicates that neurons such as nociceptive neurons can sense microbial products as alarming signals (70, 72). Neurons in the OO of vertebrates are constantly exposed to environmental pathogens. Additionally, OSNs send signals to the CNS via the OB, therefore providing a fast and direct link between the

external microbial environment and the brain. This fast route is exploited by neurotropic viruses such as HSV and influenza which target OSNs to infect CNS in animals (73, 74).

As mentioned earlier, neurons from the CNS have been shown to produce different immune mediators in response to infection or injury, particularly cytokines and chemokines. However, to date, the OSNs of any species have not been implicated in any immune role. Chapter 4 of this dissertation discusses the immunological role of OSNs and interaction of crypt neurons TrkA receptor and viral antigens (Immunity, under review).

Overall, the goal of this dissertation is to shed light on the nasal immune system and important immunological players against viral antigens in teleost. This study showed the important role of CCL19-like chemokines in nasal immunity and revealed the presence of microenvironments in OO to minimize damages to olfactory neurons of rainbow trout. We discovered the immunological role of OSNs against neurotropic viruses and showed the interaction of viral glycoprotein and TrkA receptor on crypt neurons. We demonstrated that delivery of viral antigens intranasally results in neuronal activation and infiltration of CD8 T cells from OB microvasculature to OO within minutes in TrkA dependent manner.

This dissertation has three aims: 1st. determining the role of CCL19-like as a primordial chemokine in vertebrate nasal immunity, 2nd. uncovering the presence of tissue microenvironments and regional immunity within the nasal mucosa of rainbow trout, and 3rd. establishing the immunological role of olfactory sensory neurons in teleost.

II. Significance

This dissertation is significant both from a basic and an applied point of view. Our understanding of the cross talk between olfaction and immunity is very limited. By defining how OSNs respond

to pathogens, we can further infer how vertebrates sense and respond to environmental cues and how infection and olfactory detection of pathogens contributes to the behavior, success and survival of species. These studies will also shed light on novel aspects of neuroimmune interactions, usually studied in the gut or skin.

Teleosts express a limited number of olfactory and vomeronasal receptors and therefore represent a simpler model system for the study of OSNs and their role in immunity compared to mammals.

Thus, studying teleost nasal immunity can potentially reveal primordially conserved principles of nasal immunity and/or novel mechanisms and pathways so far overlooked in mammalian studies.

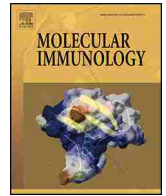
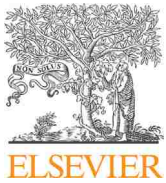
Particularly, since teleosts only have D-NALT, understanding nasal immune responses in teleosts will establish the so far unclear contributions of D-NALT to the overall nasal immune response.

As an example, this can help understand the effectiveness of nasal vaccines in humans who have undergone tonsil or adenoid surgical removal.

From an applied point of view, this dissertation carries important significance for the field of aquaculture. At present, about 50% of the total seafood that we eat originates from aquaculture (FAO, 2012). The sustainability of this industry strongly depends on the prevention of infectious diseases, which cause critical economic losses. Nasal vaccination appears as a novel and reliable method of vaccination that can avoid disease related losses and guarantee a sustainable production of fish protein via the aquaculture industry. By understanding the immunological basis of nasal vaccines in this dissertation, we will be able to expand nasal vaccination to other fish species and other diseases.

Chapter 1

Sepahi, Ali, and Irene Salinas. "The evolution of nasal immune systems in vertebrates." *Molecular immunology* (2016). <https://doi.org/10.1016/j.molimm.2015.09.008>



The evolution of nasal immune systems in vertebrates



Ali Sepahi, Irene Salinas*

Center for Evolutionary and Theoretical Immunology, Department of Biology, University of New Mexico, Albuquerque, NM, USA

ARTICLE INFO

Article history:

Received 15 July 2015

Received in revised form 5 September 2015

Accepted 6 September 2015

Available online 19 September 2015

Keywords:

Evolution

Nasal immunity

NALT

Mucosal immunity

Vertebrates

Teleost fish

ABSTRACT

The olfactory organs of vertebrates are not only extraordinary chemosensory organs but also a powerful defense system against infection. Nasopharynx-associated lymphoid tissue (NALT) has been traditionally considered as the first line of defense against inhaled antigens in birds and mammals. Novel work in early vertebrates such as teleost fish has expanded our view of nasal immune systems, now recognized to fight both water-borne and air-borne pathogens reaching the olfactory epithelium. Like other mucosa-associated lymphoid tissues (MALT), NALT of birds and mammals is composed of organized lymphoid tissue (O-NALT) (i.e., tonsils) as well as a diffuse network of immune cells, known as diffuse NALT (D-NALT). In teleosts, only D-NALT is present and shares most of the canonical features of other teleost MALT. This review focuses on the evolution of NALT in vertebrates with an emphasis on the most recent findings in teleosts and lungfish. Whereas teleost are currently the most ancient group where NALT has been found, lungfish appear to be the earliest group to have evolved primitive O-NALT structures.

© 2015 Elsevier Ltd. All rights reserved.

1. Historical aspects

Tonsillectomy or the surgical removal of tonsils is a very ancient practice. Approximately 2000 years ago, Aulus Cornelius Celsus, a Roman writer and physician, described tonsil surgery by using his fingers to remove tonsils (Koempel et al., 2006; Younis and Lazar, 2002). Today, 530,000 children under the age of 15 have their tonsils or adenoids removed in the US every year and it is still one of the most common surgical procedures in children in this country (Cullen et al., 2009; Roland et al., 2011).

The first attempt to nasally vaccinate humans against smallpox was reported in the Golden Mirror of Medicine, Chinese medical text in 1742. Nasal vaccination was done by using powdered scabs that were blown to the nose or filling the nose with a vesicle smeared cotton (Plotkin, 2014). Thus, tonsillectomy and nasal vaccination precede our understanding of nasal immune systems.

Anatomically, the human Waldeyer's ring was first described in 1884 by von Waldeyer-Hartz as a ring of lymphoid tissue in the pharyngeal wall (Cocquyt et al., 2005; Perry and Whyte, 1998). Nasopharynx-associated lymphoid tissue (NALT) was first described as a paired of lymphoid cells accumulations in the nasal passage of rat in 1947 (Kelemen, 1947) whilst the mouse NALT was first described few decades later (Belal et al., 1977). In the subsequent years, the NALT of other mammals such as monkeys

(Harkema et al., 1987; Loo and Chin, 1974) and horses (Mair et al., 1987, 1988) were described. However these studies did not include functional aspects of the nasal immune system (Kuper et al., 1992).

One of the major breakthroughs in nasal immunity field took place in the early 2000, when the first nasal vaccine for use in humans against influenza virus was licensed in the USA (FluMist) (Chen et al., 2006). To date, this vaccine remains the only nasal vaccine licensed for human use. The effectiveness and availability of this vaccine has helped the NALT community to expand basic scientific knowledge on nasal immune responses. Intranasal vaccination offers a number of advantages over other vaccination routes (Neutra and Kozlowski, 2006). Apart from the fact that is needle free and requires small amounts of antigen, intranasal delivery has been shown to stimulate not only local nasal immunity but also systemic immune responses as well as mucosal immune responses in distant mucosal sites (Fukuyama et al., 2012; Lycke, 2012; Neutra and Kozlowski, 2006; Pabst, 2015).

2. Anatomy of NALT

In endotherms, mucosa-associated lymphoid tissues (MALT) comprise a network of secondary lymphoid tissues that contain both well-organized lymphoid structures (organized MALT, O-MALT) and scattered or disseminated lymphoid cells (diffuse MALT, D-MALT) (Brandtzaeg and Pabst, 2004). Examples of O-MALT include the Peyer's patches in the gut or the tonsils in the nasopharyngeal cavity. Generally speaking we know very little about NALT (both organized and diffuse) compared to the gut-associated lym-

* Corresponding author.

E-mail address: isalin@unm.edu (I. Salinas).

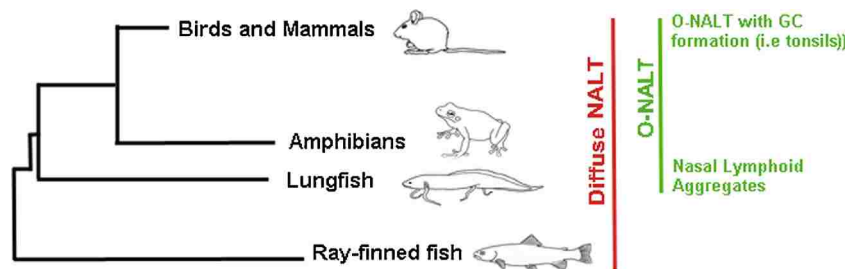


Fig. 1. Schematic diagram of the evolution of nasal immune systems in vertebrates.

phoid tissue (GALT). Furthermore, most mammalian studies focus on organized NALT (O-NALT), whereas diffuse NALT (D-NALT) has received very little attention. It is worth noting that the term “non-NALT” can also be found in the literature instead of D-NALT (Asanuma et al., 1997; Lee et al., 2015; Tamura et al., 1998). Additionally, “nasal passage (NP) leucocytes” is another term that can be found in the mammalian literature referring to D-NALT (Hiroi et al., 1998; Rodríguez-Monroy et al., 2007; Shikina et al., 2004). Despite the fact that the Society for mucosal immunology does not recommend the use of O-MALT and D-MALT (Brandtzaeg et al., 2008), numerous mammalian immunologists continue to use this terminology. Moreover, from the evolutionary immunologist point of view, O-NALT and D-NALT are useful terms considering that early vertebrates lack O-NALT (Fig. 1). In the next part of this review, we will summarize the basic anatomical aspects of NALT in different vertebrate groups.

2.1. Rodents and humans

The anatomy and structure of O-NALT have been widely studied in rodents (Mestecky et al., 2005). Murine NALT is composed of a pair of organized mucosal organs located on the roof of the soft palate at the entrance to the nasopharyngeal duct (Liang et al., 2001). NALT in mouse is considered by some to be analogous to the Waldeyer's ring in human which consists of the adenoids and tonsils (Kuper et al., 1992). Thus, in both mice and humans, O-NALT is strategically placed in the upper airways to combat air-borne antigens. Perhaps, this anatomical observation historically hindered the investigation of NALT in non-terrestrial vertebrates.

It is important to highlight that O-NALT of rodents and humans appears to be significantly different anatomically speaking. In rodents, NALT is located in a single localization bilateral at the entrance of the nasopharyngeal duct whereas in human studies conducted in children, O-NALT was mostly found in the middle concha and it consisted of disseminated lymphoid, subepithelial follicles (Debertin et al., 2003). The results from this study indicated that children have O-NALT structures in addition to a Waldeyer's ring (Debertin et al., 2003). Additionally, these differences underscore the fact that mice may not be the best models for human nasal immunity studies.

Similar to the Peyer's patches in the gut, O-NALT structures are located underlying specialized portions of the epithelium known as follicle-associated epithelium (FAE). Additionally, high endothelial venules (HEVs) control lymphocyte trafficking into O-NALT (Kiyono and Fukuyama, 2004). O-NALT structures also have distinct B-lymphocyte and T-cell zones (Bailey et al., 2005; Brandtzaeg and Pabst, 2004). Germinal center formation occurs in O-NALT in response to infection or antigenic stimulation (Zuercher et al., 2002).

As mentioned earlier, both mice and humans also possess diffuse lymphoid cells situated on the mucosa of the nasal passages called (D-NALT) (Liang et al., 2001). D-NALT includes myeloid cells and lymphoid cells (both B and T cells). The similarities and differ-

ences between mammalian O-NALT and D-NALT are summarized in Table 1.

2.2. Other mammals

In this section, we are going to focus on reports pertaining four groups of mammals: cattle, sheep, canines and rabbits. The studies in these species have been motivated by the importance of nasal vaccination in veterinary medicine.

In cattle, the tonsil (O-NALT) was first described in 1992 (Schuh and Oliphant, 1992). Cattle tonsils are located at the entry of the pharynx and are equivalent to the Waldeyer's ring in humans (Rebelatto et al., 2000). During development, adenoid can be detected at 95 days of gestation. Moreover, ciliated, microvillus cells and a loose accumulation of mononuclear cells in lamina propria is visible at 120–150 days of gestation. Small lymphoid follicles form at 4–5 months of gestation following by the appearance of goblet cells after 5 months of gestation (Schuh and Oliphant, 1992). Tonsils are well developed at birth in cattle. However, germinal center formation and increase in MHC class II expression only occur in the late natal and early post-natal period (Schuh and Oliphant, 1992). Moreover, cattle infected with foot-and-mouth disease virus (FMDV) showed increased expression of TLR-4 in NALT, indicating the importance of type I IFN responses in NALT against FMDV (Zhang et al., 2006).

Sheep O-NALT structures, similar to horse O-NALT, are clustered posterior to the opening of the Eustachian tube (Mair et al., 1988; Stanley et al., 2001). Thus, ovine NALT is highly organized and consists of discrete B and T cells areas similar to those found of humans and rodents. Furthermore, it has been shown that sheep NALT is covered by ciliated and non-ciliated cells which play an important role in antigen uptaking and processing (Stanley et al., 2001).

Peeters et al. reported the absence of typical O-NALT structures in the nasal mucosa of dogs without respiratory disease (Peeters et al., 2005). Waldeyer's ring in the dog consists of the lingual tonsil, the palatine tonsils, the soft palate tonsil and the pharyngeal tonsil or adenoid (Billen et al., 2006). The nasopharyngeal mucosa in dogs appears uniform and the nasopharyngeal tonsil is not obvious (Billen et al., 2006). The latter might be due to the fact that dogs breathe through both the nose and the mouth; therefore, exposure of the canine nasal and nasopharyngeal mucosa to inhaled antigens is decreased. This may explain why the pharyngeal tonsil is less developed in dogs than horses, cattle, sheep and pigs (Billen et al., 2006).

Casteleyn et al. (2010) histologically examined the presence of NALT in rabbits by sectioning the nasal cavity. Rabbits appear to have well organized NALT in their nasal cavities including clustered I and II lymphoid follicles separated by interfollicular regions as well as isolated lymphoid follicles. Interestingly, in the middle third of rabbit nasal cavity, NALT occupied the largest space. The rabbit and human nasal cavities occupy a similar volume considering their respective body masses. However, in comparison with rodents, O-NALT in the rabbit is more abundant. Therefore the sim-

Table 1
The differences between mice O-NALT and D-NALT.

	O-NALT	D-NALT	References
Number of lymphocytes	+	++	Rodríguez-Monroy et al. (2007)
T/B cells ratio	0.76–1.2	0.33–1.0	Asanuma et al. (1997), Rodríguez-Monroy et al. (2007)
Percentage of B cells ^a	47–79%	55–74%	Liang et al. (2001), Rodríguez-Monroy et al. (2007)
Plasma cells	+	++	Rodríguez-Monroy et al., (2007)
IgM+ B cells	47 or 85%	0.5–9%	Rodríguez-Monroy et al. (2007), Shikina et al. (2004), Smith et al. (2013)
IgA+ B cells	1–1.6%	7.7–10.8%	
B220 ^{hi} B cells	Present	Present	Rodríguez-Monroy et al. (2007)
B220 ^{hi} B220 ^{low} B cells	Absent	Present	
IgM/IgG/IgA secreting cells ratio (Uninfected)	10/3/3	10/3/3	Asanuma et al. (1997)
IgM/IgG/IgA secreting cells ratio (infected with influenza) ^b	4/50/40	1/25/10	
IgM/IgG/IgA secreting cells ratio (immunized with Cry1Ac protoxin) ^c	1/80/125	1/125/350	Rodríguez-Monroy and Moreno-Fierros (2010)
IgM/IgG/IgA secreting cells ratio (immunized with cholera toxin)	1/30/65	1/90/160	
IgA isotype class switching	Present	Absent	Shikina et al. (2004)
Class switch recombination-associated molecules	Present	Absent	
Long-lasting, specific effector antibody response ^e	Absent	Present	Liang et al. (2001)
Frequency of AFCs ^e	+	++	Liang et al. (2001)
Generation of virus-specific antibody forming cells (AFCs) ^e	+	+	
Infected/uninfected IFN- γ production ratio ^d	~1000	~700	Asanuma et al. (1997)
Infected/uninfected IL4 production ratio	1	2	
CD3 ⁺ T cells	30–40%	13–20%	Rodríguez-Monroy et al. (2007), Smith et al. (2013)
CD4 ⁺ /CD8 ⁺ T cells ratio	3–4.4	1.5–6.4	Asanuma et al. (1997), Heritage et al. (1997), Rodríguez-Monroy et al. (2007), Smith et al. (2013)
$\alpha\beta$ / $\gamma\delta$ of CD3 ⁺ T cells ratio	49–100	2.5–3	Heritage et al. (1997)
$\alpha\beta$ / $\gamma\delta$ of CD4 ⁺ CD8 ⁻ T cells ratio	49–100	49–100	
$\alpha\beta$ / $\gamma\delta$ of CD4 ⁻ CD8 ⁺ T cells ratio	49–100	9–19	
$\alpha\beta$ / $\gamma\delta$ of CD4 ⁻ CD8 ⁻ T cells ratio	0–1	0–1	
Type of CD4 ⁺ T cells	Th ₀	Th ₂	Hiroi et al. (1998), Liang et al. (2001)

Summary of major immune characteristics of mammalian organized and diffuse NALT in mice: +++=high, +=low.

^a C57BL/6 mice have higher B cells percentage compared to BALB/c mice.

^b 7 days post infection (dpi) with influenza.

^c BALB/c mice immunized intranasally.

^d 7 dpi with influenza.

^e shows responses after influenza virus infection.

ilarities between human and rabbit nasal cavities suggest that the rabbit is a better model for intranasal vaccine development than rodents are (Casteleyn et al., 2010). Additionally, rabbits have a D-NALT characterized by intraepithelial and lamina propria lymphocytes (Casteleyn et al., 2010).

2.3. Birds

Most of our knowledge on avian NALT comes from studies in chicken and duck. The nasal cavity in chickens is cone-shaped and separated into the right and left sides by a cartilaginous nasal septum. The majority of the nasal cavity is occupied by the turbinates which play a major role in preventing the entry of dust and microbes (Kang et al., 2013). Lymphoid nodules are the main

O-NALT structure in chickens. Nodules are made of B cells with developed germinal centers, surrounded by a coat of CD4⁺ T cells.

Chicken D-NALT, on the other hand, consists mostly of CD8⁺ T cells that can be found in the epithelium and in the lamina propria of the nasal mucosa (Kang et al., 2013; Ohshima and Hiramatsu, 2000). Additionally, scattered lymphoid cells are found in the paranasal organs of chickens (nasolacrimal ducts, lateral nasal glands and their ducts) (Bang and Bang, 1968; Kang et al., 2013).

NALT appears to be an important inductive site for the chicken's mucosal immune system, however, the low absorption rates of antigen by the nasal mucosa may limit induction of effective nasal immune responses (Kang et al., 2013).

The nasal cavity in duck is cone-shaped and separated into right and left sides by a nasal septum (Kang et al., 2014). At the caudal

regions of the nasal cavity there are two pairs of symmetrical lymphoid aggregates; one pair located on the dorsal side of the choanal cleft and the other pair on both sides of nasal septum (Kang et al., 2014). The FAE found in duck O-NALT, unlike that of rodents, contains almost no goblet cells. The use of liquid vaccines for ducklings and dry powder vaccine sprays for adult ducks has been recommended because liquid vaccines are unlikely to reach the NALT located on the nasal septum in adult ducks (Kang et al., 2014).

Like the chicken, ducks have diffuse lymphoid tissue and intraepithelial lymphocytes located within their nasal walls and turbinalia randomly (Kang et al., 2014).

2.4. Reptiles and amphibians

Unfortunately, NALT has been studied neither in reptiles nor in amphibians. This is despite the fact that chelonids are affected by upper respiratory tract disease (URTD) caused by *Mycoplasma agassizii* (Brown et al., 1999). The infection results in nasal discharge, nasal wheeze, conjunctivitis and inflammation of the oral mucosa. The contribution of NALT responses in *M. agassizii* infected chelonids should be investigated

Amphibians are known to have both diffuse and organized GALT and NALT (Goldstine et al., 1975). Tonsil-like structures were found in the lingual and sublingual regions of anuran amphibians (Myers, 1928). We further identified lymphoid aggregates associated with the olfactory epithelium of *Lithobates* sp. Tadpoles (Tacchi et al., 2015). Based on histological examination, these were present immediately underneath the olfactory epithelium but did not appear as organized as those found in lungfish. Contrary to birds and mammals, amphibian O-MALT is characterized by lymphoid nodules or aggregates that lack B and T cell zones or GC formation (Goldstine et al., 1975).

2.5. Sarcopterygian fishes

Sarcopterygian fish such as lungfish are the closest living sister species to all tetrapods (Zardoya and Meyer, 1996). Moreover, lungfish represent the transition from aquatic to terrestrial environments during vertebrate evolution and are exposed to both air-borne and water-borne antigens. We recently discovered that African lungfish (*Protopterus* sp.) may be the most ancient vertebrate where O-MALT, including O-NALT, is found (Fig. 1). O-NALT structures in lungfish are FAE-associated or embedded in the mucosa of the upper and lower jaw (Fig. 2). They are mostly composed of lymphocytes both B and T cells and do not display GC formation (Tacchi et al., 2015). In response to bacterial infection, lungfish O-NALT architecture and cellular composition changes, with an increase in the percentage of T and B cells compared to uninfected controls. Although not covered in the same study, we anticipate the presence of D-NALT in lungfish, but their characteristics need to be investigated. The discovery of these primordial forms of O-NALT in lungfish along with the ability to infect these animals intranasally in the laboratory makes this species an interesting system for investigating the structure, organogenesis and function of O-MALT in ectotherms.

2.6. Teleosts

Until recently, three MALT have been characterized in teleost fish: gut-associated lymphoid tissue (GALT), skin-associated lymphoid tissue (SALT) and gill-associated lymphoid tissue (Salinas et al., 2011). However, we have discovered that NALT is likely conserved in all jawed vertebrates as it was found in teleost fish. Teleost NALT resembles other teleost MALT in many regards such as the presence of diffuse lymphoid cells with no organized structures present, a predominant constitutive presence of IgT⁺

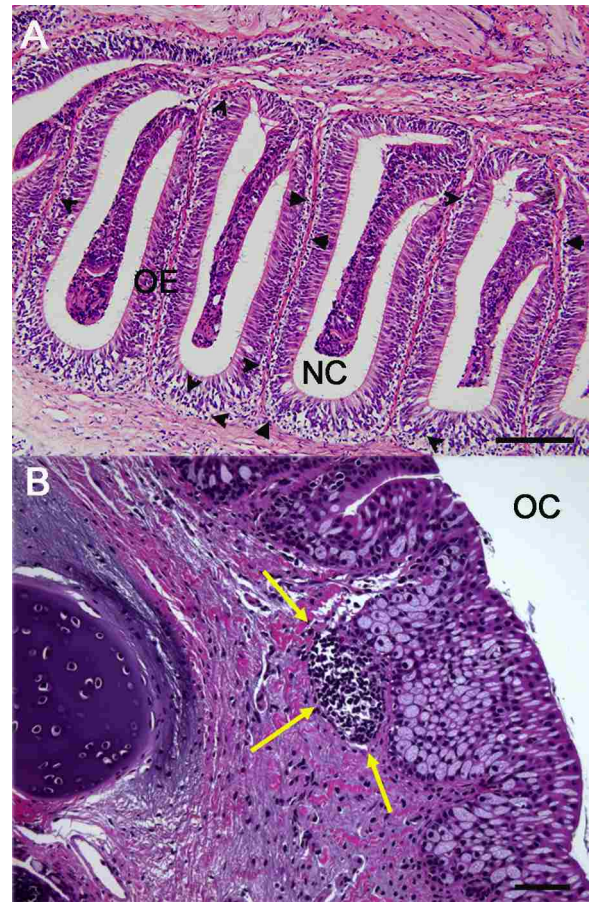


Fig. 2. (A) Light micrograph (hematoxylin and eosin stain) of paraffin sections of the olfactory organ of an Australian eel (*Anguilla australis*) showing the presence of diffuse NALT in the form of scattered lymphocytes (black arrow heads). (B) Light micrograph (hematoxylin and eosin stain) of the olfactory organ of the African lungfish (*Protopterus dolloi*) showing the presence of a primordial lymphoid aggregate (yellow arrows). NC: nasal cavity; OC: oral cavity; OE: olfactory epithelium. Scale bar = 100 μ m.

B cells and secreted IgT compared to systemic lymphoid tissues and the presence of an associated microbiota coated by mucosal immunoglobulins (Tacchi et al., 2014). This discovery broke the previous paradigm of nasal immune systems being a first line of defense against inhaled antigens.

Histological examination of the NALT of four different families of teleost fish showed that teleost NALT harbors diffuse lymphoid cells but lacks O-NALT (Tacchi et al., 2014). One of the key features of teleost MALT is the preponderant presence of IgT⁺ B cells and secreted IgT into mucosal secretions (Zhang et al., 2010). Trout D-NALT contains abundant B cells, 48.5% are IgM⁺ B cells and 51.5% are IgT⁺ B cells, following the canonical B cell composition of other trout MALT. Similarly, the ratio of secreted IgT and secreted IgM in nasal mucus is much higher than that in plasma, again highlighting that trout NALT shares the main features of other MALT in teleosts. In gut and skin, previous studies have shown that specific IgT but not IgM responses occur in the local mucosal environment in response to parasitic infections in rainbow trout (Xu et al., 2013; Zhang et al., 2010). Although we detected high levels of IgT in the nasal secretion of trout in the absence of antigenic stimulation, specific IgT responses in the olfactory organ of teleosts in response to infection or vaccination are yet to be investigated. We have demonstrated striking protection levels conferred by nasal vaccines against viral and bacterial pathogens of fish in rainbow trout however, the mechanisms underlying the observed protection are not well understood

Table 2
Requirements for the formation of NALT in mice.

KO mice with	Organogenesis of NALT	References
Id2	Absent	Fukuyama et al. (2002), Yokota et al. (1999)
Ror- γ t	Not required/well developed	Harmsen et al. (2002), Sun et al. (2000)
Lt α	Disorganized but developed with fewer number of lymphocytes	De Togni et al. (1994), Fukuyama et al. (2002), Harmsen et al. (2002)
aly/aly	Disorganized but developed with fewer number of lymphocytes	Fukuyama et al. (2002), Miyawaki et al. (1994)
IL-7 α	Disorganized but developed with decreased number of lymphocytes	Adachi et al. (1998), Fukuyama et al. (2002), Harmsen et al. (2002)
plt/plt	Developed with decreased number of lymphocytes	Fukuyama et al. (2006), Rangel-Moreno et al. (2005)
Microbiota	Developed with delay	Randall and Mebius (2014)
LT β	Developed but disorganized	Fukuyama et al. (2002), Koni et al. (1997)
TRANCE	Developed but disorganized	Ache and Young (2005), Harmsen et al. (2002)
CXCL13/CCL19/CCL21	Developed but disorganized	Ansel et al. (2000), Fukuyama et al. (2006), Rangel-Moreno et al. (2005)

and may include both humoral and cellular immunity (LaPatra et al., 2015; Tacchi et al., 2014).

Using a live attenuated infectious hematopoietic necrosis virus (IHNV) model of nasal vaccination, we were able to show that trout NALT mounts strong innate and adaptive immune responses over the course of a 28 day experiment. Whereas the expression of innate immune genes peaked at day 4 post vaccination, expression of adaptive immune genes peaked at day 14. Additionally, nasal vaccination resulted in stimulation of immune genes not only in NALT but also in the head-kidney (Tacchi et al., 2014).

Altogether, our results clearly reveal that early bony vertebrates evolved olfactory organs with strong defense functions that serve as a primary mucosal immune barrier against pathogens. Moreover, the discovery of teleost NALT and detection of nasal immune responses in trout in response to vaccination underscores the fact that strong nasal immune responses in vertebrates can take place in the absence of O-NALT. Currently, surgical ablation of O-NALT in mice is used as a tool to evaluate the specific contribution of O-NALT to mammalian nasal immune responses. This method is complex and may result in incomplete removal of all O-NALT cells. Thus, we propose that teleost NALT is an excellent model for the study of D-NALT and can provide a unique tool to understand, for instance, how tonsillectomized humans respond to nasal vaccines.

3. Evolution of NALT-specific molecules in vertebrates

The mucosal immune system has evolved complex suites of immune molecules as well as cell adhesion and trafficking molecules that separate it from the systemic immune system. For instance, trafficking of lymphocytes to NALT in mice is governed by the PNA α -L-selectin pair (Csencsits et al., 1999; Fukuyama et al., 2002), whereas the α 4 β 7-MA α CAM-1 pair governs trafficking of lymphocytes to the gut (Berlin et al., 1995).

The development of lymphoid tissues mainly relies on the lymphotoxin-driven expression of homeostatic chemokines such as CXCL13 (Ansel et al., 2000; Randall and Mebius, 2014). CXCL13 also plays an important role in maintaining the lymphoid architecture of NALT such as formation of germinal centers (Rangel-Moreno et al., 2005). In NALT, however, additional chemokines like CCL20 and CCL9 which are important in dendritic cell and B cell migration are required for development (Zhao et al., 2003). Impaired expression of CCL19/CCL21 results in defects in influenza-specific CD8 T cells responses in NALT of lymphotoxin- α -deficient (Lt α ^{-/-}) and plt/plt mice (Rangel-Moreno et al., 2005).

We know very little about the role of chemokines in the nasal immune system of vertebrates other than mice and humans. In trout, we found CCL19 expression was upregulated around 50-fold at 4 days post vaccination with live attenuated IHNV suggesting a conserved role of this chemokine in vertebrate nasal immunity (Tacchi et al., 2014).

With respect to O-MALT evolution, it has been proposed that organization of lymphocytes in structures such as lymph nodes or

O-MALT is an endotherm-restricted innovation. Lymphocyte organization requires the presence of certain molecular signals that create the adequate microenvironment for B and T cells. Most of the molecules that play a role in lymphocyte organization belong to the tumor necrosis factor superfamily (TNFSF) (Tacchi et al., 2015). In this respect, we recently provided new insights into the evolution of TNFSF and showed that it greatly diversified in African lungfish. Among TNFSF members, lymphotoxins are of particular relevance due to their function in the organization of lymphoid tissues. Interestingly, where lymphotoxin beta receptor (LTBR) is found from teleosts to humans, lymphotoxin alpha (LTA) and beta (LTB) are absent in teleosts but found in lungfish. In other words, TNFSF members known to be essential in lymphocyte organization in mammals first appeared in lungfish and are absent from teleost genomes. Moreover, a number of these TNFSF members were found to be expressed in African lungfish O-NALT (Tacchi et al., 2015).

ID2 is a transcription factor known to be essential for O-NALT formation. ID2 is involved in the induction of CD3⁺CD4⁺CD45⁺ cells (Yokota et al., 1999) and ID2 deficient mice could not develop NALT after birth (Fukuyama et al., 2002; Yokota et al., 1999). We found ID2 expressed both in trout and lungfish NALT and its expression was significantly modulated upon nasal vaccination with a viral vaccine or nasal bacterial infection, respectively (Tacchi et al., 2014). Important molecules in the formation of NALT in mice are summarized in Table 2.

4. Nasal microbiota and immunity in vertebrates

Every animal mucosal surface is colonized by millions of microorganisms forming a very ancient and successful symbiosis between prokaryotes and metazoans. The microbiota controls the immunological development of the host by different mechanisms such as inhibition of pathogen colonization on mucosal surfaces and stimulation of the host immune system (Buffie and Pamer, 2013; Kiyono and Fukuyama, 2004; Randall and Mebius, 2014). Although the number of studies revealing the importance of the microbiota in GALT development and function is vast, information regarding its effects on NALT is limited.

The nasal microbiome of human was sequenced and characterized in 2010 and further studies continue to determine its role in health and disease (Dewhirst et al., 2010). In humans, over 96% of the nasal bacterial microbiome belongs to three phyla: Actinobacteria, Firmicutes and Proteobacteria (Yan et al., 2013). In other mammalian species such as pigs, the nasal microbiome is Proteobacteria, Firmicutes and Spirochaetes (Weese et al., 2014). Nasal-associated microbiota are also present in aquatic vertebrates as evidenced by our studies in rainbow trout (Tacchi et al., 2014). The bacterial community associated with the trout olfactory organ is very diverse. 16s rDNA pyrosequencing revealed the presence of 18 total bacterial phyla, the highest number of phyla present among all body sites. The bacterial community was dominated by Proteobacteria, Actinobacteria, Bacteroidetes and Firmicutes with the

class Betaproteobacteria accounting for 15.1–53.6% of all sequences (Lowrey et al., 2015). Thus, although limited pyrosequencing data is available, it appears that Proteobacteria and Firmicutes may be the most dominant and conserved taxa among nasal microbiomes in vertebrates, further studies will confirm or reject this hypothesis. The trout nasal microbiome composition is distinct from that of any other trout mucosal surface but most closely resembles that of the skin.

The presence of unique bacterial communities in association with each mucosal anatomical site suggests a tight cross-talk between the microbiota and MALT in vertebrates. One of the ways by which the microbiota and the host immune system interact is by means of secretory immunoglobulins that help anchor microorganisms to the mucus layer, while tagging them in a process known as immune exclusion. As an example, trout nasal-associated bacteria, similar to gut and skin bacteria, are coated by secretory immunoglobulins. Particularly, in trout skin and gut mucus, the immunoglobulin isotype IgT has specialized in the role of bacteria coating (Xu et al., 2013; Zhang et al., 2010) with IgM coating significantly lower numbers of bacteria. In nasal mucus, however, an equal proportion of bacteria were coated with IgM or IgT and the proportion of bacteria coated with both isotypes was higher than that found in the gut and skin (Tacchi et al., 2014).

From mammalian studies it appears clear that the microbiota plays a key role in the form and function of NALT. For instance, the microbiota was shown to modulate local nasal T cell responses against *Mycoplasma pulmonis* infection (Henriksson et al., 2004). On the other hand, the composition of the nasal microbiome of humans is a determinant of *Staphylococcus aureus* colonization and carriage (Frank et al., 2010; Yan et al., 2013) and, in mice, it regulates the immune responses against respiratory influenza A virus infection (Ichinohe et al., 2011). Additionally, it has been shown that the number of M cells in NALT of specific pathogen free rats is lower compared to normally reared rats (Jeong et al., 2000) and the numbers of T and B cells in NALT are 2–3 times greater after an experimental infection (Asanuma et al., 1997). NALT, like most of the lymphoid organs, can develop in germ free mice. NALT development CXCL5-deficient mice in sterile conditions takes about 20 weeks, however by repeated intranasal application of heat inactivated *Propionibacterium acnes* suspension, NALT can be induced after 8 weeks (Krege et al., 2009). In the future, the specific roles of the nasal microbiota on the development and function of vertebrate NALT should be further elucidated.

5. How old is NALT?

Our current view of nasal immunity is limited and mostly restricted to mammalian studies. We provided the first evidence supporting the idea that nasal immunity is an ancient arm of the mucosal immune system of vertebrates. Furthermore, our studies underscore that D-NALT, as anticipated, precedes the appearance of O-NALT during evolution (Fig. 1). Currently, we can state that D-NALT is at least 380 MY old, although we anticipate the cartilaginous fish and even agnathans may be equipped with an equivalent immune system associated with their olfactory organs. How old is O-NALT is a separate question. We have provided evidence of primitive O-NALT structures in the African lungfish, indicating that the ancestor to all tetrapods first acquired this immunological innovation (Tacchi et al., 2015). Further studies should address the immune function of primitive O-NALT in ectotherms.

6. Concluding remarks

Olfaction is one of the most ancient and conserved sensory systems in vertebrates. It seems that the successful structure

and function of olfactory organs evolved to not only provide the exquisite detection of odorants but also to ensure that pathogens do not gain entry into hosts via this route. We hope that our pioneer studies in NALT evolution motivate more studies in non-mammalian models that complete our understanding of nasal immune systems and their evolution. Future studies in teleosts may address whether specific IgT is the main immunoglobulin isotype in nasal adaptive immune responses and whether nasal vaccination can lead to protection in other distant MALT. Lungfish studies, on the other hand, should try to address what evolutionary advantages lymphocyte organization confers at mucosal sites in the absence of germinal center formation.

Acknowledgments

This work was funded by awards NSF IOS # 1456940 and USDA AFRI # 2DN70-2RD7 to IS. Authors thank Victoria Hansen for the artwork.

References

- Ache, B.W., Young, J.M., 2005. Olfaction: diverse species, conserved principles. *Neuron* 48, 417–430.
- Adachi, S., Yoshida, H., Honda, K., Maki, K., Saijo, K., Ikuta, K., Saito, T., Nishikawa, S.-I., 1998. Essential role of IL-7 receptor alpha in the formation of Peyer's patch anlage. *Int. Immunol.* 10 (1), 1–6.
- Ansel, K.M., Ngo, V.N., Hyman, P.L., Luther, S.A., Förster, R., Sedgwick, J.D., Browning, J.L., Lipp, M., Cyster, J.G., 2000. A chemokine-driven positive feedback loop organizes lymphoid follicles. *Nature* 406, 309–314.
- Asanuma, H., Hodson Thompson, A., Iwasaki, T., Sato, Y., Inaba, Y., Aizawa, C., Kurata, T., Tamura, S.-I., 1997. Isolation and characterization of mouse nasal-associated lymphoid tissue. *J. Immunol. Methods* 202, 123–131.
- Bailey, M., Haverson, K., Inman, C., Harris, C., Jones, P., Corfield, G., Miller, B., Stokes, C., 2005. The development of the mucosal immune system pre- and post-weaning: balancing regulatory and effector function. *Proc. Nutr. Soc.* 64, 451–457.
- Bang, B.G., Bang, F., 1968. Localized lymphoid tissues and plasma cells in paracocular and paranasal organ systems in chickens. *Am. J. Pathol.* 53, 735.
- Belal, A., El-Gohery, Y., Talaat, M., 1977. Nasal and paranasal pathology in experimental bilharziasis. *J. Laryngol. Otol.* 91, 391–400.
- Berlin, C., Bargatze, R., Campbell, J., Von Andrian, U., Szabo, M., Hasslen, S., Nelson, R., Berg, E., Erlandsen, S., Butcher, E., 1995. $\alpha 4$ integrins mediate lymphocyte attachment and rolling under physiologic flow. *Cell* 80, 413–422.
- Billen, F., Peeters, D., Dehard, S., Day, M., Clercx, C., 2006. Distribution of leucocyte subsets in the canine pharyngeal tonsil. *J. Comp. Pathol.* 135, 63–73.
- Brandtzaeg, P., Kiyono, H., Pabst, R., Russell, M., 2008. Terminology: nomenclature of mucosa-associated lymphoid tissue. *Mucosal Immunol.* 1, 31–37.
- Brandtzaeg, P., Pabst, R., 2004. Let's go mucosal: communication on slippery ground. *Trends Immunol.* 25, 570–577.
- Brown, M., McLaughlin, G., Klein, P., Crenshaw, B., Schumacher, I., Brown, D., Jacobson, E., 1999. Upper respiratory tract disease in the gopher tortoise is caused by *Mycoplasma agassizii*. *J. Clin. Microbiol.* 37, 2262–2269.
- Buffie, C.G., Pamer, E.G., 2013. Microbiota-mediated colonization resistance against intestinal pathogens. *Nat. Rev. Immunol.* 13, 790–801.
- Castelny, C., Broos, A., Simoens, P., Van Den Broeck, W., 2010. NALT (nasal cavity-associated lymphoid tissue) in the rabbit. *Vet. Immunol. Immunopathol.* 133, 212–218.
- Chen, Z., Aspelund, A., Kemble, G., Jin, H., 2006. Genetic mapping of the cold-adapted phenotype of B/Ann Arbor/1/66, the master donor virus for live attenuated influenza vaccines (FluMist®). *Virology* 345, 416–423.
- Cocquyt, G., Baten, T., Simoens, P., Van Den Broeck, W., 2005. Anatomical localisation and histology of the ovine tonsils. *Vet. Immunol. Immunopathol.* 107, 79–86.
- Csencits, K.L., Jutila, M.A., Pascual, D.W., 1999. Nasal-associated lymphoid tissue: phenotypic and functional evidence for the primary role of peripheral node addressin in naive lymphocyte adhesion to high endothelial venules in a mucosal site. *J. Immunol.* 163, 1382–1389.
- Cullen, K.A., Hall, M.J., Golosinskiy, A., Statistics N.C.f.H., 2009. Ambulatory surgery in the United States, 2006. US Department of Health and Human Services, Centers for Disease Control and Prevention, National Center for Health Statistics, Maryland.
- De Togni, P., Goellner, J., Ruddle, N.H., Streeter, P.R., Fick, A., Mariathasan, S., Smith, S.C., Carlson, R., Shornick, L.P., Strauss-Schoenberger, J., 1994. Abnormal development of peripheral lymphoid organs in mice deficient in lymphotoxin. *Science* 264, 703–707.
- Debertin, A., Tschernig, T., Tönjes, H., Kleemann, W., Tröger, H., Pabst, R., 2003. Nasal-associated lymphoid tissue (NALT): frequency and localization in young children. *Clin. Exp. Immunol.* 134, 503–507.
- Dewhirst, F.E., Chen, T., Izard, J., Paster, B.J., Tanner, A.C., Yu, W.-H., Lakshmanan, A., Wade, W.G., 2010. The human oral microbiome. *J. Bacteriol.* 192, 5002–5017.

- Frank, D.N., Feazel, L.M., Bessesen, M.T., Price, C.S., Janoff, E.N., Pace, N.R., 2010. The human nasal microbiota and *Staphylococcus aureus* carriage. *PLoS One* 5, e10598.
- Fukuyama, S., Hiroi, T., Yokota, Y., Rennert, P.D., Yanagita, M., Kinoshita, N., Terawaki, S., Shikina, T., Yamamoto, M., Kurono, Y., 2002. Initiation of NALT organogenesis is independent of the IL-7R, LT β R, and NIK signaling pathways but requires the Id2 gene and CD3⁺CD4⁺CD45⁺ cells. *Immunity* 17, 31–40.
- Fukuyama, S., Nagatake, T., Kim, D.-Y., Takamura, K., Park, E.J., Kaisho, T., Tanaka, N., Kurono, Y., Kiyono, H., 2006. Cutting edge: uniqueness of lymphoid chemokine requirement for the initiation and maturation of nasopharynx-associated lymphoid tissue organogenesis. *J. Immunol.* 177, 4276–4280.
- Fukuyama, Y., Tokuhara, D., Kataoka, K., Gilbert, R.S., McGhee, J.R., Yuki, Y., Kiyono, H., Fujihashi, K., 2012. Novel vaccine development strategies for inducing mucosal immunity. *Expert Rev. Vaccines* 11, 367–379.
- Goldstine, S.N., Manickavel, V., Cohen, N., 1975. Phylogeny of gut-associated lymphoid tissue. *Am. Zool.* 15, 107–118.
- Harkema, J., Plopper, C., Hyde, D., St George, J., 1987. Regional differences in quantities of histochemically detectable mucosubstances in nasal, paranasal, and nasopharyngeal epithelium of the bonnet monkey. *J. Histochem. Cytochem.* 35, 279–286.
- Harmsen, A., Kusser, K., Hartson, L., Tighe, M., Sunshine, M.J., Sedgwick, J.D., Choi, Y., Littman, D.R., Randall, T.D., 2002. Cutting edge: organogenesis of nasal-associated lymphoid tissue (NALT) occurs independently of lymphotoxin- α (LT α) and retinoic acid receptor-related orphan receptor- γ but the organization of NALT is LT α dependent. *J. Immunol.* 168, 986–990.
- Henriksson, G., Helgeland, L., Midtvedt, T., Stiern, P., Brandtzaeg, P., 2004. Immune response to *Mycoplasma pulmonis* in nasal mucosa is modulated by the normal microbiota. *Am. J. Respir. Cell Mol. Biol.* 31, 657–662.
- Heritage, P., Underdown, B., Arsenault, A., Snider, D., McDermott, M., 1997. Comparison of murine nasal-associated lymphoid tissue and Peyer's patches. *Am. J. Respir. Crit. Care Med.* 156, 1256.
- Hiroi, T., Iwatani, K., Iijima, H., Kodama, S., Yanagita, M., Kiyono, H., 1998. Nasal immune system: distinctive Th0 and Th1/Th2 type environments in murine nasal-associated lymphoid tissues and nasal passage, respectively. *Eur. J. Immunol.* 28, 3346–3353.
- Ichinohe, T., Pang, I.K., Kumamoto, Y., Peaper, D.R., Ho, J.H., Murray, T.S., Iwasaki, A., 2011. Microbiota regulates immune defense against respiratory tract influenza A virus infection. *Proc. Natl. Acad. Sci. U. S. A.* 108, 5354–5359.
- Jeong, K., Suzuki, H., Nakayama, H., Doi, K., 2000. Ultrastructural study on the follicle-associated epithelium of nasal-associated lymphoid tissue in specific pathogen-free (SPF) and conventional environment-adapted (SPF-CV) rats. *J. Anat.* 196, 443–451.
- Kang, H., Yan, M., Yu, Q., Yang, Q., 2013. Characteristics of nasal-associated lymphoid tissue (NALT) and nasal absorption capacity in chicken. *PLoS One* 8, e84097.
- Kang, H., Yan, M., Yu, Q., Yang, Q., 2014. Characterization of Nasal cavity-associated lymphoid tissue in ducks. *Anat. Rec.* 297, 916–924.
- Kelemen, G., 1947. The junction of the nasal cavity and the pharyngeal tube in the rat. *Arch. Otolaryngol.* 45, 159–168.
- Kiyono, H., Fukuyama, S., 2004. NALT-versus Peyer's-patch-mediated mucosal immunity. *Nat. Rev. Immunol.* 4, 699–710.
- Koempel, J., Solares, C., Koltai, P., 2006. The evolution of tonsil surgery and rethinking the surgical approach to obstructive sleep-disordered breathing in children. *J. Laryngol. Otol.* 120, 993–1000.
- Koni, P.A., Sacca, R., Lawton, P., Browning, J.L., Ruddle, N.H., Flavell, R.A., 1997. Distinct roles in lymphoid organogenesis for lymphotoxins α and β revealed in lymphotoxin β -deficient mice. *Immunity* 6, 491–500.
- Krege, J., Seth, S., Hardtke, S., Davalos-Misslitz, A.C.M., Förster, R., 2009. Antigen-dependent rescue of nose-associated lymphoid tissue (NALT) development independent of LT β R and CXCR5 signaling. *Eur. J. Immunol.* 39, 2765–2778.
- Kuper, C.F., Koornstra, P.J., Hameleers, D.M., Biewenga, J., Spit, B.J., Duijvestijn, A.M., van Breda Vriesman, P.J., Sminia, T., 1992. The role of nasopharyngeal lymphoid tissue. *Immunol. Today* 13, 219–224.
- LaPatra, S., Kao, S., Erhardt, E.B., Salinas, I., 2015. Evaluation of dual nasal delivery of infectious hematopoietic necrosis virus and enteric red mouth vaccines in rainbow trout (*Oncorhynchus mykiss*). *Vaccine* 33, 771–776.
- Lee, H., Ruane, D., Law, K., Ho, Y., Garg, A., Rahman, A., Esterházy, D., Cheong, C., Goljo, E., Sikora, A., 2015. Phenotype and function of nasal dendritic cells. *Mucosal Immunol.* 8, 1083–1098.
- Liang, B., Hyland, L., Hou, S., 2001. Nasal-associated lymphoid tissue is a site of long-term virus-specific antibody production following respiratory virus infection of mice. *J. Virol.* 75, 5416–5420.
- Loo, S., Chin, K., 1974. Lymphoid tissue in the nasal mucosa of primates, with particular reference to intraepithelial lymphocytes. *J. Anat.* 117, 249–259.
- Lowrey, L., Woodhams, D.C., Tacchi, L., Salinas, I., 2015. Topographical mapping of the rainbow trout (*Oncorhynchus mykiss*) microbiome reveals a diverse bacterial community in the skin with antifungal properties. *Appl. Environ. Microbiol.* 81, 6915–6925.
- Lykke, N., 2012. Recent progress in mucosal vaccine development: potential and limitations. *Nat. Rev. Immunol.* 12, 592–605.
- Mair, T., Batten, E., Stokes, C., Bourne, F., 1987. The histological features of the immune system of the equine respiratory tract. *J. Comp. Pathol.* 97, 575–586.
- Mair, T., Batten, E., Stokes, C., Bourne, F., 1988. The distribution of mucosal lymphoid nodules in the equine respiratory tract. *J. Comp. Pathol.* 99, 159–168.
- Mestecky, J., Lamm, M.E., Ogra, P.L., Strober, W., Bienenstock, J., McGhee, J.R., Mayer, L., 2005. *Mucosal Immunology*. Academic Press, Amsterdam.
- Miyawaki, S., Nakamura, Y., Suzuka, H., Koba, M., Shibata, Y., Yasumizu, R., Ikehara, S., 1994. A new mutation, aly, that induces a generalized lack of lymph nodes accompanied by immunodeficiency in mice. *Eur. J. Immunol.* 24, 429–434.
- Myers, M.A., 1928. A study of the tonsillar developments in the lingual region of anurans. *J. Morphol.* 45, 399–439.
- Neutra, M.R., Kozlowski, P.A., 2006. Mucosal vaccines: the promise and the challenge. *Nat. Rev. Immunol.* 6, 148–158.
- Ohshima, K., Hiramatsu, K., 2000. Distribution of T-cell subsets and immunoglobulin-containing cells in nasal-associated lymphoid tissue (NALT) of chickens. *Histol. Histopathol.* 15, 713–720.
- Pabst, R., 2015. Mucosal vaccination by the intranasal route. Nose-associated lymphoid tissue (NALT) Structure, function and species differences. *Vaccine* 33, 4406–4413.
- Peeters, D., Day, M., Farnir, F., Moore, P., Clercx, C., 2005. Distribution of leucocyte subsets in the canine respiratory tract. *J. Comp. Pathol.* 132, 261–272.
- Perry, M., Whyte, A., 1998. Immunology of the tonsils. *Immunol. Today* 19, 414–421.
- Plotkin, S., 2014. History of vaccination. *Proc. Natl. Acad. Sci. U. S. A.* 111, 12283–12287.
- Randall, T., Mebius, R., 2014. The development and function of mucosal lymphoid tissues: a balancing act with micro-organisms. *Mucosal Immunol.* 7, 455–466.
- Rangel-Moreno, J., Moyron-Quiroz, J., Kusser, K., Hartson, L., Nakano, H., Randall, T.D., 2005. Role of CXCL chemokine ligand 13, CC chemokine ligand (CCL) 19, and CCL21 in the organization and function of nasal-associated lymphoid tissue. *J. Immunol.* 175, 4904–4913.
- Rebelatto, M., Mead, C., HogenEsch, H., 2000. Lymphocyte populations and adhesion molecule expression in bovine tonsils. *Vet. Immunol. Immunopathol.* 73, 15–29.
- Rodriguez-Monroy, M., Moreno-Fierros, L., 2010. Striking activation of NALT and nasal passages lymphocytes induced by intranasal immunization with Cry1Ac protoxin. *Scand. J. Immunol.* 71, 159–168.
- Rodriguez-Monroy, M.A., Rojas-Hernández, S., Moreno-Fierros, L., 2007. Phenotypic and functional differences between lymphocytes from NALT and nasal passages of mice. *Scand. J. Immunol.* 65, 276–288.
- Roland, P.S., Rosenfeld, R.M., Brooks, L.J., Friedman, N.R., Jones, J., Kim, T.W., Kuhar, S., Mitchell, R.B., Seidman, M.D., Sheldon, S.H., 2011. Clinical practice guideline polysomnography for sleep-disordered breathing prior to tonsillectomy in children. *OTO-HNS* 145, S1–S15.
- Salinas, I., Zhang, Y.-A., Sunyer, J.O., 2011. Mucosal immunoglobulins and B cells of teleost fish. *Dev. Comp. Immunol.* 35, 1346–1365.
- Schuh, J., Oliphant, L., 1992. Development and immunophenotyping of the pharyngeal tonsil (adenoid) in cattle. *J. Comp. Pathol.* 106, 229–241.
- Shikina, T., Hiroi, T., Iwatani, K., Jang, M.H., Fukuyama, S., Tamura, M., Kubo, T., Ishikawa, H., Kiyono, H., 2004. IgA class switch occurs in the organized nasopharynx-and gut-associated lymphoid tissue, but not in the diffuse lamina propria of airways and gut. *J. Immunol.* 172, 6259–6264.
- Smith, P.D., MacDonald, T.T., Blumberg, R.S., 2013. *Principles of Mucosal Immunology*. Garland Science, New York.
- Stanley, A., Huntley, J., Jeffrey, M., Buxton, D., 2001. Characterization of ovine nasal-associated lymphoid tissue and identification of M cells in the overlying follicle-associated epithelium. *J. Comp. Pathol.* 125, 262–270.
- Sun, Z., Unutmaz, D., Zou, Y.-R., Sunshine, M.J., Pierani, A., Brenner-Morton, S., Mebius, R.E., Littman, D.R., 2000. Requirement for ROR γ in thymocyte survival and lymphoid organ development. *Science* 288, 2369–2373.
- Tacchi, L., Larragoite, E., rin, T., Muñoz, P., Amemiya, C., hris, T., Salinas, I., 2015. African lungfish reveal the evolutionary origins of organized mucosal lymphoid tissue in vertebrates. *Curr. Biol.* 25, 1–8.
- Tacchi, L., Musharrafieh, R., Larragoite, E.T., Crossey, K., Erhardt, E.B., Martin, S.A., LaPatra, S.E., Salinas, I., 2014. Nasal immunity is an ancient arm of the mucosal immune system of vertebrates. *Nat. Commun.* 5, 6205.
- Tamura, S.-i., Iwasaki, T., Thompson, A.H., Asanuma, H., Chen, Z., Suzuki, Y., Aizawa, C., Kurata, T., 1998. Antibody-forming cells in the nasal-associated lymphoid tissue during primary influenza virus infection. *J. Gen. Virol.* 79, 291–299.
- Weese, J.S., Slifert, M., Jalali, M., Friendship, R., 2014. Evaluation of the nasal microbiota in slaughter-age pigs and the impact on nasal methicillin-resistant *Staphylococcus aureus* (MRSA) carriage. *BMC Vet. Res.* 10, 69.
- Xu, Z., Parra, D., Gómez, P., Salinas, I., Zhang, Y.-A., von Gersdorff Jørgensen, L., Heinecke, R.D., Buchmann, K., LaPatra, S., Sunyer, J.O., 2013. Teleost skin, an ancient mucosal surface that elicits gut-like immune responses. *Proc. Natl. Acad. Sci. U. S. A.* 110, 13097–13102.
- Yan, M., Pamp, S.J., Fukuyama, J., Hwang, P.H., Cho, D.-Y., Holmes, S., Relman, D.A., 2013. Nasal microenvironments and interspecific interactions influence nasal microbiota complexity and *S. aureus* carriage. *Cell Host Microbe* 14, 631–640.
- Yokota, Y., Mansouri, A., Mori, S., Sugawara, S., Adachi, S., Nishikawa, S.-I., Gruss, P., 1999. Development of peripheral lymphoid organs and natural killer cells depends on the helix-loop-helix inhibitor Id2. *Nature* 397, 702–706.
- Younis, R.T., Lazar, R.H., 2002. History and current practice of tonsillectomy. *Laryngoscope* 112, 3–5.
- Zardoya, R., Meyer, A., 1996. Evolutionary relationships of the coelacanth, lungfishes, and tetrapods based on the 28S ribosomal RNA gene. *Proc. Natl. Acad. Sci. U. S. A.* 93, 5449–5454.
- Zhang, Y.-A., Salinas, I., Li, J., Parra, D., Bjork, S., Xu, Z., LaPatra, S.E., Bartholomew, J., Sunyer, J.O., 2010. IgT, a primitive immunoglobulin class specialized in mucosal immunity. *Nat. Immunol.* 11, 827–835.

- Zhang, Z., Bashiruddin, J., Doel, C., Horsington, J., Durand, S., Alexandersen, S., 2006. Cytokine and Toll-like receptor mRNAs in the nasal-associated lymphoid tissues of cattle during foot-and-mouth disease virus infection. *J. Comp. Pathol.* 134, 56–62.
- Zhao, X., Sato, A., Cruz, C.S.D., Linehan, M., Luegering, A., Kucharzik, T., Shirakawa, A.-K., Marquez, G., Farber, J.M., Williams, I., 2003. CCL9 is secreted by the follicle-associated epithelium and recruits dome region Peyer's patch CD11b+ dendritic cells. *J. Immunol.* 171, 2797–2803.
- Zuercher, A.W., Coffin, S.E., Thurnheer, M.C., Fundova, P., Cebra, J.J., 2002. Nasal-associated lymphoid tissue is a mucosal inductive site for virus-specific humoral and cellular immune responses. *J. Immunol.* 168, 1796–1803.

Chapter 2

Sepahi, Ali, Luca Tacchi, Elisa Casadei, Fumio Takizawa, Scott E. LaPatra, and Irene Salinas. "CK12a, a CCL19-like chemokine that orchestrates both nasal and systemic antiviral immune responses in rainbow trout." *The Journal of Immunology* 11 (2017). DOI: <https://doi.org/10.4049/jimmunol.1700757>

CK12a, a CCL19-like Chemokine That Orchestrates both Nasal and Systemic Antiviral Immune Responses in Rainbow Trout

Ali Sepahi,* Luca Tacchi,* Elisa Casadei,* Fumio Takizawa,† Scott E. LaPatra,‡ and Irene Salinas*

Chemokines and chemokine receptors have rapidly diversified in teleost fish but their immune functions remain unclear. We report in this study that CCL19, a chemokine known to control lymphocyte migration and compartmentalization of lymphoid tissues in mammals, diversified in salmonids leading to the presence of six CCL19-like genes named CK10a, CK10b, CK12a, CK12b, CK13a, and CK13b. Salmonid CCL19-like genes all contain the DCCL-conserved motif but share low amino acid sequence identity. CK12 (but not CK10 or CK13) is constitutively expressed at high levels in all four trout MALT. Nasal vaccination with a live attenuated virus results in sustained upregulation of CK12 (but not CK10 or CK13) expression in trout nasopharynx-associated lymphoid tissue. Recombinant His-tagged trout CK12a (rCK12a) is not chemotactic in vitro but it increases the width of the nasal lamina propria when delivered intranasally. rCK12a delivered intranasally or i.p. stimulates the expression of CD8 α , granulysin, and IFN- γ in mucosal and systemic compartments and increases nasal CD8 α ⁺ cell numbers. rCK12a is able to stimulate proliferation of head kidney leukocytes from Ag-experienced trout but not naive controls, yet it does not confer protection against viral challenge. These results show that local nasal production of CK12a contributes to antiviral immune protection both locally and systemically via stimulation of CD8 cellular immune responses and highlight a conserved role for CK12 in the orchestration of mucosal and systemic immune responses against viral pathogens in vertebrates. *The Journal of Immunology*, 2017, 199: 3900–3913.

Chemokines are a family of cytokines that play important roles in homeostasis as well as immunity (1–3). As small secreted molecules, chemokines are the extracellular messengers of the immune system and largely control the extravasation of different immune cells from the bloodstream into the tissues (4). It is known that chemokine responses can be induced by a number of stimuli, including viral infection, and these responses are vital for control of the virus (5). Chemokines are classified in different families based on their amino acid sequence. Homeostatic chemokines such as CCL19, CCL21, CXCL12, and CXCL13 are expressed in lymphoid organs and regulate the mi-

gration and compartmentalization of lymphocytes and APCs within lymphoid tissues (6–9). CCL19 and CCL21 are also known to orchestrate the development and organization of secondary lymphoid organs including the nasopharynx-associated lymphoid tissue (NALT) (10, 11). Viral infections trigger CCL19 responses in mammals (12), which attract naive T and B lymphocytes to lymphoid organs after 24–48 h of infection (13).

A number of viruses are known to enter the host via the olfactory route (14–18). This route of infection provides a clear advantage to neurotropic viruses because they may gain access to the CNS via the olfactory bulb. Moreover, in mammals, viral infection of the upper respiratory surfaces may result in infection of the lungs (19–22). Finally, viral infection of nasal tissues, if not controlled locally, can trigger strong systemic responses once the virus enters the bloodstream via the nasal capillary beds. As a consequence, rapid onset of systemic antiviral immunity may be vital to control nasal viral infections.

Nasal vaccines are known to offer a number of advantages over other mucosal vaccines, including the ability to stimulate potent systemic Ab immune responses (23–26). The profuse network of capillaries that connects the olfactory organ (OO) with the systemic bloodstream may explain this property of nasal vaccines. In addition, molecular immune mechanisms connecting the nasal and systemic lymphoid tissues must be pivotal for the orchestration and rapid communication of local and systemic immune responses. In this regard, chemokines and other cytokines may provide the required signals for this communication, yet a full understanding of these mechanisms and their evolutionary origins are still missing.

We recently discovered the presence of NALT in teleost fish (27, 28) as a diffuse network of immune cells in the nasal mucosa that shares the same canonical features of other teleost MALT. We also showed that nasal vaccination of rainbow trout with a live atten-

*Center for Evolutionary and Theoretical Immunology, Department of Biology, University of New Mexico, Albuquerque, NM 87131; †Department of Pathobiology, School of Veterinary Medicine, University of Pennsylvania, Philadelphia, PA 19104; and ‡Research Division, Clear Springs Foods, Buhl, ID 83316

ORCID: 0000-0002-0988-2770 (F.T.).

Received for publication May 24, 2017. Accepted for publication September 26, 2017.

This work was supported by Agriculture and Food Research Initiative Grant D2N70-2RDN7 from the U.S. Department of Agriculture (to I.S.) and by National Institutes of Health Centers of Biomedical Research Excellence Grant P20GM103452 and National Institutes of Health Grant 2R01GM085207-05 (to J. Oriol Sunyer).

Address correspondence and reprint requests to Dr. Irene Salinas, Center for Evolutionary and Theoretical Immunology, University of New Mexico, 167 Castetter Hall, Albuquerque, NM 87131-0001. E-mail address: isalinas@unm.edu

The online version of this article contains supplemental material.

Abbreviations used in this article: BLAST, basic local alignment search tool; DC, dendritic cell; GL, gut leukocyte; HK, head kidney; HKL, HK leukocyte; IHNV, infectious hematopoietic necrosis virus; I.N., intranasally; LP, lamina propria; MHC-II, MHC class II; NALT, nasopharynx-associated lymphoid tissue; OO, olfactory organ; rCK12a, recombinant His-tagged trout CK12a; RT-qPCR, quantitative real-time PCR; SL, spleen leukocyte; VHSV, viral hemorrhagic septicemia virus; ZAS, zymosan-activated trout serum.

Copyright © 2017 by The American Association of Immunologists, Inc. 0022-1767/17/\$35.00

uated viral vaccine results in both local nasal and systemic immune responses (27, 29). The latter opened up many questions, including what are the molecular mechanisms that explain the protective effects of nasal vaccines in fish, and how are nasal and systemic immune responses orchestrated in cold-blooded vertebrates. As a preliminary effort, oligomicroarray studies following nasal vaccination with a viral vaccine revealed that early antiviral immune responses in rainbow trout NALT are characterized by dramatic increases in the expression of a CCL19-like molecule (27). Thus, we hypothesized that salmonid CCL19-like chemokines may provide the molecular link between local (nasal) and systemic immune compartments during antiviral immune responses and therefore can orchestrate both types of responses following nasal vaccination.

Evolutionarily speaking, chemokines and their receptors can be detected in lower deuterostome animals (30–32), and are considered rapidly evolving immune molecules (30, 33). To date, many chemokine and chemokine receptors have been found in bony fish (34–40), a group that has more chemokines and chemokine receptors than any other vertebrate including amphibians and mammals. Previous studies have identified rapid, tandem duplications in a number of teleost species including salmonids and zebrafish (38, 41, 42). It has been suggested that the diversification observed in the numbers and sequences of chemokines in bony fish may reflect the adaptation of the individual species to their respective biological environment (42). Despite this plethora of chemokines and chemokine receptor molecules, very little information is available with regards to their biological activities in teleost fish.

Using the DCCL amino acid signature motif, CCL19-like molecules have been previously identified in a few teleost species including turbot (*Scophthalmus maximus*) (43, 44) and striped murrelet (*Channa striatus*) (45). Their reported activities resemble canonical mammalian CCL19 functions including leukocyte trafficking, cell proliferation, and antiviral and antibacterial properties (43, 45). Recently, a study in Atlantic salmon (*Salmo salar*) used microarray to detect the increased expression of CCL19-like in the head kidneys (HK) of resistant and susceptible salmon strains challenged with infectious pancreatic necrosis virus (46). Moreover, a study on catfish showed that CCL19 gene expression is upregulated significantly following *Edwardsiella ictaluri* and *Flavobacterium columnare* infection (41). In rainbow trout, the CCL19-like CK12 was suggested to have a role in mucosal immune responses given its constitutive expression in mucosal tissues such as gills, gut, and skin (47). Furthermore, the mRNA levels of two other trout CCL19-like, CK10 and CK12 mRNA, increase following bath infection with viral hemorrhagic septicemia virus (VHSV) as well as infectious pancreatic necrosis virus at the fin base and ovary, respectively (40, 48–50). Trout CK12 expression also increased in the HK and spleen of VHSV-infected or polyinosinic-polycytidylic acid-injected trout and in trout HK leucocytes (HKLs) after in vitro exposure to polyinosinic-polycytidylic acid, infectious pancreatic necrosis virus, and VHSV (40, 48–50). However, whether teleost CCL19-like chemokines play a role in nasal immune responses deserves further investigation (27).

Because we found a clear induction of CCL19-like by oligomicroarray in trout NALT following nasal vaccination with a live attenuated viral vaccine (27), using the DCCL amino acid signature motif, we conducted further analysis in the National Center for Biotechnology Information database, in particular searching the rainbow trout and salmon genomes, to identify additional CCL19-like forms. Three CCL19-like genes have been described in rainbow trout thus far: CK10, CK12a, and CK12b (34, 38) based on expressed sequence tag libraries. However, in this study

we report that six CCL19-like genes exist in rainbow trout and salmon (CK10a, CK10b, CK12a, CK12b, CK13a, and CK13b) forming three major clusters (CK10, CK12, and CK13). Using a number of in vitro and in vivo studies, we report in this study that CCL19-like diversification resulted in the acquisition of a CCL19-like form, CK12a, which is able to induce both nasal mucosal and systemic antiviral immune responses. Our results not only highlight the conserved role of CCL19 in nasal immunity in vertebrates but also show that this chemokine facilitates the onset of systemic immune responses following nasal detection of Ags as well as the recruitment of APCs and CD8⁺ T cells to the local nasal mucosa.

Materials and Methods

Molecular identification of trout CCL19-like, sequence analysis, phylogenetic analysis, and three-dimensional structure modeling

Rainbow trout CK12a sequence was identified by the basic local alignment search tool (BLAST) (<http://blast.ncbi.nlm.nih.gov/Blast.cgi>) (51) using the expressed sequence tag sequence printed in the “Trout_imm_v1” (Agilent array design 028918) (27). The rainbow trout CK12a sequence was used to identify the sequence of rainbow trout CK13 and CK10 by BLAST against the available rainbow trout genome (52). The three rainbow trout sequences possess the canonical DCCL amino acid motif typical of vertebrate CCL19 sequences. Prediction of the open reading frame was performed with the programs BLAST and the ExPASy proteomics server (<http://ca.expasy.org/>). The open reading frame of each sequence was amplified by RT-PCR using specific primers (Table I) and the PCR products were cloned as previously described (53). A multiple sequence alignment was created using CLUSTALW (<http://align.genome.jp/>) (54). A phylogenetic tree was constructed from generated alignments using the Neighbor-Joining method within the software MEGA 7 (55); data were analyzed using Poisson correction and gaps were removed by pairwise deletions. To evaluate the topological stability of the Neighbor-Joining tree, a bootstrap of 1000 replicates was applied, with only values over 50% shown. To obtain the percentages of identity and similarities of the six sequences, the software MatGat 2.02 (56) was used. Three-dimensional prediction of protein structures for CCL19-like molecules was performed via Phyre² (57) online tool (<http://www.sbg.bio.ic.ac.uk/phyre2/html/page.cgi?id=index>), and the pdb files were modeled using PyMOL (<https://www.pymol.org>).

Constitutive expression of CK12, CK13, and CK10 by quantitative real-time PCR

RNA was extracted by homogenization in 1 ml TRIzol (Invitrogen) using tungsten carbide beads (3 mm; Qiagen) and shaking (300 times per minute) following the manufacturer’s instructions. The RNA pellet was washed in 500 ml 80% ethanol, air dried, and resuspended in RNase-free H₂O. The RNA concentration was determined by spectrophotometry (Nanodrop ND1000; LabTech) and the integrity of the RNA was determined by electrophoresis (Bioanalyzer 2100; Agilent). cDNA synthesis was performed using 1 µg of total RNA, which was denatured (65°C, 5 min) in the presence of 1 µl of oligo-dT17, 1 µl deoxynucleoside triphosphate mix 10 mM each (Promega), and RNA/DNA-free water (Sigma) in a volume of 13 µl. Synthesis was carried out using 1 µl Superscript III enzyme reverse transcriptase (Invitrogen) in the presence of 5 µl of 5× first strand buffer, 1 µl 0.1 M DTT, made up to a final volume of 25 µl with water, and incubated at 55°C for 1 h. The resultant cDNA was stored at –20°C. The expression of CK12, CK13, and CK10 was measured by quantitative real-time PCR (RT-qPCR) using specific primers (Table I). Due to the sequence similarities between CK12a and CK12b and between CK13a and CK13b, we were only able to design primers sets that would amplify all CK12 and all CK13 genes. Although it may be possible to design primers to analyze gene expression of CK10a and CK10b separately, for consistency purposes we designed primers that would amplify both CK10 genes. The RT-qPCR was performed using 3 µl of a diluted cDNA template as described in Tacchi et al. (53). Trout elongation factor EF-1α was used as control gene for normalization of expression.

Animals and nasal vaccination with viral vaccine

Triploid female adult rainbow trout (mean weight 200 g) were obtained from the Lisboa Springs Hatchery, Pecos, New Mexico. All animal studies

were reviewed and approved by the Institutional Animal Care and Use Committee at the University of New Mexico, protocol number 16-200384-MC. For nasal vaccination studies, adult rainbow trout received live attenuated infectious hematopoietic necrosis virus (IHNV) vaccine or PBS intranasally (I.N.) as described previously (27). The OOs ($n = 5$) from each group were sampled 1, 4, and 7 d postvaccination and placed in RNAlater for gene expression studies

Recombinant protein production, SDS-PAGE, and Western blot

Recombinant His-tagged trout CK12a (rCK12a) (amino acid sequence: MHHHHHHFSEVPVDCCLLTETFRPRHFKMVSYLLQTTEKGCIDATVFITKTGVRLLCTPHPTKSKWVADYIKRLERTISL) was produced in a bacterial expression system (*Escherichia coli*, expression vector E3; GenScript USA), with a theoretical molecular mass of the recombinant protein of 9.4 kDa. The endotoxin level was <0.01 endotoxin units/ μg . The recombinant protein was then refolded using gel filtration as previously described (58), and filtered and sterilized using a $0.22 \mu\text{m}$ filter. The obtained protein was analyzed by SDS-PAGE under nonreducing and reducing conditions by loading $2 \mu\text{g}$ of recombinant protein onto a 4–2% SDS-PAGE gel followed by Coomassie Blue staining to confirm the presence of a band of the expected molecular mass (~ 12 kDa) (Supplemental Fig. 1A). We only observed one band after refolding. Moreover, no aggregates were observed in the gel. The gel was transferred to a polyvinylidene difluoride membrane and incubated with anti-His-tag Ab (1:1000; Pierce) followed by incubation with HRP-labeled anti-His-tag mouse IgG1 (1:7500; Thermo Fisher Scientific) (Supplemental Fig. 1B). Recombinant protein was then refolded using gel filtration as explained previously (58).

HKL isolation and chemotaxis assays

After bleeding from the caudal vein, HKLs, spleen leukocytes (SLs), and gut leukocytes (GLs) were isolated by Percoll density gradients as described in Salinas et al. (59, 60). Cells were then washed twice, counted in a Neubauer chamber, and adjusted to 5×10^6 cells per ml. Chemotaxis assays were carried out in Transwell plates (pore size $3 \mu\text{m}$, Costar; Corning). To test the capacity of rainbow trout rCK12a to attract HKLs and SLs from naive and vaccinated trout, $400 \mu\text{l}$ of culture media containing different concentrations of rCK12a (10, 100, or 1000 ng/ml) were placed at the bottom of the wells and 5×10^5 HKLs, SLs, or GLs were carefully loaded onto the upper chamber. After 90 min at 18°C in a CO_2 chamber, cells were collected from the bottom of the plate and adherent cells detached by trypsinization. The total number of cells that had migrated to the bottom of the wells was quantified by flow cytometry in an Attune Flow Cytometer (Applied Biosystems) by counting the number of events in 2 min. Positive controls consisted of freshly isolated HKLs and SLs, which were directly placed at the bottom of the well to test the maximum collection capacity, and wells to where zymosan-activated trout serum (ZAS) (1:30) was added to the medium. The chemorepellent activity of rCK12a was tested by placing both ZAS and rCK19a (10, 100, 1000 ng/ml) at the bottom of the Transwell plates. Negative controls consisted of medium to which the same volume of PBS or an irrelevant protein (a His-tagged *Drosophila melanogaster* recombinant protein refolded as rCK12a in PBS) rather than rCK12a was added.

CFSE proliferation assay and flow cytometry

Freshly isolated rainbow trout HKL cells (10^6 cells per ml) from control or IHNV I.N. vaccinated fish ($n = 5$) were labeled with $1 \mu\text{M}$ CFSE (Molecular Probes; Thermo Fisher Scientific) according to the manufacturer's instructions. Cells were then stimulated with rCK12a (100 or 1000 ng/ml) for 7 d. Unstimulated labeled HKLs were used as negative controls. Positive controls consisted of HKLs incubated with *Vibrio anguillarum* lysate. Cell division was measured as the percentage of cells where the CFSE intensity was lower than the unstimulated control in an Attune Flow Cytometer (Applied Biosystems). A total of 20,000 events were collected per sample.

Fluorescence in situ hybridization

OO cryosections from adult control or nasally vaccinated IHNV rainbow trout were stained with rainbow trout CK12 or NON-CK12 (negative control) oligonucleotide probes labeled at their 5' ends with indocarbocyanine (Eurofins MWG Operon). The probe sequence used is shown in Table I. Hybridizations were performed at 37°C overnight with hybridization buffer ($2\times$ SSC/50% formamide) containing $1 \mu\text{g/ml}$ of the labeled probe. Slides were then washed with hybridization buffer without probes, followed by two more washes in washing buffer ($0.1\times$ SSC) and two washes in PBS at 37°C . Nuclei were stained with DAPI (5 ng/ml)

solution for 25 min at 37°C . Slides were mounted with fluorescent mounting media, and images were acquired and analyzed with a Nikon Ti fluorescence microscope and the Elements Advanced Research Software (version 4.2).

Immunofluorescence microscopy

OO cryosections from control, I.N. rCK12a-treated, and i.p. rCK12a-treated ($n = 3$) rainbow trout were stained with anti-trout $\text{CD8}\alpha^+$ and MHC class II (MHC-II) Ab as explained previously (29, 61, 62). Nuclei were stained with DAPI DNA stain and slides were observed under a Nikon Ti fluorescence microscope. A total of 10 images per sample from six different cryosections were captured, and the number of $\text{CD8}\alpha^+$ cells and MHC-II^+ cells were visually counted by two different researchers. The distance from 0 to $100 \mu\text{m}$ was considered the apical lamina propria (LP) and between 100 and $250 \mu\text{m}$ was considered the mid-LP. The width of LP in apical and mid-points of the lamella was measured in 10 different lamellae per sample. All analyses were carried out with the Nikon Elements Advanced Research Software v. 4.2.

In vitro effects of rCK12a on immune gene expression

A total of 10^6 HKLs ($n = 6$) in DMEM + 10% FBS per well were pipetted onto flat-bottom 24-well plates. After 4 h, rCK12a (100 ng/ml) or PBS (control) were added to the cell cultures for 6, 24, and 48 h. Cells were collected and placed in TRIzol (Invitrogen). Total RNA was extracted and cDNA produced as explained previously (63). Expression levels of $\text{CD8}\alpha$, $\text{CD8}\beta$, granulysin, $\text{IFN-}\gamma$, IL-7-R , CCR7 , MHC-IIb , and CXCR3 was measured by RT-qPCR using specific primers (Table I). Trout elongation factor EF-1 α was used as control gene for the normalization of expression. The relative expression level of the genes was compared with the unstimulated control and determined using the Pfaffl method (64).

In vivo delivery of rCK12a, effects on gene expression, and challenge experiments

Rainbow trout (mean weight 3 g) were divided into three experimental groups. The first was a control group that received PBS I.N. and i.p.; the second received $3 \mu\text{g}$ of refolded rCK12a in PBS I.N.; the third received $3 \mu\text{g}$ of refolded rCK12a in PBS i.p. OO and HKs ($n = 5$) were sampled at days 1, 5, and 8 after rCK12a administration. Expression of $\text{CD8}\alpha$, granulysin, $\text{IFN-}\gamma$, CCR7 , and CK12 was measured by RT-qPCR and analyzed as previously described. Then 8 d after rCK12a treatment, trout were challenged with virulent IHNV as explained previously (27). A total of 25 fish per tank in duplicate tanks were used for the challenge experiment. Controls consisted of mock-vaccinated fish (which received PBS I. N. and i.p.) and an unchallenged group. Mortalities were recorded for 28 d postchallenge.

Statistical analyses

Data are expressed as the mean \pm SEM. Gene expression data were analyzed by *t* test to identify statistically significant differences between groups. Data analysis was performed in GraphPad Prism version 5.0. One-way ANOVA and a Tukey post hoc analysis test were performed to identify statistically significant differences among groups. For the proliferation assay, a multivariate ANOVA test followed by a Fisher least significant difference post hoc test for multiple comparisons was performed. Survival proportions among experimental groups in the challenge experiment were compared using the logrank test within Prism. A *p* value < 0.05 was considered statistically significant.

Results

Salmonids possess six CCL19-like genes

Searching for the CCL19-like motif in the rainbow trout genome revealed that salmonids possess six different genes that encode CCL19-like chemokines. We named them CK12a, CK12b, CK13a, CK13b, CK10a, and CK10b (Fig. 1, Table I). Out of all the isoforms, CK12a had been identified as one of the most important immune genes upregulated in trout NALT following nasal vaccination with a viral vaccine (27). The coding regions for CK12a, CK12b, CK13a, CK13b, CK10a, and CK10b were 285, 297, 321, 324, 342, and 318 bp long, respectively. They encoded for a 95, 99, 107, 108, 114, and 106 aa-long protein, respectively (Fig. 1A). Alignment of all six rainbow trout CCL19-like sequences showed a highly variable level of conservation among them, with CK13a

and CK13b sharing 82.4% identity, whereas CK13b and CK10b are the most dissimilar with only 17% identity (Supplemental Table I). Phylogenetic analyses comparing salmonid CCL19-like molecules with other available teleost and mammalian CCL19 sequences showed that there is a clear relationship between CK12 and CK13 genes (with a bootstrap over 50%) (Fig. 1B). Meanwhile, CK10a and CK10b appear to be phylogenetically distant from the other teleost CCL19-like genes. As expected, mammalian CCL19 sequences cluster in a separate clade from the fish homologs. When comparing all the trout and human chemokines available to date, phylogenetic analysis also shows that teleost CCL19-like genes are more closely related to mammalian CCL19 genes than to other chemokine genes. Finally, screening of the Atlantic salmon and rainbow trout genomes revealed that the six CCL19-like genes are positioned in four different chromosomes in the Atlantic salmon genome and in six different scaffolds in the rainbow trout genome (Fig. 1C). However, we could not locate CK10b in the current versions of the Atlantic salmon or trout genomes. It is possible that future versions of these genomes may reveal the CK10b genomic position.

Three-dimensional protein structures of all six rainbow trout CCL19-like molecules (CK12a, CK12b, CK13a, CK13b, CK10a, and CK10b) are shown in Supplemental Fig. 2. Mammalian CCL19 has a canonical chemokine fold consisting of a flexible N terminus and N-loop followed by an antiparallel three-stranded β -sheet, a C-terminal α -helix, and a short flexible C terminus (65). Predicted rainbow trout CCL19-like structures show some commonalities but also important differences compared with mammalian CCL19. All trout CCL19-like forms have a short flexible C terminus, a C-terminal α -helix, a three-stranded β -sheet, and an N-loop. However, the N terminus differs significantly from the resolved mammalian CCL19 structure. Moreover, consistent with the low sequence identity among some of the trout CCL19-like molecules, their N termini differ considerably. Whereas CK12a has a very short flexible N terminus followed by a N terminus α -helix, CK13a, b, and CK10a all have long flexible N termini. CK12b and CK10b, in turn, had intermediate length flexible N termini. These data indicate some degree of molecular structural conservation among CK12, CK13, and CK10 molecules in salmonids.

CK12, CK13, and CK10 show distinct constitutive tissue distribution in rainbow trout

To gain some understanding of the physiological functions of the three CCL19-like genes found in rainbow trout, we measured their constitutive expression in main lymphoid organs (HK and spleen), mucosal lymphoid tissues (gut, gill, skin, and OO), neuronal tissues (brain) as well as muscle. We normalized the expression in every tissue to that of the brain. As shown in Fig. 2A–C, each CCL19-like gene displays a unique constitutive expression pattern. In agreement with a previous report (47), CK12 is primarily expressed in mucosal lymphoid tissues including the OO, with levels between 100- and 300-fold greater than those recorded in main lymphoid organs such as the spleen (Fig. 2A). CK13 was expressed in all immune tissues examined with no clear difference between mucosal and nonmucosal immune sites, although it was expressed between 1.5 and 4 times more in mucosal tissues than in the spleen (Fig. 2B). Finally, CK10 was expressed in every tissue examined, including nonimmune tissues such as the brain and the muscle (Fig. 2C). At mucosal sites, expression of CK10 was comparable to that measured in the spleen. This expression pattern may indicate a more homeostatic role for CK10 compared with the other two (Fig. 2C). Combined, these results suggested that CK12 plays a more important role in trout mucosal immunity than CK13 and CK10.

Kinetics of trout CCL19-like expression in trout NALT following nasal viral vaccination

We previously identified CCL19-like (CK12a in this study) as one of the major innate immune genes that is upregulated in NALT following nasal vaccination with an IHNV vaccine (27). To know if this response is specific to this CCL19-like form, we measured CK12, CK13, and CK10 expression in the OO of trout 1, 4, and 7 d after nasal vaccination using the same IHNV vaccine model (Fig. 2D). CK12 was upregulated 2-fold on day 1, 67-fold on day 4, and 4-fold on day 7 in the OO of vaccinated trout compared with controls. The strong upregulation of CK12 expression on day 4 was confirmed by fluorescence in situ hybridization (Supplemental Fig. 3). Fluorescence in situ hybridization staining showed that the increase in CK12 expression was due to a few high-expressing cells rather than an increase throughout the tissue.

CK13 only showed a moderate upregulation on day 1 (2-fold) and no significant changes in expression at any other time points. Interestingly, CK10 responded very differently to the other two CCL19-like genes because it was significantly downregulated (~3-fold) on day 1 and back to basal levels after 4 and 7 d. These expression patterns indicated that CK12 is the main CCL19-like gene involved in trout nasal immune responses in vivo.

rCK12a is not chemotactic in vitro

Previous studies have shown that teleost CCL19 has a canonical chemotactic activity similar to that reported in mammals (43, 45). It is important to note that although those studies call the molecule of interest CCL19, they used recombinant proteins that do not cluster with trout CK12 based on phylogenetic analysis (Fig. 1B). Moreover, a study in rainbow trout tested chemotactic activities of recombinant protein CK12b (National Center for Biotechnology Information [https://www.ncbi.nlm.nih.gov/] accession number CA346383) in HKLs, PBLs, and SLs of rainbow trout (47). They showed no chemotactic activity of 0.1, 1, and 10 ng/ml of recombinant protein CK12b toward HKLs and PBLs cells in vitro using the Transwell system. Nevertheless, they observed moderate chemotactic activity in SLs exposed to 10 ng/ml of trout rCK12b (47). We also tested the chemotactic ability of rCK12a in vitro using a Transwell assay system (Fig. 3A–E). We could not detect any significant migration of naive HKLs, SLs (Fig. 3A, 3B), or GLs (data not shown) toward a wide range of concentrations of rCK12a. We attempted to preactivate trout leukocytes with LPS (data not shown), IHNV (Fig. 3C), or PGE2 (Fig. 3D), yet no chemotaxis toward rCK12a was observed in vitro. To test whether rCK12a has chemorepellent activities, we added rCK12a to our positive control (ZAS) at different concentrations. However, we did not detect any significant difference in HKL migration between treatments (Fig. 3E), indicating that rCK12a has no chemorepellent activity.

rCK12a stimulates proliferation of HKLs from IHNV-vaccinated fish but not naive fish

To know if trout rCK12a is able to induce proliferation of trout immune cells, we used CFSE to label HKLs isolated from control and IHNV-vaccinated fish (14 d postimmunization) followed by incubation with rCK12a (100 ng or 1 μ g) or PBS for 7 d. The FACS analyses showed a significant proliferation rate in HKLs from IHNV-vaccinated fish that were treated with 1 μ g rCK12a, compared with the control (Fig. 3F). However, we did not observe any proliferation in naive HKLs that were treated with rCK12a at both doses compared with the control. Thus, the results suggest that CK12 plays a major role in cell proliferation in the Ag-experienced leukocytes.

FIGURE 1. Salmonids possess six CCL19-like genes. **(A)** Multiple sequence alignment (performed with CLUSTALW <http://align.genome.jp/>) of trout CCL19-like isoforms with the conserved DCCL motif boxed in bold. **(B)** Phylogenetic tree showing the evolutionary relationship of CCL19-like genes among fish and other vertebrates. The tree was constructed using the Neighbor-Joining method in MEGA 7. The tree was bootstrapped 1000 times, and only values over 50% are shown. Sequences used to construct the tree were obtained from the National Center for Biotechnology Information (<https://www.ncbi.nlm.nih.gov>) under the following accession numbers: trout CK1 (AF093802); trout CK2 (AF418561); trout CK4a (CA371157); trout CK4b (CA352593); trout CK5a (CA383670); trout CK5b (CA374135); trout CK6 (CA355962); trout CK7a (CA343117); trout CK7b (CA346976); trout CK8a (CB494647); trout CK8b (CA353159); trout CK9 (CA378686); trout CK12a (KF683302.1); trout CK12b (CA346383.1); trout CK13a (DV196492.3); trout CK13b (CO471983.1); CK10a (CA361535.1); trout CK10b (DV194065); trout CCL21 (CDQ86623.1 [unnamed product]); salmon CK12a (XM_014143452.1, named *S. salar* C-C motif chemokine 4-like [LOC106570886]); salmon CK12b (XP014028076.1; named *SsCCL412*); salmon CK13a (BT125229.1); salmon CK13b (XP013984336.1); salmon CK10a (ACI69602.1); salmon CK10b (XM_014172597.1, named *S. salar* C-C motif chemokine 19-like [LOC106585878]); salmon CCL21 (NP001134739.1); zebrafish CCL19b_F1QHU2; zebrafish CCL19a.2_B3DHA6; zebrafish CCL19a.1_A2BIR2; channel catfish chemokine SCYA106 (ABA54953.1); elephant shark CCL19.a (XP_007910129.1); Elephant shark CCL19.b (XP_007910128.1); striped murrelet CCL19 (AGN52674.1); human CCL1 (P22362); human CCL2 (P13500); human CCL3 (P10147); human CCL4 (P13236); human CCL5 (P13501); human CCL7 (P80098); human CCL8 (P80075); human CCL11 (P51671); human CCL13 (Q99616); human CCL14 (Q16627); human CCL15 (Q16663); human CCL16 (O15467); human CCL17 (Q92583); human CCL18 (P55774); human CCL19 (Q99731); human CCL19.2 (Q5VZ75); human CCL21 (Q6ICR7); mouse CCL19.1 (Q548P0); mouse CCL19.2 (A0A0N4SUZ8); mouse CCL21a (NP_035254.1); chicken CCL19 (R4GM50). **(C)** Genomic configuration of CCL19-like genes in the Atlantic salmon genome (top) and rainbow trout genome (bottom). Salmon CCL19-like genes are represented by gray arrows and are located in four chromosomes: ssa01 for CK13a, ssa11 for CK13b, ssa15 for CK12a, and ssa24 for CK12b and CK10. The asterisk on CK13b highlights the presence of three different variants. We were not able to locate the chromosome containing salmon CCL19c-like. In the lower part of the figure, trout CCL19-like genes are represented within several scaffolds (in black); the missing part of the sequences appears in white.

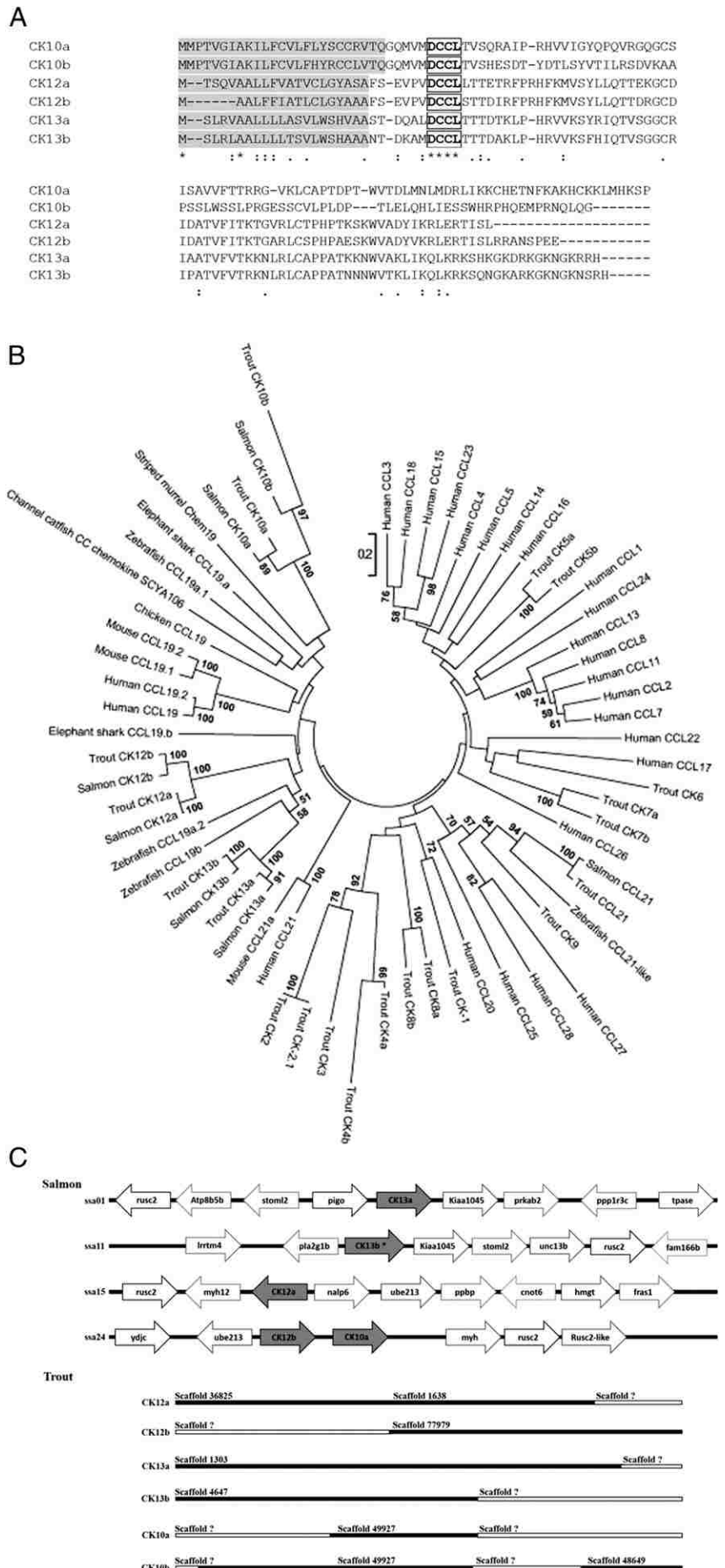


Table I. Oligonucleotides used in this study

Gene	Primer Name	Primer Sequence	Application
EF-1a	EF-1a F	5'-CAACGATATCCGTCGTGGCA-3'	RT-qPCR
	EF-1a R	5'-ACAGCGAAACGACCAAGAGG-3'	
CK12	CK12 F	5'-CTCTGAGGTACCCGTGGATTGC-3'	RT-qPCR
	CK12 R	5'-CCTTAGGGACTATTGTTCTTCAGC-3'	
CK13	CK13 F	5'-CGACCAGATACCAAGCTTCCC-3'	RT-qPCR
	CK13 R	5'-CCTTATGCGATTTCCTCTCAG-3'	
CK10	CK10 F	5'-GGCCAGATGGTATGGACTGTG-3'	RT-qPCR
	CK10 R	5'-GGTAGTGAAGACCACAGCGCTG-3'	
CD8 α	CD8 α F	5'-ATGAAAATGGTCCAAAAGTGGATGC-3'	RT-qPCR
	CD8 α R	5'-GGTTAGAAAAGTCTGTTGTTGGCTATAGG-3'	
CD8 β	CD8 β F	5'-CAACGGTGTGCTTGTGGAAAAC-3'	RT-qPCR
	CD8 β R	5'-ACACTTTTGGGTAGTCGGCTGAA-3'	
Granulysin	Granulysin F	5'-GCCACTGGCTTGTTCAGTTTGG-3'	RT-qPCR
	Granulysin R	5'-TGGTCCTCACGTCATCACTGG-3'	
IFN- γ	IFN- γ F	5'-GCTGTTCAACGGAACCTGTTT-3'	RT-qPCR
	IFN- γ R	5'-TCACTGTCCCAAACGTG-3'	
CCR7	CCR7 F	5'-TTCACTGATTACCCACAGACAATA-3'	RT-qPCR
	CCR7 R	5'-AAGCAGATGAGGGAGTAAAAGGTG-3'	
MHC II	MHC II F	5'-CATATCTCTGGAACAGATGGATA-3'	RT-qPCR
	MHC II R	5'-GCTCAACTGTCTTGTCCAGTATGGCGC-3'	
CXCR3	CXCR3 F	5'-GGACATCGCCTTTAGACAGGTG-3'	RT-qPCR
	CXCR3 R	5'-GTAGCAGTAGAGCATGACCAGC-3'	
IL-7R	IL-7R F	5'-GTGGAGAAGAATTGGTTGAC-3'	RT-qPCR
	IL-7R R	5'-CCTCCATTTTCATCATCGGTGTC-3'	
CK12 probe	5' \rightarrow 3'	5'-GGTACCCCGTGGATTGCTGTCTCCTCACCA-3' 5'-CTGAGACACGTTCCCT-3'	Fluorescence in situ hybridization

F, forward; R, reverse.

Nasal delivery of rCK12a results in infiltration of MHC-II⁺ cells into the nasal mucosa and in enlargement of the olfactory LP in trout

Nasal vaccination of rainbow trout with live attenuated IHNV vaccine results in the recruitment of myeloid and lymphoid cells to the local nasal environment (27). Leukocyte recruitment is easily visualized by histological examination due to the presence of an enlarged LP in the olfactory lamellae of vaccinated animals compared with controls (27). Furthermore, we have shown in the past that nasal delivery of IHNV vaccine results in MHC-II⁺ responses in the OO of trout (29). Because in vitro Transwell assays may not mimic in vivo immune responses, we delivered rCK12a I.N. to rainbow trout and measured the effects on MHC-II⁺ cells as well as on the width of the olfactory LP. As shown in Fig. 4, rCK12a delivery results in changes in the morphology and localization of MHC-II⁺ cells in trout NALT especially on day 5. Moreover, the olfactory LP of rCK12a-treated fish was expanded significantly compared with PBS controls in the tip of the lamella on day 1 (from ~70 to ~110 μ m), and in both the tip (from ~60 to ~130 μ m) and medial regions (from ~100 to ~200 μ m) of the LP on day 5. We observed LP expansions in the rCK12a-treated group at other time points in both the apical and mid-lamella regions but the increase was not statistically significant (Fig. 4A–C). Our analyses showed that I.N. delivery of rCK12a led to a significant (~3-fold) increase in the number of MHC-II⁺ cells in the tip on day 1 and a ~2.5-fold increase in both the tip and medial regions of the lamella on day 5 (Fig. 4D, 4E). In addition, we observed that rCK12a increased MHC-II intensity staining in OO, which may be due to the stimulation of the Ag-presenting process (Fig. 4G). Treatment with rCK12a also resulted in higher numbers of MHC-II⁺ cells in LP in all time points compared with controls; however, the increases did not reach significance (Fig. 4F). These results indicate that rCK12a has inflammatory, chemotactic properties, and suggest it can stimulate Ag presentation in vivo.

rCK12a modulates CD8⁺ T cell-related genes in rainbow trout in vitro and in vivo

Because CK12 appeared to be critical in the local nasal antiviral immune response of rainbow trout, we next asked whether locally produced CK12a may modulate immune genes that may contribute to defense against viruses in the systemic compartment. We incubated HKs with rCK12a in vitro for 6, 24, and 48 h and, using RT-qPCR, measured the expression change of CD8⁺ T cell-related immune genes (Fig. 5A, 5B). At 6 h, CD8 α , IFN- γ , and CCR7 expression was significantly upregulated, whereas after 24 h, rCK12a resulted in an upregulation of CD8 α expression; however, the change observed did not reach significance. No significant changes were recorded at 48 h (data not shown).

Administration of rCK12a i.p. or I.N. led to a downregulation of CD8 α , granulysin, and IFN- γ expression in the HK and OO 1 d postadministration (Fig. 5C–E). In contrast, on day 5, all cell-mediated immune genes were found to be upregulated in the HK and OO as a result of rCK12a both i.p. and I.N. administration (Fig. 5C–E). Similarly, on day 8 cell-mediated response genes such as CD8 α , granulysin, and IFN- γ expression levels remained significantly higher than those observed in control OO (Fig. 5C–E).

In mammals, CCR7 is known to be the receptor for CCL19 and CCL21 (66) and a CCR7 homolog has been reported in rainbow trout (37). Our RT-qPCR data show that CCR7 was significantly upregulated in the HK 1 d postadministration of rCK12a both i.p. and I.N. However, a significant downregulation in CCR7 expression was observed in the OO at this time point. On days 5 and 8, CCR7 expression was significantly higher in the OO in both the I. N.- and i.p.-administered groups compared with the control (Fig. 5F). Administration of rCK12a led to increased CK12 transcript levels in the HK 5 d after I.N. delivery and decreased expression levels on day 8 (Fig. 5G). In the OO, only I.N. administration resulted in significant increases in CK12 expression on day 8 (Fig. 5G). In agreement with our microscopy results (Fig. 4C–F), we observed a significant upregulation in MHC-II

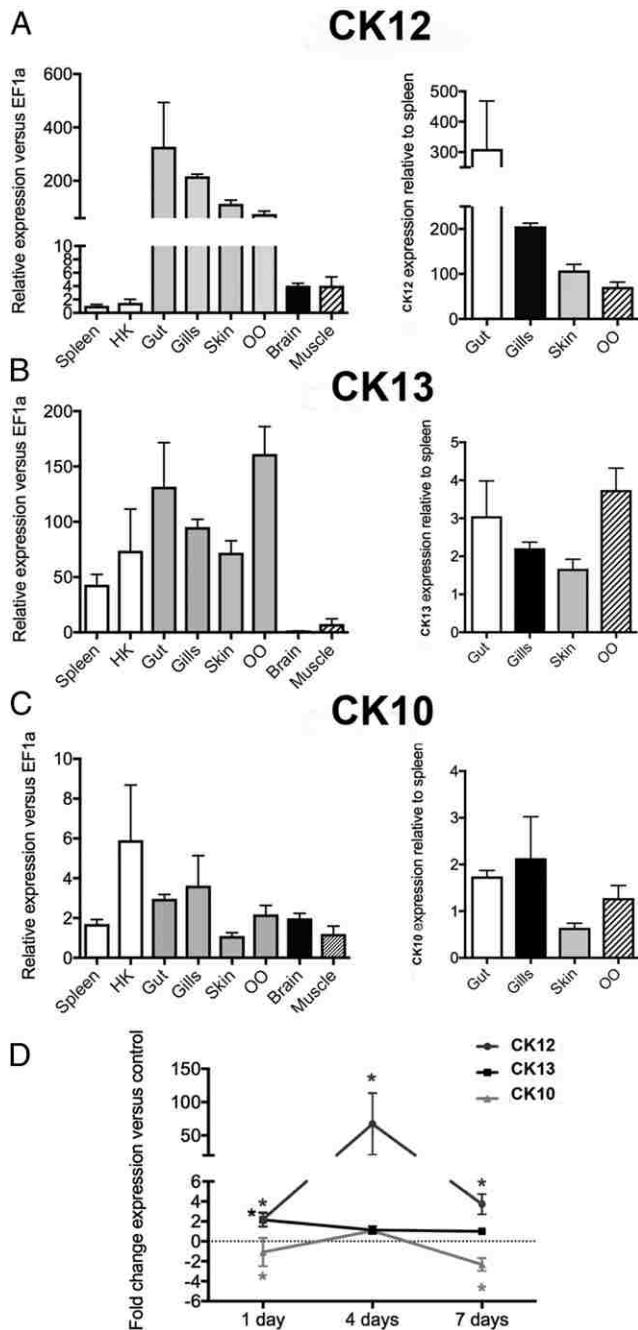


FIGURE 2. CK12a is highly expressed in mucosal tissues and is up-regulated following nasal IHNV vaccination. Tissue distribution of major isoforms of CCL19-like (CK12, CK13, and CK10) in different tissues of control trout and following IHNV vaccination was measured by RT-qPCR. Constitutive expression of CK12 (A), CK13 (B), and CK10 (C) in seven different trout tissues. Expression levels were normalized to the expression in the brain. (D) Gene expression levels of CK12, CK13, and CK10 were measured in the OO of rainbow trout 1, 4, and 7 d following I.N. IHNV vaccination (2×10^7 PFU). Gene expression levels were normalized to the housekeeping gene EF-1a and are expressed as the fold-change compared with the expression levels in mock-vaccinated controls using the Pfaffl method. Results are representative of two different experiments ($n = 6$). $*p < 0.05$.

expression in the OO 5 d postadministration (I.N.) of rCK12a (Fig. 5H), with no other changes in any other time points or tissues. Our results indicate that the presence of CK12 either in the local nasal environment or systemically results in activation of CD8⁺ T cell-related genes as well as CCR7 in rainbow trout.

In vivo delivery of rCK12a increases NALT CD8 α^+ cell numbers in rainbow trout

We showed that i.p. and I.N. delivery of rCK12a modulates CD8 α^+ T cell-related genes especially in OO both in vitro and in vivo. To test the number of CD8 α^+ T cells in OO changes following the administration of rCK12a, we next measured the total numbers of CD8 α^+ cells in the OO of rainbow trout using immunofluorescence microscopy on days 1, 5, and 8 after rCK12a delivery (i.p. or I.N.). We observed a nonsignificant increase in the number of CD8 α^+ cells on day 5 and a significant increase on day 8 (Fig. 6). This was due to increased numbers in the neuroepithelial compartment, whereas no changes were observed in the mucosal tip (data not shown). This result suggests that rCK12a may stimulate local proliferation of CD8 α^+ cells or their migration from lymphoid organs to the nasal mucosa.

I.N. or *i.p.* delivery of rCK12a does not protect rainbow trout against viral challenge

To investigate if rCK12a is sufficient to confer protection against IHNV, we administered rCK12a I.N. or i.p. to trout and challenged them 8 d later with live IHNV. No significant levels of protection were observed between rCK12a-treated and untreated (control) groups at the tested rCK12a dose and administration regimen following viral challenge (Fig. 7). Thus, when delivered alone rCK12a does not lead to protection against viral pathogen.

Discussion

Chemokines are small proteins that act as extracellular messengers of the immune system (3, 67, 68). CCL19 plays many biological roles in mammals including homing of T cells and dendritic cells (DCs) to T cell areas of lymphoid tissues, secondary lymphoid tissue organogenesis, Ab responses, and regulatory and memory T cell function (69–71). CCL19 is also one of the chemokines whose expression is induced by viral infection in a number of host-viral models (13, 71) and it contributes to inflammatory responses against viruses (71–73).

It is believed that the chemokine system appeared around 650 million years ago (31). Chemokines are present in both jawless and jawed vertebrates but not in invertebrates (31, 33). Chemokine and chemokine receptor genes have undergone several gene duplications in teleosts (31); however, the functional consequences of this molecular diversification are largely unknown. The goal of this study was to investigate the functional role of CCL19-like as a messenger between the nasal and the systemic immune compartments during antiviral immune responses in rainbow trout.

Although previous studies had reported the presence of some CCL19-like genes in salmonids, this study provides an updated and comprehensive analysis of this chemokine family using recently released genomes. Interestingly, we found an unprecedented diversity of CCL19-like genes in salmonids, with six genes in rainbow trout forming three major clusters (CK12, CK13, and CK10). This finding raised the question, are all these CCL19-like forms involved in nasal immune responses? We first observed unique tissue distribution patterns of each CCL19-like gene, with CK12 showing a more mucosal-like profile than the other two. These results are consistent with previous studies in trout, where CK12 was mainly expressed in mucosal tissues (47). It is also worth mentioning that the CK12 primers in previous studies (47) and this study amplify both CK12a and CK12b genes due to sequence similarities. Moreover, we observed that only CK12 expression was significantly upregulated in a sustained manner over

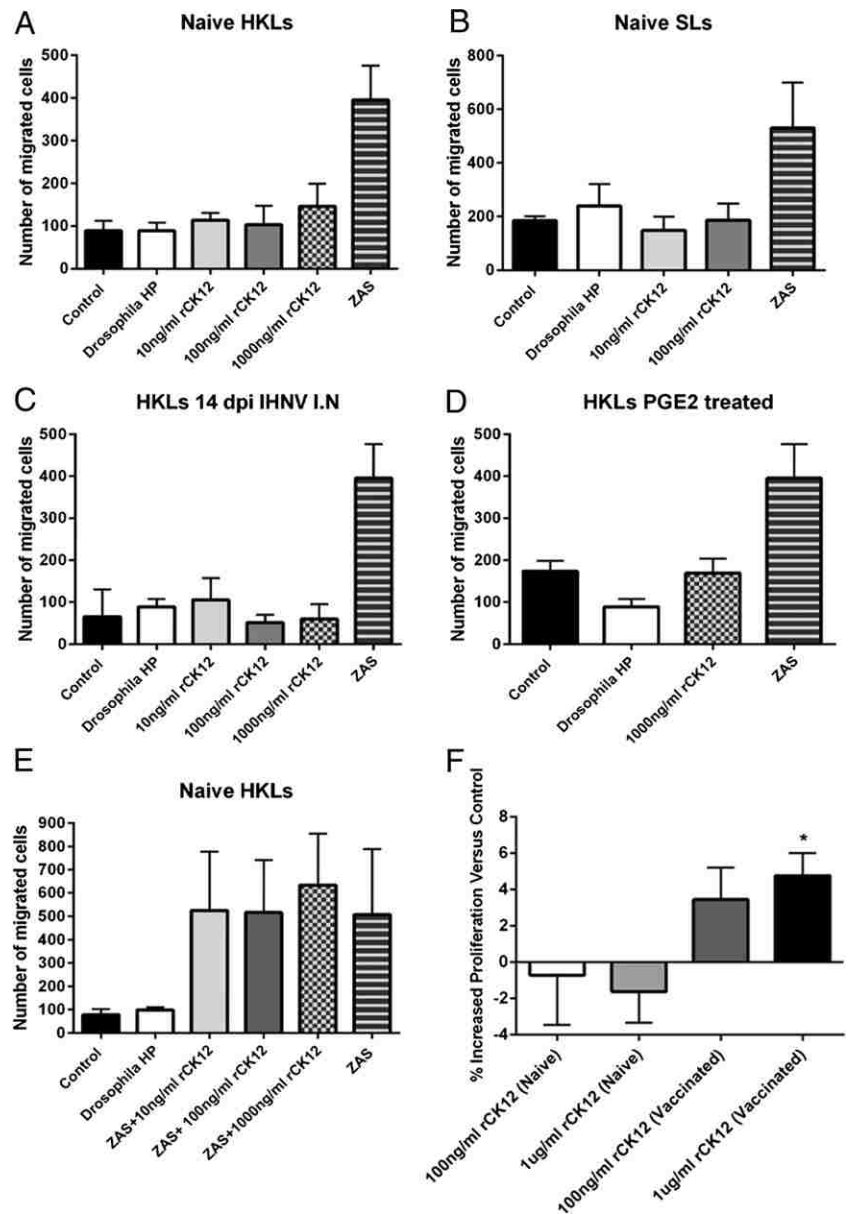


FIGURE 3. rCK12a is not chemotactic in vitro but stimulates proliferation of HKLs from IHNV-vaccinated fish. Chemotaxis assays were carried out in Transwell plates and migrated cells were measured by FACS. Chemotactic activity of rCK12a on naive HKL cells (**A**), SLs (**B**), and HK cells from IHNV-vaccinated fish (**C**), PGE2-treated HK cells (**D**) are shown. (**E**) Chemorepellent activity of rCK12a on naive HKL cells is shown. Positive controls consisted of cells migrated toward ZAS-activated trout serum. HKLs cells from control or IHNV I.N. vaccinated fish ($n = 5$) were labeled with CFSE and treated with rCK12a then proliferation was measured by FACS. (**F**) Increased proliferation (%) of HKLs from naive and IHNV-vaccinated fish incubated with or without rCK12a is shown (comparisons were carried out in cells from the same individual). Transwell experiments were conducted three independent times with $n = 3$. Proliferation experiments were conducted twice with $n = 5$. * $p < 0.05$.

a period of 7 d in the local nasal environment, supporting the idea that CK12 is specialized in nasal mucosal immune responses against viruses. These findings agree with previous studies in trout where CK12 expression increased in response to experimental rhabdovirus infection (49). Combined, the unique tissue distributions as well as the unique transcriptional responses of trout CK12, CK13, and CK10 suggest specialized functions for each of these molecules. Further studies should address the specific immune roles of CK13 and CK10 in salmonids.

Along with the local induction of CK12 in the nasal mucosa, we had previously recorded strong immune responses both in the nasal mucosa and in the main systemic lymphoid tissue of teleosts (the HK) in response to nasal vaccination with IHNV vaccine, especially 4 d postvaccination (27). These findings led us to hypothesize this CCL19-like chemokine coordinates both local and systemic antiviral immune responses in rainbow trout.

Several studies in mammals have shown that CCL19 is chemotactic for the immune cells that express its receptor CCR7, such as DCs (74, 75), B cells (76–78), CD4⁺, and CD8⁺ T cells (77–79). Because migration rates of human cells increase with increasing CCR7 ligands doses up to 1000 ng/ml in vitro (80–82), we tested

different concentrations of rCK12a up to 1000 ng/ml but we did not observe any chemotactic effects regardless of the concentration tested. These results were consistent regardless of the source of cells used (HKLs, SLs, or GLs) in vitro even when preactivated leukocytes were used. We have previously shown that HK and gut CD8 α^+ cells express CCR7 (29), indicating that the source of cells used in our studies should not be the reason why chemotaxis results were negative. Some reports have shown the importance of PGE2 on the migratory ability of CCL19 in mammalian monocytes (83–86). Thus, we also preactivated HKLs with PGE2, but still failed to observe any chemotactic effects in vitro. Testing the bioactivity of mammalian chemokines such as CCR7 ligands in vitro requires gradients generated by sustained release from microparticles (81), the presence of immobilized but not soluble chemokines (87), or the use of three-dimensional collagen gel assays where soluble CCL19 gradients are formed (87, 88). Thus, further studies may evaluate the chemoattractive activity of trout CCL19-like molecules in vitro using assays other than Transwell assays. In any case, our data highlight that trout CK12a and CK12b have distinct biological functions because CK12b has some chemotactic ability in vitro (47) whereas CK12a does not.

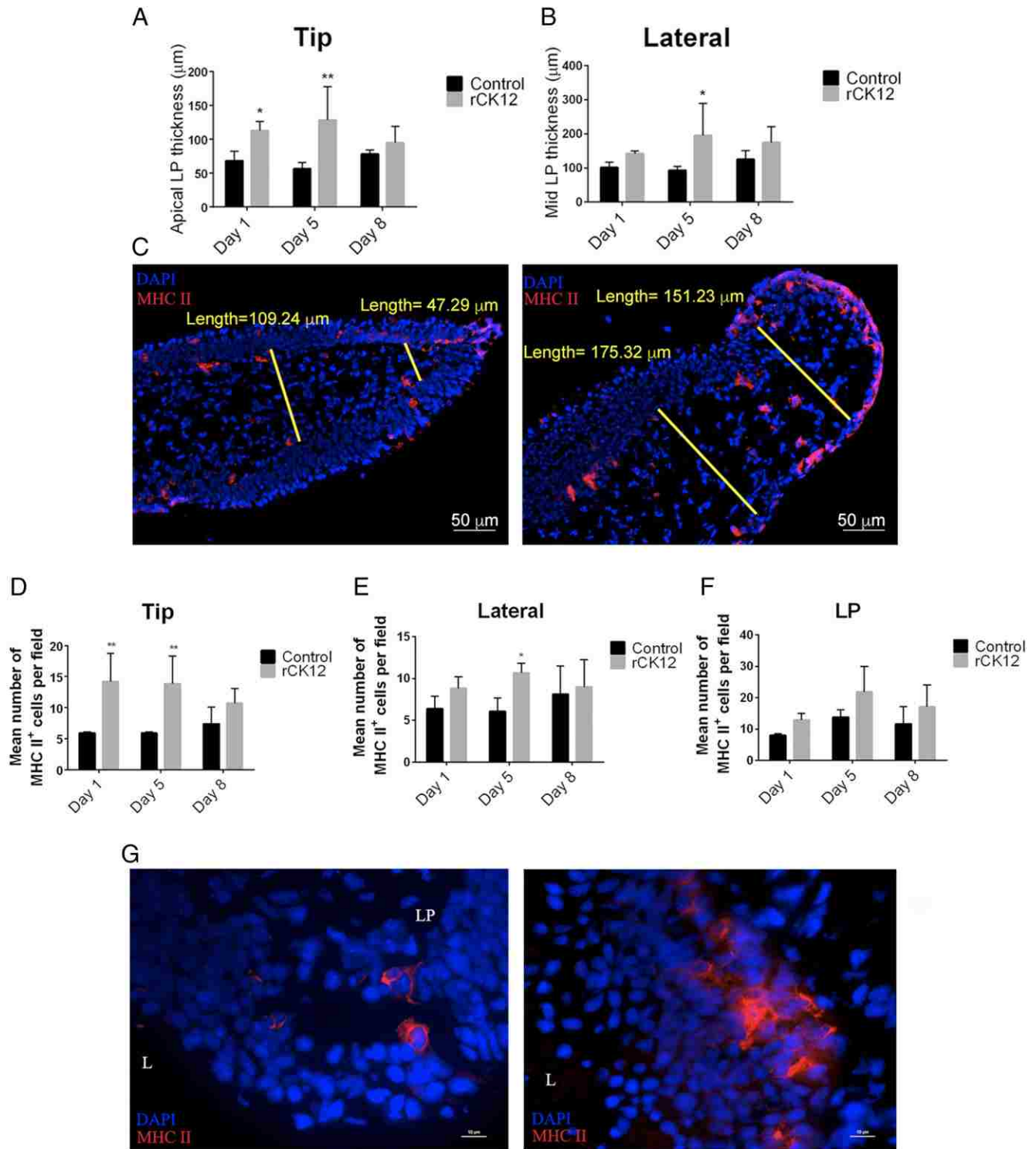


FIGURE 4. In vivo nasal delivery of rCK12a (I.N.) results in enlargement of trout OO LP. Trout were delivered rCK12a (3 µg per fish) I.N. and the OO were sampled 1, 5, and 8 d later and cryosections obtained. (A) and (B) The width of LP at the tip (100 µm from the lamellar tip) and medial (250 µm from the lamellar tip) regions of the olfactory lamella were measured by image analysis of 10 individual lamellae from three different fish per treatment. The mean distance ± SE is shown. (C) Immunofluorescence staining of control (left) and rCK12a-treated (I.N.) rainbow trout OO stained with anti-trout MHC-II Ab (red) showing our image analysis strategy and the enlargement in the apical and medial regions of the LP in the rCK12a-treated fish (right). For (C) and (G), cell nuclei were stained with DAPI DNA stain (blue). Results are representative of two different experiments ($n = 3$). Scale bar, 50 µm. (D–F) Quantification of the number of MHC-II⁺ cells present in the tip, lateral, and LP regions of control and rCK12a-treated (I.N.) rainbow trout OO ($n = 3$). * $p < 0.05$, ** $p < 0.01$. (G) Magnified view of an immunofluorescence staining of control (left) and rCK12a-treated (right) rainbow trout OO labeled with anti-trout MHC-II Ab (red) showing higher expression of MHC-II in the rCK12a-treated fish (right) compared with control (left). L, Lumen. Scale bar, 10 µm.

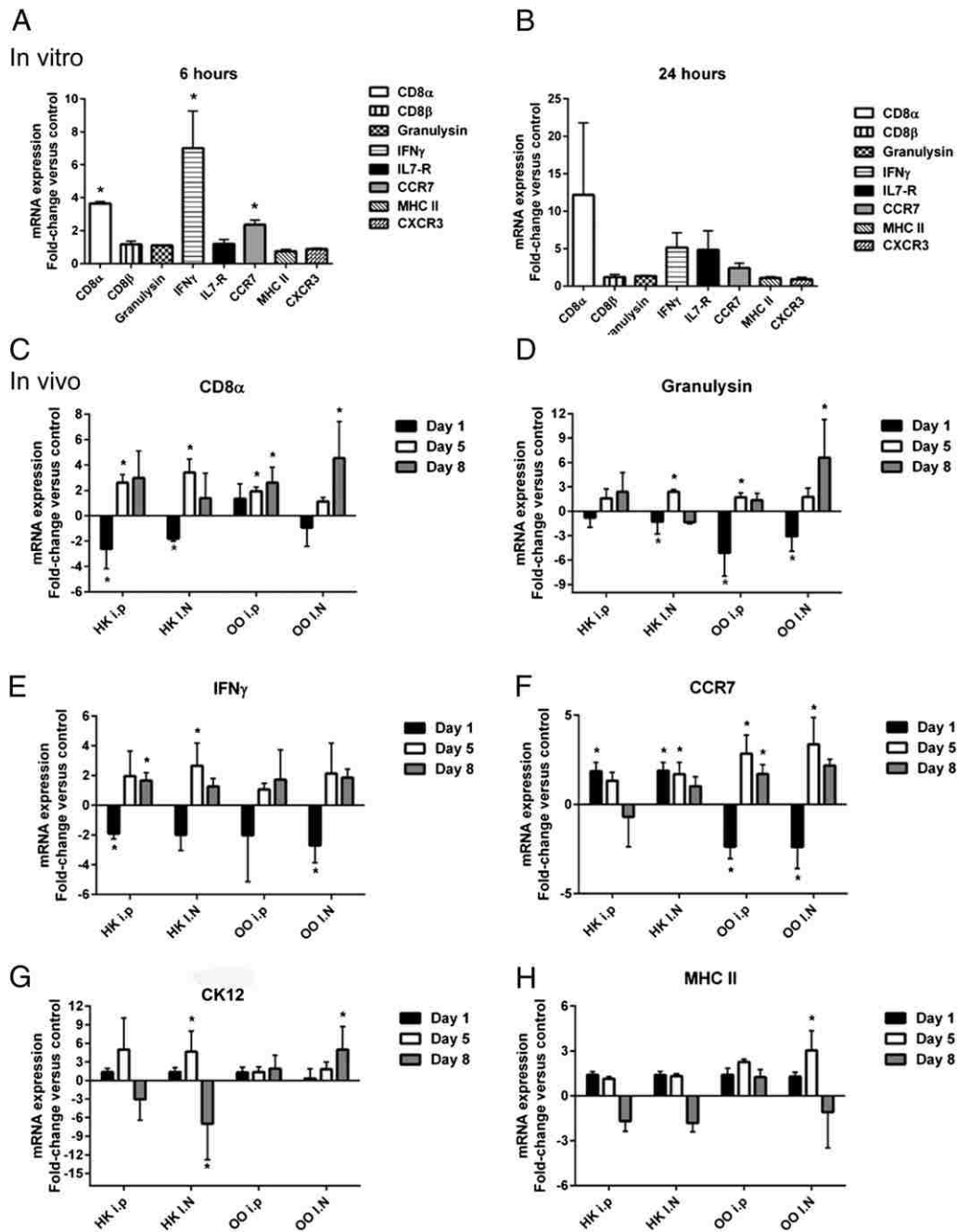


FIGURE 5. rCK12a modulates CD8⁺ T cell-related genes in rainbow trout in vitro and in vivo. Control rainbow trout HKLs were cultured in the presence of rCK12a for 6 or 24 h and expression of immune genes was measured by RT-qPCR. (A) and (B) Gene expression levels of CD8 α , CD8 β , granulysin, IFN- γ , IL-7-R, chemokine receptor CCR7, MHC-II, and CXCR3 are shown. Gene expression levels were normalized to the housekeeping gene EF-1a and expressed as the fold-change compared with the untreated HKL expression levels using the Pfaffl method. Results are representative of three different experiments ($n = 5$). For in vivo experiments, 3 μ g of rCK12a were delivered I.N. or i.p. in rainbow trout ($n = 5$), and OO and HK were sampled 1, 5, and 8 d later. * $p < 0.05$, ** $p < 0.01$. Gene expression levels of CD8 α (C), granulysin (D), IFN- γ (E), chemokine receptor CCR7 (F), CK12 (G), and MHC-II (H) are shown. Results are representative of four different experiments. * $p < 0.05$ compared with the HK.

In vivo delivery of the rCK12a (I.N.) led to expansion of LP in both the apical and mid-regions of the olfactory lamella as well as infiltration of MHC-II⁺ cells 5 d after delivery. These results are consistent with our previous work showing significant enlargement of the olfactory LP and infiltration of immune cells 4 d after nasal vaccination with IHNV vaccine (27). These data indicate that trout CK12a promotes the recruitment and extravasation of leukocytes into the nasal mucosa in vivo.

We have previously shown that I.N. delivery of IHNV vaccine changes the morphology of the MHC-II⁺ cells dramatically (29). This study revealed that delivery of rCK12a (I.N.) increases

MHC-II⁺ expression and changes in MHC-II⁺ cell morphology 5 d after the delivery. In line with our findings, mammalian studies have shown that CCL19 induces changes in morphology, activation, and maturation of MHC-II⁺ DCs in mice (71, 89). Combined, these results suggest that trout CK12a is responsible for the activation of Ag presentation in the nasal mucosa of rainbow trout in response to nasal viral Ag delivery.

CCL19 is known to modulate a myriad of adaptive immune responses in mammals including memory B and T cell function (69–71). Thus, we investigated the possible role of trout CCL19-like in the onset of secondary immune responses. We observed no

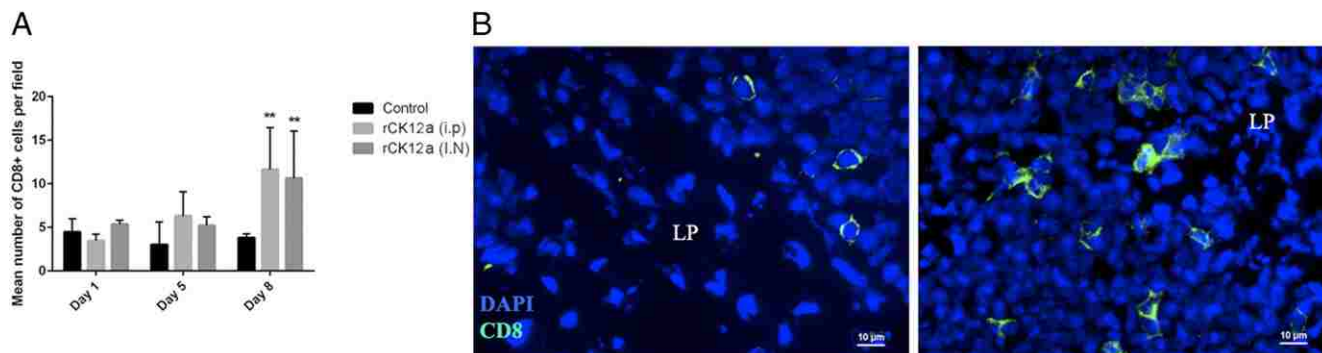


FIGURE 6. In vivo delivery of rCK12a increases NALT CD8 α^+ T cell numbers in rainbow trout. rCK12a was delivered I.N. or i.p. ($n = 5$) and the OO was sampled 1, 5, and 8 d later. Control fish received the same volume of PBS I.N. and i.p. **(A)** Quantification of the number of CD8 α^+ T cells present in neuroepithelial region of the OO of control and rCK12a-treated (I.N. or i.p.) rainbow trout ($n = 3$). $**p < 0.01$. **(B)** Representative immunofluorescence staining of control (left) and rCK12a-treated (right) rainbow trout OO labeled with anti-trout CD8 α (green) mAb showing higher number of CD8 α^+ cells in the rCK12a-treated fish (right) compared with control (left). DAPI was used to stain cell nuclei (blue). Scale bar, 10 μ m.

increased proliferation in naive HKLs incubated with rCK12a. However, HKLs extracted from IHNV-vaccinated fish responded to rCK12a stimulation with increasing proliferation rates. In support, Marsland et al. (71) reported that CCL19 did not induce any proliferation to murine naive T cells. Yet, the same study observed that CCL19 enhanced T cell proliferation in the presence of Ags (71). Overall, our findings support the idea that CCL19-like molecules have adopted multiple innate and adaptive immunological functions during evolution and that these functions are largely conserved from teleosts to mammals.

CD8 $^+$ T cells play an important role in adaptive immune responses especially against viral pathogens in vertebrates. Some reports have indicated the importance of CD8 $^+$ T cell responses at the transcript level in salmonids during IHNV infection (90–92). It is also shown that CCL19 stimulates Th1 responses rather than Th2 responses by induction of DCs in mice (71). We hypothesized that rCK12a plays an important role in the stimulation of CD8 $^+$ T cell responses. Interestingly, we observed a significant upregulation of CD8 $^+$ T cell-related genes in HKLs that were treated with rCK12a in vitro. Similarly, in vivo delivery of rCK12a (i.p. or I.N.) modulated CD8 $^+$ T cell-related genes in HK and OO, especially 5 and 8 d postdelivery. These results indicate that rCK12a is a major factor for CD8 α^+ T cell activation in trout. Importantly, we detected significant increases in the total number of CD8 α^+ cells present in the nasal mucosa

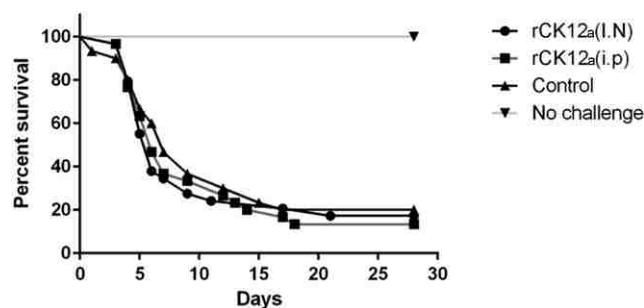


FIGURE 7. I.N. or i.p. delivery of rCK12a does not protect rainbow trout against viral challenge with IHNV. Kaplan–Meier curves showing the percent survival of rainbow trout 28 d after challenge with virulent IHNV. Then 8 d after rCK12a treatment, trout were challenged with virulent IHNV by injection. In total, 25 fish per tank in duplicate tanks were used for the challenge experiment. Controls consisted of mock-vaccinated fish (which received PBS I.N. and i.p.) and an unchallenged group.

8 d after rCK12a delivery regardless of the route (i.p. or I.N.), suggesting that CK12a mobilizes CD8 α^+ cells from systemic to nasal tissues whether produced locally or systemically. Although the effects of CCL19 on nasal CD8 responses have not been studied in mammalian models to date, our results are in line with previous work in mice where delivery of plasmid DNA encoding for CCL19 either I.N. or i.m. resulted in enhanced mucosal (vaginal) and systemic Ab responses across isotypes (93). Similarly, although in a different mucosal site, in this case the sublingual mucosa, the CCR7-CCL19/CCL21 pathway has been shown to regulate efficient Ag-specific systemic and mucosal T and B cell immune responses (94).

We recently showed that NALT CD8 α^+ cells mostly express T cell markers but not NK or DC markers, and that both nasal (but not gut) and systemic CD8 α^+ cells express similar levels of CCR7 in trout (29). Thus, direct ligand-receptor interactions may have driven the observed effects of CK12a on CD8 α^+ cells. The increased numbers of CD8 α^+ cells may have been the result of local proliferation or migration from other lymphoid sites into the nasal mucosa. Given that nasal vaccination of trout with IHNV vaccine results in negligible local proliferation (29), we believe that infiltration of the local olfactory epithelium is the main contributing mechanism by which CK12a stimulates nasal CD8 cellular responses.

Teleost MALT lack organized lymphoid structures such as LNs as well as germinal center formation (27, 28, 95). However, we recently characterized two unique tissue microenvironments with unique immune cell populations in the trout OO (29). Specifically, the apical mucosal portion of the olfactory lamella harbors clusters of CD8 $^+$ T cells and this region also has the highest expression of CK12. This is particularly interesting because the CCL19/CCR7 axis appears to be vital for the homing of naive and regulatory T lymphocytes to LNs and the strategic positioning of these cells within LNs (66, 70, 96, 97). Thus, in the absence of these organized lymphoid structures in teleosts, CCL19-like chemokines may still have evolved a role in the strategic positioning of T cells within mucosal lymphoid tissues.

Because rCK12a was able to recapitulate some of the main characteristic immune responses elicited by entire nasal vaccine formulations, we hypothesized that delivery of rCK12a in the absence of Ag may lead to protection against IHNV in naive rainbow trout. Fish were challenged 8 d after rCK12a administration because we had observed significant increases in CD8 $^+$ T cell numbers in NALT following rCK12a delivery at this time

point. However, we were not able to observe any protection against live viral challenge following administration of rCK12a (i.p. or I.N.). One explanation may be that the dose we used was too low to afford protection. In this regard, murine studies have shown no adjuvant effects of CCL19 when delivered at 50 μg per mouse but immunostimulatory effects when delivered at a dose of 100 μg per mouse (93). Our results may also be interpreted as follows: the high levels of protection against IHNV following I. N. IHNV vaccination require triggering a combination of immune factors and cells beyond CCL19 responses. Alternatively, rCK12a delivery may not result in sustaining enough immune response. Nasal vaccination with IHNV vaccine results in the presence of the Ag for 4 d in the local environment (98). Thus, a single delivery of rCK12a may not have achieved the levels of this chemokine required for protection on the day of the challenge. In addition, the half-life of the recombinant protein may require multiple administrations of rCK12a to confer protection. Finally, because we did not coadminister rCK12a with a vaccine, our results may simply indicate that rCK12a alone did not stimulate specific immune responses in naive rainbow trout. In other words, the increased CD8⁺ cell numbers we observed in the nasal mucosa are not protective unless those lymphocytes are Ag specific. Future studies should address whether code-livery of rCK12a with a vaccine enhances vaccine efficacy and/or protection.

In summary, this study demonstrates that the diversification of CCL19-like genes in salmonids resulted in the acquisition of one CCL19-like molecule, CK12, which plays a cardinal role in antiviral immune responses following nasal immunization. The ability of CCL19 to not only regulate local mucosal immune responses against viruses but also systemic ones underscores the biological role of chemokines as messengers between nasal and systemic lymphoid tissues of vertebrates. The presence of this CCL19-like-driven immune mechanism in teleost fish suggests that this chemokine has evolutionary conserved roles in vertebrate immune systems.

Acknowledgments

We thank Dr. U. Fisher for the anti-trout CD8 α antibody, Dr. C. Tafalla for the anti-trout MHC-II antibody, Dr. C. A. Johnston for the *D. melanogaster* recombinant protein, and Michael Burnett for technical assistance with microscopy. We thank Dr. G. Wiens for insightful discussions on the trout genome and trout CCL19 genes. We thank Lisboa Springs Hatchery for kindly providing animals and the staff at Clear Springs Foods Inc. for helping with sample collection.

Disclosures

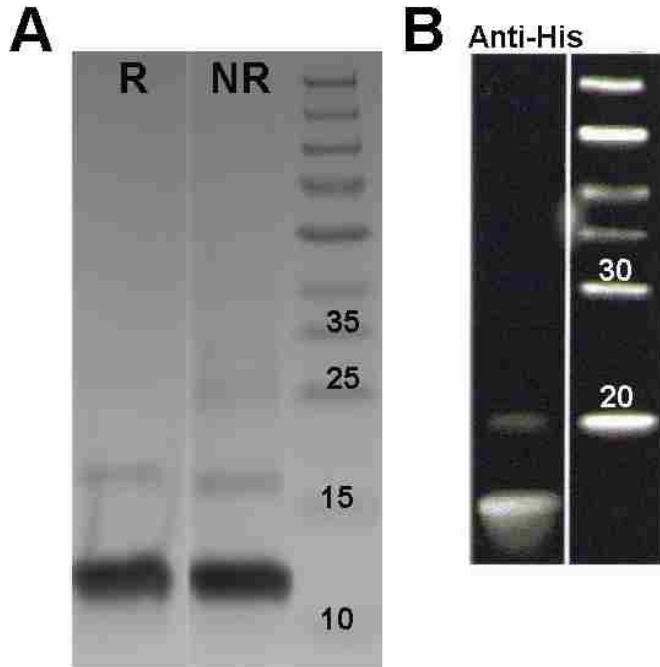
The authors have no financial conflicts of interest.

References

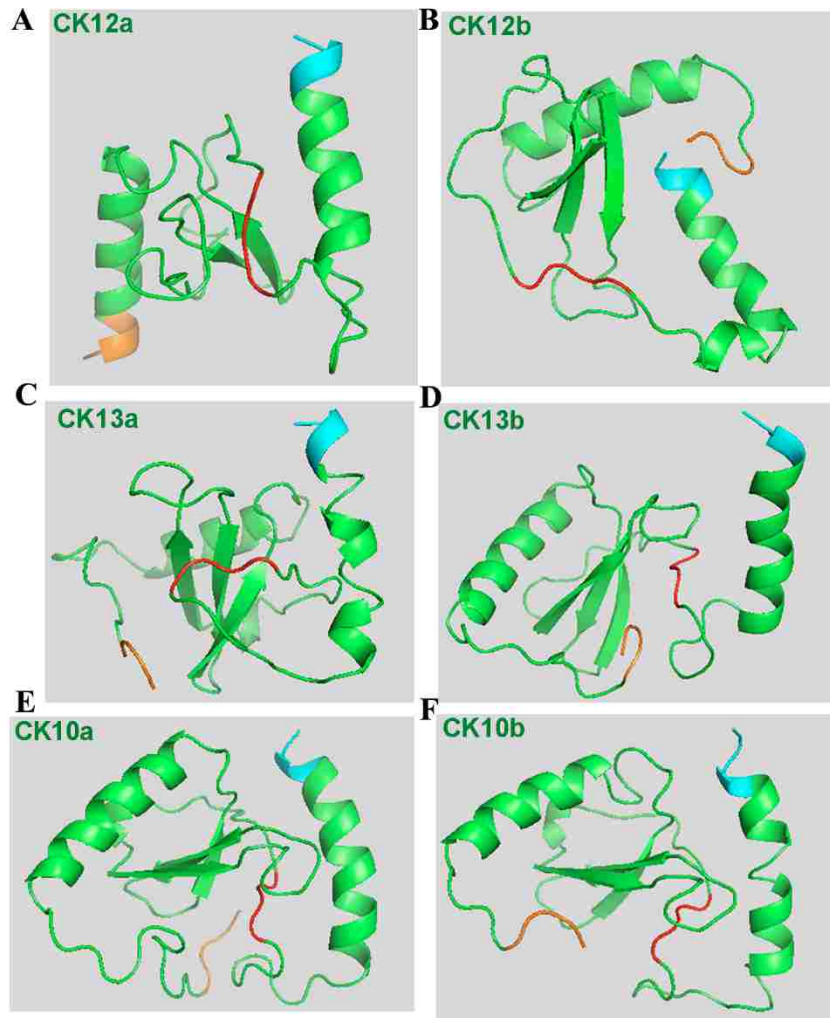
- Le, Y., Zhou, P., Iribarren, and J. Wang. 2004. Chemokines and chemokine receptors: their manifold roles in homeostasis and disease. *Cell. Mol. Immunol.* 1: 95–104.
- Viola, A., and A. D. Luster. 2008. Chemokines and their receptors: drug targets in immunity and inflammation. *Annu. Rev. Pharmacol. Toxicol.* 48: 171–197.
- Zlotnik, A., and O. Yoshie. 2000. Chemokines: a new classification system and their role in immunity. *Immunity* 12: 121–127.
- Gale, L. M., and S. R. McColl. 1999. Chemokines: extracellular messengers for all occasions? *BioEssays* 21: 17–28.
- Melchjorsen, J., L. N. Sørensen, and S. R. Paludan. 2003. Expression and function of chemokines during viral infections: from molecular mechanisms to in vivo function. *J. Leukoc. Biol.* 74: 331–343.
- Ache, B. W., and J. M. Young. 2005. Olfaction: diverse species, conserved principles. *Neuron* 48: 417–430.
- Takamura, K., S. Fukuyama, T. Nagatake, D.-Y. Kim, A. Kawamura, H. Kawachi, and H. Kiyono. 2007. Regulatory role of lymphoid chemokine CCL19 and CCL21 in the control of allergic rhinitis. *J. Immunol.* 179: 5897–5906.
- Yoshie, O., T. Imai, and H. Nomiya. 1997. Novel lymphocyte-specific CC chemokines and their receptors. *J. Leukoc. Biol.* 62: 634–644.
- Zlotnik, A., J. Morales, and J. A. Hedrick. 1999. Recent advances in chemokines and chemokine receptors. *Crit. Rev. Immunol.* 19: 1–47.
- Fukuyama, S., T. Nagatake, D.-Y. Kim, K. Takamura, E. J. Park, T. Kaisho, N. Tanaka, Y. Kuroki, and H. Kiyono. 2006. Cutting edge: uniqueness of lymphoid chemokine requirement for the initiation and maturation of nasopharynx-associated lymphoid tissue organogenesis. *J. Immunol.* 177: 4276–4280.
- Rangel-Moreno, J., J. Moyron-Quiroz, K. Kusser, L. Hartson, H. Nakano, and T. D. Randall. 2005. Role of CXC chemokine ligand 13, CC chemokine ligand (CCL) 19, and CCL21 in the organization and function of nasal-associated lymphoid tissue. *J. Immunol.* 175: 4904–4913.
- Choi, Y. K., B. A. Fallert, M. A. Murphey-Corb, and T. A. Reinhart. 2003. Simian immunodeficiency virus dramatically alters expression of homeostatic chemokines and dendritic cell markers during infection in vivo. *Blood* 101: 1684–1691.
- Piqueras, B., J. Connolly, H. Freitas, A. K. Palucka, and J. Banchereau. 2006. Upon viral exposure, myeloid and plasmacytoid dendritic cells produce 3 waves of distinct chemokines to recruit immune effectors. *Blood* 107: 2613–2618.
- Baker, H., and M. Beth Genter. 2003. The olfactory system and the nasal mucosa as portals of entry of viruses, drugs, and other exogenous agents into the brain. In *Handbook of Olfaction and Gustation*. R. Doty, ed. Marcel Dekker, New York, p. 549–574.
- Mori, I., Y. Nishiyama, T. Yokochi, and Y. Kimura. 2005. Olfactory transmission of neurotropic viruses. *J. Neurovirol.* 11: 129–137.
- Munster, V. J., J. B. Prescott, T. Bushmaker, D. Long, R. Rosenke, T. Thomas, D. Scott, E. R. Fischer, H. Feldmann, and E. de Wit. 2012. Rapid Nipah virus entry into the central nervous system of hamsters via the olfactory route. *Sci. Rep.* 2: 736.
- Morales, J. A., S. Herzog, C. Kompter, K. Frese, and R. Rott. 1988. Axonal transport of Borna disease virus along olfactory pathways in spontaneously and experimentally infected rats. *Med. Microbiol. Immunol. (Berl.)* 177: 51–68.
- Owen, S. J., M. Batzloff, F. Chehrehasa, A. Meedeniya, Y. Casart, C. A. Logue, R. G. Hirst, I. R. Peak, A. Mackay-Sim, and I. R. Beacham. 2009. Nasal-associated lymphoid tissue and olfactory epithelium as portals of entry for *Burkholderia pseudomallei* in murine melioidosis. *J. Infect. Dis.* 199: 1761–1770.
- Mizgerd, J. P. 2008. Acute lower respiratory tract infection. *N. Engl. J. Med.* 358: 716–727.
- van Riel, D., V. J. Munster, E. de Wit, G. F. Rimmelzwaan, R. A. Fouchier, A. D. Osterhaus, and T. Kuiken. 2006. H5N1 virus attachment to lower respiratory tract. *Science* 312: 399.
- Simoës, E. A. 1999. Respiratory syncytial virus infection. *Lancet* 354: 847–852.
- Hament, J.-M., J. L. Kimpen, A. Fleer, and T. F. Wolfs. 1999. Respiratory viral infection predisposing for bacterial disease: a concise review. *FEMS Immunol. Med. Microbiol.* 26: 189–195.
- Davis, S. S. 2001. Nasal vaccines. *Adv. Drug Deliv. Rev.* 51: 21–42.
- Jabbal-Gill, I. 2010. Nasal vaccine innovation. *J. Drug Target.* 18: 771–786.
- Holmgren, J., and C. Czerkinsky. 2005. Mucosal immunity and vaccines. *Nat. Med.* 11(4, Suppl.): S45–S53.
- Neutra, M. R., and P. A. Kozlowski. 2006. Mucosal vaccines: the promise and the challenge. *Nat. Rev. Immunol.* 6: 148–158.
- Tacchi, L., R. Musharrafieh, E. T. Larragoite, K. Crossey, E. B. Erhardt, S. A. M. Martin, S. E. LaPatra, and I. Salinas. 2014. Nasal immunity is an ancient arm of the mucosal immune system of vertebrates. *Nat. Commun.* 5: 5205.
- Sepahi, A., and I. Salinas. 2016. The evolution of nasal immune systems in vertebrates. *Mol. Immunol.* 69: 131–138.
- Sepahi, A., E. Casadei, L. Tacchi, P. Muñoz, S. E. LaPatra, and I. Salinas. 2016. Tissue microenvironments in the nasal epithelium of rainbow trout (*Oncorhynchus mykiss*) define two distinct CD8 α + cell populations and establish regional immunity. *J. Immunol.* 197: 4453–4463.
- Nomiya, H., N. Osada, and O. Yoshie. 2011. A family tree of vertebrate chemokine receptors for a unified nomenclature. *Dev. Comp. Immunol.* 35: 705–715.
- DeVries, M. E., A. A. Kelvin, L. Xu, L. Ran, J. Robinson, and D. J. Kelvin. 2006. Defining the origins and evolution of the chemokine/chemokine receptor system. *J. Immunol.* 176: 401–415.
- Flajnik, M., and L. Du Pasquier. 2013. Evolution of the immune system. In *Fundamental Immunology*, 7th Ed., W. Paul, ed. Lippincott Williams & Wilkins, Philadelphia, p. 67–128.
- Nomiya, H., N. Osada, and O. Yoshie. 2010. The evolution of mammalian chemokine genes. *Cytokine Growth Factor Rev.* 21: 253–262.
- Laing, K. J., and C. J. Secombes. 2004. Trout CC chemokines: comparison of their sequences and expression patterns. *Mol. Immunol.* 41: 793–808.
- Dixon, B., B. Shum, E. J. Adams, K. E. Magor, R. P. Hedrick, D. G. Muir, and P. Parham. 1998. CK-1, a putative chemokine of rainbow trout (*Oncorhynchus mykiss*). *Immunol. Rev.* 166: 341–348.
- Dixon, B., A. Luque, B. Abós, R. Castro, L. González-Torres, and C. Tafalla. 2013. Molecular characterization of three novel chemokine receptors in rainbow trout (*Oncorhynchus mykiss*). *Fish Shellfish Immunol.* 34: 641–651.
- Ordás, M. C., R. Castro, B. Dixon, J. O. Sunyer, S. Björk, J. Bartholomew, T. Korytar, B. Köllner, A. Cuesta, and C. Tafalla. 2012. Identification of a novel CCR7 gene in rainbow trout with differential expression in the context of mucosal or systemic infection. *Dev. Comp. Immunol.* 38: 302–311.

38. Peatman, E., and Z. Liu. 2007. Evolution of CC chemokines in teleost fish: a case study in gene duplication and implications for immune diversity. *Immunogenetics* 59: 613–623.
39. Lally, J., F. Al-Anouti, N. Bols, and B. Dixon. 2003. The functional characterisation of CK-1, a putative CC chemokine from rainbow trout (*Oncorhynchus mykiss*). *Fish Shellfish Immunol.* 15: 411–424.
40. Bird, S., and C. Tafalla. 2015. Teleost chemokines and their receptors. *Biology (Basel)* 4: 756–784.
41. Fu, Q., Y. Yang, C. Li, Q. Zeng, T. Zhou, N. Li, Y. Liu, Y. Li, X. Wang, S. Liu, et al. 2017. The chemokine superfamily: II. The 64 CC chemokines in channel catfish and their involvement in disease and hypoxia responses. *Dev. Comp. Immunol.* 73: 97–108.
42. Nomiyama, H., K. Hieshima, N. Osada, Y. Kato-Unoki, K. Otsuka-Ono, S. Takegawa, T. Izawa, A. Yoshizawa, Y. Kikuchi, S. Tanase, et al. 2008. Extensive expansion and diversification of the chemokine gene family in zebrafish: identification of a novel chemokine subfamily CX. *BMC Genomics* 9: 222.
43. Chen, C., Y. H. Hu, Z. Z. Xiao, and L. Sun. 2013. SmCCL19, a CC chemokine of turbot *Scophthalmus maximus*, induces leukocyte trafficking and promotes antiviral and anti-bacterial defense. *Fish Shellfish Immunol.* 35: 1677–1682.
44. Chen, S. L., Y. Liu, X. L. Dong, and L. Meng. 2010. Cloning, characterization, and expression analysis of a CC chemokine gene from turbot (*Scophthalmus maximus*). *Fish Physiol. Biochem.* 36: 147–155.
45. Arockiaraj, J., P. Bhatt, R. Harikrishnan, M. V. Arasu, and N. A. Al-Dhabi. 2015. Molecular and functional roles of 6C CC chemokine 19 in defense system of striped mullet *Channa striatus*. *Fish Shellfish Immunol.* 45: 817–827.
46. Reyes-López, F. E., J. S. Romeo, E. Vallejos-Vidal, S. Reyes-Cerpa, A. M. Sandino, L. Tort, S. Mackenzie, and M. Imarai. 2015. Differential immune gene expression profiles in susceptible and resistant full-sibling families of Atlantic salmon (*Salmo salar*) challenged with infectious pancreatic necrosis virus (IPNV). *Dev. Comp. Immunol.* 53: 210–221.
47. Montero, J., M. C. Ordas, A. Alejo, L. Gonzalez-Torres, N. Sevilla, and C. Tafalla. 2011. CK12, a rainbow trout chemokine with lymphocyte chemoattractant capacity associated to mucosal tissues. *Mol. Immunol.* 48: 1102–1113.
48. Montero, J., J. Garcia, M. C. Ordas, I. Casanova, A. Gonzalez, A. Villena, J. Coll, and C. Tafalla. 2011. Specific regulation of the chemokine response to viral hemorrhagic septicemia virus at the entry site. *J. Virol.* 85: 4046–4056.
49. Chaves-Pozo, E., J. Montero, A. Cuesta, and C. Tafalla. 2010. Viral hemorrhagic septicemia and infectious pancreatic necrosis viruses replicate differently in rainbow trout gonad and induce different chemokine transcription profiles. *Dev. Comp. Immunol.* 34: 648–658.
50. Montero, J., E. Chaves-Pozo, A. Cuesta, and C. Tafalla. 2009. Chemokine transcription in rainbow trout (*Oncorhynchus mykiss*) is differently modulated in response to viral hemorrhagic septicemia virus (VHSV) or infectious pancreatic necrosis virus (IPNV). *Fish Shellfish Immunol.* 27: 661–669.
51. Altschul, S. F., W. Gish, W. Miller, E. W. Myers, and D. J. Lipman. 1990. Basic local alignment search tool. *J. Mol. Biol.* 215: 403–410.
52. Berthelot, C., F. Brunet, D. Chalopin, A. Juanchich, M. Bernard, B. Noël, P. Bento, C. Da Silva, K. Labadie, A. Alberti, et al. 2014. The rainbow trout genome provides novel insights into evolution after whole-genome duplication in vertebrates. *Nat. Commun.* 5: 3657.
53. Tacchi, L., E. Larragoite, and I. Salinas. 2013. Discovery of J chain in African lungfish (*Protopterus dolloi*, *Sarcopterygii*) using high throughput transcriptome sequencing: implications in mucosal immunity. *PLoS One* 8: e70650.
54. Chenna, R., H. Sugawara, T. Koike, R. Lopez, T. J. Gibson, D. G. Higgins, and J. D. Thompson. 2003. Multiple sequence alignment with the Clustal series of programs. *Nucleic Acids Res.* 31: 3497–3500.
55. Kumar, S., G. Stecher, and K. Tamura. 2016. MEGA7: molecular evolutionary genetics analysis version 7.0 for bigger datasets. *Mol. Biol. Evol.* 33: 1870–1874.
56. Campanella, J. J., L. Bitnicka, and J. Smalley. 2003. MatGAT: an application that generates similarity/identity matrices using protein or DNA sequences. *BMC Bioinformatics* 4: 29.
57. Kelley, L. A., S. Mezulis, C. M. Yates, M. N. Wass, and M. J. Sternberg. 2015. The Phyre2 web portal for protein modeling, prediction and analysis. *Nat. Protoc.* 10: 845–858.
58. Zhang, Y.-A., I. Salinas, J. Li, D. Parra, S. Bjork, Z. Xu, S. E. LaPatra, J. Bartholomew, and J. O. Sunyer. 2010. IgT, a primitive immunoglobulin class specialized in mucosal immunity. *Nat. Immunol.* 11: 827–835.
59. Salinas, I., E. W. Maas, and P. Muñoz. 2011. Characterization of acid phosphatases from marine scuticociliate parasites and their activation by host's factors. *Parasitology* 138: 836–847.
60. Salinas, I., J. Meseguer, and M. Á. Esteban. 2007. Assessment of different protocols for the isolation and purification of gut associated lymphoid cells from the gilthead seabream (*Sparus aurata* L.). *Biol. Proced. Online* 9: 43–55.
61. Takizawa, F., J. M. Dijkstra, P. Kotterba, T. Korytár, H. Kock, B. Köllner, B. Jaureguierry, T. Nakanishi, and U. Fischer. 2011. The expression of CD8 α discriminates distinct T cell subsets in teleost fish. *Dev. Comp. Immunol.* 35: 752–763.
62. Granja, A. G., E. Leal, J. Pignatelli, R. Castro, B. Abós, G. Kato, U. Fischer, and C. Tafalla. 2015. Identification of teleost skin CD8 α + dendritic-like cells, representing a potential common ancestor for mammalian cross-presenting dendritic cells. *J. Immunol.* 195: 1825–1837.
63. Sepahi, A., H. Cordero, H. Goldfine, M. Á. Esteban, and I. Salinas. 2016. Symbiont-derived sphingolipids modulate mucosal homeostasis and B cells in teleost fish. *Sci. Rep.* 6: 39054.
64. Pfaffl, M. W. 2001. A new mathematical model for relative quantification in real-time RT-PCR. *Nucleic Acids Res.* 29: e45.
65. Veldkamp, C. T., E. Kiermaier, S. J. Gabel-Eissens, M. L. Gillitzer, D. R. Lippner, F. A. DiSilvio, C. J. Mueller, P. L. Wantuch, G. R. Chaffee, M. W. Famiglietti, et al. 2015. Solution structure of CCL19 and identification of overlapping CCR7 and PSGL-1 binding sites. *Biochemistry* 54: 4163–4166.
66. Förster, R., A. C. Davalos-Misslitz, and A. Rot. 2008. CCR7 and its ligands: balancing immunity and tolerance. *Nat. Rev. Immunol.* 8: 362–371.
67. Parkin, J., and B. Cohen. 2001. An overview of the immune system. *Lancet* 357: 1777–1789.
68. Baggiolini, M. 1998. Chemokines and leukocyte traffic. *Nature* 392: 565–568.
69. Randall, T. D., D. M. Carragher, and J. Rangel-Moreno. 2008. Development of secondary lymphoid organs. *Annu. Rev. Immunol.* 26: 627–650.
70. Comerford, I., Y. Harata-Lee, M. D. Bunting, C. Gregor, E. E. Kara, and S. R. McColl. 2013. A myriad of functions and complex regulation of the CCR7/CCL19/CCL21 chemokine axis in the adaptive immune system. *Cytokine Growth Factor Rev.* 24: 269–283.
71. Marsland, B. J., P. Böttig, M. Bauer, C. Ruedl, U. Lässing, R. R. Beerli, K. Dietmeier, L. Ivanova, T. Pfister, L. Vogt, et al. 2005. CCL19 and CCL21 induce a potent proinflammatory differentiation program in licensed dendritic cells. *Immunity* 22: 493–505.
72. Bachmann, M. F., M. Kopf, and B. J. Marsland. 2006. Chemokines: more than just road signs. *Nat. Rev. Immunol.* 6: 159–164.
73. Luther, S. A., and J. G. Cyster. 2001. Chemokines as regulators of T cell differentiation. *Nat. Immunol.* 2: 102–107.
74. Haessler, U., M. Pisano, M. Wu, and M. A. Swartz. 2011. Dendritic cell chemotaxis in 3D under defined chemokine gradients reveals differential response to ligands CCL21 and CCL19. *Proc. Natl. Acad. Sci. USA* 108: 5614–5619.
75. Randolph, G. J. 2001. Dendritic cell migration to lymph nodes: cytokines, chemokines, and lipid mediators. *Semin. Immunol.* 13: 267–274.
76. Corcione, A., N. Arduino, E. Ferretti, L. Raffaghello, S. Roncella, D. Rossi, F. Fedeli, L. Ottonello, L. Trentin, F. Dallegrì, et al. 2004. CCL19 and CXCL12 trigger in vitro chemotaxis of human mantle cell lymphoma B cells. *Clin. Cancer Res.* 10: 964–971.
77. Reif, K., K. Okkenhaug, T. Sasaki, J. M. Penninger, B. Vanhaesebroeck, and J. G. Cyster. 2004. Cutting edge: differential roles for phosphoinositide 3-kinases, p110 γ and p110 δ , in lymphocyte chemotaxis and homing. *J. Immunol.* 173: 2236–2240.
78. Okada, T., V. N. Ngo, E. H. Ekland, R. Förster, M. Lipp, D. R. Littman, and J. G. Cyster. 2002. Chemokine requirements for B cell entry to lymph nodes and Peyer's patches. *J. Exp. Med.* 196: 65–75.
79. Bromley, S. K., S. Y. Thomas, and A. D. Luster. 2005. Chemokine receptor CCR7 guides T cell exit from peripheral tissues and entry into afferent lymphatics. *Nat. Immunol.* 6: 895–901.
80. Riol-Blanco, L., N. Sánchez-Sánchez, A. Torres, A. Tejedor, S. Narumiya, A. L. Corbí, P. Sánchez-Mateos, and J. L. Rodríguez-Fernández. 2005. The chemokine receptor CCR7 activates in dendritic cells two signaling modules that independently regulate chemotaxis and migratory speed. *J. Immunol.* 174: 4070–4080.
81. Wang, Y., and D. J. Irvine. 2011. Engineering chemoattractant gradients using chemokine-releasing polysaccharide microspheres. *Biomaterials* 32: 4903–4913.
82. Campbell, J. J., K. E. Murphy, E. J. Kunkel, C. E. Brightling, D. Soler, Z. Shen, J. Boisvert, H. B. Greenberg, M. A. Viera, S. B. Goodman, et al. 2001. CCR7 expression and memory T cell diversity in humans. *J. Immunol.* 166: 877–884.
83. Muthuswamy, R., J. Mueller-Berghaus, U. Haberkorn, T. A. Reinhardt, D. Schandorf, and P. Kalinski. 2010. PGE(2) transiently enhances DC expression of CCR7 but inhibits the ability of DCs to produce CCL19 and attract naive T cells. *Blood* 116: 1454–1459.
84. Scandella, E., Y. Men, S. Gillessen, R. Förster, and M. Groettrup. 2002. Prostaglandin E2 is a key factor for CCR7 surface expression and migration of monocyte-derived dendritic cells. *Blood* 100: 1354–1361.
85. Scandella, E., Y. Men, D. F. Legler, S. Gillessen, L. Priklér, B. Ludewig, and M. Groettrup. 2004. CCL19/CCL21-triggered signal transduction and migration of dendritic cells requires prostaglandin E2. *Blood* 103: 1595–1601.
86. Côté, S. C., S. Pasvanis, S. Bounou, and N. Dumais. 2009. CCR7-specific migration to CCL19 and CCL21 is induced by PGE(2) stimulation in human monocytes: involvement of EP(2)/EP(4) receptors activation. *Mol. Immunol.* 46: 2682–2693.
87. Schumann, K., T. Lämmermann, M. Brückner, D. F. Legler, J. Polleux, J. P. Spatz, G. Schuler, R. Förster, M. B. Lutz, L. Sorokin, and M. Sixt. 2010. Immobilized chemokine fields and soluble chemokine gradients cooperatively shape migration patterns of dendritic cells. *Immunity* 32: 703–713.
88. Lämmermann, T., B. L. Bader, S. J. Monkley, T. Worbs, R. Wedlich-Söldner, K. Hirsch, M. Keller, R. Förster, D. R. Critchley, R. Fässler, and M. Sixt. 2008. Rapid leukocyte migration by integrin-independent flowing and squeezing. *Nature* 453: 51–55.
89. Yanagawa, Y., and K. Onoé. 2002. CCL19 induces rapid dendritic extension of murine dendritic cells. *Blood* 100: 1948–1956.
90. Purcell, M. K., K. M. Nichols, J. R. Winton, G. Kurath, G. H. Thorgaard, P. Wheeler, J. D. Hansen, R. P. Herwig, and L. K. Park. 2006. Comprehensive gene expression profiling following DNA vaccination of rainbow trout against infectious hematopoietic necrosis virus. *Mol. Immunol.* 43: 2089–2106.
91. Hansen, J. D., and S. La Patra. 2002. Induction of the rainbow trout MHC class I pathway during acute IHNV infection. *Immunogenetics* 54: 654–661.
92. Ballesteros, N. A., M. Alonso, S. R. Saint-Jean, and S. I. Perez-Prieto. 2015. An oral DNA vaccine against infectious haematopoietic necrosis virus (IHNV) encapsulated in alginate microspheres induces dose-dependent immune responses and significant protection in rainbow trout (*Oncorhynchus mykiss*). *Fish Shellfish Immunol.* 45: 877–888.
93. Hu, K., S. Luo, L. Tong, X. Huang, W. Jin, W. Huang, T. Du, Y. Yan, S. He, G. E. Griffin, et al. 2013. CCL19 and CCL28 augment mucosal and systemic

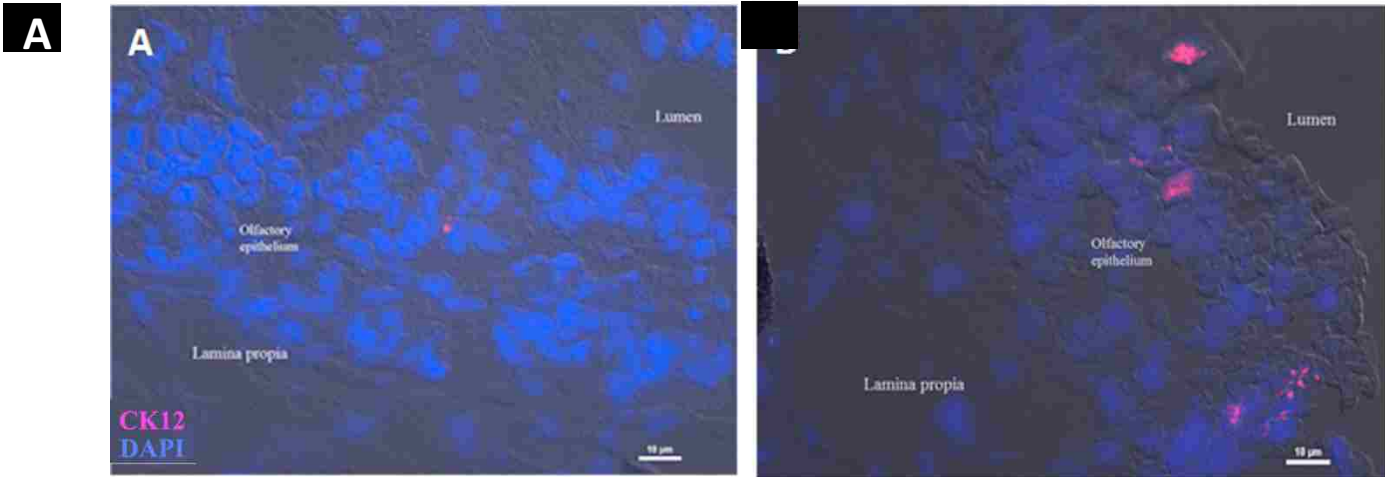
- immune responses to HIV-1 gp140 by mobilizing responsive immunocytes into secondary lymph nodes and mucosal tissue. *J. Immunol.* 191: 1935–1947.
94. Song, J.-H., J.-I. Kim, H.-J. Kwon, D.-H. Shim, N. Parajuli, N. Cuburu, C. Czerkinsky, and M.-N. Kweon. 2009. CCR7-CCL19/CCL21-regulated dendritic cells are responsible for effectiveness of sublingual vaccination. *J. Immunol.* 182: 6851–6860.
95. Salinas, I. 2015. The mucosal immune system of teleost fish. *Biology (Basel)* 4: 525–539.
96. Groom, J. R. 2015. Moving to the suburbs: T-cell positioning within lymph nodes during activation and memory. *Immunol. Cell Biol.* 93: 330–336.
97. von Andrian, U. H., and T. R. Mempel. 2003. Homing and cellular traffic in lymph nodes. *Nat. Rev. Immunol.* 3: 867–878.
98. Larragoite, E. T., L. Tacchi, S. E. LaPatra, and I. Salinas. 2016. An attenuated virus vaccine appears safe to the central nervous system of rainbow trout (*Oncorhynchus mykiss*) after intranasal delivery. *Fish Shellfish Immunol.* 49: 351–354.



Supplemental Figure 1: Production of trout recombinant protein CK12a (rCK12a). rCK12a was produced by bacterial expression system and then refolded by gel filtration. **(A)** SDS-PAGE confirmed the presence of the recombinant protein (rCK12a) band at expected molecular weight (12 KDa). R: reducing and NR: non-reducing conditions. **(B)** Immunoblot using anti-Histag antibody confirmed the presence of the recombinant protein (rCK12a) band at expected molecular weight.



Supplemental Figure 2: 3-D protein structure prediction of the six CCL19-like molecules. (A) CK12a, (B) CK12b, (C) CK13a, (D) CK13b, (E) CK10a and (F) CK10b was performed via Phyre2 online tool (<http://www.sbg.bio.ic.ac.uk/phyre2/html/page.cgi?id=index>) and the .pdb files were modeled using PyMOL.



Supplemental Figure 3: CK12 expression is up-regulated in the olfactory organ following nasal vaccination with IHNV (4 dpi). Olfactory organ cryosections from adult control or nasally vaccinated IHNV rainbow trout (4 dpi) were stained with rainbow trout CK12 oligonucleotide probes labeled at their 5' ends with indodicarbocyanine. **(A)** FISH staining of control olfactory organ and **(B)** IHNV vaccinated (4 dpi) olfactory organ labelled with CK12 probe (Cy5, pink). DAPI was used to stain cell nuclei (blue). Fluorescence images were overlaid with differential interference contrast (DIC) image. Scale bars: 10 μm .

S.1

	1. CK12a	2. CK12b	3. CK13a	4. CK13b	5. CK10a	6. CK10b
1. CK12a		74.8	40.7	34.9	28.2	19.8
2. CK12b	87.9		37	33.9	25.6	17.2
3. CK13a	58.9	58.9		82.4	32.5	17.9
4. CK13b	56.5	56.5	88.9		31.9	17
5. CK10a	42.1	43	52.6	49.1		39.7
6. CK10b	38.7	35.8	36.4	34.3	57	

Identity
Similarity

Supplemental Table I: MatGAT output for % of identity and similarities of the six CCL19-like sequences of rainbow trout (*Oncorhynchus mykiss*). Scoring matrix Blosom50 was used in the comparison. % of similarity is shown in light grey and % of identity in dark grey.

Chapter 3

*Sepahi, Ali, Elisa Casadei, Luca Tacchi, Pilar Muñoz, Scott E. LaPatra, and Irene Salinas. "Tissue microenvironments in the nasal epithelium of rainbow trout (*Oncorhynchus mykiss*) define two distinct CD8 α + cell populations and establish regional immunity." The Journal of Immunology (2016). DOI: <https://doi.org/10.4049/jimmunol.1600678>*

Tissue Microenvironments in the Nasal Epithelium of Rainbow Trout (*Oncorhynchus mykiss*) Define Two Distinct CD8 α ⁺ Cell Populations and Establish Regional Immunity

Ali Sepahi,* Elisa Casadei,* Luca Tacchi,* Pilar Muñoz,[†] Scott E. LaPatra,[‡] and Irene Salinas*

Mucosal surfaces require balancing different physiological roles and immune functions. To effectively achieve multifunctionality, mucosal epithelia have evolved unique microenvironments that create unique regional immune responses without impairing other normal physiological functions. Whereas examples of regional immunity are known in other mucosal epithelia, to date, no immune microenvironments have been described in the nasal mucosa, a site where the complex functions of olfaction and immunity need to be orchestrated. In this study we identified the presence of CD8 α ⁺ cells in the rainbow trout (*Oncorhynchus mykiss*) nasal epithelium. Nasal CD8 α ⁺ cells display a distinct phenotype suggestive of CD8⁺ T cells with high integrin β ₂ expression. Importantly, nasal CD8 α ⁺ cells are located in clusters at the mucosal tip of each olfactory lamella but scattered in the neuroepithelial region. The grouping of CD8 α ⁺ cells may be explained by the greater expression of CCL19, ICAM-1, and VCAM-1 in the mucosal tip compared with the neuroepithelium. Whereas viral Ag uptake occurred via both tip and lateral routes, tip-resident MHC class II⁺ cells are located significantly closer to the lumen of the nasal cavity than are their neuroepithelial counterparts, therefore having quicker access to invading pathogens. Our studies reveal compartmentalized mucosal immune responses within the nasal mucosa of a vertebrate species, a strategy that likely optimizes local immune responses while protecting olfactory sensory functions. *The Journal of Immunology*, 2016, 197: 4453–4463.

Animal mucosal barriers are complex tissues that carry many important physiological functions. In addition to their main physiological role, every mucosal epithelium is a first line of defense against pathogen invasion and has important immune roles. To increase immune surveillance and regulate immune responses, mucosal barriers have evolved unique microenvironments allowing for regional tissue immunity (1–3). For instance, different segments of the intestine have distinctive immune responses, such as the small intestine, where immune tolerance to food Ags is important, versus the colon, where constitutive antibacterial immunity or symbiosis is essential (4). The increasing amount of work pertaining to the number and complexity of mucosal microenvironments has made clear that mucosal organs, previously thought to be immunologically uniform, are immunologically heterogeneous. This heterogeneity helps them support multiple physiological functions while mounting efficient immune responses. However, apart from

the intestine, there are very few well-documented examples of regional immunity in other mucosal surfaces.

Regional immune specialization relies on specific anatomical distributions of innate and adaptive immune cells (5, 6). The latter is achieved by a number of molecular mechanisms. For instance, selective expression of chemokines and chemokine receptors is known to govern the localization and circulation of lymphocytes within primary and secondary lymphoid organs (4, 7–9). Additionally, expression of unique integrins on the surface of lymphocytes and specific adhesion molecules also allows tissue-specific homing of lymphocytes to different mucosal regions (7–9). In this respect, intestinal epithelial cells, via expression of different immune molecules, determine the specificity of lymphocyte trafficking and the nature of local immune specialization (10–12).

Ag presentation via MHC class II (MHC-II) molecules is an important component of any immune response, including viral immune responses. In this respect, the expression of MHC-II is also variable in different regions of the intestine (5, 13), and professional APCs in mammals have compartment-specific properties (2, 5, 14). Importantly, epithelial cells, despite not being considered professional APCs, express MHC-II (15–17), and the levels and patterns of expression change under pathological conditions (18, 19).

Generally speaking, mucosal surfaces establish a highly regulatory immune environment that dampens excessive inflammatory responses with the goal of protecting barrier integrity. In the case of the nasal mucosa, highly regulated immune responses may be critical for the correct functioning of the sensitive neuronal tissue, the olfactory neuroepithelium. As the olfactory epithelium is often subject to numerous infections, rapid removal of microbes and debris from this tissue must be essential to maintain its integrity. Thus, to preserve olfactory sensory function while still fighting nasal pathogens, we hypothesized that the nasal mucosa may establish unique microenvironments that meet its immune requirements without compromising olfaction.

*Center for Evolutionary and Theoretical Immunology, Department of Biology, University of New Mexico, Albuquerque, NM 87131; [†]Departamento de Sanidad Animal, Facultad de Veterinaria, Campus de Excelencia Internacional Regional Campus Mare Nostrum, Universidad de Murcia, 30100 Murcia, Spain; and [‡]Clear Springs Foods Research Division, Buhl, ID 83316

Received for publication April 18, 2016. Accepted for publication September 29, 2016.

This work was supported by U.S. Department of Agriculture AFRI Grant 2DN70-2RDN7 (to I.S.) and by National Institutes of Health COBRE Grant P20GM103452.

Address correspondence and reprint requests to Dr. Irene Salinas, Center for Evolutionary and Theoretical Immunology, University of New Mexico, 167 Castetter Hall, Albuquerque, NM 87131-0001. E-mail address: isalinas@unm.edu

The online version of this article contains supplemental material.

Abbreviations used in this article: DC, dendritic cell; EdU, 5-ethynyl-2'-deoxyuridine; HK, head kidney; IHNV, infectious hematopoietic necrosis virus; LCM, laser capture microdissection; MHC-II, MHC class II; NALT, nasopharynx-associated lymphoid tissue; RT-qPCR, real-time quantitative PCR.

Copyright © 2016 by The American Association of Immunologists, Inc. 0022-1767/16/\$30.00

The teleost and mammalian olfactory organs are highly conserved anatomically speaking and their cellular and molecular mechanisms are largely similar (20). In both cases, the olfactory organ is a complex sensory organ made up of many different cell types. In humans, different regions of the nasal cavity contain different densities and distributions of ciliated, columnar, and goblet cells (21–23). In particular, the chemosensory portion of the nasal cavity, the olfactory epithelium, contains no goblet cells (24). In teleosts, the olfactory organ is also divided into sensory and nonsensory regions; however, the location of these regions varies in different species (25, 26). The sensory region of the olfactory lamella contains olfactory sensory neurons, including ciliated, microvillus, and crypt cells (26–28), whereas the nonsensory region is a mucosal epithelium characterized by the presence of goblet cells. Recently, a nasopharynx-associated lymphoid tissue (NALT) was described in rainbow trout (*Oncorhynchus mykiss*) (29, 30). Teleost NALT was described as a diffuse network of myeloid and lymphoid cells located in the olfactory organ of fish (29, 30). However, the histological regionalization present in teleosts and mammals led us to hypothesize that regional immunity may exist in different portions of the vertebrate nasal cavity.

The present study demonstrates the presence of two different microenvironments (mucosal and neuroepithelial) in the olfactory organ of rainbow trout. The mucosal tip of the epithelium harbors clusters of CD8 α ⁺ cells whereas few numbers are found in the neuroepithelium. CD8 α ⁺ cell localization corresponds with a higher expression of chemokine and chemokine receptor pairs (CCL19 and CCR7) in the mucosal tip versus the neuroepithelial side. Sorted nasal lymphoid CD8 α ⁺ cells have a CD8 α ⁺ T cell phenotype rather than an NK cell or dendritic cell (DC) phenotype. Furthermore, based on MHC-II staining patterns, we report important differences in Ag presentation in the two microenvironments both in control and vaccinated animals. This represents an example of unique nasal immune microenvironments in a vertebrate species and suggests that regional immunity may be a mechanism by which the nasal mucosa is able to mount effective immune responses without impinging crucial neural functions.

Materials and Methods

Animals, nasal vaccination, and tissue sampling

Triploid female adult rainbow trout (mean weight, 200 g) were obtained from the Lisboa Springs Hatchery (Pecos, NM). All animal studies were reviewed and approved by the Institutional Animal Care and Use Committee at the University of New Mexico (protocol no. 16-200384-MC). Head kidney (HK) leukocytes, GALT leukocytes, and NALT leukocytes were isolated as explained elsewhere (30). For nasal immunization studies, adult rainbow trout ($n = 10$) received live attenuated infectious hematopoietic necrosis virus (IHNV) vaccine or PBS as described in (30). Five fish from each group were sampled 4 and 8 d after vaccination. The olfactory organs were snap frozen and cryoblocks used for immunostaining as described below.

Flow cytometry and cell sorting of CD8 α ⁺ T cells

HK leukocytes, gut leukocytes, and nasal leukocytes ($n = 6$) were stained with rat anti-trout CD8 α Ab (31) followed by FITC-labeled anti-rat IgG. After washing, a total of 30,000 cells were recorded using an Attune flow cytometer (Life Technologies). The percentage of CD8 α ⁺ cells was quantified as the percentage of FITC⁺ cells within the lymphocyte gate using their forward light scatter area/side light scatter area profile. A doublet exclusion gate based on the forward light scatter area/forward light scatter height profile was then applied to ensure that only singlets were analyzed. CD8 α ⁺ cells from the lymphocyte gate of HK, gut, and NALT cell suspensions ($n = 9$) were sorted using a Sony iCyt SY3200 high-speed cell sorter at the University of New Mexico Shared Flow Cytometry facility.

Light microscopy, transmission electron microscopy, and immunofluorescence microscopy

Control adult rainbow trout olfactory organs ($n = 5$) were fixed in 10% neutral buffered formalin overnight at 4°C and then transferred to 70% ethanol. Samples were then embedded in paraffin and 5- μ m-thick sections stained with H&E. For transmission electron microscopy, the olfactory organs ($n = 2$) of rainbow trout that had received live attenuated IHNV vaccine intranasally an hour prior to sampling were fixed overnight at 4°C in 2.5% (v/v) glutaraldehyde in PBS, then transferred to 1% osmium tetroxide (w/v) in PBS for 2 h at 4°C. After washing in PBS (three times, 10 min), samples were dehydrated in a graded series of ethanol (10–100%) through changes of propylene oxide. Samples were then embedded in Epon resin, sectioned, and stained with uranyl acetate and lead citrate before being examined in a Philips Tecnai 12 transmission electron microscope. For immunostaining, trout olfactory organs were snap frozen in OCT for cryosectioning and 5- μ m-thick cryosections were postfixed in acetone followed by 4% paraformaldehyde and labeled with rat anti-trout CD8 α Ab (31), followed by FITC donkey anti-rat IgG (Jackson Immuno-Research Laboratories). For detection of MHC-II⁺ cells in the nasal mucosa, cryosections were stained with mouse anti-trout MHC-II β -chain IgG (2 μ g/ml) (32) followed by Alexa Fluor 647 donkey anti-mouse IgG (2 μ g/ml). For detection of IHNV, a pool of anti-IHNV mAbs containing mAbs 1H8, 6A7, and 5AG (2 μ g/ml) followed by Cy3 anti-mouse IgG (1 μ g/ml; Jackson ImmunoResearch Laboratories) was used. Nuclei were stained with DAPI. Samples were observed under a Nikon Ti microscope and images captured and measured with the Nis-Elements Advanced Research software. Positive cells were scored manually.

Laser capture microdissection

Adult trout control cryosections from the olfactory organ were used to perform laser capture microdissection (LCM). Ten sections, 5 μ m thick each, from each fish ($n = 3$) were used to obtain the mucosal regions (tips) of each lamella or the lateral regions and valleys (neuroepithelium) of each lamella. Tissues were captured using an Arcturus LCM system (Thermo Fisher Scientific), and similar numbers of LCM captures were performed for both side and tip. RNA was extracted using the PicoPure RNA isolation kit as per the manufacturer's instructions. Whenever different RNA amounts were obtained, they were adjusted to make them identical prior to the cDNA synthesis. The experiment was repeated three independent times.

Gene expression analysis by real-time quantitative PCR

Total RNA from sorted CD8⁺ T cells was obtained using the GenElute single-cell RNA purification kit (Sigma-Aldrich) following the manufacturer's instructions. Total RNA from LCM-collected tissue samples was obtained using the Arcturus PicoPure RNA isolation kit as per the manufacturer's instructions. cDNA synthesis was performed using 500 ng of total RNA, which was denatured (65°C, 5 min) in the presence of 1 μ l of oligo(dT)17, 1 μ l of 2'-deoxynucleoside 5'-triphosphate mix (10 mM each; Promega), and RNA/DNA-free water (Sigma-Aldrich) in a volume of 13 μ l. Synthesis was carried out using 1 μ l of SuperScript III enzyme reverse transcriptase (Invitrogen) in the presence of 5 μ l of 5 \times first-strand buffer, 1 μ l of 0.1 M DTT, made up to a final volume of 25 μ l with water, and incubated at 55°C for 1 h. The resultant cDNA was stored at -20°C. The expression of CD3, CD8 α , IFN- γ , CCR7, IL7-R, CD103, integrin β_2 , FcR γ , DC-SIGN, MHC-II, CD83, and CD141 in HK, gut, and nasal CD8 α ⁺ cells was measured by real-time quantitative PCR (RT-qPCR) using specific primers (Supplemental Table I). The expression of CD8 α , CD8 β , TCR α , TCR β , TCR δ , TCR γ , L-selectin, VCAM-1, ICAM-1, integrin β_2 , CCL19 and CCR7 in LCM-dissected nasal samples was measured by RT-qPCR using specific primers (Supplemental Table I). The quantitative PCR was performed using 3 μ l of a diluted cDNA template as described in Tacchi et al. (33). The relative expression level of the genes was determined using the Pfaffl method (34) as previously described (33). Using this method, the fold change difference in expression in the mucosal tip compared with the neuroepithelium (lateral) was quantified by considering the neuroepithelium samples as controls. The expression in the neuroepithelium was set to 1 and used as control.

Protein sequence analysis

Protein sequences for integrin β_2 were obtained from the UniProt database (<http://www.uniprot.org/>) and aligned using ClustalW (<http://www.align.genome.jp/>) (35); subsequently, a phylogenetic tree was created using the neighbor-joining method (bootstrap 10,000) within the software MEGA 6.06 (36). Furthermore, to create the similarity and homology

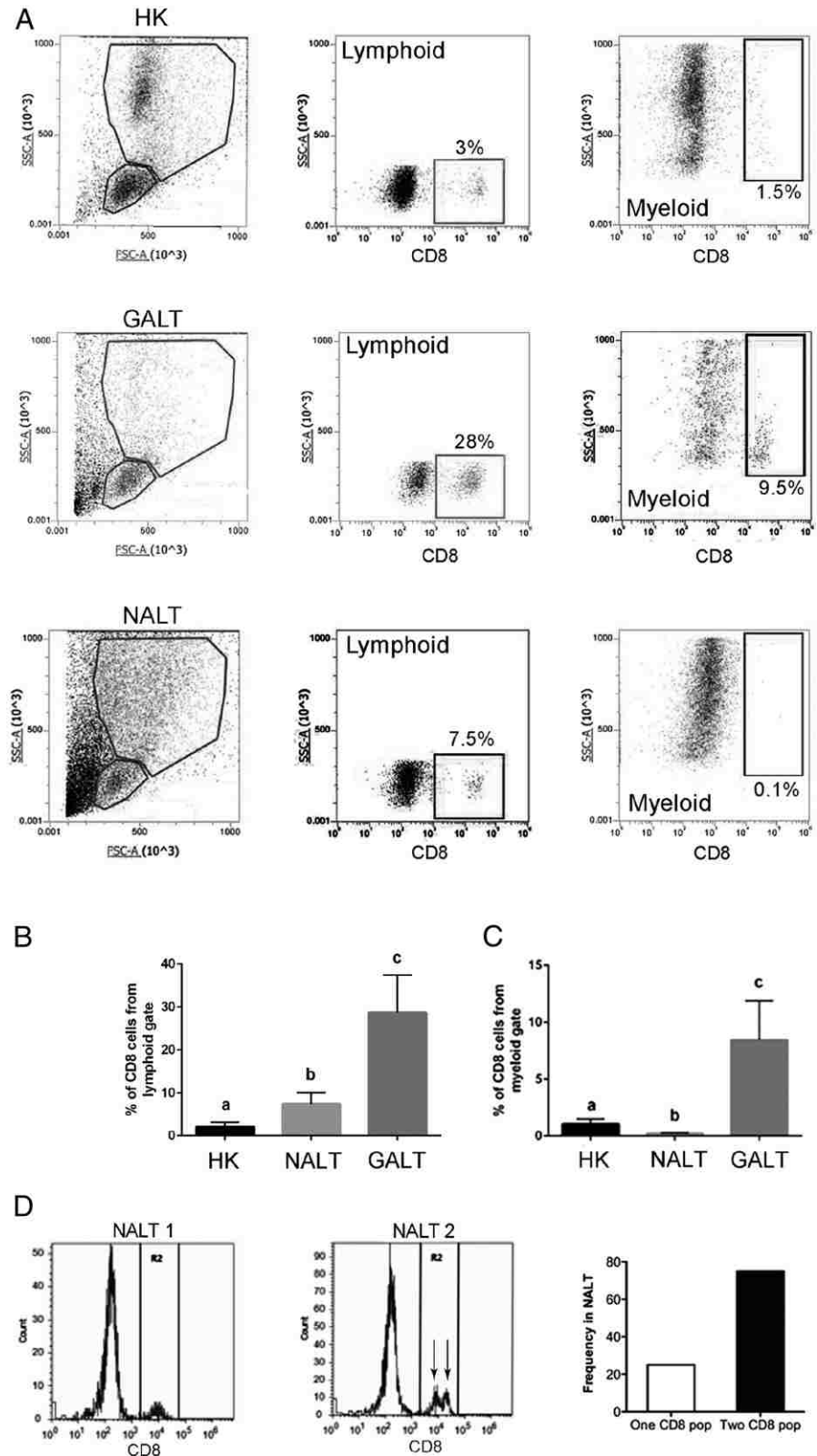
table the software MatGAT 2.02 (37) was used. All integrin β_2 sequences were searched for conserved motifs by using the National Center for Biotechnology Information Batch conserved domain database (<http://www.ncbi.nlm.nih.gov/Structure/cdd/wrpsb.cgi>) (38).

In vivo 5-ethynyl-2'-deoxyuridine proliferation assay

For proliferation assays, 100-g rainbow trout were intranasally vaccinated with live attenuated IHNV vaccine as explained elsewhere (33). Twenty-four

hours prior to sampling, trout received 500 μg of 5-ethynyl-2'-deoxyuridine (EdU) by i.p. injection. The olfactory organs from control and vaccinated trout ($n = 4$) were collected on days 4 and 8 postvaccination and snap frozen in OCT. Proliferating cells were detected using the Click-iT EdU Alexa Fluor 647 imaging kit (Thermo Fisher Scientific) as per the manufacturer's instructions. The percentage of proliferating cells in the tip and lateral regions was calculated by counting the number of Alexa Fluor 647–positive cells per field in 10 different fields ($\times 60$) of each region per specimen under a Nikon Ti inverted fluorescence microscope.

FIGURE 1. Characterization of NALT CD8 α^+ T cells in rainbow trout by FACS. **(A)** Representative dot plots of control trout HK leukocytes and NALT and GALT leukocytes stained with anti-trout CD8 α showing the percentage of positive cells from the lymphocyte and myeloid gates. **(B)** Mean percentage of CD8 α^+ cells in control rainbow trout HK, NALT, and GALT cell suspensions within the lymphocyte gate ($n = 6$) analyzed by FACS. **(C)** Mean percentage of CD8 α^+ cells in control rainbow trout HK, NALT, and GALT cell suspensions within the myeloid gate ($n = 6$) analyzed by FACS. **(D)** FACS histograms of anti-trout CD8 α -stained NALT cell suspensions showed one peak in some fish whereas other fish have two separate positive peaks. The frequency of fish that contained one CD8 α^+ subpopulation and two CD8 α^+ subpopulations is represented. Different letters indicate statistically significant differences among groups ($p < 0.05$). Results are representative of three different experiments.



Statistical analysis

Results are expressed as the mean \pm SE. Data analysis was performed in GraphPad Prism version 5.0. The RT-qPCR measurements were analyzed by *t* test to identify statistically significant differences between groups. One-way ANOVA and a Tukey post hoc analysis test were performed to identify statistically significant differences among groups. For the proliferation assay a multivariate ANOVA test followed by a Fisher least significant difference post hoc test for multiple comparisons was performed. The *p* values < 0.05 were considered statistically significant.

Results

Trout NALT contains CD8 α^+ cells that display a unique mucosal T cell phenotype

Previous studies had reported the presence of CD8 α^+ cells in trout mucosal tissues such as intestine and gills (31). Importantly, intestine and gill CD8 α^+ cells expressed immune markers different from those expressed by systemic (HK) CD8 α^+ cells. Thus, we asked whether trout NALT also contains CD8 α^+ cells. By FACS we found that lymphoid CD8 α^+ cells represent $\sim 8\%$ of the NALT lymphocyte gate whereas in HK and GALT they represent ~ 3 and $\sim 30\%$, respectively (Fig. 1A, 1B). Within the myeloid gate, NALT CD8 α^+ cells accounted for $\sim 0.1\%$ of the cells, whereas in HK and GALT, these accounted for 1.5 and 9.5%, respectively (Fig. 1A, 1C). Interestingly, most of the fish ($\sim 75\%$) showed two different CD8 α^+ cell populations in NALT, one with a higher CD8 α^+ stain intensity and a second one with a lower CD8 α^+ stain intensity (Fig. 1D). These two (high and low) populations were not observed in the rest of the organs examined.

To know whether nasal CD8 α^+ cells constitute a unique cell population different from systemic CD8 α^+ cells or other mucosal CD8 α^+ cells, we sorted nasal, HK, and gut CD8 α^+ cells from the lymphocyte gate and measured the expression of CD3, CD8 α , CCR7, IFN- γ , IL7-R, CD103, integrin β_2 , FcR γ , DC-SIGN, MHC-II, CD83, and CD141 by RT-qPCR (Fig. 2). Gut CD8 α^+ cells expressed higher levels of CD3 and CD8 α (4- and 14.4-fold, respectively) than did HK CD8 α^+ cells (Fig. 2A, 2B). Nasal CD8 α^+ cells also expressed significantly higher levels (5.8-fold) of CD8 α transcripts than did HK CD8 α^+ cells (Fig. 2B). Importantly, both nasal and gut CD8 α^+ cells expressed IFN- γ at higher levels (~ 3 -fold) than did HK CD8 α^+ cells (Fig. 2D), whereas no differences in the levels of CCR7 expression were detected in the CD8 α^+ cells from the three organs (Fig. 2C). Alternatively, gut CD8 α^+ cells expressed significantly higher levels of IL-7R and CD103 (~ 2 -fold and ~ 20 -fold, respectively) than did HK and nasal CD8 α^+ cells (Fig. 2E, 2F). Because integrins are known to play a crucial role in directing lymphocytes to mucosal sites and create tissue microenvironments, we measured expression levels of one integrin β_2 . This integrin was selected as our candidate nasal integrin based on previous microarray results (30). We found that nasal CD8 α^+ cells expressed almost 50-fold more integrin β_2 than did HK CD8 α^+ cells and ~ 2.5 -fold more than did gut CD8 α^+ cells (Fig. 2G). The low expression levels of FcR γ (Fig. 2H), DC-SIGN (Fig. 2I), and MHC-II (Fig. 2J) indicated that nasal lymphoid CD8 α^+ cells are CD8 α^+ T cells and not NK cells or DC-SIGN $^+$ DCs. Specifically, DC-SIGN expression was lowest in the gut CD8 α^+ cells (Fig. 2I) whereas MHC-II expression in nasal CD8 α^+ cells was 10-fold lower than in HK and gut CD8 α^+ cells (Fig. 2J). CD83 expression was ~ 3.5 -fold higher in nasal CD8 α^+ cells than in HK and gut CD8 α^+ cells (Fig. 2K). Finally, expression of CD141 was low in HK and nasal but high (4.2-fold) in gut CD8 α^+ cells (Fig. 2L), suggesting the presence of some DC-SIGN $^-$ /CD141 $^+$ DC contamination in the gut but not nasal CD8 α population. Collectively, these results indicated that nasal CD8 α^+ cells have a unique phenotype (i.e., high CD8 α and IFN- γ expression) that is more

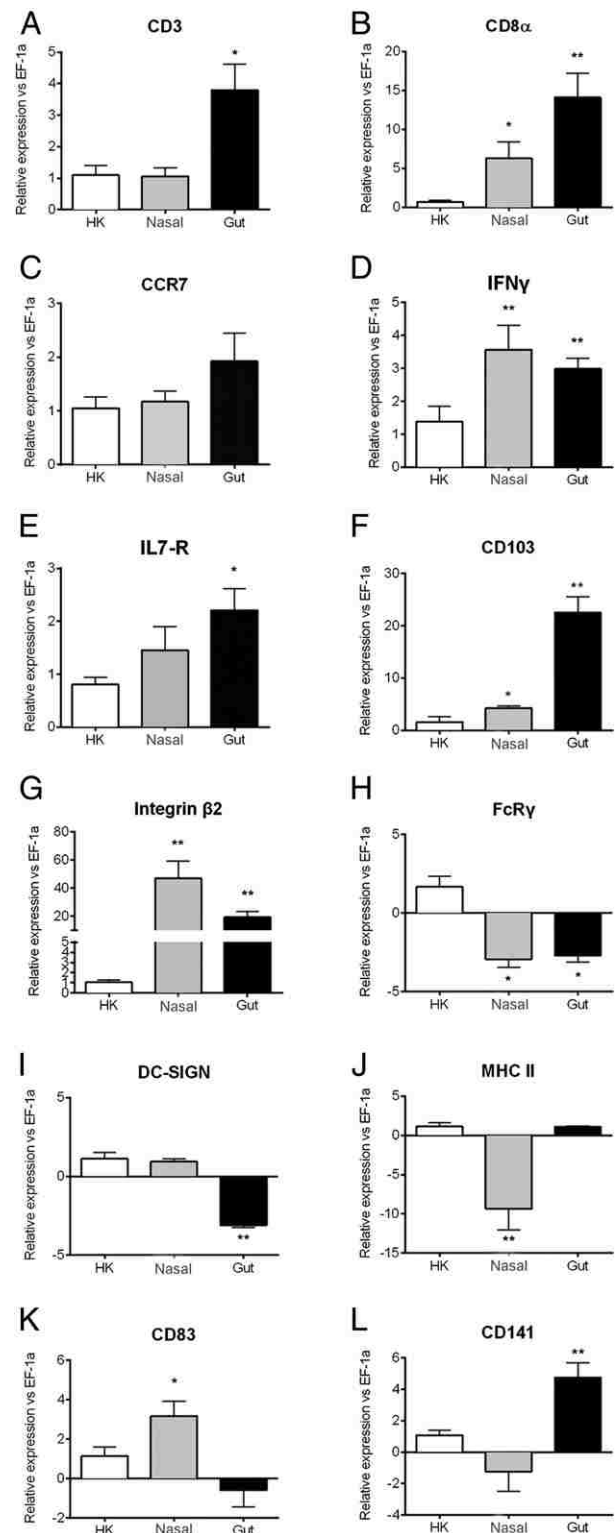


FIGURE 2. Trout NALT CD8 α^+ cells have a CD8 T cell phenotype that is different to HK and gut CD8 α^+ cells. CD8 α^+ cells from control rainbow trout HK, NALT, and GALT ($n = 9$) were sorted and total RNA was extracted to quantify gene expression levels by RT-qPCR. Gene expression levels of CD3 (A), CD8 α (B), chemokine receptor CCR7 (C), IFN- γ (D), IL-7R (E), CD103 (F), integrin β_2 (G), FcR γ (H), DC-SIGN (I), MHC-II (J), CD83 (K), and CD141 (L) are shown. Gene expression levels were normalized to the housekeeping gene EF-1 α and expressed as the fold change increase compared with the HK expression levels using the Pfaffl method. Results are representative of three different experiments. * $p < 0.05$, ** $p < 0.01$ compared with the HK.

similar to that of other mucosal CD8 α^+ cells than systemic CD8 α^+ cells. Moreover, gut and nasal CD8 α^+ cells appear to represent distinct subsets with high integrin β_2 expression specifically defining nasal CD8 α^+ cells.

The trout nasal mucosa harbors two distinct CD8 α^+ cell populations, one at the mucosal tip and one at the lateral neuroepithelium

We next examined the localization of CD8 α^+ cells in the trout olfactory organ focusing on the two main tissue compartments (mucosal and neuroepithelial) as shown in Fig. 3A. H&E staining of adult trout olfactory organ revealed clusters of cells with lymphocyte morphology in the mucosal tip but not the lateral regions of the olfactory organ (Fig. 3B). By immunostaining, CD8 α^+ cells were identified in both tissue microenvironments, albeit with important differences. At the mucosal tip, clusters of CD8 α^+ cells were observed beneath the goblet cells. In this region, CD8 α^+ cell clusters consisted an average of 12 cells (Fig. 3C, 3E). Alternatively, we found scattered CD8 α^+ cells within the neuroepithelial region of the olfactory organ (Fig. 3D). These cells were not very abundant (one to two cells per field) and did not form clusters (Fig. 3E). Moreover, staining showed that some CD8 α^+ cells were located intraepithelially in both tip and lateral neuroepithelium (Fig. 3C, 3D). Double staining with anti-CD8 anti-MHC-II Abs showed no double-positive cells in both regions (Supplemental Fig. 2). Thus, based on these observations we concluded that the mucosal tip constitutes a microenvironment specialized in CD8 α^+ cell-mediated immunity in rainbow trout.

T cell markers, adhesion molecules, chemokines, and chemokine receptor expression occur primarily in the microenvironment of the mucosal tip

To further understand the preferential localization of CD8 α^+ cells to the mucosal tip, we used LCM to dissect the two nasal microenvironments and measure a number of immune cell markers as well as adhesion molecules and chemokines. As expected, the mucosal tip expressed significantly higher levels of all T cell markers (between 4- and 8-fold), except for TCR γ , than did the neuroepithelium (Fig. 4A). Because we had identified integrin β_2 as an integrin highly expressed by nasal CD8 α^+ T cells, we measured this integrin in LCM-dissected tissue microenvironments as well as their putative adhesion molecule ligands VCAM-1, ICAM-1, and L-selectin. Our results show that the mucosal tip expresses all three adhesion molecules as well as the integrin β_2 at greater levels (between 2- and 3-fold) than does the lateral neuroepithelium (Fig. 4B), therefore creating the microenvironment that ensures preferential trafficking of CD8 α^+ cells to this area. We performed searches for a number of vertebrate integrin β_2 molecules as well as phylogenetic analyses that revealed a high degree of conservation between rainbow trout integrin β_2 and the other vertebrate integrin β_2 molecules. Trout integrin β_2 had an identity/similarity of 50.6/67.4 and 50.2/66.5% with chicken and human integrin β_2 , respectively (Supplemental Fig. 1). Importantly, all vertebrate integrin β_2 molecules, including trout integrin β_2 , contained three canonical conserved motifs for integrin β_2 : the von Willebrand factor type A domain, the integrin β cytoplasmic domain, and the β tail domain. Finally, we measured the expression levels of the chemokine CCL19 and its putative receptor

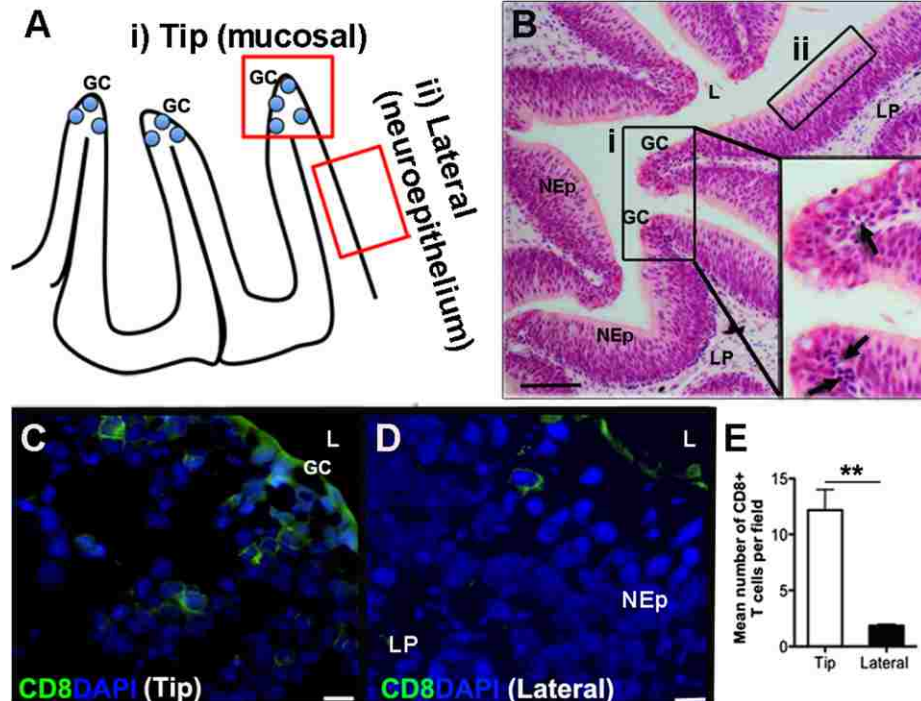


FIGURE 3. CD8 α^+ cells are clustered at the mucosal tip of the olfactory lamellae in rainbow trout. **(A)** Schematic diagram of the histological organization of the trout olfactory organ showing the mucosal tip area with goblet cells (i) and the lateral neuroepithelium (ii). **(B)** Representative H&E stain of adult rainbow trout olfactory organ showing clusters of lymphocyte-like cells at the mucosal tip (i) (and inset) of the lamella (black arrows) but not in the lateral region (ii). Scale bar, 150 μ m. **(C)** Immunofluorescence staining of a control rainbow trout olfactory organ cryosection stained with anti-trout CD8 α (FITC, green) showing a cluster of CD8 α^+ cells at the mucosal tip. **(D)** Immunofluorescence staining of a control rainbow trout olfactory organ cryosection stained with anti-trout CD8 α showing an isolated CD8 α^+ cell in the lateral neuroepithelium. For (C) and (D), cell nuclei were stained with DAPI DNA stain (blue). Results are representative of three different experiments ($n = 5$). Scale bars, 5 μ m. **(E)** Quantification of the number of CD8 α^+ cells present in the tip and lateral regions of control rainbow trout ($n = 6$). ** $p < 0.01$ for differences between both regions. GC, goblet cell; L, lumen; LP, lamina propria; NEp, neuroepithelium.

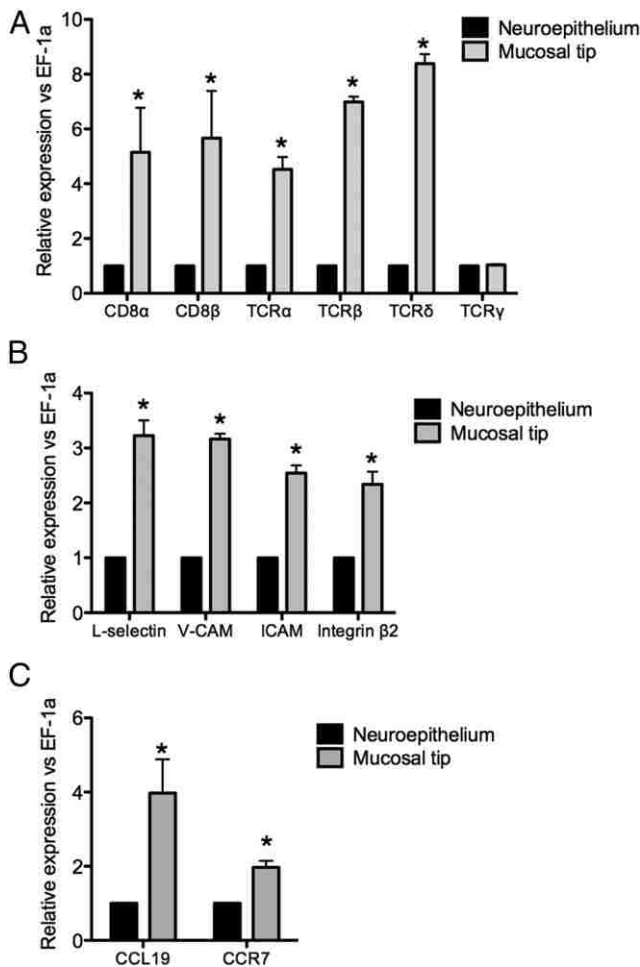


FIGURE 4. Two unique tissue microenvironments are present in the trout olfactory organ. Control trout olfactory organ cryosections were dissected by LCM to separate the mucosal tip and the lateral regions. Total RNA from each region was purified and gene expression was quantified by RT-qPCR. **(A)** Gene expression levels in the mucosal tip and neuroepithelium of T cell-related markers. **(B)** Gene expression levels of adhesion molecules and ligands. **(C)** Gene expression levels of the chemokine CCL19 and its putative receptor CCR7. Gene expression levels were normalized to the housekeeping gene EF-1 α and are expressed as the fold change increase compared with the expression levels in the neuroepithelium using the Pfaffl method. Results are representative of three different experiments ($n = 3$). $*p < 0.05$.

CCR7. We selected this molecule based on our previously published microarray results (30) and found that the mucosal tip expresses greater amounts of this chemokine and its putative receptor (4- and 2-fold, respectively) than does the neuroepithelium (Fig. 4C). These results therefore indicate that the expression of immune markers, adhesion molecules, and chemokines is preferentially compartmentalized to the mucosal tip of the trout olfactory organ whereas the neuroepithelial regions express lower levels of these molecules. These data show that the establishment of two unique CD8 α^+ cell populations in trout NALT is warranted by the regional expression of chemokine pairs and adhesion molecules that attract integrin β_2^{high} lymphocytes.

Viral Ag uptake takes place via both nasal microenvironments in rainbow trout

We hypothesized that one of the specialized immune functions of the mucosal tip could be the preferential uptake of Ags due to the greater production of mucosal secretions in this region. To test this

hypothesis, we examined the uptake of live attenuated IHNV through the two regions 1 h after nasal delivery. Immunostaining using anti-IHNV Abs recognizing the virus glycoprotein (G protein) (39) showed that both the mucosal tip and the lateral neuroepithelial region were able to uptake the viral Ag (Fig. 5A, 5B). This finding was confirmed by transmission electron microscopy (Fig. 5C, 5D) and by RT-qPCR (Fig. 5E) used to detect viral RNA in LCM-dissected tip and lateral regions. Thus, these results indicate that at least with our Ag model, no preferential uptake of Ag occurs in the mucosal tip. This result supports the previous notion that IHNV is a neurotropic virus (40, 41) and therefore the trout olfactory sensory neurons are a portal of entry for this virus in the olfactory organ.

MHC-II⁺ expression in the tip and lateral nasal microenvironments

Despite that both the tip and lateral regions had taken up viral Ag, we hypothesized that Ag presentation may be different in the two microenvironments. MHC-II⁺ cells with the morphology of professional APCs were observed in both the tip and lateral regions of control trout nasal mucosa (Fig. 6A). Interestingly, in the lateral region the MHC-II⁺ cells were located at the base, near the basal membrane, whereas in the tip, they were closer to the apical portion of the epithelium (Fig. 6A). As a consequence, when we measured the distance between the MHC-II⁺ cells and the lumen of the nasal cavity, we found that in the tip the mean distance was $\sim 25 \mu\text{m}$, whereas in the lateral region it was $\sim 120 \mu\text{m}$ (Fig. 6B). Thus, professional APCs located at the tip have quicker access to nasal pathogens than lateral APCs. In response to nasal vaccination with IHNV, the morphology of the MHC-II⁺ cells dramatically changed, particularly 4 d postvaccination in the lateral region (Fig. 6C). Importantly, the epithelial cells of the mucosal tip displayed MHC-II staining 4 d postvaccination (Fig. 6D) and the staining was no longer present on day 8 (Fig. 6F). Both at days 4 and 8, the lamina propria at the insertion of the lamellae to the midline raphe showed a dramatic influx of MHC-II⁺ cells not observed in the control fish (Fig. 6C, 6E).

Cell proliferation in response to nasal viral vaccination is compartmentalized in the mucosal tip microenvironment

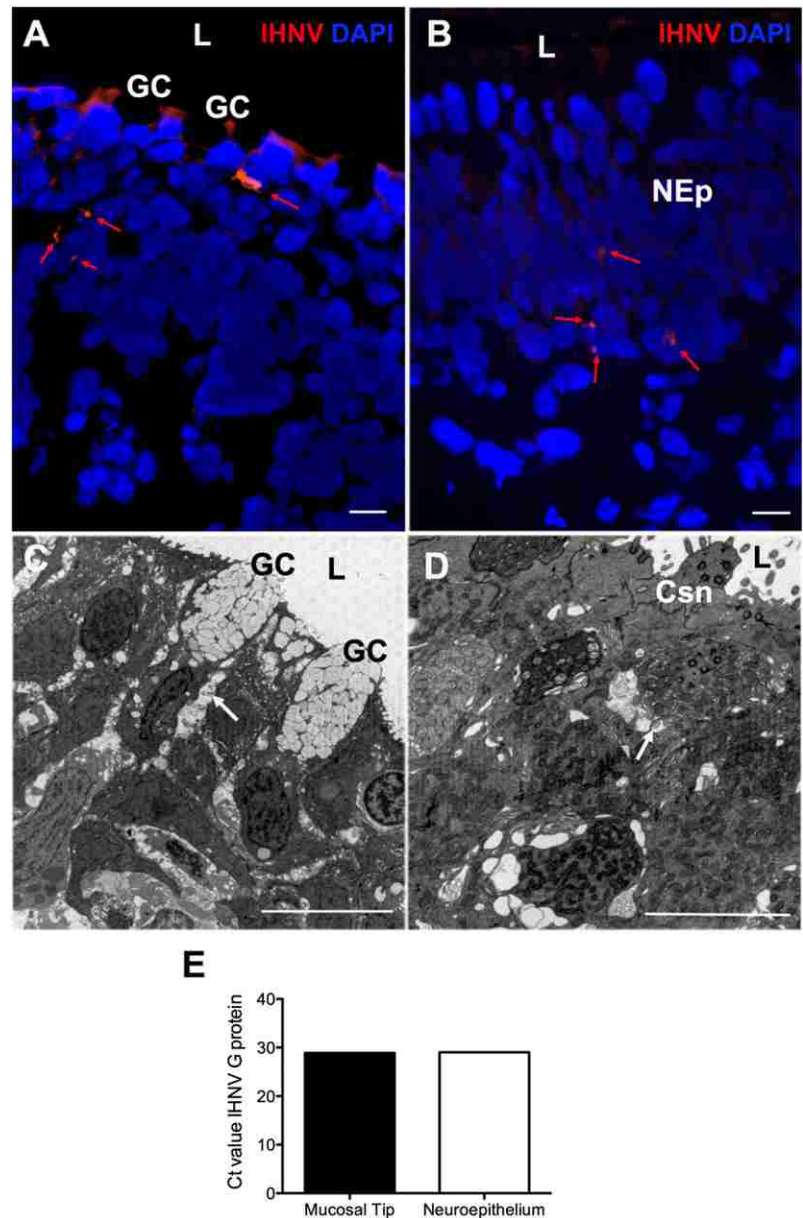
To know whether nasal vaccination resulted in cell proliferation in vivo we used the EdU assay. Overall, we observed limited amounts of cell proliferation in the olfactory organ even following nasal vaccination at day 4. At day 8, we found significantly higher numbers of EdU⁺ cells in the tip but not the lateral neuroepithelium of vaccinated fish compared with controls (Fig. 7). Thus, in response to Ag stimulation, cell proliferation is primarily contained in the mucosal tip of the olfactory organ, suggesting a protective response of the sensory regions during the course of the immune response.

Discussion

Mucosal barriers are multifunctional epithelia that perform key physiological functions while protecting the host against infection. Vertebrates have evolved strategies to limit immune responses at unique sites within mucosal barriers, a phenomenon also known as regional immunity (5, 42–44). Regional immunity examples are well documented in the intestinal mucosa of mammals (1, 5, 6, 45); however, to date, no examples have been illustrated in the nasal mucosa.

The olfactory epithelium of both aquatic and terrestrial vertebrates is often subjected to microbial invasion. Owing to the delicate nature of the sensory regions in this organ, we hypothesized that regional immunity may be critical to ensure adequate olfactory function in vertebrates. NALT was recently discovered in teleosts (30) and reported

FIGURE 5. Viral Ag uptake takes place both via the mucosal tip and the lateral neuroepithelium. Twenty-five microliters of live attenuated IHNV (10^5 PFU) or PBS (control) was delivered intranasally to rainbow trout ($n = 3$), and trout olfactory organs were collected 1 h later to localize Ag uptake. **(A)** Immunofluorescence staining with anti-IHNV Abs (Cy3, red) showing the presence of viral Ags (red arrows) at the mucosal tip region of the olfactory organ of an IHNV-vaccinated rainbow trout. Scale bar, 5 μ m. **(B)** Immunofluorescence staining with anti-IHNV Abs showing the presence of viral Ags (red arrows) at the lateral region of the olfactory organ of an IHNV-vaccinated rainbow trout. Scale bar, 5 μ m. No Ag was detected in the control PBS group (data not shown). In **(A)** and **(B)**, cell nuclei were stained with DAPI DNA stain (blue). **(C)** Transmission electron micrograph showing the presence of viral Ags at the mucosal tip region of the olfactory organ of IHNV vaccinated rainbow trout 1 h after nasal vaccination. Scale bar, 10 μ m. **(D)** Transmission electron micrograph showing the presence of viral Ags at the lateral region of the olfactory organ of IHNV-vaccinated rainbow trout 1 h after nasal vaccination. Scale bar, 5 μ m. White arrows point to viral particles. **(E)** Detection of IHNV G protein RNA levels by RT-qPCR in the tip and lateral regions of IHNV-vaccinated rainbow trout 1 h after nasal vaccination using LCM-dissected regions from olfactory organ cryosections. One pool for each region obtained from three different fish was tested. No IHNV G protein RNA could be detected in PBS controls (data not shown). Gene expression levels are shown as the Ct value and were normalized against the EF-1 α house-keeping gene. Results are representative of one experiment ($n = 3$). Csn, ciliated olfactory sensory neuron; GC, goblet cell; L, lumen; NEp, neuroepithelium.



to have the same canonical features of other teleost MALT. Using rainbow trout as a model, we show that immune responses in the nasal mucosa are not homogeneous and that at least two unique microenvironments in the mucosal (nonsensory) and sensory regions of the teleost olfactory organ exist.

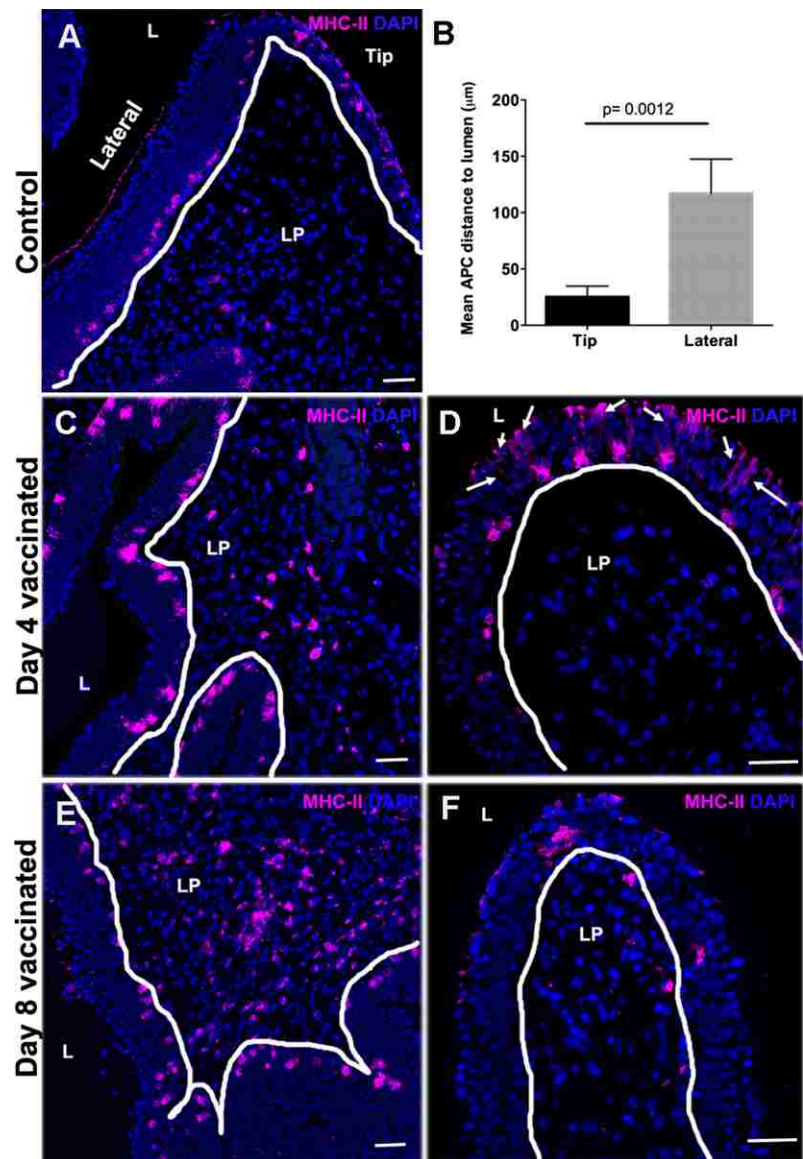
CD8 T cells are a key component of the vertebrate mucosal immune system. In this study, we identified the presence of CD8 α^+ T cells in trout NALT. Compared to HK, NALT harbors a greater proportion of CD8 α^+ cells, but not as abundant as the percentage found in GALT. The olfactory organs of all vertebrates are profusely irrigated by capillaries. Thus, the intermediate percentages of CD8 α^+ cells found in NALT may reflect a greater influence of the systemic compartment in this tissue compared with the gut. Interestingly, we observed that some animals contained two different subpopulations of CD8 α^+ cells expressing different levels of CD8 α . Future studies should further address the meaning of this finding.

Mucosal epithelia use a number of receptor–ligand interactions to guide the trafficking of immune cells and establish regional immunity. For instance, CD8 $^+$ T cells express different selectins–selectin

ligands, chemokine receptors, and integrins depending on the activation state of the cell (46), which define their tissue distribution and enable regional immunity. Thus, mucosal lymphocytes often express unique adhesion molecules that allow their specific homing to the mucosal regions expressing the corresponding ligand (4, 44, 47, 48). Mucosal CD8 α^+ cells are abundant in rainbow trout gut and gill (31). In this study, we identified the presence of CD8 α^+ T cells in teleost NALT. CD8 α^+ cells were not uniformly scattered in the nasal epithelium but rather formed clusters at the tip of each lamella, in the mucosal regions. Interestingly, trout skin CD8 $^+$ T cells are twice as abundant in the anterior region than in the posterior region of the body by flow cytometry (49); however, whether they form cell clusters similar to those observed in NALT is unknown.

Because NALT CD8 α^+ cells mostly expressed T cell markers but not NK or DC markers, we concluded that this NALT population represents CD8 α^+ T cells. Based on our microscopy results, no double CD8 $^+$ /MHC-II $^+$ cells were identified in NALT. Recently, CD8 $^+$ /MHC-II $^+$ cells within the myeloid gate with a DC-like cell phenotype have been characterized in the skin of rainbow trout (32). Thus, it seems that this population is absent at this mucosal site in trout.

FIGURE 6. MHC-II expression in the two nasal tissue microenvironments in response to viral nasal vaccination. **(A)** Immunofluorescence image of a control cryosection of the trout olfactory organ stained with anti-MHC-II (Alexa Fluor 647; magenta) and containing both the lateral neuroepithelium and the mucosal tip. The distance from the nucleus of the MHC-II⁺ cells to the lumen of the nasal cavity was measured with the Nikon Nis Advanced Research software in 50 cells from each region from three different fish. The mean distance \pm SE is shown in **(B)**. Trout were vaccinated intranasally with IHNV vaccine and the olfactory organs were sampled 4 and 8 d later. Cryosections were stained with anti-MHC-II Ab. An influx of MHC-II⁺ cells was observed in the lamina propria at the midline raphe level 4 d postvaccination **(C)**. Note that the MHC-II⁺ cells in the neuroepithelium show an activated stellate morphology. At 4 d postvaccination, the epithelial cells at the tip of the lamellae increased their MHC-II⁺ expression (white arrows) and MHC-II⁺ cells in the tip of the lamella also showed signs of activation but did not have a stellate morphology **(D)**. Eight days postvaccination, the influx of MHC-II⁺ cells in the lamina propria at the raphae region was more evident **(E)**; however, neuroepithelial MHC-II⁺ cells did not appear as activated as on day 4. At the tip, epithelial cell expression of MHC-II had already decreased **(F)**. For **(A)** and **(C)–(F)**, the white line delineates the basal membrane. Cell nuclei were stained with DAPI DNA stain (blue). Results are representative of one experiment ($n = 5$). Scale bars, 50 μ m. L, lumen; LP, lamina propria.



In agreement with previous studies on trout (31), we observed that GALT and NALT CD8 α ⁺ cells have a phenotype reminiscent of effector CD8 T cells with high IFN- γ expression. We also observed greater levels of IL-7R expression in mucosal CD8 α ⁺ cells than in HK CD8 α ⁺ cells. In mammals, increased expression of IL-7R identifies the effector CD8⁺ T cells that will differentiate into memory cells (50). Moreover, anatomic location plays an inductive role in the memory differentiation program of mammalian CD8⁺ T cells. Specifically, the gut microenvironment generates virus-specific intraepithelial lymphocytes that do not resemble central or effector memory CD8⁺ T cells isolated from spleen or blood (51). The markers that differentiate different subsets of CD8⁺ T cells in teleost fish are thus far unknown. If IL-7R function is conserved across the vertebrate lineage, our results indicate that trout memory T cells reside primarily in the gut. Further studies should ascertain the unique aspects of mucosal memory T cells in teleosts.

CD83 is expressed on the surface of mammalian DCs as well as activated B cells and T cells (52–56). Studies on teleost fish have found surface CD83 expression on DCs (57). Whether CD83 expression is a hallmark of certain teleost lymphocytes is unknown. Our results may suggest that nasal CD8⁺ T cells express

CD83. Further studies should address the function of teleost CD83 expression on T cells.

Previous work from our laboratory had identified CCL19 as one of the nasal-related genes whose expression greatly increased in the olfactory organ of trout in response to nasal vaccination with IHNV (30). CCR7, the receptor for CCL19 and CCL21 in mammals, is an important player for the migration of T lymphocytes into secondary lymphoid organs through high endothelial venules (58). Additionally, CCR7 has been implicated in the microenvironmental positioning of lymphocytes in secondary lymphoid organs (43, 59) and downregulation of CCR7 results in the retention of tissue-resident memory T cells (48). In this study, we demonstrate that trout CD8 α ⁺ cells express CCR7 and that levels of expression are comparable in mucosal and systemic T cells. Previous studies reported lack of CCR7 expression in trout blood T lymphocytes but strong CCR7 mRNA expression in trout spleen T lymphocytes (60). This result may reflect the presence of multiple CD8⁺ T cell subsets, including naive, effector, and memory T cells within each lymphoid tissue with varying levels of CCR7 expression at least based on the mammalian literature (46, 61). Importantly, we found that the mucosal tip expresses greater levels of CCL19 than does the neuroepithelium, creating the adequate microenvironment likely

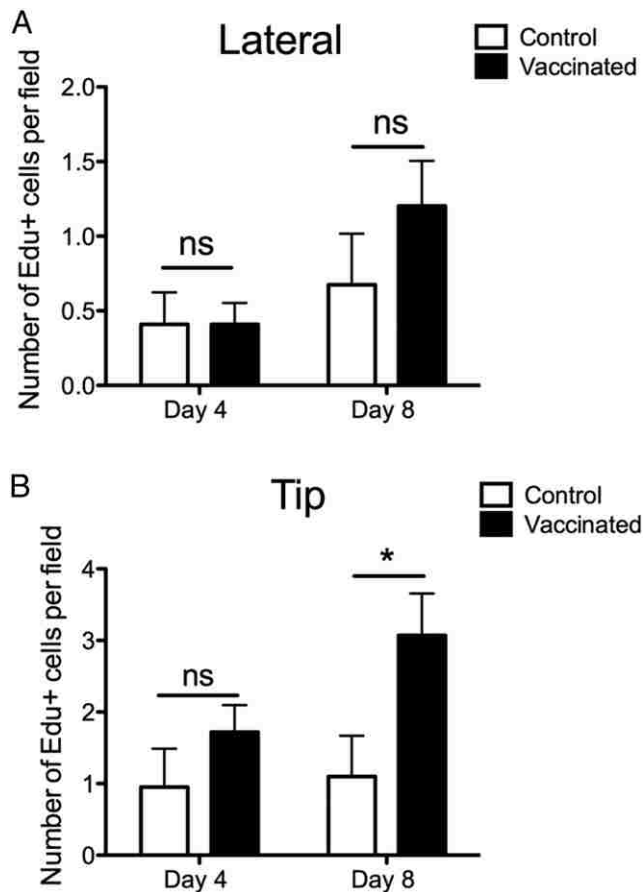


FIGURE 7. In vivo cell proliferation in response to nasal vaccination is limited to the mucosal tip of the nasal epithelium. Trout were vaccinated intranasally with IHNV vaccine and the olfactory organs were sampled 4 and 8 d later. Trout were injected i.p. with EdU 24 h prior to sampling. Cryosections were used to count the number of Alexa Fluor 647–positive cells per field in 10 different fields ($\times 60$) from the lateral neuroepithelium region (**A**) or from the mucosal tip region (**B**) per specimen under a Nikon Ti inverted fluorescence microscope. * $p < 0.05$ by two-way ANOVA analysis followed by Bonferroni multiple comparisons test. Results are representative of one experiment ($n = 4$). ns, not significant.

necessary for the retention and positioning of CD8 α^+ cells in clusters observed in this region. Based on our previous studies, we predict that expression of CCL19 by local epithelial cells or endothelial cells in the trout olfactory organ in response to vaccination may be a key mechanism by which CCR7 $^+$ T cells are recruited to the local environment. Further studies will address the sources of CCL19 production in trout NALT.

A number of receptor–ligand interactions are known to specifically guide lymphocytes to NALT in mammals. These include L-selectin/PNAd, VCAM-1/ $\alpha_4\beta_1$ integrin, ICAM-1/ $\alpha_1\beta_2$, and CCR7/CCL19, CCL21 (46, 62, 63). To date, the phenotype of teleost NALT lymphocytes (B or T cells) had not been characterized. In this study, we report that most of the molecules that dictate the tissue localization of NALT lymphocytes appear to have a conserved expression pattern in early vertebrates and mammals, including L-selectin, VCAM-1, ICAM-1, integrin β_2 , and CCL19. Our study reveals unique differences not only between systemic and NALT CD8 α^+ cells but also between GALT and NALT CD8 α^+ cells in rainbow trout. Mammalian tissue-resident CD8 $^+$ memory T cells express the α -chain (CD103) of the integrin $\alpha_E\beta_7$ (64–66). Previously, CD103 and integrin β_7 were shown to be abundantly expressed in thymic and mucosal (gill and gut) trout CD8 α^+

lymphocytes (31). Moreover, unlike their mucosal counterparts, trout splenic CD8 $^+$ T cells do not express CD103 (32). In this study, we show that trout nasal CD8 α^+ lymphocytes have a significantly lower expression of CD103 but much higher expression of integrin β_2 than do gut CD8 α^+ lymphocytes. Thus, the adhesion molecules that guide immune cells to NALT and GALT compartments are unique and specific in teleost fish. Another important difference between gut and nasal CD8 $^+$ cells is the expression of CD141. We found very low levels of expression of CD141 in systemic (HK) and nasal CD8 $^+$ T cells but high expression in gut CD8 $^+$ cells. Our results are in agreement with a previous study that showed low CD141 expression in trout splenic CD8 $^+$ T cells (32). With regard to the high CD103 and CD141 expression in gut, it is noteworthy that teleost and mammalian DCs can also express CD103 and CD141 (32, 67–69), and therefore the presence of few CD8 $^+$ /DC-SIGN $^-$ /CD103 $^+$ /CD141 $^+$ DCs or DC progenitors in the gut CD8 α^+ cell population, although unlikely, cannot be ruled out. Because mammalian migratory CD103 $^+$ and lymphoid-resident CD8 $^+$ DCs share many attributes, and may even belong to a common sublineage (70), it is possible that these lineages are also complex and related to each other in teleosts.

The positioning of professional APCs at mucosal surfaces may critically impact the kinetics of effectiveness of the immune responses against any invading pathogen. Based on their distance to the lumen, any nasal Ag would reach mucosal tip APCs much faster than neuroepithelium-resident APCs. In other words, we propose that the onset of NALT immune responses takes place first at the mucosal tip and then the neuroepithelium. With respect to non-professional APCs, it is known that intestinal epithelial cells display a highly dynamic phenotype and radically change their immunological function from the transport and assembly of S-IgA in the crypts to the expression of MHC-II as they mature and migrate up the villi (71). Additionally, in response to chronic *Helicobacter hepaticus* infection, IFN- γ induces expression of MHC-II on intestinal epithelial cells in mice (19). In this study, we found that nasal viral vaccine delivery leads to important changes in MHC-II expression in both the mucosal tip and lateral neuroepithelium microenvironments. Importantly, 4 d after vaccination, the epithelial cells present at the tip expressed MHC-II, a time when we had previously reported an upregulation of many innate immune genes, including IFN- γ . Thus, similar to mammalian intestinal epithelial cells, trout nasal epithelial cells upregulate MHC-II expression in response to antigenic stimulation and can contribute to Ag presentation in the mucosal tip microenvironment.

The olfactory epithelium is one of the few neuronal tissues with regenerative capacity (72–74). Our proliferation experiments indicate that a few cells divide in the trout olfactory organ in the absence of antigenic stimulation and that the proliferation rate increases moderately 8 d after vaccination. Importantly, the proliferation rate increased significantly in the tip but not the neuroepithelium, suggesting that the mucosal region plays a greater role in the local immune response than does the sensory region.

Different theories trying to explain the evolutionary forces driving regional and tissue-specific immunity have been proposed. For instance, an evolutionary bias toward specific protection of pathogen entry sites has been proposed (4). In our model, both microenvironments appeared equally suitable for Ag uptake. However, because Ag uptake was only quantified at one time point, it is possible that during the course of an infection or immunization, the mucosal tip may receive a higher Ag load than does the neuroepithelium, thus requiring the recruitment of specific immune cell subsets as suggested by others (4, 44).

In summary, the present study reveals the presence of distinctive immune cells, molecules, and immune responses in the mucosal

and sensorial regions of the nasal epithelium of a vertebrate species, the rainbow trout. We predict that similar microenvironments may be also present in the nasal cavity of other vertebrates, including humans. Furthermore, our results indicate that the molecular mechanisms that allow regional immunity appear conserved in teleosts and mammals. These findings provide an important basis for the understanding of local tissue immune responses in the nasal mucosa of animals and for the rational design of intranasal vaccines.

Acknowledgments

We thank Dr. U. Fisher and Dr. F. Takizawa for the anti-trout CD8 α Ab and Dr. C. Tafalla for the anti-trout MHC-II Ab. We thank Lisboa Springs Hatchery for providing animals and the staff at Clear Springs Foods Inc. for helping with sample collection.

Disclosures

The authors have no financial conflicts of interest.

References

- Mowat, A. M. 2003. Anatomical basis of tolerance and immunity to intestinal antigens. *Nat. Rev. Immunol.* 3: 331–341.
- Belkaid, Y., and G. Oldenhove. 2008. Tuning microenvironments: induction of regulatory T cells by dendritic cells. *Immunity* 29: 362–371.
- Vickery, B. P., A. M. Scurlock, S. M. Jones, and A. W. Burks. 2011. Mechanisms of immune tolerance relevant to food allergy. *J. Allergy Clin. Immunol.* 127: 576–584.
- Kunkel, E. J., and E. C. Butcher. 2002. Chemokines and the tissue-specific migration of lymphocytes. *Immunity* 16: 1–4.
- Mowat, A. M., and W. W. Agace. 2014. Regional specialization within the intestinal immune system. *Nat. Rev. Immunol.* 14: 667–685.
- Brandtzaeg, P., E. S. Baekkevold, I. N. Farstad, F. L. Jahnsen, F.-E. Johansen, E. M. Nilsen, and T. Yamana. 1999. Regional specialization in the mucosal immune system: what happens in the microcompartments? *Immunol. Today* 20: 141–151.
- Bourges, D., C. Chevalere, C. Wang, M. Berri, X. Zhang, L. Nicaise, F. Meurens, and H. Salmon. 2007. Differential expression of adhesion molecules and chemokines between nasal and small intestinal mucosae: implications for T- and sIgA⁺ B-lymphocyte recruitment. *Immunology* 122: 551–561.
- Mikhak, Z., W. W. Agace, and A. D. Luster. 2015. Lymphocyte trafficking to mucosal tissues. In *Mucosal Immunol*, 4th Ed., J. Mestecky, W. Strober, M. W. Russell, B. L. Kelsall, H. Cheroutre, and B. N. Lambrecht, eds. Elsevier Science, Oxford, U.K., p. 805–830.
- Miyasaka, M., and T. Tanaka. 2004. Lymphocyte trafficking across high endothelial venules: dogmas and enigmas. *Nat. Rev. Immunol.* 4: 360–370.
- Farber, D. L., N. A. Yudanin, and N. P. Restifo. 2014. Human memory T cells: generation, compartmentalization and homeostasis. *Nat. Rev. Immunol.* 14: 24–35.
- Cepek, K. L., S. K. Shaw, C. M. Parker, G. J. Russell, J. S. Morrow, D. L. Rimm, and M. B. Brenner. 1994. Adhesion between epithelial cells and T lymphocytes mediated by E-cadherin and the $\alpha^E\beta_7$. *Nature* 372: 190–193.
- Mora, J. R., M. R. Bono, N. Manjunath, W. Weninger, L. L. Cavanagh, M. Roseblatt, and U. H. Von Andrian. 2003. Selective imprinting of gut-homing T cells by Peyer's patch dendritic cells. *Nature* 424: 88–93.
- Sidhu, N. K., G. M. Wright, R. J. Markham, W. P. Ireland, and A. Singh. 1992. Quantitative regional variation in the expression of major histocompatibility class II antigens in enterocytes of the mouse small intestine. *Tissue Cell* 24: 221–228.
- Mann, E. R., D. Bernardo, N. R. English, J. Landy, H. O. Al-Hassi, S. T. Peake, R. Man, T. R. Elliott, H. Spranger, G. H. Lee, et al. 2016. Compartment-specific immunity in the human gut: properties and functions of dendritic cells in the colon versus the ileum. *Gut* 65: 256–270.
- Bland, P. W., and L. G. Warren. 1986. Antigen presentation by epithelial cells of the rat small intestine. I. Kinetics, antigen specificity and blocking by anti-Ia antisera. *Immunology* 58: 1–7.
- Kaiserlian, D., K. Vidal, and J. P. Revillard. 1989. Murine enterocytes can present soluble antigen to specific class II-restricted CD4⁺ T cells. *Eur. J. Immunol.* 19: 1513–1516.
- Mayer, L., and R. Shlien. 1987. Evidence for function of Ia molecules on gut epithelial cells in man. *J. Exp. Med.* 166: 1471–1483.
- Mulder, D. J., A. Pooni, N. Mak, D. J. Hurlbut, S. Basta, and C. J. Justinich. 2011. Antigen presentation and MHC class II expression by human esophageal epithelial cells: role in eosinophilic esophagitis. *Am. J. Pathol.* 178: 744–753.
- Thelemann, C., R. O. Eren, M. Coutaz, J. Brasseit, H. Bouzourene, M. Rosa, A. Duval, C. Lavanchy, V. Mack, C. Mueller, et al. 2014. Interferon- γ induces expression of MHC class II on intestinal epithelial cells and protects mice from colitis. *PLoS One* 9: e86844.
- Saraiva, L. R., G. Ahuja, I. Ivandic, A. S. Syed, J. C. Marioni, S. I. Korsching, and D. W. Logan. 2015. Molecular and neuronal homology between the olfactory systems of zebrafish and mouse. *Sci. Rep.* 5: 11487.
- Thaete, L. G., S. S. Spicer, and A. Spock. 1981. Histology, ultrastructure, and carbohydrate cytochemistry of surface and glandular epithelium of human nasal mucosa. *Am. J. Anat.* 162: 243–263.
- Dahl, R., and N. Mygind. 1998. Anatomy, physiology and function of the nasal cavities in health and disease. *Adv. Drug Deliv. Rev.* 29: 3–12.
- Reznik, G. K. 1990. Comparative anatomy, physiology, and function of the upper respiratory tract. *Environ. Health Perspect.* 85: 171–176.
- Gizurason, S. 2012. Anatomical and histological factors affecting intranasal drug and vaccine delivery. *Curr. Drug Deliv.* 9: 566–582.
- Patle, P. J., and V. V. Baile. 2014. Olfactory sensory neuron morphotypes in the featherback fish, *Notopterus notopterus* (Osteoglossiformes: Notopteridae). *Ann. Neurosci.* 21: 51–56.
- Laberge, F., and T. J. Hara. 2001. Neurobiology of fish olfaction: a review. *Brain Res. Brain Res. Rev.* 36: 46–59.
- Hamdani, H., and K. B. Døving. 2007. The functional organization of the fish olfactory system. *Prog. Neurobiol.* 82: 80–86.
- Hansen, A., and E. Zeiske. 1998. The peripheral olfactory organ of the zebrafish, *Danio rerio*: an ultrastructural study. *Chem. Senses* 23: 39–48.
- Sepahi, A., and I. Salinas. 2016. The evolution of nasal immune systems in vertebrates. *Mol. Immunol.* 69: 131–138.
- Tacchi, L., R. Musharrafieh, E. T. Larragoite, K. Crossey, E. B. Erhardt, S. A. Martin, S. E. LaPatra, and I. Salinas. 2014. Nasal immunity is an ancient arm of the mucosal immune system of vertebrates. *Nat. Commun.* 5: 5205.
- Takizawa, F., J. M. Dijkstra, P. Kotterba, T. Korytár, H. Kock, B. Köllner, B. Jaureguiberry, T. Nakanishi, and U. Fischer. 2011. The expression of CD8 α discriminates distinct T cell subsets in teleost fish. *Dev. Comp. Immunol.* 35: 752–763.
- Granja, A. G., E. Leal, J. Pignatelli, R. Castro, B. Abós, G. Kato, U. Fischer, and C. Tafalla. 2015. Identification of teleost skin CD8 α^+ dendritic-like cells, representing a potential common ancestor for mammalian cross-presenting dendritic cells. *J. Immunol.* 195: 1825–1837.
- Tacchi, L., E. Larragoite, and I. Salinas. 2013. Discovery of J chain in African lungfish (*Protopterus dolloi*, Sarcopterygii) using high throughput transcriptome sequencing: implications in mucosal immunity. *PLoS One* 8: e70650.
- Pfaffl, M. W. 2001. A new mathematical model for relative quantification in real-time RT-PCR. *Nucleic Acids Res.* 29: e45.
- Chenna, R., H. Sugawara, T. Koike, R. Lopez, T. J. Gibson, D. G. Higgins, and J. D. Thompson. 2003. Multiple sequence alignment with the Clustal series of programs. *Nucleic Acids Res.* 31: 3497–3500.
- Tamura, K., G. Stecher, D. Peterson, A. Filipski, and S. Kumar. 2013. MEGA6: molecular evolutionary genetics analysis version 6.0. *Mol. Biol. Evol.* 30: 2725–2729.
- Campanella, J. J., L. Bitincka, and J. Smalley. 2003. MatGAT: an application that generates similarity/identity matrices using protein or DNA sequences. *BMC Bioinformatics* 4: 29.
- Marchler-Bauer, A., M. K. Derbyshire, N. R. Gonzales, S. Lu, F. Chitsaz, L. Y. Geer, R. C. Geer, J. He, M. Gwadz, D. I. Hurwitz, et al. 2015. CDD: NCBI's conserved domain database. *Nucleic Acids Res.* 43: D222–D226.
- Huang, C., M. Chien, M. Landolt, and J. Winton. 1994. Characterization of the infectious hematopoietic necrosis virus glycoprotein using neutralizing monoclonal antibodies. *Dis. Aquat. Organ.* 18: 29–35.
- LaPatra, S. E., K. A. Lauda, G. R. Jones, S. C. Walker, B. S. Shewmaker, and A. W. Morton. 1995. Characterization of IHNV isolates associated with neurotropism. *Vet. Res.* 26: 433–437.
- Müller, A., B. J. Sutherland, B. F. Koop, S. C. Johnson, and K. A. Garver. 2015. Infectious hematopoietic necrosis virus (IHNV) persistence in sockeye salmon: influence on brain transcriptome and subsequent response to the viral mimic poly (I:C). *BMC Genomics* 16: 634.
- Butcher, E. C., M. Williams, K. Youngman, L. Rott, and M. Briskin. 1999. Lymphocyte trafficking and regional immunity. *Adv. Immunol.* 72: 209–253.
- Campbell, D. J., C. H. Kim, and E. C. Butcher. 2003. Chemokines in the systemic organization of immunity. *Immunity* 19: 58–71.
- Campbell, J. J., and E. C. Butcher. 2000. Chemokines in tissue-specific and microenvironment-specific lymphocyte homing. *Curr. Opin. Immunol.* 12: 336–341.
- Kunkel, E. J., J. J. Campbell, G. Haraldsen, J. Pan, J. Boisvert, A. I. Roberts, E. C. Ebert, M. A. Vieira, S. B. Goodman, M. C. Genovese, et al. 2000. Lymphocyte CC chemokine receptor 9 and epithelial thymus-expressed chemokine (TECK) expression distinguish the small intestinal immune compartment: epithelial expression of tissue-specific chemokines as an organizing principle in regional immunity. *J. Exp. Med.* 192: 761–768.
- Nolz, J. C., G. R. Starbeck-Miller, and J. T. Harty. 2011. Naive, effector and memory CD8 T-cell trafficking: parallels and distinctions. *Immunotherapy* 3: 1223–1233.
- Johnston, B., and E. C. Butcher. 2002. Chemokines in rapid leukocyte adhesion triggering and migration. *Semin. Immunol.* 14: 83–92.
- Sheridan, B. S., and L. Lefrançois. 2011. Regional and mucosal memory T cells. *Nat. Immunol.* 12: 485–491.
- Leal, E., A. G. Granja, C. Zarza, and C. Tafalla. 2016. Distribution of T cells in rainbow trout (*Oncorhynchus mykiss*) skin and responsiveness to viral infection. *PLoS One* 11: e0147477.
- Kaech, S. M., J. T. Tan, E. J. Wherry, B. T. Konieczny, C. D. Surh, and R. Ahmed. 2003. Selective expression of the interleukin 7 receptor identifies effector CD8 T cells that give rise to long-lived memory cells. *Nat. Immunol.* 4: 1191–1198.
- Masopust, D., V. Vezys, E. J. Wherry, D. L. Barber, and R. Ahmed. 2006. Cutting edge: gut microenvironment promotes differentiation of a unique memory CD8 T cell population. *J. Immunol.* 176: 2079–2083.
- Aerts-Togaert, C., C. Heirman, S. Tuytaerts, J. Cortals, J. L. Aerts, A. Bonehill, K. Thielemans, and K. Breckpot. 2007. CD83 expression on dendritic cells and T cells: correlation with effective immune responses. *Eur. J. Immunol.* 37: 686–695.

53. Ohta, Y., E. Landis, T. Boulay, R. B. Phillips, B. Collet, C. J. Secombes, M. F. Flajnik, and J. D. Hansen. 2004. Homologs of CD83 from elasmobranch and teleost fish. *J. Immunol.* 173: 4553–4560.
54. Zhou, L.-J., and T. F. Tedder. 1995. Human blood dendritic cells selectively express CD83, a member of the immunoglobulin superfamily. *J. Immunol.* 154: 3821–3835.
55. Kozlow, E. J., G. L. Wilson, C. H. Fox, and J. H. Kehrl. 1993. Subtractive cDNA cloning of a novel member of the Ig gene superfamily expressed at high levels in activated B lymphocytes. *Blood* 81: 454–461.
56. Zhou, L.-J., R. Schwarting, H. M. Smith, and T. F. Tedder. 1992. A novel cell-surface molecule expressed by human interdigitating reticulum cells, Langerhans cells, and activated lymphocytes is a new member of the Ig superfamily. *J. Immunol.* 149: 735–742.
57. Shao, T., L.-Y. Zhu, L. Nie, W. Shi, W.-R. Dong, L.-X. Xiang, and J.-Z. Shao. 2015. Characterization of surface phenotypic molecules of teleost dendritic cells. *Dev. Comp. Immunol.* 49: 38–43.
58. Förster, R., A. C. Davalos-Miszlitz, and A. Rot. 2008. CCR7 and its ligands: balancing immunity and tolerance. *Nat. Rev. Immunol.* 8: 362–371.
59. Förster, R., A. Schubel, D. Breitfeld, E. Kremmer, I. Renner-Müller, E. Wolf, and M. Lipp. 1999. CCR7 coordinates the primary immune response by establishing functional microenvironments in secondary lymphoid organs. *Cell* 99: 23–33.
60. Ordás, M. C., R. Castro, B. Dixon, J. O. Sunyer, S. Bjork, J. Bartholomew, T. Korytar, B. Köllner, A. Cuesta, and C. Tafalla. 2012. Identification of a novel CCR7 gene in rainbow trout with differential expression in the context of mucosal or systemic infection. *Dev. Comp. Immunol.* 38: 302–311.
61. Campbell, J. J., K. E. Murphy, E. J. Kunkel, C. E. Brightling, D. Soler, Z. Shen, J. Boisvert, H. B. Greenberg, M. A. Vierra, S. B. Goodman, et al. 2001. CCR7 expression and memory T cell diversity in humans. *J. Immunol.* 166: 877–884.
62. Johansen, F.-E., E. S. Baekkevold, H. S. Carlsen, I. N. Farstad, D. Soler, and P. Brandtzaeg. 2005. Regional induction of adhesion molecules and chemokine receptors explains disparate homing of human B cells to systemic and mucosal effector sites: dispersion from tonsils. *Blood* 106: 593–600.
63. Schriever, F., D. Korinth, A. Salah, P. Lefterova, I. G. Schmidt-Wolf, and S. I. Behr. 1997. Human T lymphocytes bind to germinal centers of human tonsils via integrin α_4 /VCAM-1 and LFA-1/ICAM-1 and -2. *Eur. J. Immunol.* 27: 35–39.
64. Gebhardt, T., P. G. Whitney, A. Zaid, L. K. Mackay, A. G. Brooks, W. R. Heath, F. R. Carbone, and S. N. Mueller. 2011. Different patterns of peripheral migration by memory CD4⁺ and CD8⁺ T cells. *Nature* 477: 216–219.
65. Masopust, D., D. Choo, V. Vezys, E. J. Wherry, J. Duraiswamy, R. Akondy, J. Wang, K. A. Casey, D. L. Barber, K. S. Kawamura, et al. 2010. Dynamic T cell migration program provides resident memory within intestinal epithelium. *J. Exp. Med.* 207: 553–564.
66. Mueller, S. N., T. Gebhardt, F. R. Carbone, and W. R. Heath. 2013. Memory T cell subsets, migration patterns, and tissue residence. *Annu. Rev. Immunol.* 31: 137–161.
67. del Rio, M. L., G. Bernhardt, J. I. Rodriguez-Barbosa, and R. Förster. 2010. Development and functional specialization of CD103⁺ dendritic cells. *Immunol. Rev.* 234: 268–281.
68. Kilshaw, P. J. 1993. Expression of the mucosal T cell integrin α M290 β 7 by a major subpopulation of dendritic cells in mice. *Eur. J. Immunol.* 23: 3365–3368.
69. Jongbloed, S. L., A. J. Kassianos, K. J. McDonald, G. J. Clark, X. Ju, C. E. Angel, C.-J. J. Chen, P. R. Dunbar, R. B. Wadley, V. Jeet, et al. 2010. Human CD141⁺ (BDCA-3)⁺ dendritic cells (DCs) represent a unique myeloid DC subset that cross-presents necrotic cell antigens. *J. Exp. Med.* 207: 1247–1260.
70. Jiao, Z., S. Bedoui, J. L. Brady, A. Walter, M. Chopin, E. M. Carrington, R. M. Sutherland, S. L. Nutt, Y. Zhang, H.-J. Ko, et al. 2014. The closely related CD103⁺ dendritic cells (DCs) and lymphoid-resident CD8⁺ DCs differ in their inflammatory functions. *PLoS One* 9: e91126.
71. Russell, M. W., J. Mestecky, W. Strober, B. N. Lambrecht, B. L. Kelsall, and H. Cheroutre. 2015. Overview: the mucosal immune system. In *Mucosal Immunol*, 4th Ed. J. Mestecky, W. Strober, M. W. Russell, B. L. Kelsall, H. Cheroutre, and B. N. Lambrecht, eds. Elsevier Science, Oxford, U.K., p. 3–8.
72. Graziadei, P. P., and G. A. Graziadei. 1979. Neurogenesis and neuron regeneration in the olfactory system of mammals. I. Morphological aspects of differentiation and structural organization of the olfactory sensory neurons. *J. Neurocytol.* 8: 1–18.
73. Loo, A. T., S. L. Youngentob, P. F. Kent, and J. E. Schwob. 1996. The aging olfactory epithelium: neurogenesis, response to damage, and odorant-induced activity. *Int. J. Dev. Neurosci.* 14: 881–900.
74. Leung, C. T., P. A. Coulombe, and R. R. Reed. 2007. Contribution of olfactory neural stem cells to tissue maintenance and regeneration. *Nat. Neurosci.* 10: 720–726.

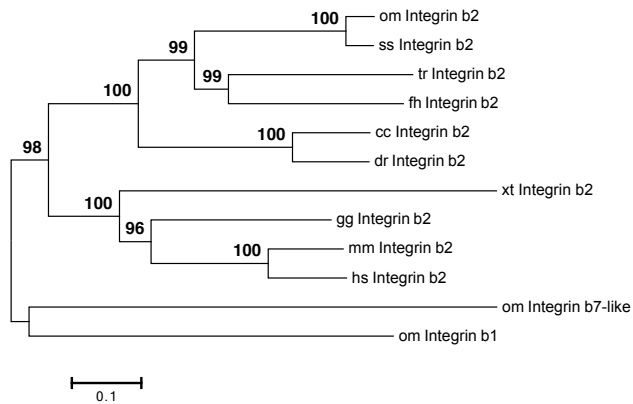
Table 1: Primers used in this study for RT-qPCR

Gene	Primer name	Primer sequence (5'→3')
EF-1 α	EF-1 α F EF-1 α R	CAACGATATCCGTCGTGGCA ACAGCGAAACGACCAAGAGG
Integrin β 2	β -Integrin-2 F β -Integrin-2 R	GGAAGTGCATCGAGTGTCTGG CCTCACGTCACAAGGCTTACC
CD3 $\gamma\delta$	CD3 F CD3 R	CCTGATTGGAGTAGCTGTCTAC GCTGTACTCAGATCTGTCCATGC
CD8 α	CD8 α F CD8 α R	ATGAAAATGGTCCAAAAGTGGATGC GGTTAGAAAAGTCTGTTGTTGGCTATAGG
CD8 β	CD8 β F CD8 β R	CAACGGTGTGCTTGTGGAAAAC ACACTTTTTGGGTAGTCGGCTGAA
CCL19.1	CCL19.1 F CCL19.1 R	CTCTGAGGTACCCGTGGATTGC CCTTAGGGACTATTGTTCTTCAGC
CCR7	CCR7 F CCR7 R	TTCACTGATTACCCACAGACAATA AAGCAGATGAGGGAGTAAAAGGTG
ICAM1	ICAM1 F ICAM1 R	CCTCACCTTGCTAGGCAGAG CGTTTGAGCTCAAGAGGAAAGG
IFN γ	IFN γ F IFN γ R	GCTGTTCAACGGAAAACCTGTTT TCACTGTCCTCAAACGTG
IL-7R	IL-7R F IL-7R R	GTGGAGAAGAATTGGTTGAC CCTCCATTTTCATCATCGGTGTC
L-selectin	L-selectin F L-selectin R	CCTCATCCCTCACTCATCAGTTC CCTCTAACTCTCTGTCTCCC
TCR α	TCR α F TCR α R	CAGCTTGAAGTCAAGAAATAC TATCAGCACGTTGAAAACGAT
TCR β	TCR β F TCR β R	CTCCGCTAAGGAGTGTGAAGATAG CAGGCCATAGAAGGTACTCTTAGC
TCR δ	TCR δ F TCR δ R	AACACTCTCCATCCTCACCC TGACAGAAGCAGTTGTAGCC
TCR γ	TCR γ F TCR γ R	CACCCTGCTATGTCTGGCTA CCATTCATGCTCCACAGAAC
FcR γ	FcR γ F FcR γ R	TACTCCAACCTCCATCTACTC CTGTGGATACCCGCCAGTGA
DC-SIGN	DC-SIGN F DC-SIGN R	CAGCAAGAAACAGCATGACGCTCTG CCCATGTGATCCTCCTGACT
CD83	CD83 F CD83 R	GGTGAGGTGGTACAAGCTGGGTG TGTGGACTCAAGGCAATCTG
CD141	CD141 F CD141 R	GGAGATTTGCTTGTAGGCTTAACGG ACTTTTTCTGACAAGGTCGTTCTG
MHC II	MHC II F MHC II R	CATATTCTCTGGAACAGATGGATA GCTCAACTGTCTTGTCCAGTATGGCGC

CD103	CD103 F CD103 R	AGGAGTGATCTTAAAACACCCCAAG TGGCAGACACAACACTGTAACCTAA
VCAM1	VCAM1 F VCAM1 R	GGTTGAGAAGCATCAGTACCAGC GGTGTCTTGATGTTGTCCTTGG
IHNV G	IHNV-G1035 F IHNV-G1147 R	CATGTCCATCCCCCAGAACT GGACAACCTGTTCCACCTTGTGTT

Supplemental Fig. 1

A



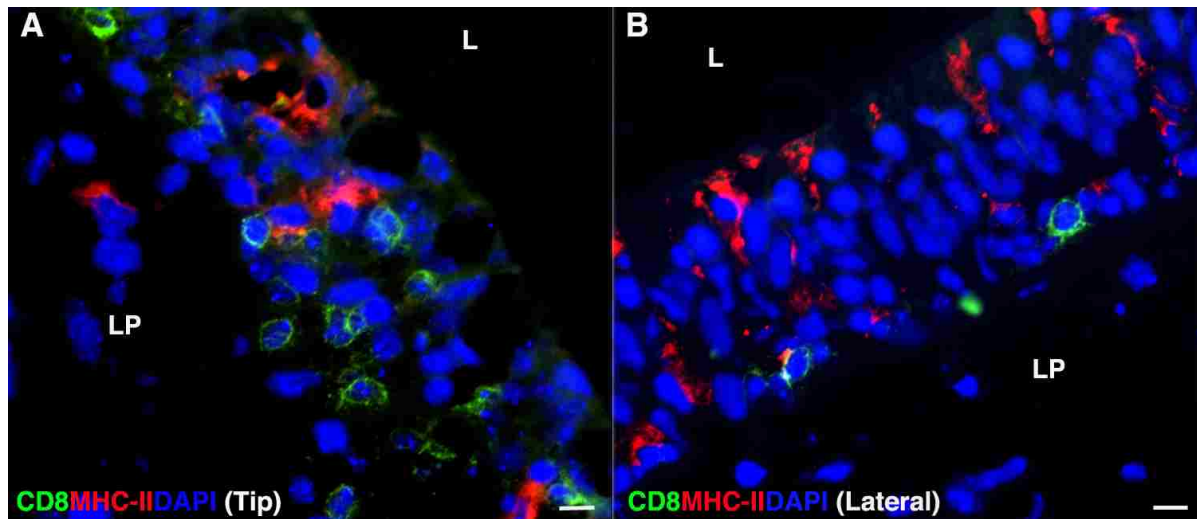
B

	1	2	3	4	5	6	7	8	9	10
1. om Integrin b2		92.5	58.3	59.4	60.2	61.8	44.6	50.6	49.2	50.2
2. ss Integrin b2	95.5		58.9	59.5	60.5	62.1	44.6	50.7	49.3	50.4
3. cc Integrin b2	71.8	73.5		81.9	52.5	54.6	45.7	50.4	49.9	49.9
4. dr Integrin b2	72.7	73.1	90		52.8	54.3	45.1	50.1	49.3	50.3
5. tr Integrin b2	75.4	76.2	68.3	69.8		63.5	43.5	47.8	48.1	48.7
6. fh Integrin b2	77.3	77.9	73.6	73.3	77.4		43.3	47.5	48.7	49.1
7. xt Integrin b2	62.5	62.5	61.7	63.3	61.1	62.8		52.8	52.3	51.6
8. gg Integrin b2	67.4	66.9	65.1	66.1	64.9	67.4	67.4		62.5	63.7
9. mm Integrin b2	66.4	66.5	67.2	67.4	65.8	67.1	68.6	77.4		81.8
10. hs Integrin b2	66.5	66.3	67.8	68.1	64.9	67.8	67.1	78	90.3	

Identity
Similarity

Supplemental Figure 1. Phylogenetic analysis of rainbow trout integrin $\beta 2$. (A) Phylogenetic tree showing the evolutionary relationship of integrin $\beta 2$ proteins in vertebrates. Tree was generated using the Neighbour-Joining method in MEGA 6.06 and bootstrapped 10,000 times, and only values over 90% are shown. Integrin $\beta 2$ GenBank accession numbers used are as follows: rainbow trout (om) (NP_001117907.1), salmon (ss) (NP_001158796.1), carp (cc) (BAB39131.1), zebrafish (dr) (XP_686012.3), Fugu (tr) (XP_003961738.1), mummichog (fh) (XP_012713602.1), tropical clawed frog (xt) (XP_012826644.1), chicken (gg) (XP_015144621.1), mouse (mm) (P11835.2) and human (hs) (NP_000202.3). Rainbow trout (om) integrin $\beta 7$ -like and rainbow trout (om) integrin $\beta 1$ GenBank accession numbers used are: CDQ74299.1 and CDQ66682.1, respectively. (B) MatGAT output for global similarity and identity over the full length of different vertebrate integrin $\beta 2$ protein sequences. Scoring matrix Blosum50 was used in the comparison. % of similarity is shown in light grey and % of identity in dark grey.

Supplemental Fig. 2



Supplemental Figure 2: Nasal CD8 α + cells do not express MHC-II. Double immunofluorescence staining of a control rainbow trout olfactory organ cryosection stained with anti-trout CD8 α (FITC, green), anti-trout MHC-II (Alexa 647, red) and DAPI DNA stain (blue). (A) Mucosal tip immunofluorescence image. (B) Lateral neuroepithelium immunofluorescence image. L: lumen. LP: lamina propria. Scale bar = 5 μ m. Results are representative of ten different cryosections per fish (N=3).

Chapter 4

Sepahi, Ali, Aurora, Kraus, Chris Johnston., Jorge Galindo-Villegas., Cecilia Kelly., Diana Garcia-Moreno., Pilar Muñoz., Victoriano Mulero., Mar Huertas and Irene Salinas. "Olfactory sensory neurons mediate ultra-rapid antiviral immune responses in teleosts in a TrkA-dependent manner". Immunity. Under review

1 **Olfactory sensory neurons mediate ultra-rapid antiviral immune responses in teleosts in a**
2 **TrkA-dependent manner**

3 Ali Sepahi ¹, Aurora Kraus ¹, Christopher A Johnston ², Jorge Galindo-Villegas ³, Cecilia Kelly ¹,
4 Diana García-Moreno ³, Pilar Muñoz ⁴, Victoriano Mulero ², Mar Huertas ⁵, Irene Salinas ^{1*}

5 ¹ *Center of Evolutionary and Theoretical Immunology, Biology Department, University of New Mexico,*
6 *New Mexico, USA.*

7 ² *Biology Department, University of New Mexico, New Mexico, USA.*

8 ³ *Department of Cell Biology and Histology, Faculty of Biology, IIMIB-Arrixaca, Campus Universitario*
9 *de Espinardo, University of Murcia, 30100 Murcia, SPAIN.*

10 ⁴ *Department of Faculty of Veterinary, University of Murcia, Murcia, SPAIN.*

11 ⁵ *Department of Biology, Texas State University, San Marcos, Texas, USA.*

12 *Lead contact: Dr. Irene Salinas. Center of Evolutionary and Theoretical Immunology, Biology
13 Department, University of New Mexico, New Mexico, USA. Phone: +15052770039. email:
14 isalinas@unm.edu

15 **Summary**

16 The nervous system is known to regulate host immune responses. However, the ability of neurons
17 to detect danger and initiate immune responses at barrier tissues is unclear. Vertebrate olfactory
18 sensory neurons (OSNs) are located in direct contact with the external environment and therefore
19 directly exposed to pathogens. Here, we report that nasal delivery of rhabdoviruses induced
20 apoptosis in crypt OSNs in rainbow trout olfactory organ (OO) via the interaction of the OSN
21 TrkA receptor with viral glycoprotein. This signal resulted in pro-inflammatory responses in the
22 OO and dampened inflammation in the olfactory bulb (OB). CD8 α^+ cells infiltrated the OO within
23 minutes of nasal viral delivery and this response was abrogated when TrkA was blocked.
24 Infiltrating CD8 α^+ cells originated from the microvasculature surrounding the OB and not the
25 periphery. Ablation of crypt neurons in zebrafish resulted in increased susceptibility to rhabdoviral
26 challenge. Our results, therefore, indicate a novel function for OSNs as a first layer of pathogen
27 detection in vertebrates.

28 **Keywords:** olfaction; sensory neurons; crypt neurons; TrkA; viral immunity; teleost fish; viral
29 glycoprotein

30 **Introduction**

31 The interactions between the nervous system and the immune system are multiple and complex.
32 Both systems are specialized in sensing and responding to environmental signals and, evolutionary
33 speaking, these two systems may have originated from a common ancestral precursor (Arendt,
34 2008). Sensory neurons have been shown to participate in immune responses in several animal
35 models. For instance, in mice, nociceptor sensory neurons can be directly activated by bacteria to
36 control pain and modulate inflammatory responses (Chiu et al., 2013; Pinho-Ribeiro et al., 2017)
37 at several sites including the skin, joints, lungs and gastrointestinal tract (Pinho-Ribeiro et al.,
38 2017). Moreover, sensory neurons are critical for suppressing innate immune responses triggered
39 by pathogens and restore host homeostasis in invertebrates (Sun et al., 2012).

40 Vertebrate olfactory sensory neurons (OSNs) rapidly sense chemical stimuli present in the
41 environment and transduce odorant-encoded signals into electrical signals that travel to the
42 olfactory bulb (OB) via the olfactory nerve, where they are integrated and transferred to other parts
43 of the central nervous system (CNS). OSNs are one of the few neurons in the vertebrate body that
44 are in direct contact with the external environment, yet the interactions between microbes and
45 OSNs remain unknown. OSNs are also in close proximity to a local network of immune cells
46 known as the nasopharynx-associated lymphoid tissue (NALT) which is present in both teleosts
47 and mammals (Sepahi and Salinas, 2016; Tacchi et al., 2014). The cross-talk between OSNs and
48 NALT during the course of an immune response has not yet been investigated.

49 Teleost fish are known to have four different OSN types: ciliated, microvillous, crypt, and kappe
50 neurons (Ahuja et al., 2014). The specific odors recognized by crypt neurons and their function
51 are still enigmatic although recent evidence suggests that these neurons are responsible for kin
52 recognition in zebrafish (Biechl et al., 2016). Crypt neurons only express one type of olfactory
53 receptor, the vomeronasal receptor 1-like Ora4 and can be identified by their tropomyosin-related
54 kinase A receptor (TrkA) immunoreactivity (Ahuja et al., 2013; Catania et al., 2003; Germana et
55 al., 2004). The interaction between TrkA and endogenous ligands, such as nerve growth factor
56 (NGF), induces internalization of TrkA into endosomes (Grimes et al., 1996). While TrkA

57 activation by NGF regulates neuronal differentiation, growth and survival (Cattaneo and McKay,
58 1990; Sofroniew et al., 2001), previous studies have shown the ability of pathogens to hijack the
59 TrkA system to infect hosts. For instance, *Trypanosoma cruzi* activates TrkA receptors and uses
60 TrkA as a vehicle for host cell invasion (de Melo-Jorge and PereiraPerrin, 2007). Additionally,
61 herpes simplex virus (HSV2) G protein modulates TrkA in order to guide axons to the infection
62 site and facilitate neuronal infection (Cabrera et al., 2015).

63 Many neurotropic viruses exploit the olfactory route to infect CNS tissues (Koyuncu et al., 2013;
64 Mori et al., 2005). In this context, murine studies suggest that nasal infection with neurotropic
65 viruses can stimulate immune responses in the olfactory organ (OO) as well as the OB within hours
66 of virus delivery (Leyva-Grado et al., 2010; Majde et al., 2007). Thus, currently, the OB in mice
67 is considered as an immune effector organ capable of eliciting pro-inflammatory immune
68 responses and containing pathogen infections to protect the CNS (Durrant et al., 2016). These local
69 immune responses are isolated from the systemic immune compartment since the blood brain
70 barrier (BBB) remains intact early during viral infection (Bi et al., 1995; D'Agostino et al., 2012).

71 In this study, we report that crypt neurons expressing TrkA are fast sensors of viruses in the
72 olfactory mucosa and critical regulators of antiviral immune responses in teleost fish. These
73 sensory neurons enter apoptosis within minutes of nasal delivery of infectious hematopoietic
74 necrosis virus (IHNV), an aquatic rhabdovirus with neurotropic characteristics (LaPatra et al.,
75 1995), via the interaction of the TrkA receptor neuron with viral glycoprotein (G protein). Upon
76 exposure to virus, TrkA-dependent neuronal activation rapidly elicits pro-inflammatory immune
77 responses in the OO and dampens inflammation in the OB. Furthermore, viral sensing by crypt
78 neurons induces infiltration of CD8 α^+ T cells from the microvasculature surrounding the OB into
79 the OO and specific ablation of crypt neurons results in increased susceptibility to rhabdoviral
80 challenge. Our results reveal that pathogen sensing by sensory neurons precedes that of the
81 immune system and that initial signals derived from neurons allow quick orchestration of immune
82 responses between the nasal mucosa and the CNS.

83 **Results**

84 *Nasal delivery of neurotropic virus induces caspase-3 dependent apoptosis fo TrkA⁺ crypt neurons*

85 Neurotropic viruses such as rhabdoviruses can infect OSNs and transneuronally infect the CNS
86 (Koyuncu et al., 2013; Mori et al., 2005). Viruses can also cause caspase-dependent apoptosis in
87 neurons via NGF signals (Allsopp et al., 1998; Chou et al., 2000; Gomes-Leal et al., 2006; Lavoie
88 et al., 2005). We first confirmed that anti-TrkA antibody exclusively labels crypt neurons in trout.
89 As previously reported, TrkA⁺ cells in the OO of trout had typical morphology and apical
90 localization of crypt cells (Figure 1A). Immunoblotting of total tissue lysates with rabbit anti-TrkA
91 antibody showed a band at the expected size of ~140kDa in OO and brain but not in the head-
92 kidney (HK), the main hematopoietic tissue in bony fish (Figure S1A). Microscopy results
93 confirmed the absence of TrkA⁺ cells in HK (Figure S1B) indicating trout immune cells are not
94 TrkA⁺. When we delivered live attenuated IHNV intranasally (IN) into rainbow trout, we observed
95 a significant decrease in the number of TrkA⁺ crypt cells in the OO compared to control fish 15
96 min, 1 h and 1 day after treatment (Figure 1 A, B, E & L). The number of TrkA⁺ crypt cells returned
97 to basal levels by day 4 suggesting that that replacement from progenitors takes approximately 4
98 days to complete. Loss of TrkA reactivity 15 min after viral delivery was associated with presence
99 of apoptotic morphology in the remaining TrkA⁺ crypt cells (Figure 1C, G & I) compared to
100 controls (Figure 1D, H & J). Moreover, staining with anti-caspase 3 antibody confirmed that crypt
101 neurons were undergoing apoptosis through caspase 3 pathway at this time point (Figure 1F). Since
102 TrkA signaling may result in cell death in sensory neurons (Nikoletopoulou et al., 2010) , we
103 pharmacologically blocked TrkA with the drug AG879. Nasal delivery of AG879 30 min prior to
104 IHNV nasal delivery (Figure 1K) rescued 50% of TrkA reactivity in crypt neurons (Figure 1M).
105 Combined, these results indicate that aquatic rhabdoviruses result in crypt neuron cells death in
106 the OO of rainbow trout in a TrkA-dependent manner.

107 *Rainbow trout smell neurotropic virus*

108 Exposure of either live attenuated IHNV or culture medium used to grow the virus elicited strong
109 olfactory responses and followed a dose-dependent pattern characteristic of activation of olfactory
110 receptors (Figure 2A). Both the virus and the culture medium elicited highly sensitive olfactory
111 responses, which could be detected up to a 1:10⁵ dilution by electro-olfactogram (EOG). However,
112 IHNV elicited greater olfactory responses than medium at the 1: 100 dilution. Differences in the
113 slopes of the linear dose responses also suggested activation of a different receptor set for each
114 stimulus. Thus, we performed cross adaptation experiments in which the OO was continuously

115 saturated with IHNV (adapted stimulus), and then measured olfactory responses to IHNV (self-
116 adapted control) or a mix of IHNV with medium by EOG (see material and methods for details).
117 We repeated the same experiment saturating the OO with medium and then measuring responses
118 to medium alone or the IHNV and medium mix. If IHNV and medium activate different receptors,
119 we would expect that OO saturated with IHNV will have a smaller olfactory response to a
120 concentrated solution of IHNV due to fewer IHNV receptors available for activation. In turn, we
121 would expect a greater response for the mix of IHNV and medium since medium-specific receptors
122 but no IHNV-specific receptors would be available for activation. In agreement, cross-adaptation
123 odorant assays showed that, after saturation of olfactory receptors with the adapting solution,
124 normalized self-adapted controls had significant lower responses (26–40 %) than the mixture of
125 live attenuated IHNV and culture medium (Figure 2B), which implied different activation of
126 receptors by the virus and medium, respectively.

127 Since we hypothesized that viral detection is TrkA receptor-mediated, we expected a decrease of
128 olfactory responses after nasal exposure to TrkA inhibitor AG879. Inhibition curves showed that
129 AG879 affected the olfactory responses to virus and culture medium in concentrations of the drug
130 as low as 10^{-8} M, with a total inhibition of activity at 10^{-5} M (Figure 2C & D). The inhibition of
131 olfactory responses by the drug was stronger for the virus than the medium, with an inhibition of
132 50% of olfactory responses (EC50) by AG879 of $10^{-6.3}$ M, and 10^{-6} M for virus and medium
133 respectively. Inhibitory curves also showed hormesis at 10^{-7} M for the virus but not for the
134 medium, implying a positive effect of the drug for virus detection at very low concentrations.
135 Combined, these experiments demonstrate the rainbow trout is able to smell viruses via TrkA
136 signaling.

137 *Neurotropic viruses activate sensory neurons in the OO and OB in a TrkA-dependent manner*

138 Studies in fish have demonstrated that pERK staining and *c-fos* gene expression are suitable
139 markers of neuronal activation upon odorant exposure in OO and CNS (Dieris et al., 2017; Lau et
140 al., 2011). However, whether viruses activate neurons in the OO and OB has not been investigated
141 to date. Incubation of OO single cell suspensions with IHNV *in vitro* showed a significant increase
142 in pERK labeling after 15 min as measured by flow cytometry (Figure S2A & B). These results
143 were confirmed *in vivo* since we detected pERK staining in the OO and OB of IHNV-treated fish

144 but not controls (Figure 3A-D). OB neuronal activation was due to viral-derived signals present in
145 the OO since IHNV could not be detected in the OB 15 min after nasal delivery (Figure S3A-D).
146 Interestingly, pERK positive cells in the OO of IHNV-treated fish were localized in the middle of
147 the neuroepithelium and did not have a crypt neuron morphology, indicating that OSNs other than
148 crypt neurons become activated following nasal viral delivery (Figure 3C). We also found a
149 significant upregulation in *c-fos* expression in the OO but not the OB, in fish that received IHNV
150 compared to controls (Figure 3E-G). Inhibition of TrkA signaling pathway with AG879 before IN
151 IHNV delivery blocked neuronal activation as evidenced by the lack of pERK staining in the OO
152 and OB and absence of *c-fos* up-regulation in the OO (Figure 3E-G). Combined, these data indicate
153 that IHNV induces OSN activation through a TrkA-dependent pathway or, alternatively, that crypt
154 neuron cell death results in activation of other OSNs.

155 *Nasal delivery of viruses results in ultra-rapid innate immune responses in the olfactory mucosa*
156 *and the CNS in a TrkA-dependent manner*

157 We previously reported that nasal delivery of live attenuated IHNV results in the recruitment of
158 myeloid and lymphoid cells to the local nasal environment 4 days after treatment in trout (Sepahi
159 et al., 2017; Tacchi et al., 2014). Here, we report that leukocyte recruitment occurs as early as 15
160 min after IHNV delivery as visualized by the enlarged lamina propria (LP) of the olfactory
161 lamellae of IHNV-treated fish compared to control fish (Figure S4A-C). Histological changes in
162 the OO were paralleled by changes in innate immune gene expression. Specifically, we observed
163 a significant upregulation of *ck10*, a CCL19-like chemokine in rainbow trout (Sepahi et al., 2017),
164 and *ptgs2b* in OO 15 min after IHNV delivery. In the OB, in turn, we observed a significant
165 downregulation in expression of *ck10* and no significant change in expression of *ptgs2b* (Figure
166 4A). *ifng* expression was down-regulated both in the OO (2-fold) and the OB (4-fold) (Figure 4A)
167 whereas no significant changes in *tnfa* expression were recorded in any tissue for any of the
168 treatments. Importantly, when we pharmacologically blocked TrkA, we could revert IHNV-
169 elicited changes in innate immune gene expression in both the OO and OB (Figure 4A). These
170 results indicate antiviral pro-inflammatory immune responses in the nasal mucosa are
171 accompanied by dampened antiviral immune responses in the OB and that both types of responses
172 require TrkA activation in crypt neurons.

173 *CD8 α T cells rapidly infiltrate the olfactory organ in a TrkA-dependent manner*

174 Gene expression data indicated that local immune responses in the OO of fish are initiated within
175 minutes of viral exposure. We next evaluated changes in leukocyte populations in the OO and
176 systemic circulation by flow cytometry following IHNV IN delivery. The percentages of trout
177 IgM⁺, IgT⁺ B cells and CD8α⁺ T cells remained unchanged in in PBLs 15 min after nasal viral
178 delivery compared to control fish (Figure 4B & D). In turn, the percentage of CD8α⁺ T cells
179 increased from 7% in controls to 24% in IHNV-treated fish in the OO. Additionally, whereas no
180 significant changes in IgM⁺ B cells were observed, we recorded a decrease in the percentage of
181 IgT⁺ B cells after nasal viral exposure (Figure 4C, E, F & G). To test whether signals derived from
182 crypt neurons are responsible for the observed infiltration of CD8α⁺ T cells into the OO, we
183 blocked TrkA with AG879, as explained in Figure 1K. We found that AG879 treatment abolished
184 both the decrease in the percentage of IgT⁺ B cells and the increase in CD8α⁺ T cells (Figure 4F
185 & G). These results indicate that crypt neurons trigger ultra-rapid cellular immune responses
186 against rhabdoviruses in a TrkA-dependent manner.

187 *CD8α T cells infiltrates originate in the OB microvasculature*

188 Neurotropic virus can hijack TrkA receptor to infect neurons and induce apoptosis (Allsopp et al.,
189 1998; Chou et al., 2000; Gluska et al., 2014; Gomes-Leal et al., 2006; Lavoie et al., 2005). TrkA
190 expressing crypt neurons project to a single target glomerulus in the OB (Ahuja et al., 2013) and
191 we showed that nasal delivery of virus results in neuronal activation in the OO and OB. Moreover,
192 we found that PBLs populations do not change following nasal viral delivery in trout. We therefore
193 hypothesized that ultra-rapid infiltration of CD8α⁺ T cells in the OO might originate from a pool
194 of lymphocytes present at the OB microvasculature that are recruited after neuronal signals. To
195 test this, we collected the blood from the microvasculature surrounding the OB, 15 min after IN
196 delivery of IHNV and evaluated changes in the percentage of cells within the lymphocyte gate as
197 well as CD8α⁺ T cells, IgM⁺ and IgT⁺ B cells by flow cytometry. We observed a significant
198 decrease in the percentage of cells within the lymphocyte gate 15 min after nasal delivery of IHNV
199 (Figure 5A & C). Analyses of OB microvasculature leukocytes showed no significant changes in
200 the percentage of IgM⁺ or IgT⁺ B cells but a significant decrease in the percentage of CD8α⁺ T
201 cells from ~2% to ~0.5% (Figure 5B & D). Intravenous administration of FITC- conjugated
202 dextran indicated that these effects occur without any changes in the blood barrier integrity of

203 IHNV-treated fish (Figure S3E-H). Combined, these results indicate an ultra-rapid shunting of
204 CD8 α^+ T cells from the OB to the OO.

205 *The interaction between IHNV viral glycoprotein (G protein) and TrkA is necessary for the onset*
206 *of nasal antiviral immune responses*

207 Since HSV Secreted G protein has been previously shown to interact with mouse TrkA (Cabrera
208 et al., 2015), we hypothesized that IHNV G protein may be the ligand for TrkA in rainbow trout
209 crypt neurons. Amino acid sequence analysis of vertebrate TrkA molecules showed a high (>50%)
210 conservation among mouse, human and rainbow trout TrkA (Figure 6A) including amino acid
211 sites known to interact with NGF (Wiesmann et al., 1999), whereas comparison of IHNV G protein
212 and HSV secreted G protein indicated a low degree of amino acid conservation (Figure S5A). In
213 order to test whether IHNV G protein alone is able to recapitulate IHNV-induced changes in crypt
214 neurons and elicit nasal CD8 α^+ T cell immune responses, we produced FLAG-tagged IHNV G
215 protein in a mammalian expression system (Figure S5B) and delivered 100 ng of recombinant
216 IHNV G protein IN to rainbow trout. Microscopy results showed the co-localization of TrkA and
217 IHNV G protein 15 min after administration of FLAG-tagged IHNV G protein (Figure 6B). We
218 also observed a significant decrease in the number of TrkA $^+$ cells 15 min after IN delivery of
219 FLAG-tagged IHNV G protein (Figure 6C) similar to what we observed following IHNV
220 treatment. Moreover, nasal delivery of FLAG-tagged IHNV G protein resulted in a significant
221 increase in the number of CD8 α^+ T cells present in trout OO 15 min after nasal delivery (Figure
222 6D). To further confirm that IHNV G protein is responsible for TrkA-mediated nasal immune
223 responses, we performed *in vivo* antibody neutralization experiments using a monoclonal anti-
224 IHNV G protein antibody or a monoclonal anti-IHNV N protein antibody as a control. Blocking
225 IHNV G protein but not N protein rescued the loss of TrkA reactivity in crypt neurons and
226 abolished the infiltration of CD8 α^+ T cells into the trout OO 15 min after IN delivery (Figures 6E
227 & F). These experiments demonstrated that the interaction between viral G protein and the crypt
228 neuron TrkA receptor is necessary and sufficient to elicit OO immune responses.

229 *Crypt neurons are involved in survival to rhabdoviral infection*

230 Our results thus far provided evidence for the role of crypt neurons in the immune crosstalk
231 between the olfactory organ and the CNS. Next, we asked whether viral detection by crypt neurons

232 is necessary for survival against rhabdoviral infection using a zebrafish model (Figure 7A). To
233 that end, we generated a transgenic zebrafish line which expressed the Gal4.VP16 transactivator
234 under the *ora4* promoter and the GFP under the heart specific promoter *cmlc2* for rapid screening
235 under the fluorescence microscope (Figure 7A). Crossing of this line with the a line which
236 expresses bacterial nitroreductase fused to mCherry revealed the presence of *ora+* crypt neurons
237 from 2 dpf onward (Figure 7A & 7B). . Addition of the prodrug metronidazole (Mtz) into the
238 zebrafish water tanks at 2 dpf for 24 h resulted in 100% ablation of crypt neurons, that started to
239 regenerate 5 days later (7 dpf) (Figure 7B & 7C). Infection of and *ora4+* crypt neuron ablated
240 zebrafish with spring viraemia of carp virus (SVCV) resulted on defects in CCL19-like expression
241 patterns in response to infection (Figure 7D), as measured by RT-qPCR. Crypt neuron ablation
242 resulted in no significant differences in SVCV viral loads 15 min after exposure but increased
243 SVCV loads 2 days post-infection (dpi) (Figure 7E). Importantly, challenge with SVCV revealed
244 that, in the absence of crypt neurons, zebrafish are more susceptible to viral infection (Figure 7F).
245 These results demonstrate that crypt neurons induce immune responses in response to viral
246 infection and that these responses are essential for viral clearance and host survival.

247

248 **Discussion**

249 The multifaceted, complex and bidirectional interactions between the nervous and the immune
250 system highlight the importance of neuro-immune communication for the success and survival of
251 all species. Apart from homeostatic functions, neuro-immune interactions are vital for the
252 protection of neuronal tissues from invading pathogens as well as from damaging host immune
253 responses. For instance, *Caenorhabditis elegans* responds to microorganisms by utilizing its
254 nervous system, which triggers a protective behavioral avoidance response (Bargmann et al., 1990;
255 Zhang et al., 2005). This behavior depends on G protein-coupled receptors (GPCRs) expressed by
256 chemosensory neurons (McMullan et al., 2012).

257 Viral pathogens have evolved different strategies to invade the CNS including exploiting the
258 olfactory route or crossing the BBB (Koyuncu et al., 2013; Mori et al., 2005). HSV-1, influenza A
259 virus, parainfluenza viruses, are some examples of viral pathogens that enter the CNS through
260 olfactory organ in mammals (Detje et al., 2009; Koyuncu et al., 2013; Mori et al., 2005). CNS
261 immune responses need to be quick and tightly controlled because, otherwise, they may lead to

262 meningitis, encephalitis, meningoencephalitis, or even death (Koyuncu et al., 2013). The present
263 study reveals a novel model of viral recognition by the vertebrate nervous system in which OSNs
264 are able to sense microbial-derived signals and use electrical decoding to trigger ultra-fast immune
265 responses in teleosts.

266 We have identified a specific type of OSN, the crypt neuron, that acts as a canary in the coal-mine
267 in the bony fish olfactory organ. We envisage 3 features of crypt neurons that make them ideal for
268 pathogen detection: (i) they are strategically located in the most apical part of the teleost olfactory
269 epithelium and so are the most exposed to invading microorganisms; (ii) they only constitute ~1-
270 2% of all cells in the OO of trout, making TrkA-mediated cell death an exquisitely specific
271 mechanism of triggering immune responses without compromising large numbers of OSNs; and
272 (iii) because crypt neurons are replaced within few days, the refractory period to recover pathogen
273 sensors in the trout OO is relatively quick. The effects of a secondary pathogen encounter prior to
274 crypt neuron regeneration remain to be explored but it is possible that compensatory mechanisms
275 are in place while crypt neurons replenish.

276 Viral-induced cell death allows crypt neurons to efficiently orchestrate innate immune responses
277 such as induction of CCL19-like and the recruitment of CD8⁺ T cells to the local nasal
278 environment. CD8⁺ T cells have been shown to prevent HSV-1 reactivation without destroying
279 the infected sensory neurons in the trigeminal ganglia of mice (Liu et al., 2000). Thus, the CD8⁺
280 T cell infiltrates detected in the teleost OO after nasal IHNV delivery may play a critical role in
281 the elimination of the virus without destruction of OSNs. Future studies will aim to further
282 understand the role of fast-recruited CD8 T cells in the nasal mucosa.

283 TrkA molecular receptor is known to be utilized by several pathogens including parasites such as
284 *Trypanosoma* (de Melo-Jorge and PereiraPerrin, 2007) and viruses such as HSV (Cabrera et al.,
285 2015) in order to invade host neurons or to change neuronal behavior. Interestingly, secreted HSV
286 G protein is able to bind TrkA in mouse skin neurons and modify neuronal dendrite outgrowth
287 (Cabrera et al., 2015). Additionally, HSV-2 secreted G protein, is known to bind chemokines and
288 enhance in this manner cell migration (Martínez-Martín et al., 2016). We provided evidence that
289 the G protein of aquatic rhabdoviruses such as IHNV also interacts with TrkA⁺ crypt neurons.
290 These findings suggest that G proteins from different neurotropic viruses have co-opted binding
291 TrkA expressed in different neuronal types as a strategy to invade their hosts. Importantly, our

292 work shows that the arms race between host and pathogen has resulted in efficient immune
293 responses evoked by the TrkA-viral G protein interaction.

294 One of the most striking findings of the present study was the immunological cross-talk between
295 the OO and the OB. Previous studies in mice have shown that infiltration of CCR7⁺ CD8⁺ T cells
296 from the lymph nodes into the OB occurs in response to neurotropic viral infection of the OB
297 (Cupovic et al., 2016). Our experiments revealed that the expression of CK10, a CCL19-like
298 chemokine in trout (Sepahi et al., 2017), is quickly up-regulated on in the OO and down-regulated
299 in the OB in response to nasal viral delivery and that zebrafish larvae where crypt neurons had
300 been ablated showed dysregulated CCL19-like expression patterns. These findings suggest that
301 the CCL19-CCR7 CD8 T cell axis is a conserved hallmark of viral neuronal infections in both
302 bony fish and mammals. Importantly, the present study shows that a type of OSN, the crypt neuron,
303 regulates antiviral immunity not only at the site of antigen encounter, but also in the OB, even in
304 the absence of viral antigens in this tissue. Through a mechanism not explored in the present study,
305 the OB turns viral-evoked electrical signals into immune responses within minutes. Future studies
306 should address which molecules (i.e neurotransmitters or neuropeptides) are responsible for the
307 changes in the OB microvasculature and T cell migration following nasal viral delivery.

308 In conclusion, our findings demonstrate a new mechanism of neuroimmune interaction by which
309 OSNs can rapidly initiate antiviral immune responses in the OO-OB axis via a TrkA-sensing
310 mechanism of viral G proteins. Understanding how the interaction between viral antigens and
311 OSNs regulates innate and adaptive immune responses in the nasal mucosa and CNS can
312 potentially help improve the efficacy and safety of nasal vaccines.

313

314 **Acknowledgements**

315 The authors would like to thank Dr. E. Casadei for cloning the IHNV G protein, Hossein
316 Goudarzi for his help with graphical abstract and I. Fuentes and P. Martínez for their excellent
317 technical assistance, Dr. Pilar Fernández-Somalo for the SVCV strain, and Profs. D. Halpern and
318 Parsons for the the Tg(UAS-E1b:nfsb-mCherry)^{c264}, Dr. Weiming Li for his help with the
319 preliminary data in the electrophysiology assays.

320 This work was supported by USDA AFRI Grant 2DN70-2RDN7 to IS, NSF IOS award 1755348

321 to IS, and NIH COBRE grant P20GM103452 as well as Spanish Ministry of Economy and
322 Competiveness (grant BIO2014-52655-R and BIO2017-84702-R to VM), co-funded with Fondos
323 Europeos de Desarrollo Regional/European Regional Development Funds. Cecelia Kelly was
324 funded by the Stephanie Ruby Fellowship and NSF award 1456940 to IS.

325

326 **Author contributions:**

327 AS performed most of the trout experiments, analyzed data and wrote the manuscript, AK
328 performed confocal microscopy, sequence alignments and zebrafish gene expression experiments,
329 PM performed TEM and light microscopy experiments, JGV performed zebrafish infections and
330 ablation experiments, CK and DGM made transgenic zebrafish, CJ made recombinant protein, MH
331 performed electrophysiology experiments, VM conceived zebrafish experiments and wrote the
332 manuscript, IS conceived the study, analyzed data and wrote the manuscript. All authors approved
333 the manuscript before submission.

334

335 **Declaration of interests:**

336 Authors declare no competing interests

337

338 **References:**

339 Ahuja, G., Ivandić, I., Saltürk, M., Oka, Y., Nadler, W., and Korsching, S.I. (2013). Zebrafish crypt neurons
340 project to a single, identified mediodorsal glomerulus. *Scientific reports* 3.
341 Ahuja, G., Nia, S.B., Zapolko, V., Shiriagin, V., Kowatschew, D., Oka, Y., and Korsching, S.I. (2014). Kappe
342 neurons, a novel population of olfactory sensory neurons. *Scientific reports* 4, 4037.
343 Allsopp, T.E., Scallan, M.F., Williams, A., and Fazakerley, J.K. (1998). Virus infection induces neuronal
344 apoptosis: A comparison with trophic factor withdrawal. *Cell Death Differ.* 5.
345 Arendt, D. (2008). The evolution of cell types in animals: emerging principles from molecular studies. *Nat.*
346 *Rev. Genet.* 9, 868.
347 Bargmann, C., Thomas, J., and Horvitz, H. (1990). Chemosensory cell function in the behavior and
348 development of *Caenorhabditis elegans*. In *Cold Spring Harbor Symp. Quant. Biol.* (Cold Spring Harbor
349 Laboratory Press), pp. 529-538.
350 Bi, Z., Barna, M., Komatsu, T., and Reiss, C.S. (1995). Vesicular stomatitis virus infection of the central
351 nervous system activates both innate and acquired immunity. *J. Virol.* 69, 6466-6472.
352 Biechl, D., Tietje, K., Gerlach, G., and Wullimann, M.F. (2016). Crypt cells are involved in kin recognition in
353 larval zebrafish. *Scientific reports* 6, 24590.
354 Cabrera, J.R., Viejo-Borbolla, A., Martinez-Martín, N., Blanco, S., Wandosell, F., and Alcamí, A. (2015).
355 Secreted herpes simplex virus-2 glycoprotein G modifies NGF-TrkA signaling to attract free nerve endings
356 to the site of infection. *PLoS Pathog.* 11, e1004571.

357 Catania, S., Germana, A., Laura, R., Gonzalez-Martinez, T., Ciriaco, E., and Vega, J. (2003). The crypt
358 neurons in the olfactory epithelium of the adult zebrafish express TrkA-like immunoreactivity. *Neurosci.*
359 *Lett.* *350*, 5-8.

360 Cattaneo, E., and McKay, R. (1990). Proliferation and differentiation of neuronal stem cells regulated by
361 nerve growth factor. *Nature* *347*, 762.

362 Chiu, I.M., Heesters, B.A., Ghasemlou, N., Von Hehn, C.A., Zhao, F., Tran, J., Wainger, B., Strominger, A.,
363 Muralidharan, S., and Horswill, A.R. (2013). Bacteria activate sensory neurons that modulate pain and
364 inflammation. *Nature* *501*, 52.

365 Chou, T.T., Trojanowski, J.Q., and Lee, V.M.-Y. (2000). A novel apoptotic pathway induced by nerve growth
366 factor-mediated TrkA activation in medulloblastoma. *J. Biol. Chem.* *275*, 565-570.

367 Cupovic, J., Onder, L., Gil-Cruz, C., Weiler, E., Caviezel-Firner, S., Perez-Shibayama, C., Rülcke, T.,
368 Bechmann, I., and Ludewig, B. (2016). Central nervous system stromal cells control local CD8+ T cell
369 responses during virus-induced neuroinflammation. *Immunity.* *44*, 622-633.

370 D'Agostino, P.M., Kwak, C., Vecchiarelli, H.A., Toth, J.G., Miller, J.M., Masheeb, Z., McEwen, B.S., and
371 Bulloch, K. (2012). Viral-induced encephalitis initiates distinct and functional CD103+ CD11b+ brain
372 dendritic cell populations within the olfactory bulb. *Proc. Natl. Acad. Sci. U. S. A* *109*, 6175-6180.

373 Davison, J.M., Akitake, C.M., Goll, M.G., Rhee, J.M., Gosse, N., Baier, H., Halpern, M.E., Leach, S.D., and
374 Parsons, M.J. (2007). Transactivation from Gal4-VP16 transgenic insertions for tissue-specific cell labeling
375 and ablation in zebrafish. *Dev. Biol.* *304*, 811-824.

376 de Melo-Jorge, M., and PereiraPerrin, M. (2007). The Chagas' disease parasite *Trypanosoma cruzi* exploits
377 nerve growth factor receptor TrkA to infect mammalian hosts. *Cell Host Microbe* *1*, 251-261.

378 Detje, C.N., Meyer, T., Schmidt, H., Kreuz, D., Rose, J.K., Bechmann, I., Prinz, M., and Kalinke, U. (2009).
379 Local type I IFN receptor signaling protects against virus spread within the central nervous system. *J.*
380 *Immunol.* *182*, 2297-2304.

381 Dieris, M., Ahuja, G., Krishna, V., and Korsching, S.I. (2017). A single identified glomerulus in the zebrafish
382 olfactory bulb carries the high-affinity response to death-associated odor cadaverine. *Scientific reports* *7*.

383 Durrant, D.M., Ghosh, S., and Klein, R.S. (2016). The olfactory bulb: an immunosensory effector organ
384 during neurotropic viral infections. *ACS chemical neuroscience* *7*, 464-469.

385 Galindo-Villegas, J., García-Moreno, D., de Oliveira, S., Meseguer, J., and Mulero, V. (2012). Regulation of
386 immunity and disease resistance by commensal microbes and chromatin modifications during zebrafish
387 development. *Proc. Natl. Acad. Sci. U. S. A* *109*, E2605-E2614.

388 Germana, A., Montalbano, G., Laura, R., Ciriaco, E., Del Valle, M., and Vega, J.A. (2004). S100 protein-like
389 immunoreactivity in the crypt olfactory neurons of the adult zebrafish. *Neurosci. Lett.* *371*, 196-198.

390 Gluska, S., Zahavi, E.E., Chein, M., Gradus, T., Bauer, A., Finke, S., and Perlson, E. (2014). Rabies virus hijacks
391 and accelerates the p75NTR retrograde axonal transport machinery. *PLoS Pathog.* *10*, e1004348.

392 Gomes-Leal, W., Martins, L., Diniz, J., Dos Santos, Z., Borges, J., Macedo, C., Medeiros, A., De Paula, L.,
393 Guimaraes, J., and Freire, M. (2006). Neurotropism and neuropathological effects of selected
394 rhabdoviruses on intranasally-infected newborn mice. *Acta Trop.* *97*, 126-139.

395 Grimes, M.L., Zhou, J., Beattie, E.C., Yuen, E.C., Hall, D.E., Valletta, J.S., Topp, K.S., LaVail, J.H., Bunnett,
396 N.W., and Mobley, W.C. (1996). Endocytosis of activated TrkA: evidence that nerve growth factor induces
397 formation of signaling endosomes. *J. Neurosci.* *16*, 7950-7964.

398 Koyuncu, O.O., Hogue, I.B., and Enquist, L.W. (2013). Virus infections in the nervous system. *Cell Host*
399 *Microbe* *13*, 379-393.

400 Kwan, K.M., Fujimoto, E., Grabher, C., Mangum, B.D., Hardy, M.E., Campbell, D.S., Parant, J.M., Yost, H.J.,
401 Kanki, J.P., and Chien, C.B. (2007). The Tol2kit: a multisite gateway-based construction kit for Tol2
402 transposon transgenesis constructs. *Dev. Dyn.* *236*, 3088-3099.

403 LaPatra, S., Lauda, K., Jones, G., Walker, S., Shewmaker, B., and Morton, A. (1995). Characterization of
404 IHNV isolates associated with neurotropism. *Vet. Res.* *26*, 433-437.

405 Lau, B.Y., Mathur, P., Gould, G.G., and Guo, S. (2011). Identification of a brain center whose activity
406 discriminates a choice behavior in zebrafish. *Proc. Natl. Acad. Sci. U. S. A* *108*, 2581-2586.

407 Lavoie, J.-F., LeSauter, L., Kohn, J., Wong, J., Furtoss, O., Thiele, C.J., Miller, F.D., and Kaplan, D.R. (2005).
408 TrkA induces apoptosis of neuroblastoma cells and does so via a p53-dependent mechanism. *J. Biol. Chem.*
409 *280*, 29199-29207.

410 Leyva-Grado, V.H., Churchill, L., Harding, J., and Krueger, J.M. (2010). The olfactory nerve has a role in the
411 body temperature and brain cytokine responses to influenza virus. *Brain, behavior, and immunity* *24*, 281-
412 288.

413 Liu, T., Khanna, K.M., Chen, X., Fink, D.J., and Hendricks, R.L. (2000). CD8+ T cells can block herpes simplex
414 virus type 1 (HSV-1) reactivation from latency in sensory neurons. *J. Exp. Med.* *191*, 1459-1466.

415 López-Muñoz, A., Roca, F.J., Sepulcre, M.P., Meseguer, J., and Mulero, V. (2010). Zebrafish larvae are
416 unable to mount a protective antiviral response against waterborne infection by spring viremia of carp
417 virus. *Dev. Comp. Immunol.* *34*, 546-552.

418 Majde, J.A., Bohnet, S.G., Ellis, G.A., Churchill, L., Leyva-Grado, V., Wu, M., Szentirmai, E., Rehman, A., and
419 Krueger, J.M. (2007). Detection of mouse-adapted human influenza virus in the olfactory bulbs of mice
420 within hours after intranasal infection. *J. Neurovirol.* *13*, 399-409.

421 Martínez-Martín, N., Viejo-Borbolla, A., and Alcami, A. (2016). Herpes simplex virus particles interact with
422 chemokines and enhance cell migration. *J. Gen. Virol.* *97*, 3007-3016.

423 McMullan, R., Anderson, A., and Nurrish, S. (2012). Behavioral and immune responses to infection require
424 Gαq-RhoA signaling in *C. elegans*. *PLoS Pathog.* *8*, e1002530.

425 Mori, I., Nishiyama, Y., Yokochi, T., and Kimura, Y. (2005). Olfactory transmission of neurotropic viruses. *J.*
426 *Neurovirol.* *11*, 129-137.

427 Nikolettou, V., Lickert, H., Frade, J.M., Rencurel, C., Giallonardo, P., Zhang, L., Bibel, M., and Barde,
428 Y.-A. (2010). Neurotrophin receptors TrkA and TrkC cause neuronal death whereas TrkB does not. *Nature*
429 *467*, 59.

430 Pfaffl, M.W. (2001). A new mathematical model for relative quantification in real-time RT-PCR. *Nucleic*
431 *Acids Res.* *29*, 2002-2007.

432 Pinho-Ribeiro, F.A., Verri Jr, W.A., and Chiu, I.M. (2017). Nociceptor sensory neuron-immune interactions
433 in pain and inflammation. *Trends Immunol.* *38*, 5-19.

434 Ristow, S.S., LaPatra, S.E., Dixon, R., Pedrow, C.R., Shewmaker, W.D., Park, J.-W., and Thorgaard, G.H.
435 (2000). Responses of cloned rainbow trout *Oncorhynchus mykiss* to an attenuated strain of infectious
436 hematopoietic necrosis virus. *Dis. Aquat. Org.* *42*, 163-172.

437 Sepahi, A., Casadei, E., Tacchi, L., Muñoz, P., LaPatra, S.E., and Salinas, I. (2016a). Tissue
438 microenvironments in the nasal epithelium of rainbow trout (*Oncorhynchus mykiss*) define two distinct
439 CD8α+ cell populations and establish regional immunity. *J. Immunol.* *197*, 4453-4463.

440 Sepahi, A., Cordero, H., Goldfine, H., Esteban, M.Á., and Salinas, I. (2016b). Symbiont-derived sphingolipids
441 modulate mucosal homeostasis and B cells in teleost fish. *Scientific reports* *6*, 39054.

442 Sepahi, A., and Salinas, I. (2016). The evolution of nasal immune systems in vertebrates. *Mol. Immunol.*
443 *69*, 131-138.

444 Sepahi, A., Tacchi, L., Casadei, E., Takizawa, F., LaPatra, S.E., and Salinas, I. (2017). CK12a, a CCL19-like
445 chemokine that orchestrates both nasal and systemic antiviral immune responses in Rainbow trout. *J.*
446 *Immunol.* *199*, 3900-3913.

447 Sofroniew, M.V., Howe, C.L., and Mobley, W.C. (2001). Nerve growth factor signaling, neuroprotection,
448 and neural repair. *Annu. Rev. Neurosci.* *24*, 1217-1281.

449 Sun, J., Liu, Y., and Aballay, A. (2012). Organismal regulation of xbp-1-mediated unfolded protein response
450 during development and immune activation. *EMBO Rep.* *13*, 855-860.

451 Tacchi, L., Larragoite, E., and Salinas, I. (2013). Discovery of J Chain in African Lungfish (*Protopterus dolloi*,
452 *Sarcopterygii*) Using High Throughput Transcriptome Sequencing: Implications in Mucosal Immunity. PLoS
453 One 8, e70650.
454 Tacchi, L., Musharrafieh, R., Larragoite, E.T., Crossey, K., Erhardt, E.B., Martin, S.A., LaPatra, S.E., and
455 Salinas, I. (2014). Nasal immunity is an ancient arm of the mucosal immune system of vertebrates. Nat.
456 Commun. 5, 6205.
457 Takizawa, F., Dijkstra, J.M., Kotterba, P., Korytář, T., Kock, H., Köllner, B., Jaureguiberry, B., Nakanishi, T.,
458 and Fischer, U. (2011). The expression of CD8 α discriminates distinct T cell subsets in teleost fish. Dev.
459 Comp. Immunol. 35, 752-763.
460 Westerfield, M. (2000). The Zebrafish Book. A Guide for the Laboratory Use of Zebrafish *Danio**
461 (*Brachydanio*) rerio. (Eugene, OR.: University of Oregon Press.).
462 Wiesmann, C., Ultsch, M.H., Bass, S.H., and de Vos, A.M. (1999). Crystal structure of nerve growth factor
463 in complex with the ligand-binding domain of the TrkA receptor. Nature 401, 184.
464 Zhang, Y.-A., Salinas, I., Li, J., Parra, D., Bjork, S., Xu, Z., LaPatra, S.E., Bartholomew, J., and Sunyer, J.O.
465 (2010). IgT, a primitive immunoglobulin class specialized in mucosal immunity. Nat. Immunol. 11, 827-
466 835.
467 Zhang, Y., Lu, H., and Bargmann, C.I. (2005). Pathogenic bacteria induce aversive olfactory learning in
468 *Caenorhabditis elegans*. Nature 438, 179-184.

469

470 **Figure legends:**

471 Figure 1: Nasal delivery of neurotropic virus induces caspase-3 dependent apoptosis to TrkA+
472 crypt neurons

473 Immunofluorescence microscopy image of rainbow trout olfactory organ cryosections (A) Control
474 and (B) 15 min after nasal IHNV delivery stained with anti-TrkA (FITC, green) show a decrease
475 in the number of TrkA⁺ crypt neurons following IN delivery of IHNV. Nuclei were stained with
476 nuclear stain DAPI (blue). Confocal microscopy images of rainbow trout olfactory organ
477 cryosections (C) Control and (D) 15 min after nasal IHNV delivery stained with anti-TrkA (FITC,
478 green) showing changes in TrkA reactivity with the characteristic morphology of cell apoptosis in
479 TrkA⁺ cells following IN delivery of IHNV. Cell nuclei were stained with DAPI (blue). Scale bar,
480 20 μ m. Immunofluorescence staining of an IHNV-vaccinated rainbow trout olfactory organ with
481 anti-TrkA (FITC, green) (E) and anti-caspase 3 (Cy5, magenta) (F) showing co-localization of
482 caspase-3 staining in low-TrkA⁺ crypt neurons. Scale bar, 20 μ m. Cell nuclei were stained with
483 DAPI DNA stain (blue). Results are representative of three independent experiments (N = 5) L,
484 lumen; LP, lamina propria. Semithin sections of control (G) and nasal IHNV treated (H) rainbow
485 trout olfactory organ indicate that crypt neurons undergo cell death within 15 min of viral delivery.
486 Scale bar A-H, 20 μ m. Transmission electron micrograph showing a crypt neuron in control trout
487 olfactory epithelium (I) and a crypt neuron undergoing cell death in nasal IHNV treated rainbow

488 trout 15 min after nasal vaccination (**J**). Scale bar, 2 μm . (**K**) Schematic diagram of the
489 experimental design used in TrkA-blocking experiment. AG879 (TrkA blocker) or vehicle were
490 delivered IN and 30 min later IHNV or PBS (control) were delivered to the nasal cavity of trout.
491 OO and OB were collected 15 min after IHNV delivery. (**L**) Quantification of the mean number
492 of TrkA⁺ crypt neurons in control and nasal IHNV treated rainbow trout olfactory organ 15 min,
493 1 h, 1 day and 4 days after nasal viral delivery showing that TrkA reactivity begins to recover on
494 day 4 as measured by immunofluorescence microscopy (N = 3). Results are expressed as mean \pm
495 SEM. Unpaired *t*-test **p* < 0.05, ***p* < 0.01. (**M**) AG879 pre-treatment partially abolishes loss of
496 IHNV-induced TrkA reactivity in crypt neurons (N = 3). Results are expressed as mean \pm SEM
497 and statistical. One-way ANOVA and a Tukey post hoc analysis test were performed to identify
498 statistically significant differences among groups. *P* < 0.05.

499

500 Figure 2: Rainbow trout smell neurotropic virus

501 (**A**) Olfactory responses to live attenuated IHNV and medium where the virus was grown (negative
502 control) produce different dose-response curves in rainbow trout measured by electro-olfactogram
503 (EOG). Responses were normalized to the L-Serine control. Data are represented as the mean \pm
504 SEM (N = 8). (**B**) Live attenuated IHNV activates a set of receptors different than those activated
505 by virus-free supernatants (negative control). Cross-adaptation experiments compared olfactory
506 responses to live attenuated IHNV (self-adapted control, SAC) or a mix of live attenuated and the
507 virus-free supernatant (Mix IHNV-M) when the olfactory epithelium was saturated with live
508 attenuated IHNV (adapted stimuli) odors. Same experiments were performed using the IHNV
509 culture medium as adapted stimuli. Paired *t*-test showed significant differences (*p* < 0.05) between
510 both SAC and Mix. (**C**) AG879 treatment results in stronger inhibition of olfactory responses in
511 live attenuated IHNV than in virus-free supernatant (**D**). Pharmacological inhibition of olfactory
512 responses was total at concentrations of the drug $>10^{-5}$ M. Paired *t*-test showed significant
513 differences (*p* < 0.05) between EC₅₀.

514

515 Figure 3: Nasal IHNV delivery activates sensory neurons in the OO and OB in a TrkA-dependent
516 manner.

517 Immunofluorescence staining of control rainbow trout OO (A) and OB (B) cryosections stained
518 with anti-pERK (FITC, green) showing absence of neuronal activation. Immunofluorescence

519 staining of OO (C) and OB (D) cryosections of trout nasally treated with IHNV stained with anti-
520 pERK antibody (FITC, green) showing neuronal activation 15 min after viral delivery.
521 Immunofluorescence staining rainbow trout OO (E) and OB (F) treated with AG879 + IHNV with
522 anti-pERK showing AG879 inhibition of viral-induced neuronal activation in both OO and OB.
523 Scale bar, 10 μ m. For (A-F), cell nuclei were stained with DAPI DNA stain. (G) Gene expression
524 levels of *c-fos* (neuronal activation marker) in control, nasal IHNV treated, AG879 only treated
525 and IHNV + AG879 groups as measured by RT-qPCR. Gene expression levels were normalized
526 to the housekeeping gene EF-1a and expressed as the fold-change compared to the control group
527 using the Pfaffl method. Results are representative of three independent experiments (N = 5).
528 Results were analyzed by unpaired t-test *p < 0.05, **p < 0.01.

529
530 Figure 4: Viral nasal delivery results in ultra-rapid immune responses in the OO and OB of rainbow
531 trout in a TrkA-dependent manner.

532 (A) Gene expression levels of the chemokine *ck10* (CCL19-like), *ptgs2b*, *ifng* and *tnfa* in OO and
533 OB in of control, IHNV-treated, AG879 treated and AG879 + IHNV treated trout. Gene expression
534 levels were measured by RT-qPCR and normalized to the housekeeping gene *ef1a*. Data are
535 expressed as the mean fold change compared to the control group using the Pfaffl method. Results
536 are representative of three different experiments (N = 5). Results were analyzed by unpaired t-test
537 *p < 0.05. (B) Representative dot plots of control and IHNV-treated rainbow trout PBLs stained
538 with mouse anti-trout IgM, mouse anti-trout IgT and rat anti-trout CD8 α showing the mean
539 percentage of positive cells from the lymphocyte gate. (C) Representative dot plots of control and
540 IHNV, AG879 and AG879 + IHNV trout OO lymphocytes stained with mouse anti-trout IgM,
541 mouse anti-trout IgT and rat anti-trout CD8 α showing the mean percentage of positive cells from
542 the lymphocyte gate. (D) Quantification of flow cytometry data in (B) indicating no significant
543 changes in the percentage of IgM⁺, IgT⁺ and CD8 α ⁺ cells in PBLs 15 min after nasal IHNV
544 delivery. Results are representative of three independent experiments (N = 5). NS = not significant.
545 (E-G) Quantification of flow cytometry data shown in (C) indicating significant decrease in the
546 percentage of IgT⁺ B cells and increase in the percentage of CD8 α ⁺ T cells in the OO 15 min after
547 nasal IHNV delivery and inhibition of such responses when AG879 is administered 30 min before
548 IHNV treatment. Results are representative of three different experiments (N = 5). One-way
549 ANOVA and a Tukey post hoc analysis test were performed to identify statistically significant

550 differences among groups. * $p < 0.05$, ** $p < 0.01$. **(H-J)** Immunofluorescence staining of a control
551 **(H)** IHNV only **(I)** and AG879+IHNV **(J)** rainbow trout OO cryosection stained with anti-CD8 α
552 (FITC, green). Scale bar, 10 μm . Cell nuclei were stained with DAPI DNA stain. L, lumen; LP,
553 lamina propria.

554

555 Figure 5: CD8 α T cells infiltrating the trout OO originate from the OB microvasculature but not
556 from peripheral blood.

557 **(A)** Representative dot plots of control and IHNV-treated trout of cells obtained from the OB
558 microvasculature showing the percentage of cells within the lymphocyte gate in each group. **(B)**
559 Representative dot plots of cells obtained from the OB microvasculature of control and IHNV-
560 treated rainbow trout stained with mouse anti-trout IgM, mouse anti-trout IgT and rat anti-trout
561 CD8 α showing the mean percentage of positive cells within the lymphocyte gate. **(C)**
562 Quantification of flow cytometry data presented in **(A)** showing a significant decrease in the
563 percentage of cells within the lymphocyte gate in IHNV-treated group compared to controls. **(D)**
564 Quantification of flow cytometry data shown **(B)** indicating a significant decrease in the percentage
565 of CD8 α^+ in the OB microvasculature 15 min after nasal IHNV delivery. Results are representative
566 of three different experiments (N = 5). Results were analyzed by unpaired t-test NS = not
567 significant.

568

569 Figure 6: The interaction between viral glycoprotein (G protein) and crypt neuron TrkA is
570 necessary for inducing crypt neuron-mediated nasal immune responses in trout.

571 **(A)** Multiple sequence alignment (performed with CLUSTALW <http://align.genome.jp/>) of
572 rainbow trout, mouse and human TrkA domain 5 (domain known to interact with cognate ligand)
573 showing conservation of aa at sites previously described to be critical for NGF binding to TrkA.
574 **(B)** Nasal delivery of recombinant IHNV G protein recapitulates IHNV-induced changes in crypt
575 neurons and CD8 T cell immune responses. Immunofluorescence staining of trout olfactory
576 organs 15 min after receiving PBS or 100 ng of recombinant FLAG-tagged IHNV G protein
577 intranasally stained with anti-TrkA (FITC, green), anti-FLAG (Cy3, magenta) and DAPI (blue)
578 showing the co-localization of TrkA and IHNV G protein in the FLAG-tagged IHNV G protein
579 delivered group but not controls. **(C)** Quantification of the mean number of TrkA $^+$ crypt neurons
580 in the OO of control trout and trout that received recombinant FLAG-tagged IHNV G protein IN

581 (N = 3). **(D)** Quantification of the mean number of CD8 α^+ T cells in control and FLAG-tagged
582 IHNV G protein treated rainbow trout OO (N = 3) by immunofluorescence microscopy. **(E)** *In*
583 *vivo* antibody blocking of IHNV G protein reverts IHNV-induced changes in crypt neurons and
584 CD8 T cell immune responses. Live attenuated IHNV was incubated with anti-IHNV G protein
585 monoclonal antibody, anti-IHNV N protein monoclonal antibody or not treated for 30 min at RT
586 prior to *in vivo* nasal delivery. Quantification of the mean number of TrkA $^+$ crypt neurons by
587 immunofluorescence microscopy in control, anti-G protein antibody treated + IHNV, anti-N
588 protein antibody treated IHNV and IHNV alone in the OO of rainbow trout (N = 3). **(F)**
589 Quantification of the mean number of CD8 α^+ T cells by immunofluorescence microscopy in the
590 OO of control, anti-G protein antibody treated + IHNV, anti-N protein antibody treated IHNV and
591 IHNV-treated rainbow trout (N = 3). Results are representative of two independent experiments
592 (N = 3). One-way ANOVA and a Tukey post hoc analysis test were performed to identify
593 statistically significant differences among groups. * $p < 0.05$, ** $p < 0.01$.

594

595 Figure 7: Ablation of crypt neurons results in increased susceptibility to rhabdoviral infection in
596 zebrafish.

597 **(A)** Schematic representation of the generation of *ora4* transgenic zebrafish and ablation of crypt
598 neurons by delivery of the prodrug metronidazole (Mtz) into the water for 24 h. **(B-CD)** Expression
599 of CCL19-like in whole zebrafish larvae 15 min after infection with SVCV as measured by RT-
600 qPCR. Each symbol represents a pool of 10 larvae. Results are expressed as the fold-change in
601 expression compared to uninfected controls. Expression levels were normalized to the *rps11* as
602 house-keeping gene. Data are expressed as the mean fold change compared to the control group
603 using the Pfaffl method. Results are representative of three different experiments (N = 5). Results
604 were analyzed by unpaired t-test. **(E)** Relative SVCV viral loads as measured by N protein
605 expression levels 15 min and 2 days after SVCV infection in ORA4 $^+$ zebrafish and ORA4 $^+$ + Mtz
606 (ablated) zebrafish. Each symbol represents a pool of 10 larvae. Results are expressed as mean
607 level of N protein expression measured by RT-qPCR compared to uninfected controls. ND: non-
608 detectable. P-values were obtained by unpaired t-test **(F)** Percent survival of wildtype (ORA4-)
609 and transgenic (ORA4+) zebrafish larvae that were ablated (+ Mtz) or not in response to SVCV
610 infection. Results are representative of two independent experiments (N = 30 per group). Statistical
611 analysis was performed by Gehan-Breslow-Wilcoxon method ($p < 0.05$).

612
613
614

615 **STAR METHODS**

616 **Animals, nasal delivery of virus and tissue sampling**

617 All rainbow trout studies were reviewed and approved by the Institutional Animal Care and Use
618 Committee (IACUC) at the University of New Mexico, protocol number 16-200384-MC. For nasal
619 delivery of virus studies, rainbow trout (mean weight of 50-150 g) received 30 µl of live attenuated
620 infectious hematopoietic necrosis virus (IHNV) (2×10^8 PFU/ml) or phosphate buffer saline (PBS)
621 in each nare. For TrkA blocking experiment, rainbow trout (N = 20) received 30 µl of 10 µM
622 AG879 or vehicle 30 min before viral delivery as described in diagram (Figure 1K). Olfactory
623 Organ (OO) and olfactory bulbs (OB) were snap frozen and cryoblocks used for immunostaining
624 or kept in RNAlater for gene expression studies.

625 Zebrafish (*Danio rerio* H.) were obtained from the Zebrafish International Resource Center
626 and mated, staged, raised and processed as described (Westerfield, 2000). The line *Tg(UAS-*
627 *E1b:nfsb-mCherry)*^{c264} was previously reported (Davison et al., 2007) The experiments performed
628 comply with the Guidelines of the European Union Council (Directive 2010/63/EU) and the
629 Spanish RD 53/2013. Experiments and procedures were performed as approved by the Bioethical
630 Committees of the University of Murcia (approval numbers #537/2011, #75/2014 and #216/2014).

631 **Electrophysiological recordings**

632 Rainbow trout were anesthetized in a solution of MS222 at 0.1 g/l, and then immobilized with an
633 intra-muscular injection of gallamine triethiodide (3 mg/kg of body weight, in 0.9% saline). Fish
634 were then secured in a V-shape Plexiglas stand partially inundated, whereby gills could be
635 continuously irrigated with aeriated anesthetic solution of MS222 at 0.05 g/l. The olfactory rosette
636 was surgically exposed and borosilicate electrodes, filled with a solution of 3 M KCL in 0.4% agar
637 and connected to solid state electrodes with Ag/AgCl pellets, were placed between olfactory
638 lamellae (signal electrode) and external skin (reference electrode). The olfactory epithelium was
639 continuously irrigated with tap charcoal filtered water and the stimulus was released directly into
640 the nose through a borosilicate tube. The olfactory responses generated after release of the stimuli

641 for 4 s were filtered and amplified by a NeuroLog DC filter and pre-amplifier integrated by an
642 Axon Digidata 1550B, and stored on a PC running Axoscope 10.6 software.

643 *Dose response experiments.* Stimuli were serially diluted from a 1:100 to 1:1000 000 from a stock
644 solution, and applied to the nose to measure amplitude of the olfactory responses. These responses
645 were blank subtracted (i.e. the response to tap charcoal filtered water) and normalized to those of
646 *L*-serine at 10^{-5} M. IHNV stock was a vaccine solution with inactivated IHNV at 2×10^8 PFU and
647 culture medium stock was the supernatant of the vaccine after being centrifuged at 50000 rpm for
648 20 min at 5 °C.

649 *Cross-adaptation experiments.* We identified dilutions of IHNV and medium that evoked the same
650 EOG amplitude (called the ‘unadapted’ response). Then the olfactory rosette was continually
651 exposed to IHNV solution at the concentration of the unadapted response at least 1 min, and the
652 response to a sample at double concentration of unadapted response IHNV was recorded (called
653 the self-adapted control, SAC). After that, the response to a mixture IHNV and medium, both at
654 same concentration that unadapted response, was recorded (Mix). Both measures, Mix and SAC,
655 were then calculated as a percentage of the unadapted response. After adaptation, the olfactory
656 rosette was flushed with charcoal filtered water for 20 min, and the process repeated using medium
657 as the adapting solution and IHNV or the mixture IHNV and medium as stimuli. Half of the fish
658 were adapted first to IHNV and the other half first to control.

659 *Inhibition curves.* Responses to 1:1000 to IHNV or medium were recorded (both showed similar
660 amplitude in their olfactory responses). Then the olfactory rosette was continuously exposed to
661 increasing concentrations of AG879 from 10^{-9} M to 10^{-5} M and, under each adapting concentration
662 of the drug, it was measured the olfactory responses to 1:1000 of IHNV or medium. Responses
663 were calculated as ratio between 1:1000 odorant after adaptation to drug solution and 1:1000
664 odorant before adapted to drug. All graphs were produced with Sigma plot 11.0 and EC50
665 concentrations were calculated using the Pharmacology module of the same program.

666 **Histology, transmission electron microscopy and immunofluorescence microscopy**

667 For transmission electron microscopy (TEM), the OO (N = 3) of rainbow trout that had received
668 live attenuated IHNV IN 15 min prior to sampling were fixed overnight at 4 °C in 2.5 % (v/v)
669 glutaraldehyde in PBS, then transferred to 1 % osmium tetroxide (w/v) in PBS for 2 h at 4 °C.

670 After washing in PBS (3 times, 10 min), samples were dehydrated in a graded series of ethanol
671 (10–100 %) through changes of propylene oxide. Samples were then embedded in Epon resin,
672 sectioned and stained with uranyl acetate and lead citrate before being examined in a PHILIPS
673 TECNAI 12 transmission-electron microscope. Additionally, semithin sections were stained with
674 toluidine blue. The conjugated antibodies used for immunostaining are listed in the **Key Resources**
675 **Table**. Trout OO and OB were snap frozen in OCT and 5- μm -thick cryosections were fixed in
676 4% paraformaldehyde for 3 min, blocked and labeled with rat anti-trout CD8 α (1:50 dilution),
677 anti- pERK (1:50 dilution), anti-human TrkA (1:100 dilution) and rabbit anti-mouse caspase 3
678 (1:100 dilution) antibody for immunostaining. Nuclei were stained with DAPI. Samples were
679 observed under a Nikon Ti or Zeiss confocal microscopes. To test the permeability of BBB 15 min
680 after nasal viral delivery, 50 μl of FITC-conjugated 10 kDa dextran particles in PBS were injected
681 i.v into 10 g rainbow trout (N = 6) 1 hour before sampling. Trout then received IHNV or PBS IN
682 and 15 min later, trout heads were snap frozen, embedded in OCT and cryosections were examined
683 for fluorescence microscopy.

684 **Western blot, cell isolation and flow cytometry**

685 The conjugated antibodies used for western blot and Flow cytometry are listed in the **Key**
686 **Resources Table**. Olfactory Organ (OO), head kidney (HK), and brain (B) were extracted and
687 prepared for Western blotting as explained elsewhere (Sepahi et al., 2016b). Briefly, tissues were
688 lysed in RIPA buffer and 10 μl of lysed tissues were mixed with 10 μl of Laemmli buffer under
689 non-reducing conditions. Samples were boiled for 3 min at 97 °C and resolved on 4–15% SDS-
690 PAGE gels. Gels were run for 50 min at 120 V and transferred onto PVDF membranes. Membranes
691 were blocked in PBS-T containing 5% non-fat milk overnight at 4 °C. Membranes were incubated
692 with anti-TrkA (1:1000) for 90 min, washed three times in PBS-T and then incubated for 60 min
693 with HRP-anti-rabbit IgG (1:2500). Detection was performed using ECL Western Blotting
694 Substrate. Immunoblots were scanned using a ChemiDoc Touch Imaging System and band
695 densitometry was analyzed with Image Lab Software.

696 Isolation of trout OO cells was carried out as explained elsewhere (Tacchi et al., 2014). Briefly,
697 trout OO were obtained by means of mechanical agitation of both olfactory rosettes in DMEM
698 medium (supplemented with 5% FBS, 100 U/ml penicillin and 100 $\mu\text{g}/\text{ml}$ streptomycin) at 4 °C
699 for 30 min. Leukocytes were collected, and the aforementioned procedure was repeated four times.

700 Thereafter, the OO pieces were treated with PBS (containing 0.37 mg/ml EDTA and 0.14 mg/ml
701 dithiothreitol) for 30 min followed by enzymatic digestion with collagenase (0.15 mg/ml) for 2 h
702 at 20 °C. All cell fractions obtained the OO following the mechanical and enzymatic treatments
703 were pooled, washed with modified DMEM. OB microvessels were extracted then 40 µl of DMEM
704 containing heparin were added to the cavity to collect the remaining blood from the microvessels.
705 This step was repeated twice. Cells were isolated by forcing the tissue through a 100-µm pore
706 nylon cell strainer and washed in DMEM three times. Cell suspensions were counted in a
707 haemocytometer and stained with CD8α, IgM and IgT antibodies as explained elsewhere (Sepahi
708 et al., 2016a). After washing, a total of 30,000 cells were recorded using an Attune NxT flow
709 cytometer. The percentage of CD8α⁺, IgM⁺ and IgT⁺ cells was quantified as the percentage of
710 FITC⁺ cells within the lymphocyte gate using their FSC/SSC profile.

711

712 **Gene expression analysis by real-time quantitative PCR**

713 Total RNA from OO and OB samples were collected and placed in 1 ml TRIzol for RNA extraction
714 according to the manufacturer's instructions. cDNA synthesis was performed as explained
715 elsewhere (Sepahi et al., 2016b). The resultant cDNA was stored at -20 °C. The expression of
716 *pgs2b*, *IFN-γ*, *TNFα*, *CK10* (CCL19-like) and *c-fos* for rainbow trout and *CCL19-like* and *SVCV*
717 N protein for zebrafish were measured by RT-qPCR using specific primers (**Key Resources**
718 **Table**). The qPCR was performed using 3 µl of a diluted cDNA template as described in (Tacchi
719 et al., 2013). The relative expression level of the genes was determined using the Pfaffl method
720 (Pfaffl, 2001) as previously described (Tacchi et al., 2013).

721 **DNA constructs and generation of transgenic zebrafish larvae**

722 Three kb of the upstream regulatory sequence of the *ora4* gene, which includes its 5'UTR
723 (Ensembl accession number ENSDARG00000078223) was amplified using PfuUltra II Fusion HS
724 DNA Polymerase, the primers 5'-aaggtaccgtgaatgcgtgtgtgatg-3 and 5'-
725 aaaggatccgctgaagatgctccagagtcc-3, and zebrafish larval genomic DNA as template. The amplicon
726 was digested with *KpnI/BamHI*, cloned in the p5E-MCS vector (#228) of the Tol2kit and the
727 *ora4::Gal4VP16* construct were then generated by MultiSite Gateway assemblies using LR
728 Clonase II Plus according to standard protocols and using Tol2kit vectors described previously
729 (Kwan et al., 2007).

730 The lines *Tg(ora4::Gal4VP16)^{ums4}* were generated by microinjecting 0.5-1 nl into the yolk
731 sac of one-cell-stage embryos a solution containing 100 ng/μl *ora4::Gal4VP16* construct and 50
732 ng/μl Tol2 RNA in microinjection buffer (0.5x Tango buffer and 0.05 % phenol red solution) using
733 a pneumatic microinjector .

734 **Cell ablation and live imaging of zebrafish larvae**

735 The lines *Tg(UAS-E1b:nfsb-mCherry)^{c264}* and *Tg(ora4::Gal4VP16)^{ums4}* were crossed.
736 Their offspring were treated at 48 h post-fertilization (hpf) for 24 h with 12 mM metronidazole
737 and kept in dark (Davison et al., 2007). Images were first obtained at 48 hpf as described below.
738 Thereafter, starting from 72 hpf the prodrug was removed, and larvae imaged once a day up to 120
739 hpf to confirm the ablation of *ora4*⁺ crypt neurons.

740 For live imaging, larvae were anesthetized in tricaine as previously described (Galindo-
741 Villegas et al., 2012). Images were captured with an epifluorescence MZ16FA stereomicroscope
742 (Leica) equipped with green and red fluorescent filters while animals were kept constantly at
743 28.5°C.

744 **Viral challenge in zebrafish**

745 The SVCV isolate 56/70 was propagated in EPC cells and titrated in 96-well plates. Thirty
746 72 hpf zebrafish larvae per group in triplicate were challenged for 24 h at 25°C in disposable Petri
747 dishes by immersion in 10⁸ TCID₅₀/fish SVCV. After challenge, the remaining fish in each group
748 were transferred to fresh plates containing egg water and monitored every 12 h over a 6-day period
749 to score mortality (López-Muñoz et al., 2010).

750 **Statistical analysis**

751 Results are expressed as the mean ± SE. Data analysis was performed in GraphPad Prism version
752 5.0. The RT-qPCR measurements were analyzed by *t*-test to identify statistically significant
753 differences between groups. One-way ANOVA and a Tukey post hoc analysis test were performed
754 to identify statistically significant differences among groups. Statistical analysis for survival assay
755 was carried out using PRISM 7 for Mac OS X (GraphPad). Gehan-Breslow-Wilcoxon method was
756 performed following a log-rank test and confirmed with Kaplan-Meier curve to ensure

757 compatibility and avoid deviations due a lack of proportional hazard. P-value of < 0.05 was
758 considered statistically significant.

759 **Contact for reagent and resource sharing**

760 Further information and requests for resources and reagents should be directed to and will be
761 fulfilled by the Lead Contact, Irene Salinas (isalinas@unm.edu)

762

763

764 **Supplemental Figure legends**

765 Supplementary Fig. 1: (A) Detection of TrkA in trout OO and brain but not HK lysates by
766 immunoblotting. Immunoblots detecting TrkA showed a band at the expected size (~140 KDa) in
767 OO and brain. (B) Immunofluorescence staining of control rainbow trout HK cryosection stained
768 with anti-TrkA antibody (FITC, green) confirming absence of TrkA⁺ cells. Cell nuclei were stained
769 with DAPI DNA stain (blue). Scale bar: 20 μ m.

770 Supplementary Fig. 2: IHNV activates sensory neurons in the OO *in vitro* (A) Representative dot
771 plots of control (left) and IHNV (right) trout OO extracted cells stained with anti-pERK antibody
772 showing the mean percentage of positive cells. (B) Quantification of flow cytometry data in (A)
773 indicating a significant increase in the percentage of pERK⁺ cells 15 min after adding IHNV
774 (multiplicity of infection 1:3) *in vitro*. Results are representative of three independent experiments
775 (N = 5). *p < 0.05

776 Supplementary Fig. 3: Nasal delivery of IHNV does not result in presence of virus in the OB and
777 does not alter BBB integrity 15 min after delivery. (A) Immunofluorescence staining with anti-
778 IHNV Abs (Cy3, red) showing no IHNV staining in the OO of control rainbow trout. (B)
779 Immunofluorescence staining with anti-IHNV Abs (Cy3, red) showing the presence of IHNV (red
780 arrows) in the OO of IHNV treated rainbow trout 15 min after nasal delivery. (C)
781 Immunofluorescence staining with anti-IHNV Abs (Cy3, red) showing no detection of IHNV at
782 OB of control rainbow trout. (D) Immunofluorescence staining with anti-IHNV Abs (Cy3, red)
783 showing the absence of IHNV in the OB of IHNV treated rainbow trout 15 min after nasal delivery.
784 Scale bar, 20 μ m. (E-H) Intravenous injection of FITC- conjugated dextran showing that no

785 changes in the BBB integrity in IHNV-treated fish as demonstrated by the absence of FITC
786 staining in the OB. Scale bar: 100 μ m.

787 Supplementary Fig. 4: Leukocyte recruitment occurs as early as 15 min after IHNV delivery as
788 visualized by enlargement lamina propria (LP) of the olfactory lamellae of IHNV-treated
789 compared to control fish. (A) Immunofluorescence staining of control (left) and IHNV-treated
790 (right) rainbow trout OO stained with anti-trout TrkA (FITC, green) showing our image analysis
791 strategy and the enlargement in the apical and medial regions of the LP in the IHNV-treated fish.
792 Cell nuclei were stained with DAPI DNA stain (blue). Results are representative of two different
793 experiments (N = 3). Scale bar, 20 μ m. (B) The width of LP at the apical (100 μ m from the lamellar
794 tip) and lateral (250 μ m from the lamellar tip) regions of the olfactory lamella were measured by
795 image analysis of 10 individual lamellae from three different fish per treatment. The mean distance
796 \pm SE is shown. (C) Representative hematoxylin-eosin stain of adult rainbow trout olfactory organ
797 showing Leukocyte recruitment occurs as early as 15 min after IHNV delivery of the olfactory
798 lamellae of IHNV-treated (middle and right) compared to control fish (left). L, lumen; LP, lamina
799 propria. Scale bar: 50 μ m.

800 Supplementary Fig. 5: A low degree of amino acid conservation between IHNV G protein and
801 HSV secreted G protein indicated. (A) Amino acid sequence alignment of HSV-2 sG protein
802 (accession number GD_HHV23) and trout IHNV G protein (sequenced obtained from the live
803 attenuated IHNV used in this study) performed in CLUSTALW showing a low degree of amino
804 acid conservation (B) Production of recombinant FLAG-tagged IHNV G protein by mammalian
805 expression system. Immunoblot using anti-Flag antibody confirmed the presence of the
806 recombinant protein (IHNV G protein) band at expected (~50 KDa) molecular weight.

807

808

809

810

811

812

813

814

REAGENT or RESOURCE	SOURCE	IDENTIFIER
Antibodies		
Trk A anti-rabbit polyclonal IgG	Santa Cruz Biotechnology	Cat# sc-118 RRID:AB_632556
Caspase-3 anti-rabbit polyclonal IgG	Abcam	Cat# ab13847 RRID:AB_443014
Cy3 AffiniPure Goat anti-rabbit IgG (H+L)	Jackson ImmunoResearch	Cat# 111-165-144 RRID:AB_2337913
Phospho-p44/42 MAPK(ERK1/2) anti-rabbit polyclonal IgG	Cell signaling	Cat# 9101 RRID:AB_331646
FITC affiniPure donkey anti-rat IgG	Jackson ImmunoResearch	Cat#712-095-153 RRID:AB_2340655
FITC donkey anti-rabbit IgG	Jackson ImmunoResearch	Cat# 115-165-003 RRID:AB_2340598
Rat anti-trout CD8 α polyclonal IgG	(Takizawa et al., 2011)	
Rabbit anti-trout IgT	(Zhang et al., 2010)	
Mouse anti-trout IgM	(Zhang et al., 2010) (1.14)	
Mouse anti-IHNV mAb	(Sepahi et al., 2016a)	Pool of anti-IHNV mAbs containing mAbs 1H8, 6A7, and 5AG (2 mg/ml)
Cy3 anti-mouse IgG	Jackson ImmunoResearch	Cat# 715-165-150 RRID:AB_2340813
Peroxidase AffiniPure Donkey Anti-Rabbit IgG (H+L)	Jackson ImmunoResearch	Cat# 711-035-152 RRID:AB_10015282
Mouse anti-FLAG M2 IgG	Sigma	Cat# F3165 RRID: AB_259529
Monoclonal ANTI-FLAG [®] M2-Cy3 [™] antibody produced in mouse	Sigma	Cat# A9594 RRID: AB_439700
murine mAb: anti-Infectious hematopoietic necrosis virus G (anti-IHNV G)	EVAg	Cat# 015A-01754
murine mAb: anti-Infectious hematopoietic necrosis virus N (anti-IHNV N)	EVAg	Cat# 015A-01753
Bacterial and Virus Strains		

Live attenuated infectious haematopoietic necrosis virus (IHNV)	(Ristow et al., 2000)	Passaged from IHNV Strain 220-90
Spring Viremia Carp Virus (SVCV)	(Galindo-Villegas et al., 2012)	Strain 56/70
Biological Samples		
Triploid female rainbow trout adult olfactory organ, olfactory bulb, blood	Lisboa Springs hatchery, New Mexico	
Zebrafish larvae (entire organism)	ZIRC, Oregon , USA	
pcDNA3.1-IHNV expression plasmid	This paper	
FreeStyle 293-F cells and expression system	ThermoFisher	Cat# R79007
Chemicals, Peptides, and Recombinant Proteins		
Ampicillin	Sigma Aldrich	Cat# 69-52-3
L-Serine	Acros Organics	Cat# 132660250
Ethyl 3-aminobenzoate methanesulfonate salt (MS-222)	Sigma Aldrich	Cat# 886-86-2
Gallamine triethiodide	Sigma Aldrich	Cat# G8134-25G
RNAlater	Ambion	Cat# AM7021
Paraformaldehyde	Sigma Aldrich	Cat# 30525-89-4
Absolute Blue qPCR SYBR Green ROX Mix	Thermo Scientific	Cat# AB4162B
2-(4-Amidinophenyl)-6-indolecarbamide dihydrochloride (DAPI)	Sigma Aldrich	Cat# 28718-90-3
TRIzol™ Reagent	Thermo Scientific	Cat# 15596018
Tyrphostin AG879	Sigma Aldrich	Cat# 148741-30-4
Tyrphostin AG879	Cayman Chemical	Cat# 10793
SuperScript™ III First-Strand Synthesis System	Thermo Scientific	Cat# 18080051
Fluorescein isothiocyanate–dextran	Sigma	Cat# FD10S
DMEM high glucose	Gibco	Cat# 11995040
Fetal bovine serum	Hyclone	Cat# SH30071.03
Penicillin-Streptomycin (10,000 U/mL)	Gibco	Cat# 15140122
StartingBlock™ T20 (TBS) Blocking Buffer	ThermoFisher	Cat# 37543
Metronidazole	Sigma-Aldrich	Cat# M3761
PfuUltra II Fusion HS DNA Polymerase	Agilent	Cat# 600670
Anti-FLAG M2 Magnetic Beads	Sigma	Cat# M8823 RRID:AB_2637089
3X-FLAG peptide	Sigma	Cat# F4799

Recombinant IHNV glycoprotein	This paper	N/A
Gallamine triethiodide	Sigma Aldrich	Cat# G8134-25G
Potassium chloride	Acros Organics	Cat# 196770010
Agar	VWR	Cat# J637
Critical Commercial Assays		
Gateway™ LR Clonase™ II Enzyme mix	ThermoFisher Scientific	Cat# 11791100
GenElute™ Single Cell RNA Purification Kit	Sigma Aldrich	Cat# RNB300
Deposited Data		
Experimental Models: Cell Lines		
Experimental Models: Organisms/Strains		
Triploid female adult rainbow trout	Lisboa Springs Hatchery (Pecos, NM)	N/A
Wild type zebrafish strains AB	Zebrafish International Resource Center	ZFIN:ZDB-GENO-960809-7
Zebrafish: <i>Tg(UAS-E1b:NTR-mCherry)^{c264}</i>	Zebrafish International Resource Center	ZFIN ID: ZDB-ALT-070316-1
Zebrafish: <i>Tg(ora4:gal4)</i>	This paper	N/A
Oligonucleotides		
<i>flag-ihnv</i> , primers AATAGGTACCGCCATGGATTACAAGGATGACGAC GATAAGGACACCACGATCACCCTCCGCTC (forward) and AATACTCGAGCTAGTGGAGTGATTGAAGGTCGAA TGAG (reverse)	This paper	N/A
<i>ef-1a</i> , primers CAACGATATCCGTCGTGGCA (forward) and ACAGCGAAACGACCAAGAGG (reverse)	N/A	N/A
<i>ck10</i> , primers GGCCAGATGGTGTGGACTGTG (forward) and GGTAGTGAAGACCACAGCGCTG (reverse)	N/A	N/A
<i>lfnγ</i> , primers GCTGTTCAACGGAAAACCTGTTT (forward) and TCACTGTCCTCAAACGTG (reverse)	N/A	N/A
<i>c-fos</i> , primers CGTCCTTCATCCCTACTGTTACC (forward) and TGTTCCATTTTGCCTCTGC (reverse)	N/A	N/A

<i>tnfa</i> , primers GGGGACAAACTGTGGACTGA (forward) and GAAGTTCTTGCCCTGCTCTG (reverse)	N/A	N/A
<i>ZF rps11</i> , primers CCCAGAGAAGCTATTGATGGC (forward) and CCCATGCTTCAGGGATGTGA (reverse)	N/A	N/A
<i>svcv (N protein)</i> , primers ATCAGGCCGATTATCCTTCCA (forward) and AGATAAGCATTACATGCTGTAT (reverse)	N/A	N/A
<i>ZF ccl19-like</i> , primers GCCCACGTGATGCTGTAATA (forward) and ACAGCGTCTCTCGATGAACC (reverse)	N/A	N/A
Software and Algorithms		
GraphPad Prism version 5.0 & 7.0	GraphPad	https://www.graphpad.com/scientific-software/prism/ RRID:SCR_002798
Sigma Plot version 11	Systat Software Inc	https://systatsoftware.co
Axoscope 10.6	Axon Instruments	https://www.moleculardevices.com/systems/axon-conventional-patch-clamp/digidata-1550b-plus-humsilencer#tab-2
Other		
Transmission Electronic Microscope	PHILIPS TECNAI 12	
ABI Prism 7000	Applied Biosystems	
TissueLyser II	Qiagen	
NanoDrop	Thermo Scientific	ND 1000
Nikon Eclipse Ti microscope	Nikon	
Attune Flow Cytometer	Thermo Scientific	
Micro HM 550 Cryostat	Thermo Scientific	

Zeiss confocal microscope	Zeiss	LSM 780
Fluorescence stereomicroscope	Leica	MZ16FA
Biological safety cabinet	Telstar	Class II/B3
Axon digidata 1550B plus hum silencer	Axon Instruments	Digidata 1550B1
Neurolog AC/DC amplifier	Digitimer	NL106
Neurolog Band-Pass Filter	Digitimer	NL 125/6
Neurolog DC Preamplifier with head stage	Digitimer	NL102G
Nikon zoom stereomicroscope	Nikon	SMZ800N
Flaming/Brown Micropipette Puller	Sutter Instrument Co	P-97
Pneumatic Microinjector	Narishige	IM-300

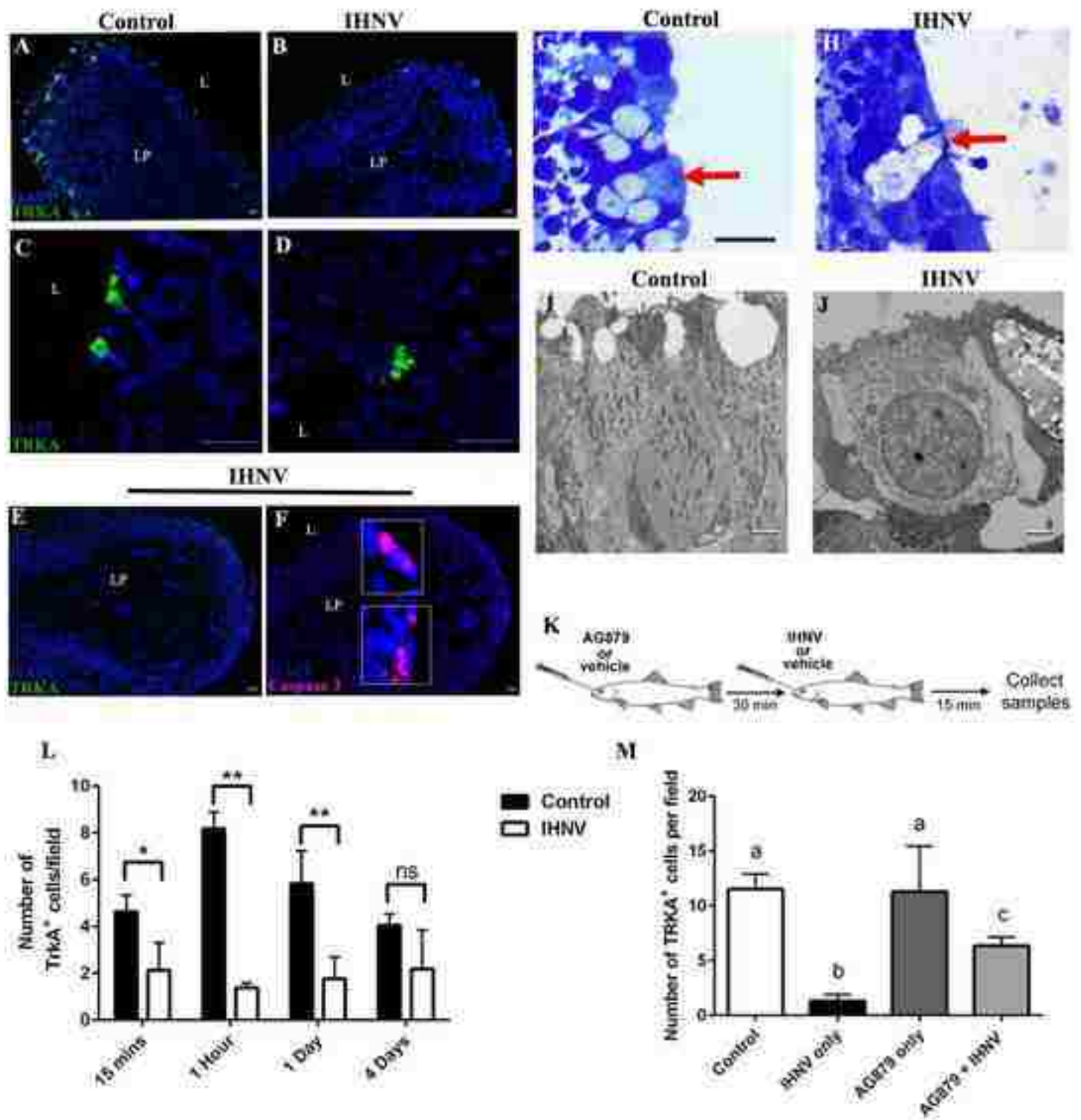
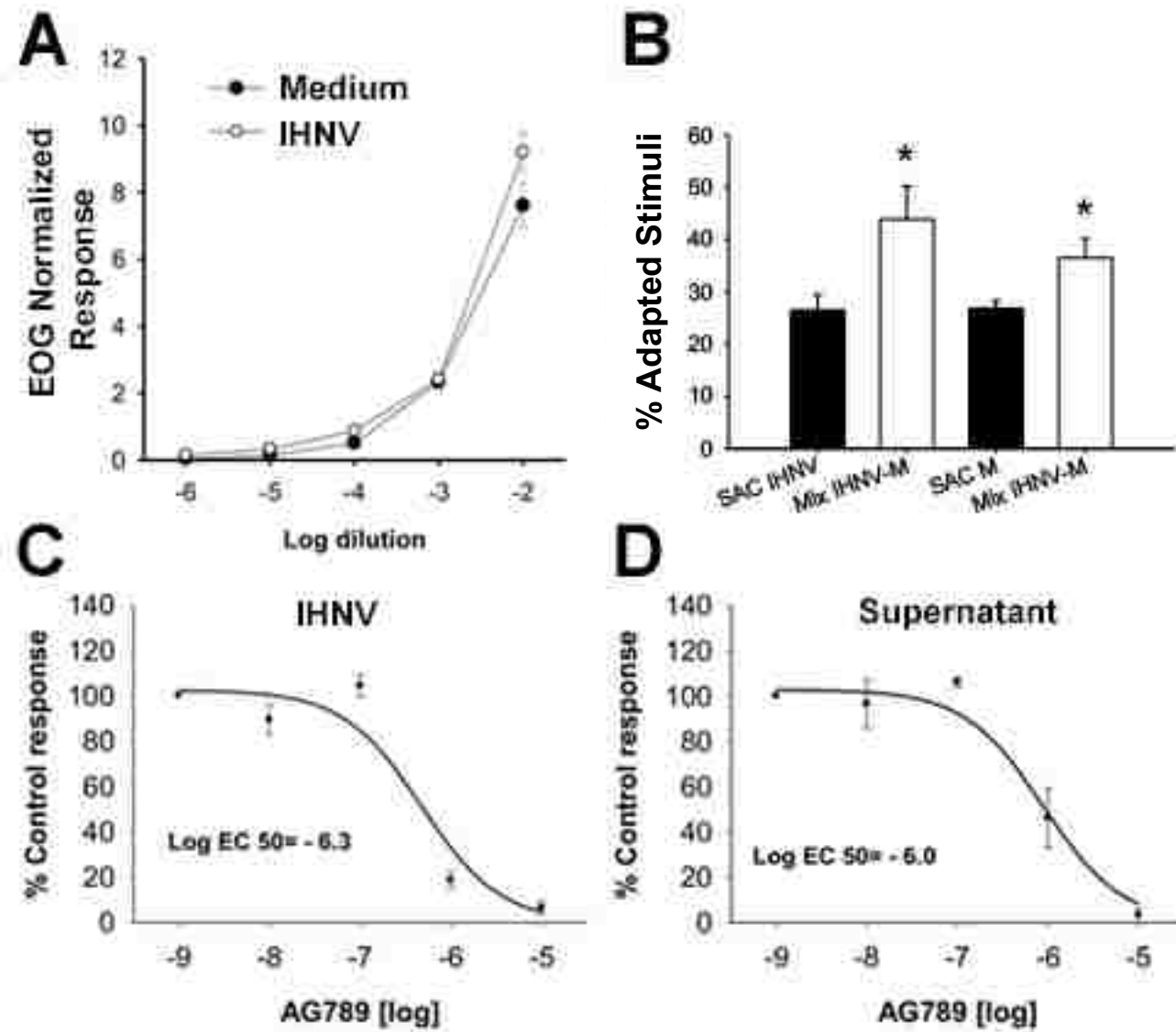
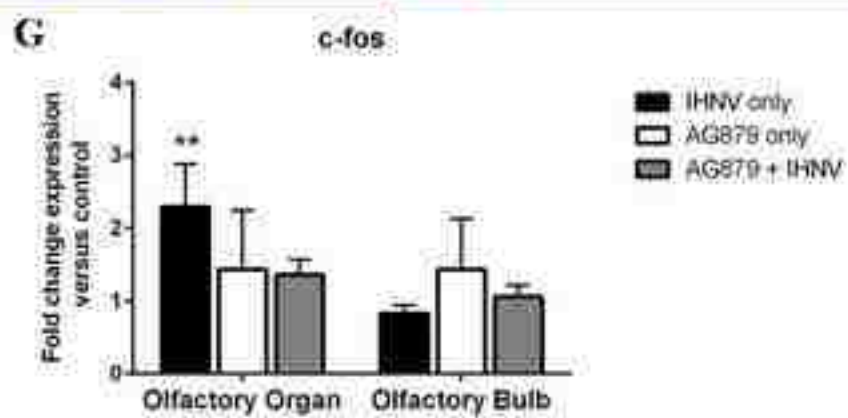
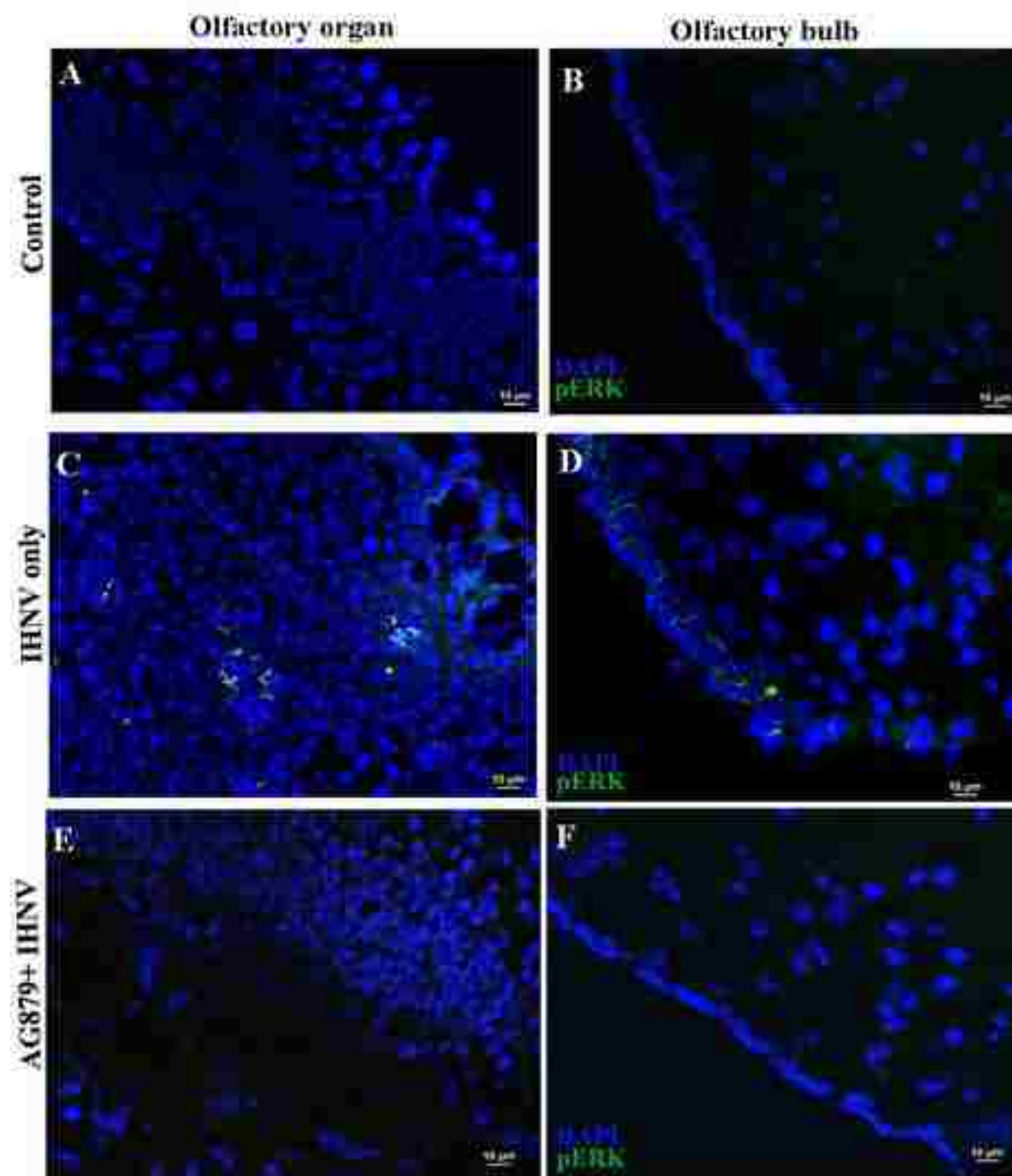
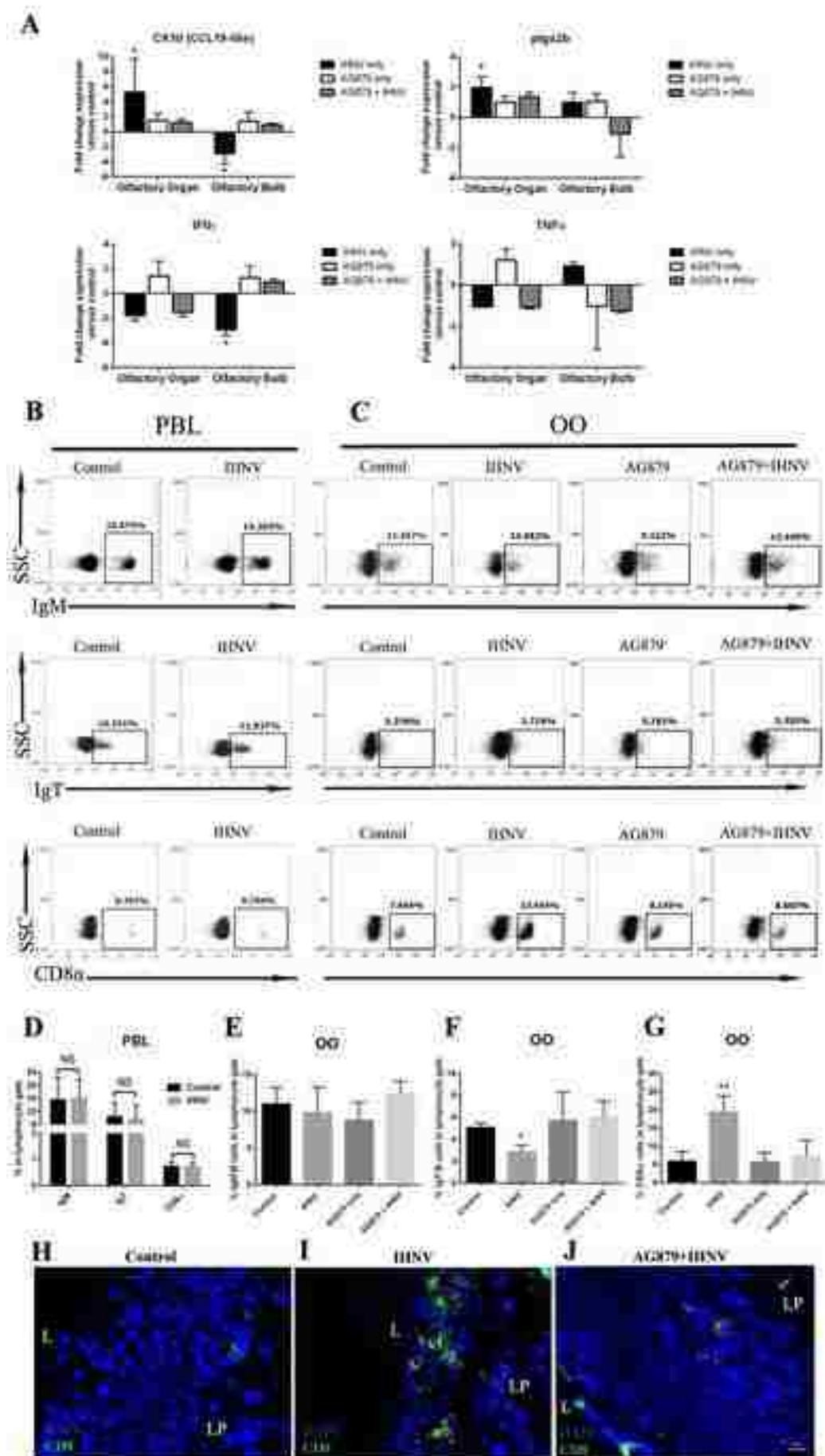
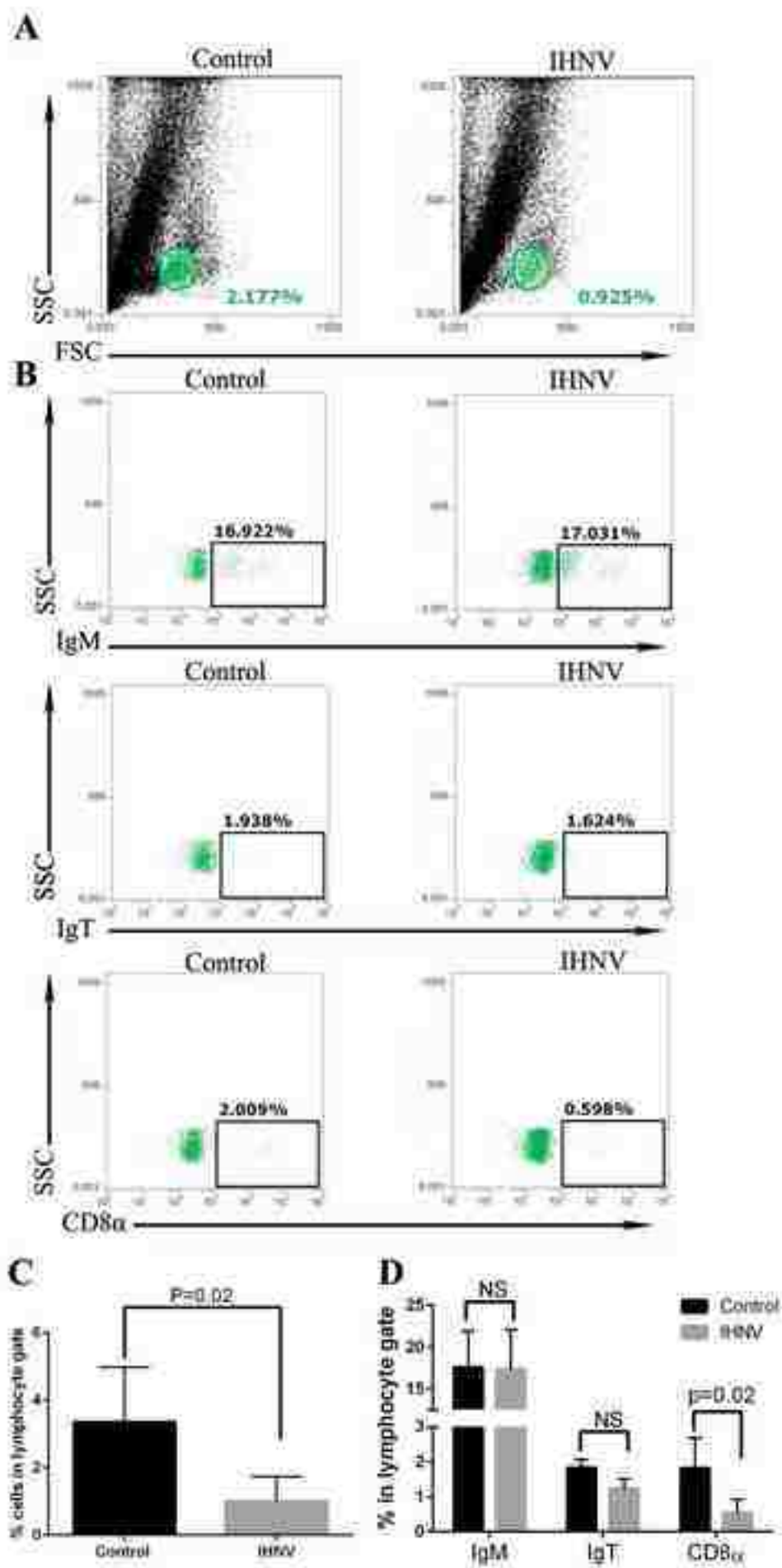


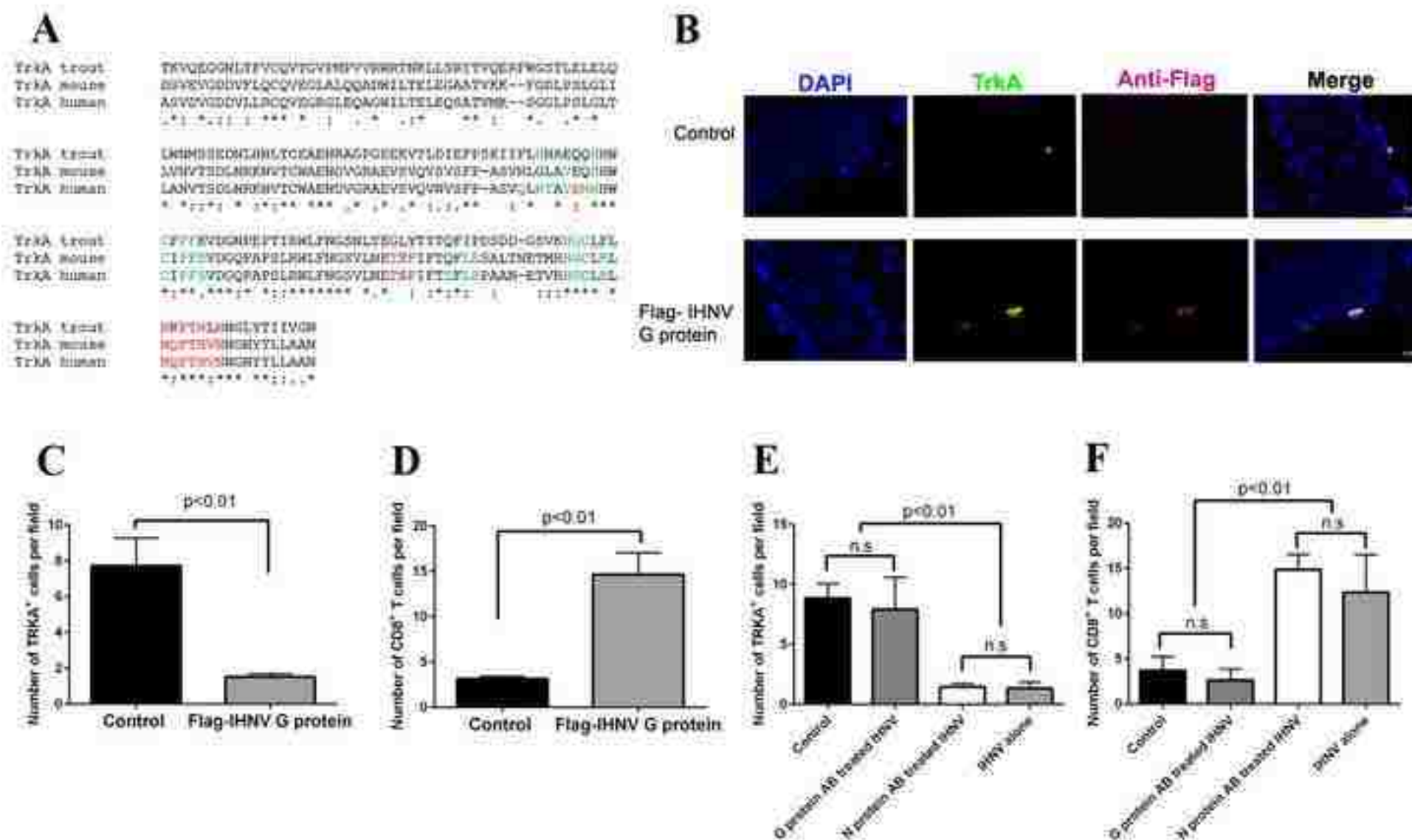
Figure 2

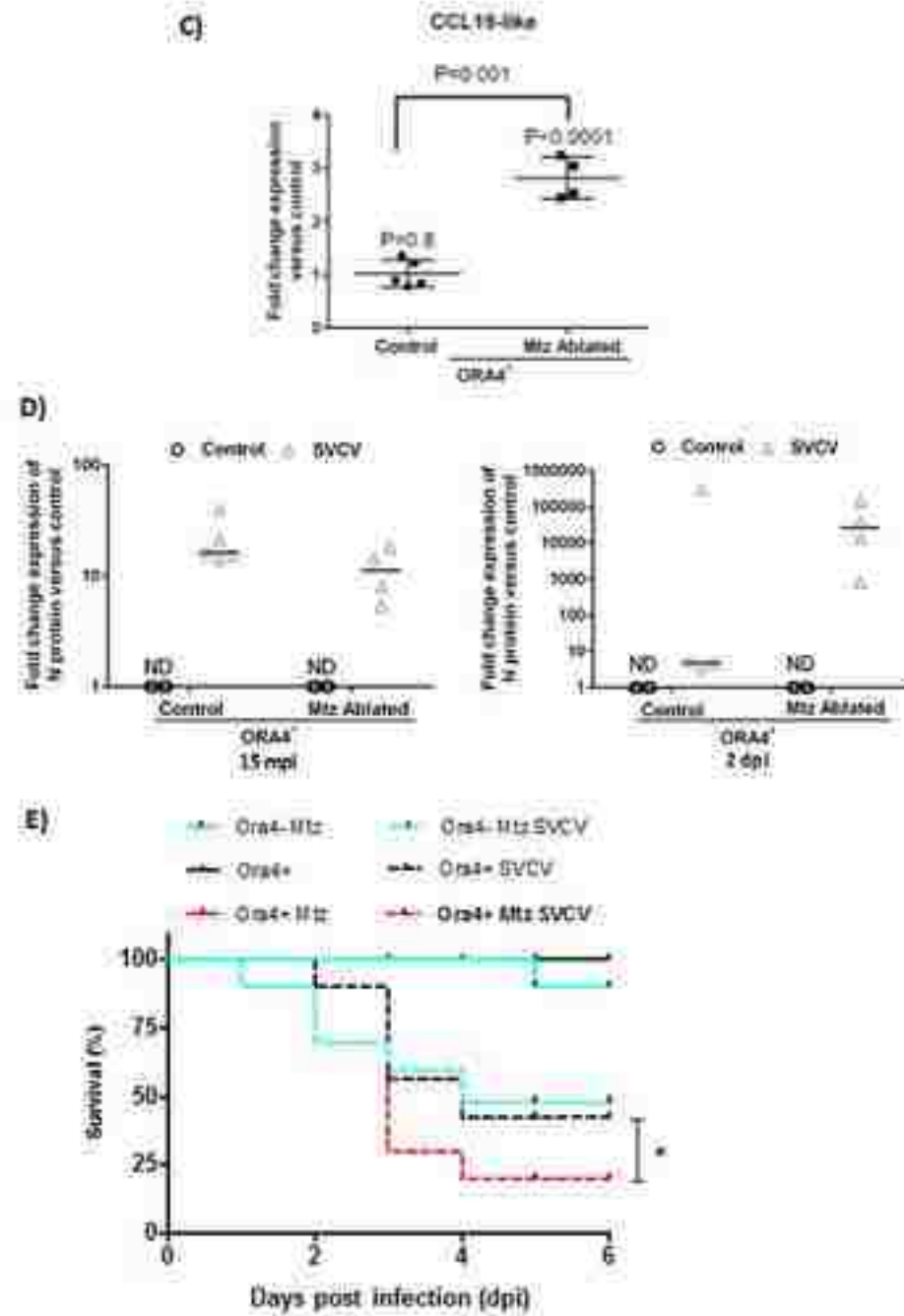
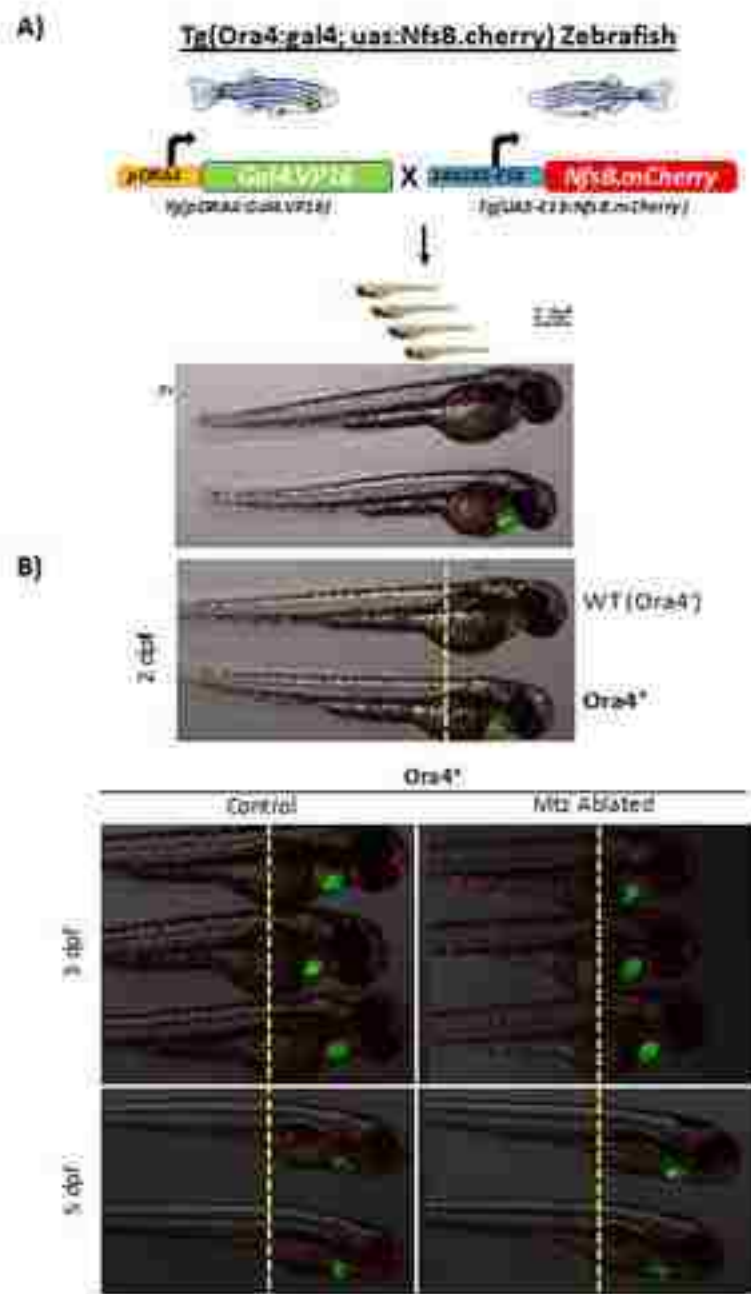


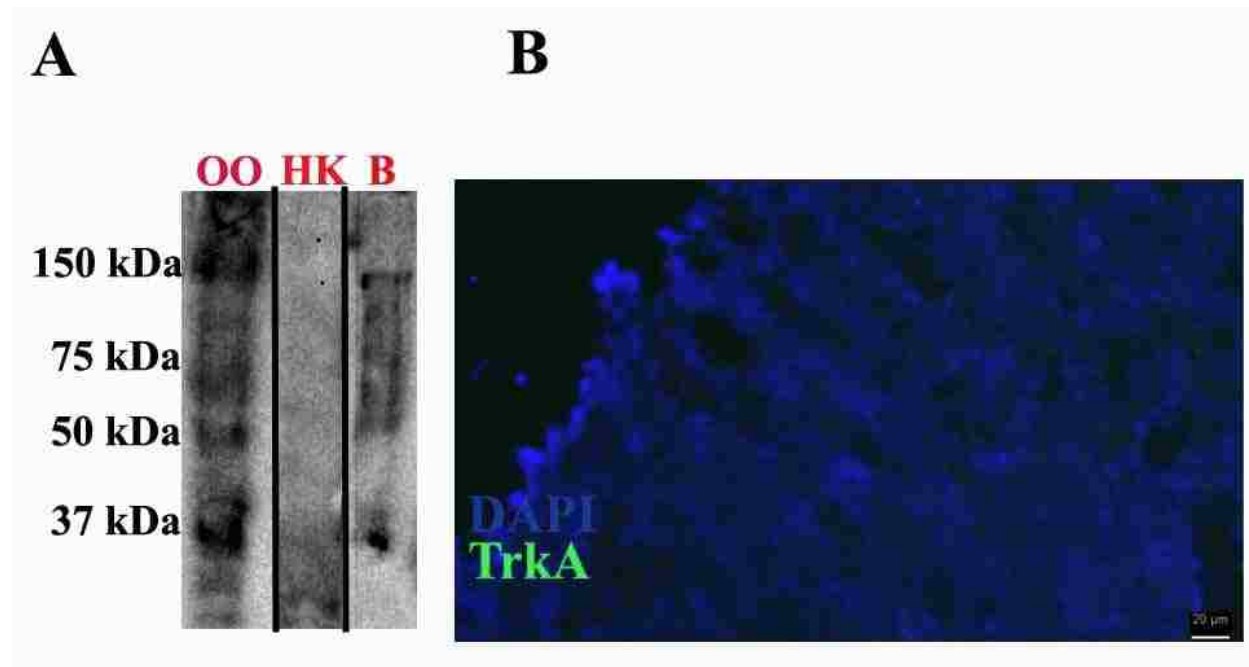




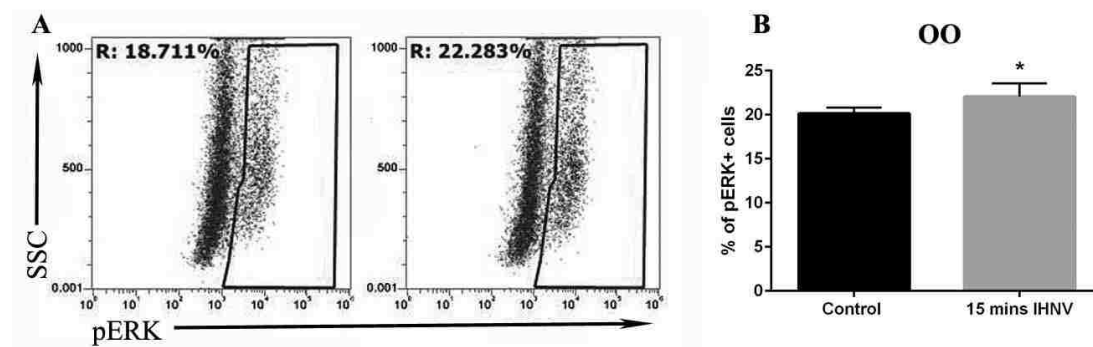




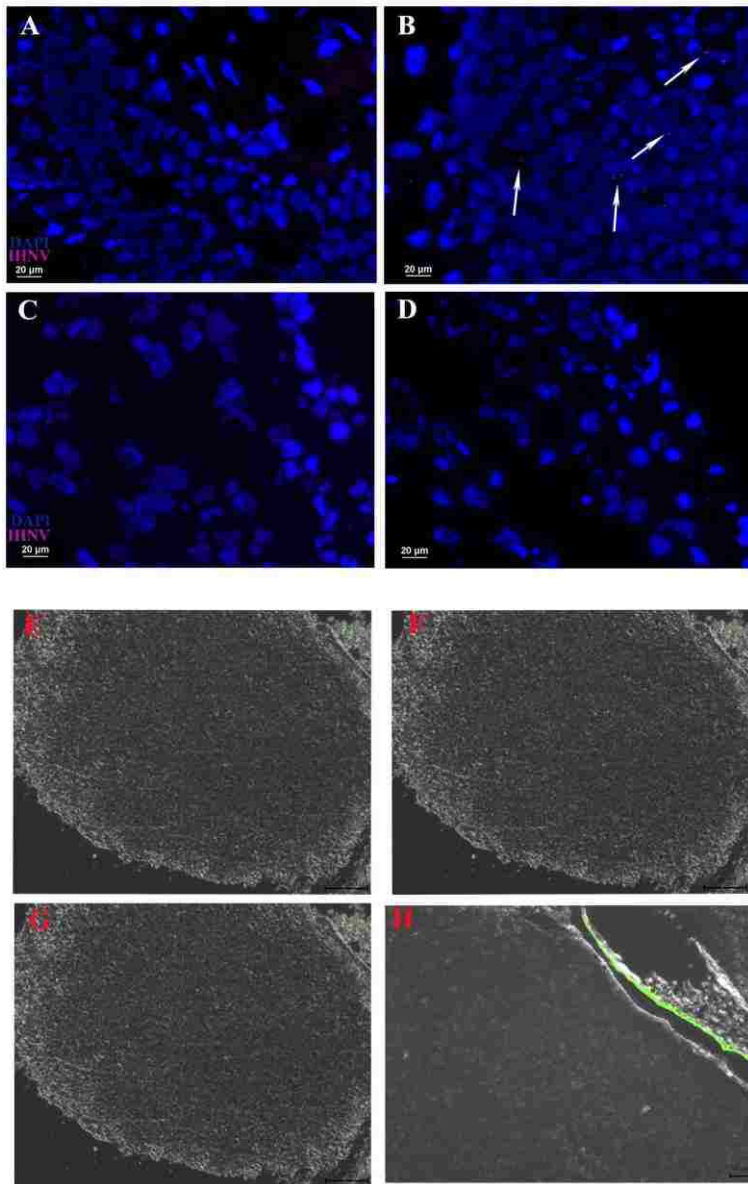




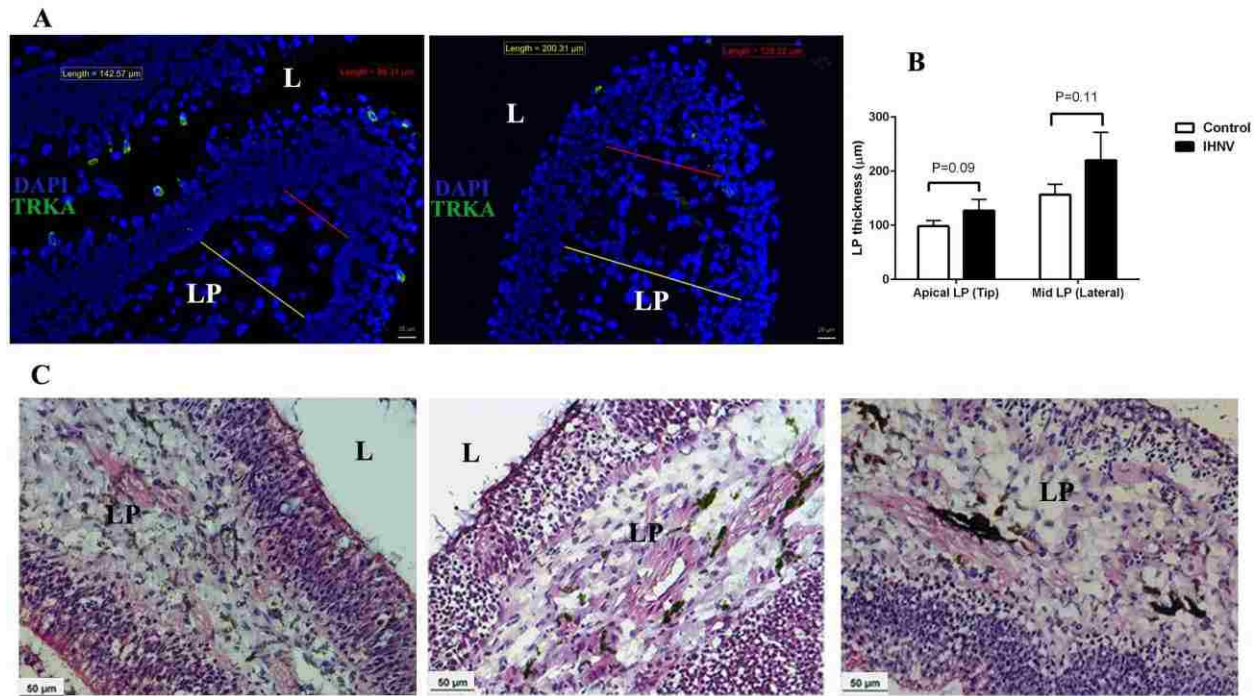
Supplementary Fig. 1: (A) Detection of TrkA in trout OO and brain but not HK lysates by immunoblotting. Immunoblots detecting TrkA showed a band at the expected size (~140 kDa) in OO and brain. (B) Immunofluorescence staining of control rainbow trout HK cryosection stained with anti-TrkA antibody (FITC, green) confirming absence of TrkA⁺ cells. Cell nuclei were stained with DAPI DNA stain (blue). Scale bar: 20 μm.



Supplementary Fig. 2: IHNV activates sensory neurons in the OO *in vitro* (A) Representative dot plots of control (left) and IHNV (right) trout OO extracted cells stained with anti-pERK antibody showing the mean percentage of positive cells. (B) Quantification of flow cytometry data in (A) indicating a significant increase in the percentage of pERK⁺ cells 15 min after adding IHNV (multiplicity of infection 1:3) *in vitro*. Results are representative of three independent experiments (n = 5). *p < 0.05



Supplementary Fig. 3: Nasal delivery of IHNV does not result in presence of virus in the OB and does not alter BBB integrity 15 min after IN delivery. (A) Immunofluorescence staining with anti-IHNV Abs (Cy3, red) showing no IHNV staining in the OO of control rainbow trout. (B) Immunofluorescence staining with anti-IHNV Abs (Cy3, red) showing the presence of IHNV (red arrows) in the OO of IHNV treated rainbow trout 15 min after nasal delivery. (C) Immunofluorescence staining with anti-IHNV Abs (Cy3, red) showing no detection of IHNV at OB of control rainbow trout. (D) Immunofluorescence staining with anti-IHNV Abs (Cy3, red) showing the absence of IHNV in the OB of IHNV treated rainbow trout 15 min after nasal delivery. Scale bar, 20 μm . (E-H) Intravenous injection of FITC- conjugated dextran showing that no changes in the BBB integrity in IHNV-treated fish as demonstrated by the absence of FITC staining in the OB. Scale bar: 100 μm .



Supplementary Fig. 4: Leukocyte recruitment occurs as early as 15 min after IHNV delivery as visualized by enlargement lamina propria (LP) of the olfactory lamellae of IHNV-treated compared to control fish. (A) Immunofluorescence staining of control (left) and IHNV-treated (right) rainbow trout OO stained with anti-trout TrkA (FITC, green) showing our image analysis strategy and the enlargement in the apical and medial regions of the LP in the IHNV-treated fish. Cell nuclei were stained with DAPI DNA stain (blue). Results are representative of two different experiments ($n = 3$). Scale bar, 20 μm . (B) The width of LP at the apical (100 μm from the lamellar tip) and lateral (250 μm from the lamellar tip) regions of the olfactory lamella were measured by image analysis of 10 individual lamellae from three different fish per treatment. The mean distance \pm SEM is shown. (C) Representative hematoxylin-eosin stain of adult rainbow trout olfactory organ showing Leukocyte recruitment occurs as early as 15 min after IHNV delivery of the olfactory lamellae of IHNV-treated (middle and right) compared to control fish (left). L, lumen; LP, lamina propria. Scale bar: 50 μm .

A

```

HSV-2 sG -----MGRITSGYG--IAALLVAVVGLRWCAKYALADPSLQAD
IHNV G      : : * . * . * . * . * . * . * . * . * . *
HSV-2 sG PNRFRGHQLFVLDRLID-----PFGVGRVYHIQPSLEDFQPPSIF
IHNV G      : : * . * . * . * . * . * . * . * . * . *
HSV-2 sG IIVVYAVLER-----ACRSVLLHAFSEAFQVIRGASDEARQITYNLTI
IHNV G      : : * . * . * . * . * . * . * . * . * . *
HSV-2 sG AWR-----MENDCAIPITVMEITCFPH-----KSLGVCEIR-TQRRNS
IHNV G      : : * . * . * . * . * . * . * . * . * . *
HSV-2 sG -----YDSFSAVSEDLGFLMHAFAFETAGT
IHNV G      : : * . * . * . * . * . * . * . * . * . *
HSV-2 sG YLRLVKIKDQWIEITQFILEHRAASCKYALFLRFPFACLTSGAYQGVV
IHNV G      : : * . * . * . * . * . * . * . * . * . *
HSV-2 sG VDSIDMGK-----IIPENQRIVAKYELKAGMGGKFPFVITLLPEL
IHNV G      : : * . * . * . * . * . * . * . * . * . *
HSV-2 sG SDTINATQELVFEEDSALLEDDAGT-----
IHNV G      : : * . * . * . * . * . * . * . * . * . *
HSV-2 sG -----VSSQIPRWNIPTQVAFHSAFAAFSHPGLIKALAGST
IHNV G      : : * . * . * . * . * . * . * . * . * . *

HSV-2 sG -----LAVLVGGIAFWRRRAQAPRRLRLEPHRUD--DAP
IHNV G      : : * . * . * . * . * . * . * . * . * . *
HSV-2 sG FSNQDFY
IHNV G      : : * .

```

B

Supplementary Fig. 5: A low degree of amino acid conservation between IHNV G protein and HSV secreted G protein indicated. (A) Amino acid sequence alignment of HSV-2 sG protein (accession number GD_HHV23) and trout IHNV G protein (sequenced obtained from the live attenuated IHNV used in this study) performed in CLUSTALW showing a low degree of amino acid conservation (B) Production of recombinant FLAG-tagged IHNV G protein by mammalian expression system. Immunoblot using anti-Flag antibody confirmed the presence of the recombinant protein (IHNV G protein) band at expected (~50 KDa) molecular weight.

VII. Summary of findings

This dissertation investigates the antiviral immune responses in the olfactory organ of the teleost fish. The major findings of this dissertation are summarized below.

1. CCL19-like chemokine orchestrates both nasal and systemic antiviral responses in rainbow trout (O. mykiss)

In chapter 2, we reported six CCL19 genes in salmonids, CK12a, CK12b, CK13a, CK13b, CK10a and CK10b. Out of all the isoforms, CK12a had been previously identified as one of the most important immune genes upregulated in trout NALT following nasal vaccination with a viral vaccine (42). Phylogenetically speaking, salmonid CK12 and CK13 clustered together and salmonid CK12 was more similar to mammalian CCL19 compared to the other two main isoforms. We showed that CK12 was mainly expressed in trout mucosal tissues and its expression in the olfactory organ increased up to 50-fold after IHNV nasal vaccination. Recombinant protein CK12 (rCK12) was not chemotactic *in vitro* but it increased the width of the nasal lamina propria when delivered intranasally *in vivo*, suggesting an inflammatory function. rCK12a when delivered I.N or i.p. also stimulated the expression of CD8 α , granulysin, and IFN γ in mucosal and systemic compartments and increased numbers of nasal CD8 α^+ and APC cell numbers. However, *in vivo* delivery of rCK12 did not confer protection against viral antigens. Overall, this chapter highlights the significant role of CCL19-like chemokines in nasal and systemic immunity of rainbow trout (28).

2. Tissue microenvironments in the nasal epithelium of rainbow trout (O. mykiss) define two distinct CD8 α^+ cell populations and establish regional immunity

In chapter 3, we identified the presence of CD8 α^+ cells in the rainbow trout nasal epithelium. We showed nasal CD8 α^+ cells display a distinct phenotype of CD8 $^+$ T cells. We observed that nasal

CD8 α ⁺ cells were mainly located in clusters at the mucosal tip of olfactory lamella but scattered in the neuroepithelial region. Their cluster at the tip of olfactory lamella could be explained by the greater expression of CCL19, ICAM-1, and VCAM-1 in the mucosal tip compared to the neuroepithelium. Whilst viral antigen uptake occurred via both tip and lateral routes, tip resident MHC-II⁺ cells were located significantly closer to the lumen of the nasal cavity than their neuroepithelial counterparts, providing quicker access to lumen antigens. Our results support the idea of compartmentalized immune responses within the nasal mucosa of teleosts that likely evolved as a sparing mechanism to protect olfactory sensory function (43).

3. Olfactory sensory neurons mediate ultra-rapid antiviral immune responses in teleost fish in a TrkA-dependent manner

In chapter 4, we report that nasal delivery of rhabdoviruses induced apoptosis in crypt OSNs in rainbow trout OO via the interaction of the OSN TrkA receptor with viral glycoprotein. This signal resulted in pro-inflammatory responses in the OO and dampened inflammation in the OB. CD8 α ⁺ T cells infiltrated the OO within minutes of nasal viral delivery and this response was abrogated when TrkA was blocked. Infiltrating CD8 α ⁺ T cells originated from the microvasculature surrounding the OB and not the periphery (**Figure 2**). Finally, ablation of crypt neurons in a transgenic zebrafish model resulted in increased susceptibility to rhabdoviral challenge. Our results, therefore, indicate a novel function for OSNs as a first layer of pathogen detection in vertebrates.

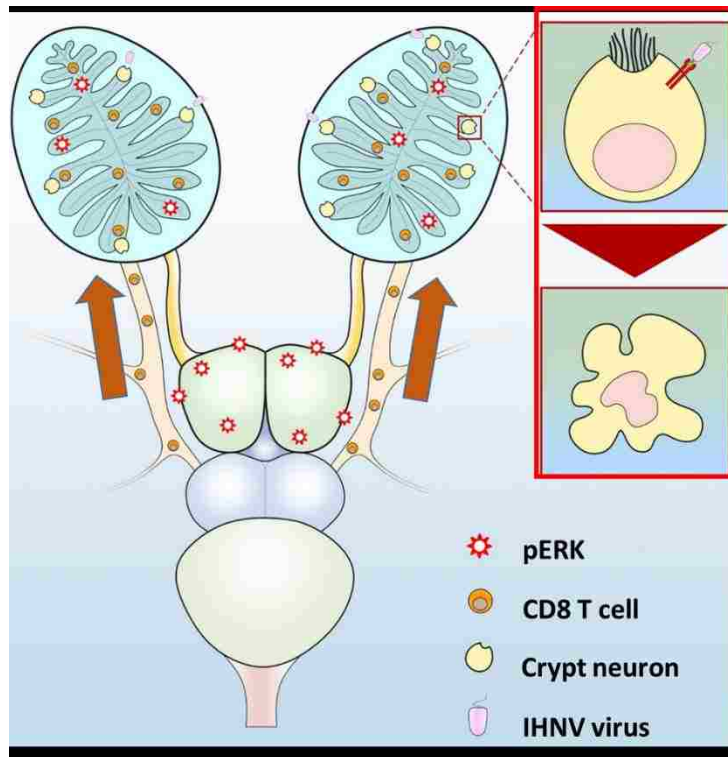


Figure 2: Nasal delivery of neurotropic virus A) Induce apoptosis crypt neurons, red box B) Induce neuronal activation in OO and OB labeled, pERK C) Infiltrate CD8 T cells from OB to OO, orange arrow

VIII. Conclusion

The immune responses at tissue barriers are complex due to the multifunctional nature of these tissues. The olfactory organ, responsible for detection of chemical cues in the environment, also plays a role in defense against infection. However, the immunological principles that govern nasal immunity are poorly understood even in mammals. The current dissertation represents the first in-depth anatomical, cellular and molecular characterization of the nasal immune system of a teleost fish. This work has revealed some of the key players in nasal immunity of teleosts (i.e. CCL19) and showed the unique immune regulatory mechanisms in the OO of fish that preserve neurons from inflammatory damages. The intimate relationship between neurons and immune cells in the teleost olfactory system offers an excellent platform for the study of neuroimmune interactions in

vertebrates. As an example, we provide evidence for the immune role of crypt neurons against viral pathogens provides the first evidence for the immunological role of OSNs in vertebrates.

IX. References:

1. Medzhitov, R., and C. Janeway. 2000. Innate immune recognition: mechanisms and pathways. *Immunol. Rev.* 173: 89-97.
2. Medzhitov, R., and C. Janeway. 2000. Innate immunity. *N. Engl. J. Med.* 343: 338-344.
3. Criscitiello, M. F., and P. de Figueiredo. 2013. Fifty shades of immune defense. *PLoS Pathog.* 9: e1003110.
4. Pradeu, T., and L. Du Pasquier. 2018. Immunological memory: What's in a name? *Immunol. Rev.* 283: 7-20.
5. West, C., and N. Silverman. 2017. Drosophilosophical: Re-thinking Adaptive Immunity in the Fly. *Cell* 169: 188-190.
6. Janeway, C., K. P. Murphy, P. Travers, and M. Walport. 2008. *Janeway's immunobiology*. Garland Science.
7. Vivier, E., and B. Malissen. 2005. Innate and adaptive immunity: specificities and signaling hierarchies revisited. *Nat. Immunol.* 6: 17-21.
8. Banyer, J., N. Hamilton, I. Ramshaw, and A. Ramsay. 1999. Cytokines in innate and adaptive immunity. *Rev. Immunogenet.* 2: 359-373.
9. Belardelli, F., and M. Ferrantini. 2002. Cytokines as a link between innate and adaptive antitumor immunity. *Trends Immunol.* 23: 201-208.
10. Viola, A., and A. D. Luster. 2008. Chemokines and their receptors: drug targets in immunity and inflammation. *Annu. Rev. Pharmacol. Toxicol.* 48: 171-197.
11. Charo, I. F., and R. M. Ransohoff. 2006. The many roles of chemokines and chemokine receptors in inflammation. *N. Engl. J. Med.* 354: 610-621.
12. Griffith, J. W., C. L. Sokol, and A. D. Luster. 2014. Chemokines and chemokine receptors: positioning cells for host defense and immunity. *Annu. Rev. Immunol.* 32: 659-702.
13. Fukuyama, S., T. Nagatake, D.-Y. Kim, K. Takamura, E. J. Park, T. Kaisho, N. Tanaka, Y. Kurono, and H. Kiyono. 2006. Cutting edge: uniqueness of lymphoid chemokine requirement for the initiation and maturation of nasopharynx-associated lymphoid tissue organogenesis. *J. Immunol.* 177: 4276-4280.
14. Rangel-Moreno, J., J. Moyron-Quiroz, K. Kusser, L. Hartson, H. Nakano, and T. D. Randall. 2005. Role of CXC chemokine ligand 13, CC chemokine ligand (CCL) 19, and CCL21 in the organization and function of nasal-associated lymphoid tissue. *J. Immunol.* 175: 4904-4913.
15. Marsland, B. J., P. Böttig, M. Bauer, C. Ruedl, U. Lässig, R. R. Beerli, K. Dietmeier, L. Ivanova, T. Pfister, and L. Vogt. 2005. CCL19 and CCL21 induce a potent proinflammatory differentiation program in licensed dendritic cells. *Immunity.* 22: 493-505.
16. Magnado'ttir, B. 2006. Innate immunity of fish (overview). *Fish Shellfish Immunol.* 20: 137-151.

17. Magor, B. G., and K. E. Magor. 2001. Evolution of effectors and receptors of innate immunity. *Dev. Comp. Immunol.* 25: 651-682.
18. Whyte, S. K. 2007. The innate immune response of finfish - A review of current knowledge. *Fish Shellfish Immunol.* 23: 1127-1151.
19. Uribe, C., H. Folch, R. Enriquez, and G. Moran. 2011. Innate and adaptive immunity in teleost fish: a review. *Vet. Med. (Praha)* 56: 486-503.
20. Flajnik, M. F., and M. Kasahara. 2010. Origin and evolution of the adaptive immune system: genetic events and selective pressures. *Nat. Rev. Genet.* 11: 47-59.
21. Sunyer, J. O. 2013. Fishing for mammalian paradigms in the teleost immune system. *Nat. Immunol.* 14: 320-326.
22. Zapata, A., and C. Amemiya. 2000. Phylogeny of lower vertebrates and their immunological structures. In *Origin and evolution of the vertebrate immune system*. Springer. 67-107.
23. Nomiyama, H., K. Hieshima, N. Osada, Y. Kato-Unoki, K. Otsuka-Ono, S. Takegawa, T. Izawa, A. Yoshizawa, Y. Kikuchi, and S. Tanase. 2008. Extensive expansion and diversification of the chemokine gene family in zebrafish: identification of a novel chemokine subfamily CX. *BMC Genomics* 9: 222.
24. Alejo, A., and C. Tafalla. 2011. Chemokines in teleost fish species. *Dev. Comp. Immunol.* 35: 1215-1222.
25. Liao, Z., Q. Wan, X. Xiao, J. Ji, and J. Su. 2018. A systematic investigation on the composition, evolution and expression characteristics of chemokine superfamily in grass carp *Ctenopharyngodon idella*. *Dev. Comp. Immunol.*
26. Laing, K. J., and C. J. Secombes. 2004. Trout CC chemokines: comparison of their sequences and expression patterns. *Mol. Immunol.* 41: 793-808.
27. Peatman, E., and Z. Liu. 2007. Evolution of CC chemokines in teleost fish: a case study in gene duplication and implications for immune diversity. *Immunogenetics* 59: 613-623.
28. Sepahi, A., L. Tacchi, E. Casadei, F. Takizawa, S. E. LaPatra, and I. Salinas. 2017. CK12a, a CCL19-like chemokine that orchestrates both nasal and systemic antiviral immune responses in Rainbow trout. *J. Immunol.* 199: 3900-3913.
29. Brandtzaeg, P., and R. Pabst. 2004. Let's go mucosal: communication on slippery ground. *Trends Immunol.* 25: 570-577.
30. Salinas, I., Y.-A. Zhang, and J. O. Sunyer. 2011. Mucosal immunoglobulins and B cells of teleost fish. *Dev. Comp. Immunol.* 35: 1346-1365.
31. Sepahi, A., and I. Salinas. 2016. The evolution of nasal immune systems in vertebrates. *Mol. Immunol.* 69: 131-138.
32. Kuper, C. F., P. J. Koornstra, D. M. Hameleers, J. Biewenga, B. J. Spit, A. M. Duijvestijn, P. J. van Breda Vriesman, and T. Sminia. 1992. The role of nasopharyngeal lymphoid tissue. *Immunol. Today.* 13: 219-224.
33. Liang, B., L. Hyland, and S. Hou. 2001. Nasal-associated lymphoid tissue is a site of long-term virus-specific antibody production following respiratory virus infection of mice. *J. Virol.* 75: 5416-5420.
34. Asanuma, H., C. Aizawa, T. Kurata, and S.-i. Tamura. 1998. IgA antibody-forming cell responses in the nasal-associated lymphoid tissue of mice vaccinated by intranasal, intravenous and/or subcutaneous administration. *Vaccine.* 16: 1257-1262.
35. Wu, H. Y., E. Nikolova, K. Beagley, and M. Russell. 1996. Induction of antibody-secreting cells and T-helper and memory cells in murine nasal lymphoid tissue. *Immunology* 88: 493-500.
36. Heritage, P., M. Brook, B. Underdown, and M. McDermott. 1998. Intranasal immunization with polymer-grafted microparticles activates the nasal-associated lymphoid tissue and draining lymph nodes. *Immunology* 93: 249-256.


37. Harmsen, A., K. Kusser, L. Hartson, M. Tighe, M. J. Sunshine, J. D. Sedgwick, Y. Choi, D. R. Littman, and T. D. Randall. 2002. Cutting edge: organogenesis of nasal-associated lymphoid tissue (NALT) occurs independently of lymphotoxin-alpha (LT alpha) and retinoic acid receptor-related orphan receptor-gamma, but the organization of NALT is LT alpha dependent. *J Immunol* 168: 986-990.
38. Wiley, J. A., M. P. Tighe, and A. G. Harmsen. 2005. Upper respiratory tract resistance to influenza infection is not prevented by the absence of either nasal-associated lymphoid tissue or cervical lymph nodes. *J Immunol* 175: 3186-3196.
39. Tamura, S.-i., T. Iwasaki, A. H. Thompson, H. Asanuma, Z. Chen, Y. Suzuki, C. Aizawa, and T. Kurata. 1998. Antibody-forming cells in the nasal-associated lymphoid tissue during primary influenza virus infection. *J. Gen. Virol.* 79: 291-299.
40. Zuercher, A. W., S. E. Coffin, M. C. Thurnheer, P. Fundova, and J. J. Cebra. 2002. Nasal-associated lymphoid tissue is a mucosal inductive site for virus-specific humoral and cellular immune responses. *J Immunol* 168: 1796-1803.
41. Rudraraju, R., S. Surman, B. Jones, R. Sealy, D. L. Woodland, and J. L. Hurwitz. 2011. Phenotypes and functions of persistent Sendai virus-induced antibody forming cells and CD8+ T cells in diffuse nasal-associated lymphoid tissue typify lymphocyte responses of the gut. *Virology* 410: 429-436.
42. Tacchi, L., R. Musharrafieh, E. T. Larragoite, K. Crossey, E. B. Erhardt, S. A. Martin, S. E. LaPatra, and I. Salinas. 2014. Nasal immunity is an ancient arm of the mucosal immune system of vertebrates. *Nat. Commun.* 5: 6205.
43. Sepahi, A., E. Casadei, L. Tacchi, P. Muñoz, S. E. LaPatra, and I. Salinas. 2016. Tissue microenvironments in the nasal epithelium of rainbow trout (*Oncorhynchus mykiss*) define two distinct CD8 α + cell populations and establish regional immunity. *J. Immunol.* 197: 4453-4463.
44. Eisthen, H. L. 1997. Evolution of vertebrate olfactory systems. *Brain. Behav. Evol.* 50: 222-233.
45. Saraiva, L. R., G. Ahuja, I. Ivandic, A. S. Syed, J. C. Marioni, S. I. Korsching, and D. W. Logan. 2015. Molecular and neuronal homology between the olfactory systems of zebrafish and mouse. *Sci. Rep.* 5: 11487.
46. Gross, E., J. Swenberg, S. Fields, and J. Popp. 1982. Comparative morphometry of the nasal cavity in rats and mice. *J. Anat.* 135: 83.
47. Morrison, E. E., and R. M. Costanzo. 1992. Morphology of olfactory epithelium in humans and other vertebrates. *Microsc. Res. Tech.* 23: 49-61.
48. Døving, K. B., and D. Trotier. 1998. Structure and function of the vomeronasal organ. *J. Exp. Biol.* 201: 2913-2925.
49. Hansen, A., K. T. Anderson, and T. E. Finger. 2004. Differential distribution of olfactory receptor neurons in goldfish: structural and molecular correlates. *J. Comp. Neurol.* 477: 347-359.
50. Hansen, A., S. H. Rolen, K. Anderson, Y. Morita, J. Caprio, and T. E. Finger. 2003. Correlation between olfactory receptor cell type and function in the channel catfish. *J Neurosci* 23: 9328-9339.
51. Keverne, E. B. 1999. The vomeronasal organ. *Science* 286: 716-720.
52. Meredith, M. 2001. Human vomeronasal organ function: a critical review of best and worst cases. *Chem. Senses* 26: 433-445.
53. Ferrando, S., and L. Gallus. 2013. Is the olfactory system of cartilaginous fishes a vomeronasal system? *Front Neuroanat.* 7.
54. Nakamuta, S., N. Nakamuta, K. Taniguchi, and K. Taniguchi. 2013. Localization of the primordial vomeronasal organ and its relationship to the associated gland in lungfish. *J. Anat.* 222: 481-485.
55. Ubeda-Bañon, I., P. Pro-Sistiaga, A. Mohedano-Moriano, D. Saiz-Sanchez, C. De la Rosa-Prieto, N. Gutierrez-Castellanos, E. Lanuza, F. Martinez-Garcia, and A. Martinez-Marcos. 2011. Cladistic analysis of olfactory and vomeronasal systems. *Front Neuroanat.* 5.
56. Buck, L., and R. Axel. 1991. A novel multigene family may encode odorant receptors: a molecular basis for odor recognition. *Cell* 65: 175-187.

57. Dulac, C., and R. Axel. 1995. A novel family of genes encoding putative pheromone receptors in mammals. *Cell* 83: 195-206.
58. Døving, K. B. 2007. The functional organization of the fish olfactory system. *Prog. Neurobiol.* 82: 80-86.
59. Taniguchi, K., and K. Taniguchi. 2014. Phylogenetic Studies on the Olfactory System in Vertebrates. *J Vet Med Sci* 76: 781.
60. Oka, Y., L. R. Saraiva, and S. I. Korsching. 2011. Crypt neurons express a single V1R-related ora gene. *Chem. Senses*: bjr095.
61. Hamdani, e. H., and K. Døving. 2007. The functional organization of the fish olfactory system. *Prog. Neurobiol.* 82: 80.
62. Hansen, A., and E. Zeiske. 1998. The peripheral olfactory organ of the zebrafish, *Danio rerio*: an ultrastructural study. *Chem. Senses* 23: 39-48.
63. Hansen, A., and B. S. Zielinski. 2005. Diversity in the olfactory epithelium of bony fishes: development, lamellar arrangement, sensory neuron cell types and transduction components. *J. Neurocytol.* 34: 183-208.
64. Belanger, R. M., C. M. Smith, L. D. Corkum, and B. S. Zielinski. 2003. Morphology and histochemistry of the peripheral olfactory organ in the round goby, *Neogobius melanostomus* (Teleostei: Gobiidae). *J. Morphol.* 257: 62-71.
65. Germana, A., G. Montalbano, R. Laura, E. Ciriaco, M. Del Valle, and J. A. Vega. 2004. S100 protein-like immunoreactivity in the crypt olfactory neurons of the adult zebrafish. *Neurosci. Lett.* 371: 196-198.
66. Vielma, A., A. Ardiles, L. Delgado, and O. Schmachtenberg. 2008. The elusive crypt olfactory receptor neuron: evidence for its stimulation by amino acids and cAMP pathway agonists. *J. Exp. Biol.* 211: 2417-2422.
67. Ahuja, G., I. Ivandić, M. Saltürk, Y. Oka, W. Nadler, and S. I. Korsching. 2013. Zebrafish crypt neurons project to a single, identified mediodorsal glomerulus. *Sci Rep.* 3.
68. Catania, S., A. Germana, R. Laura, T. Gonzalez-Martinez, E. Ciriaco, and J. Vega. 2003. The crypt neurons in the olfactory epithelium of the adult zebrafish express TrkA-like immunoreactivity. *Neurosci. Lett.* 350: 5-8.
69. Biechl, D., K. Tietje, G. Gerlach, and M. F. Wullmann. 2016. Crypt cells are involved in kin recognition in larval zebrafish. *Sci Rep.* 6: 24590.
70. Veiga-Fernandes, H., and D. Mucida. 2016. Neuro-immune interactions at barrier surfaces. *Cell* 165: 801-811.
71. Arendt, D. 2008. The evolution of cell types in animals: emerging principles from molecular studies. *Nat. Rev. Genet.* 9: 868.
72. Chiu, I. M., B. A. Heesters, N. Ghasemlou, C. A. Von Hehn, F. Zhao, J. Tran, B. Wainger, A. Strominger, S. Muralidharan, and A. R. Horswill. 2013. Bacteria activate sensory neurons that modulate pain and inflammation. *Nature* 501: 52.
73. Koyuncu, O. O., I. B. Hogue, and L. W. Enquist. 2013. Virus infections in the nervous system. *Cell Host Microbe* 13: 379-393.
74. Mori, I., Y. Nishiyama, T. Yokochi, and Y. Kimura. 2005. Olfactory transmission of neurotropic viruses. *J. Neurovirol.* 11: 129-137.

Appendix A

Sepahi, Ali, Héctor Cordero, Howard Goldfine, Maria Ángeles Esteban, and Irene Salinas.
"Symbiont-derived sphingolipids modulate mucosal homeostasis and B cells in teleost fish."
Scientific Reports 6 (2016). doi:10.1038/srep39054

SCIENTIFIC REPORTS



OPEN

Symbiont-derived sphingolipids modulate mucosal homeostasis and B cells in teleost fish

Ali Sepahi^{1,*}, Héctor Cordero^{1,2,*}, Howard Goldfine³, María Ángeles Esteban² & Irene Salinas¹

Received: 22 August 2016
Accepted: 16 November 2016
Published: 14 December 2016

Symbiotic bacteria and mucosal immunoglobulins have co-evolved for millions of years in vertebrate animals. Symbiotic bacteria products are known to modulate different aspects of the host immune system. We recently reported that *Flectobacillus major* is a predominant species that lives in the gill and skin mucosal surfaces of rainbow trout (*Oncorhynchus mykiss*). *F. major* is known to produce sphingolipids of a unique molecular structure. Here we propose a role for *F. major* and its sphingolipids in the regulation of B cell populations in rainbow trout, as well as an essential role for sphingolipids in trout mucosal homeostasis. We found that *F. major*-specific IgT titers are confined to the gill and skin mucus, whereas *F. major*-specific IgM titers are only detected in serum. Live *F. major* cells are able to stimulate sustained IgT expression and secretion in gills. *F. major* sphingolipids modulate the growth of trout total skin and gill symbiotic bacteria. *In vivo* systemic administration of *F. major* sphingolipids changes the proportion of IgT⁺ to IgM⁺ B cells in trout HK. These results demonstrate the key role of the symbiont *F. major* and its sphingolipids in mucosal homeostasis via the modulation of mucosal and systemic Igs and B cells.

The co-existence of beneficial microorganisms and the mucosal barriers of animals is one of the most conserved and successful associations found in nature. Microorganisms are known to provide the animal host with numerous physiological benefits including metabolic, developmental and immunological ones^{1–6}. At the same time, the animal host needs to tolerate symbionts while fighting pathogens, a complex process for the animal's immune system^{1,7,8}.

Teleost fish such as rainbow trout (*Oncorhynchus mykiss*) have numerous mucosal barriers such as the gut, skin, gills and olfactory organ that separate them from the environment. Each of these surfaces is colonized by a distinct and diverse bacterial community^{1,9–12}. Although the presence of these complex microbial communities has been reported in a number of teleosts, the specific mechanisms by which the fish host benefits from this association are largely unknown.

Mucosa-associated lymphoid tissues (MALT) of teleost fish are characterized by a unique distribution of B cells compared to systemic lymphoid tissues, with 50% of all B cells being IgT⁺ B cells and 50% IgM⁺ B cells^{11,13–15}. Importantly, teleost mucosal secretions contain one major immunoglobulin (Ig) isotype, IgT, specialized in mucosal immunity^{11,13–16}. Compartmentalized IgT responses against pathogenic bacteria and parasites can be detected in mucosal secretion of trout whereas IgM responses are mainly systemic^{11,13–15}. Additionally, rainbow trout IgT is the main Ig to coat bacterial symbionts, supporting the role of IgT in mucosal homeostasis^{11,13–15}. Thus, IgT similar to IgA in mammals, is essential for the correct functioning of the teleost mucosal immune system.

A recent topographical map of the bacterial microbiome of adult rainbow trout revealed that the skin and gill bacterial communities are dominated by one species of bacteria, *Flectobacillus major*¹². Until then, *F. major* had not been reported to be a member of the microbiome of any fish species, likely due to the lack of pyrosequencing studies from these two sites. This strong association, nevertheless, suggested that *F. major* may play a major role in the gill and skin mucosal immune system of rainbow trout.

¹Center for Evolutionary and Theoretical Immunology, Department of Biology, University of New Mexico, Albuquerque, NM, USA. ²Fish Innate Immune System Group, Department of Cell Biology and Histology, Faculty of Biology, Regional Campus of International Excellence "Campus Mare Nostrum", University of Murcia, Murcia, Spain. ³Department of Microbiology, University of Pennsylvania Perelman School of Medicine, Philadelphia, PA 19104, USA. *These authors contributed equally to this work. Correspondence and requests for materials should be addressed to I.S. (email: isalinas@unm.edu)

Specific Ig	Sample	Positive/Total
IgM	Serum	4/11
	Skin mucus with bacteria	0/6
	Skin mucus without bacteria	0/6
	Gill mucus with bacteria	0/6
	Gill mucus without bacteria	0/6
	Gut mucus with bacteria	0/6
	Gill mucus without bacteria	0/6
IgT	Serum	0/6
	Skin mucus with bacteria	6/6
	Skin mucus without bacteria	0/6
	Gill mucus with bacteria	6/6
	Gill mucus without bacteria	6/6
	Gut mucus with bacteria	0/6
	Gut mucus without bacteria	0/6

Table 1. Detection of specific immunoglobulins against *Flectobacillus major* in serum and mucus of rainbow trout (*Oncorhynchus mykiss*).

Sphingolipids are known to perform several immune-related functions^{17–19}. For instance, sphingolipids have antimicrobial properties and they are able to modulate immune cells by formation of secondary messengers such as ceramides and sphingosine-1 phosphate (S1P) that are involved in immune cell development, differentiation, activation and proliferation¹⁷. The sphingosine-1 phosphate receptor (S1P1) is mainly expressed by lymphocytes and determines their migration patterns from and into the secondary lymphoid organs and thymus^{20–23}. Moreover, S1P/S1P1 regulate peritoneal B cell trafficking and intestinal IgA production in mice^{24,25}.

Sphingolipids are produced by most eukaryotic cells but are rare in prokaryotes, whose membranes comprise only glycerol-based phospholipids²⁶. However, a few bacterial species possess both phospholipids and sphingolipids^{27–29}. Importantly, bacterial derived sphingolipids can have unique properties compared to those synthesized by eukaryotes³⁰. Interestingly, *F. major* is known to produce large quantities of a unique type of glycosphingolipid^{31,32}, but the biological functions of these sphingolipids have not been investigated.

Here we propose that *F. major* and *F. major*-derived sphingolipids play a key role in the modulation of trout mucosal homeostasis and B cell populations. *F. major*-specific IgT antibodies were found in the gill mucus of healthy rainbow trout whereas *F. major*-specific IgM antibodies were confined to the serum. *F. major* stimulated sustained IgT but not IgM expression in gill tissue. Sphingolipid metabolism was not only essential for *F. major* growth but also impaired the growth of other resident aerobic bacterial symbionts. Finally, we demonstrate that *F. major* sphingolipids control the distribution of IgT and IgM B cells at mucosal and mucosal sites *in vivo*. Our results show for the first time that sphingolipids produced by a bacterial symbiont are able to modulate B cells and Igs in vertebrates.

Results

***F. major*-specific IgT is found in trout mucus and *F. major*-specific IgM in serum.** We found specific *F. major*-IgM antibodies (titers between 1/4 and 1/6) in the serum of 36% of all analyzed specimens. However, *F. major*-specific IgT could not be detected in serum samples (Table 1, Fig. 1). In mucus, specific IgM titres were undetectable in all cases (Fig. 1). However, *F. major*-specific IgT titers were found both in gill and skin mucus but not gut mucus, with higher titers found in the gills compared to skin (Table 1, Fig. 1). Interestingly, upon symbiont removal, specific IgT could no longer be detected in skin mucus samples indicating that all the *F. major*-specific IgT in skin mucus was bound to bacteria present in the samples. In contrast, removal of bacteria from gill mucus did not eliminate the presence of specific IgT in the sample, indicating that *F. major*-specific IgT antibodies are present in free form (unbound to bacteria) in trout gill mucus (Table 1, Fig. 1). These results demonstrated the presence of Ig responses to symbiotic bacteria in mucosal and systemic compartments of teleost fish.

***F. major* induces sustained expression of IgT but not IgM in trout gill explants.** Trout gill explants incubated with 10⁴ cfu/ml of *F. major* showed significantly higher expression of IgT (between 2 and 4 fold higher than controls) at 6, 24 and 48 h whereas the lower dose (10² cfu/ml) did not significantly change IgT expression. IgM expression was transiently up-regulated at 6 h with 10⁴ cfu/ml *F. major* (Fig. 2a and b) with no changes recorded at later time points or at the lower dose tested. IgT expression was not modified in head kidney leukocytes (HKLs) at any time point or dose tested. IgM expression was significantly lower (2-fold) at 6 h in the presence of 10⁴ cfu/ml *F. major* and 2-fold higher at 48 h with the same bacterial dose (Fig. 2c and d). No changes in IgM expression were detected in HKLs incubated with 10² cfu/ml *F. major*. This experiment showed that the symbiont *F. major* is capable of modifying IgT and IgM transcript levels, but primarily stimulates mucosal IgT expression.

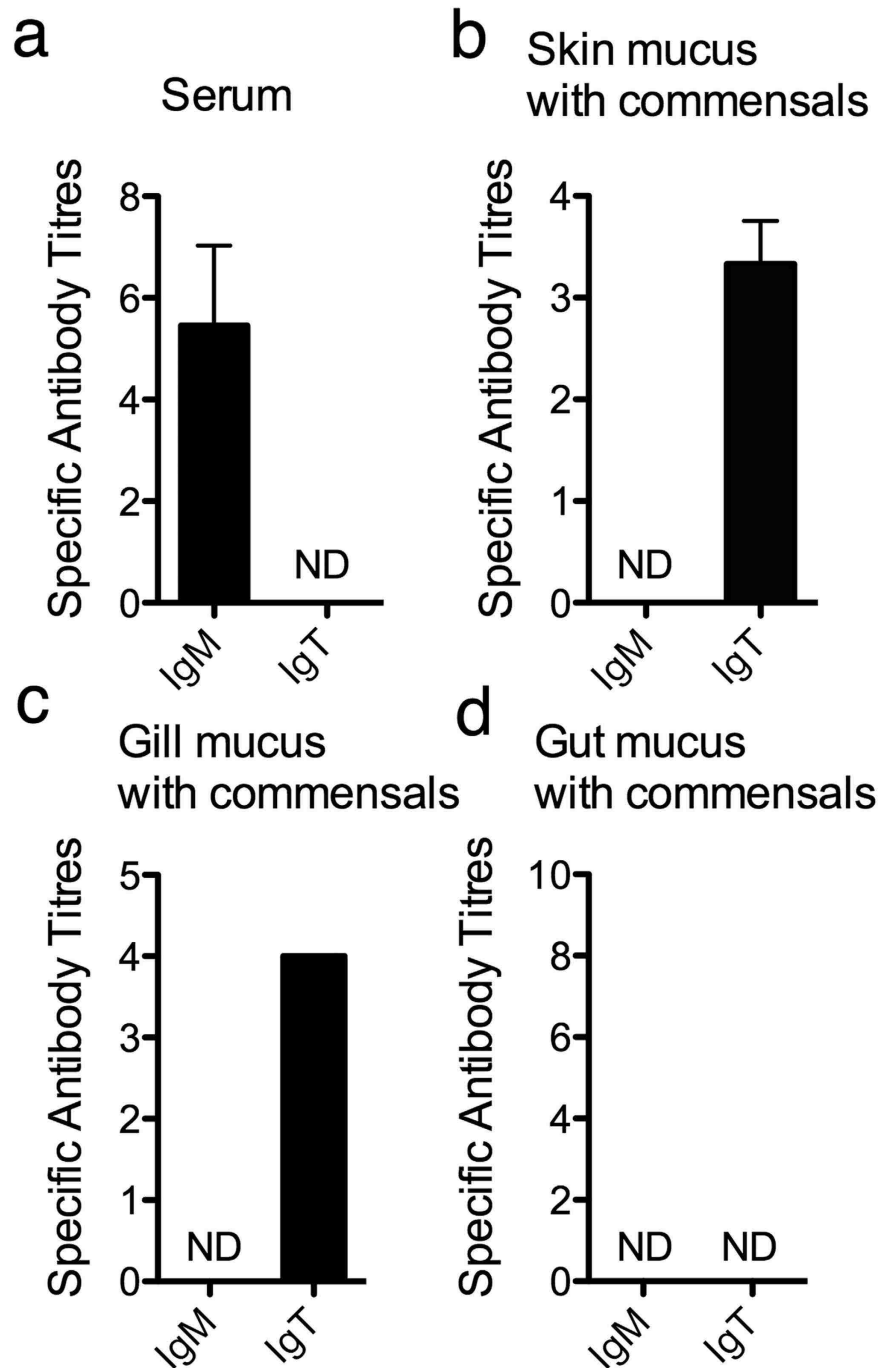


Figure 1. *F. major*-specific IgM and IgT can be detected in hatchery rainbow trout (*O. mykiss*). Antibody titres were measured by ELISA. Results are expressed as the mean titre of all fish that tested positive \pm SEM (N = 6–10). Groups are *F. major*-specific IgM and IgT titres in rainbow trout serum (a) *F. major*-specific IgM and IgT titres in rainbow trout gill mucus containing bacteria (b) *F. major*-specific IgM and IgT titres in rainbow trout skin mucus containing bacteria (c) *F. major*-specific IgM and IgT titres in rainbow trout gut mucus containing bacteria (d).

***F. major* sphingolipids affect the growth of total trout aerobic symbionts.** The growth of the total skin microbiota (TSM) of rainbow trout increased in the presence *F. major* sphingolipids at the four tested concentrations (0.1 μ M, 1 μ M, 10 μ M and 100 μ M) compared to the negative control groups (BSA only) although only the 0.1 and 100 μ M doses resulted in significant growth enhancement at 24 h (Fig. 3a,b). In the case of ceramide, the substrate for the sphingolipid synthesis pathway, no significant effects on TSM growth were recorded except for a reduction in growth at 24 h in the presence of 1 μ M ceramide (Fig. 3c,d). Regarding total aerobic gill microbiota (TGM) of rainbow trout, significant growth enhancement was observed in the presence of the highest (100 μ M) and lowest (0.1 μ M) doses of sphingolipids from *F. major* (Fig. 3e,f). Ceramide treatment, on the other

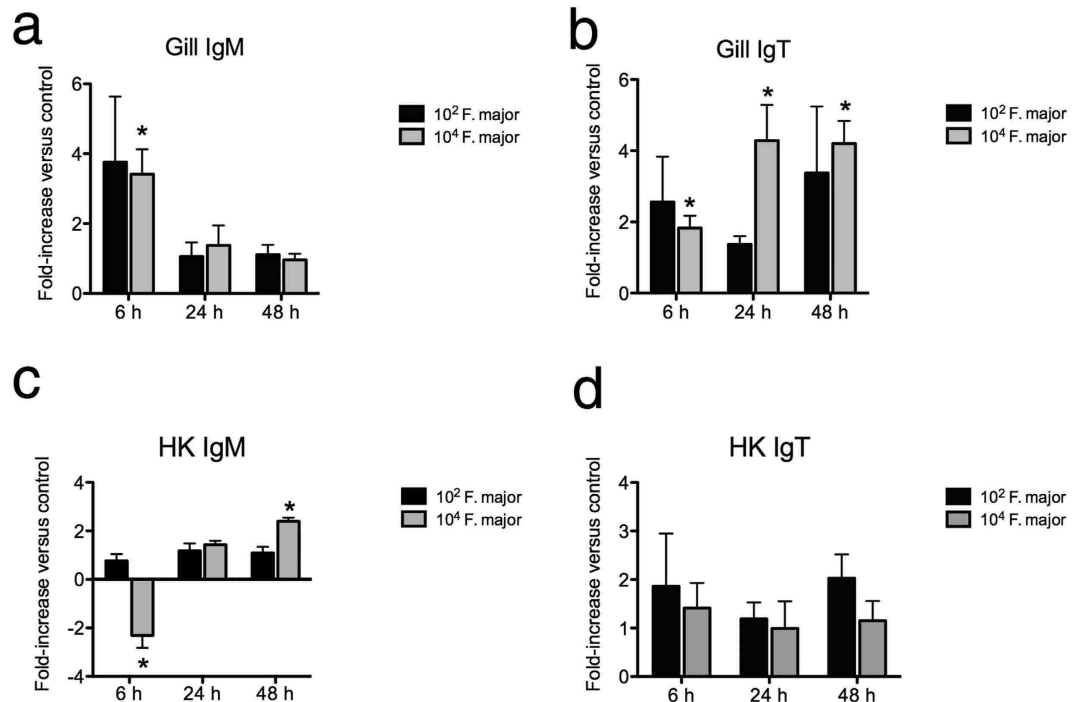


Figure 2. *F. major* stimulates IgM and IgT expression in gill and HK *in vitro* in a dose-dependent manner. (a) IgM expression in trout gill following incubation with 10² cfu/ml or 10⁴ cfu/ml *F. major* for 6, 24 or 48 h. (b) IgT expression in trout gill following incubation with 10² cfu/ml or 10⁴ cfu/ml *F. major* for 6, 24 or 48 h. (c) IgM expression in trout HK following incubation with 10² cfu/ml or 10⁴ cfu/ml *F. major* for 6, 24 or 48 h. (d) IgT expression in trout HK following incubation with 10² cfu/ml or 10⁴ cfu/ml *F. major* for 6, 24 or 48 h. Results are expressed as the mean fold-change compared to unstimulated control as measured by RT-qPCR (N = 5). *Denotes statistically significant changes compared to the unstimulated control (p < 0.05).

hand, caused a dose-dependent growth enhancement on TGM after 24 h (Fig. 3g,h). These results indicated that *F. major*-derived sphingolipids promote TSM and TGM growth when present at low or high doses.

***F. major* regulates the expression of genes involved in the sphingolipid and phospholipid metabolism of the host.** Since *F. major* may be a source of sphingolipids to the trout host, we sought to test whether this bacterium can modify the expression of genes involved in the sphingolipid and phospholipid metabolic pathways of the host. Incubation of gill explants with 10⁴ cfu/ml *F. major* led to significant down-regulation of S1P1, cytosolic phospholipase A2 (cPLA) and alkaline ceramidase (CDase) after 48 h, with the greatest inhibition (~40-fold) observed for S1P1 transcripts. S1P1 expression was also significantly down-regulated (~10-fold) in gill explants incubated with 10² cfu/ml *F. major* for 48 h. Finally, CDase expression was significantly lower (3-fold) at 24 h in gill explants incubated with 10² cfu/ml *F. major* (Fig. 4a–c). Thus, *F. major* appeared to regulate three genes involved in the host's sphingolipid and phospholipid metabolism at mucosal sites.

Phylogenetic analysis of salmonid S1P1. In order to gain further insights into the evolution of S1P1 in vertebrates we datamined S1P1 molecules in NCBI as well as the rainbow trout and Atlantic salmon genomes. S1P1 sequence alignment is shown in Supplementary Fig. S1. We identified two S1P1 genes in both rainbow trout and salmon that shared a high degree of amino acid sequence identity with other teleost S1P1 molecules as well as mammalian S1P1 (Supplementary Fig. S2). The Neighbour Joining tree (Supplementary Fig. S3) showed that all salmonid S1P1 form a clade that is closely related to other teleost S1P1 molecules. Teleost S1P1 clade is closely related to all tetrapod S1P1 molecules. Finally, evaluation of synteny revealed a high degree of conservation in the local genomic regions surrounding S1P1 across vertebrate species (Supplementary Fig. S4). The genes in conserved synteny included coiled-coil domain containing 76 [Source:ZFIN; Acc:ZDB-GENE-050327-19], leucine rich repeat containing 39 [Source:ZFIN; Acc:ZDB-GENE-050417-279], dihydrolipoamide branched chain transacylase E2 [Source:ZFIN; Acc:ZDB-GENE-050320-85], RNA terminal phosphate cyclase domain 1 [Source:ZFIN; Acc:ZDB-GENE-030131-9687], CDC14 cell division cycle 14 homolog A, b [Source:ZFIN; Acc:ZDB-GENE-070705-309], G protein-coupled receptor 88 [Source:HGNC Symbol; Acc:4539], vascular cell adhesion molecule 1 [Source:ZFIN; Acc:ZDB-GENE-070209-238], solute carrier family 30 (zinc transporter), member 7 [Source:ZFIN; Acc:ZDB-GENE-030131-5650], DPH5 homolog (*S. cerevisiae*) [Source:ZFIN; Acc:ZDB-GENE-041114-85] and sphingosine-1-phosphate receptor 1 [Source:ZFIN; Acc:ZDB-GENE-001228-2].

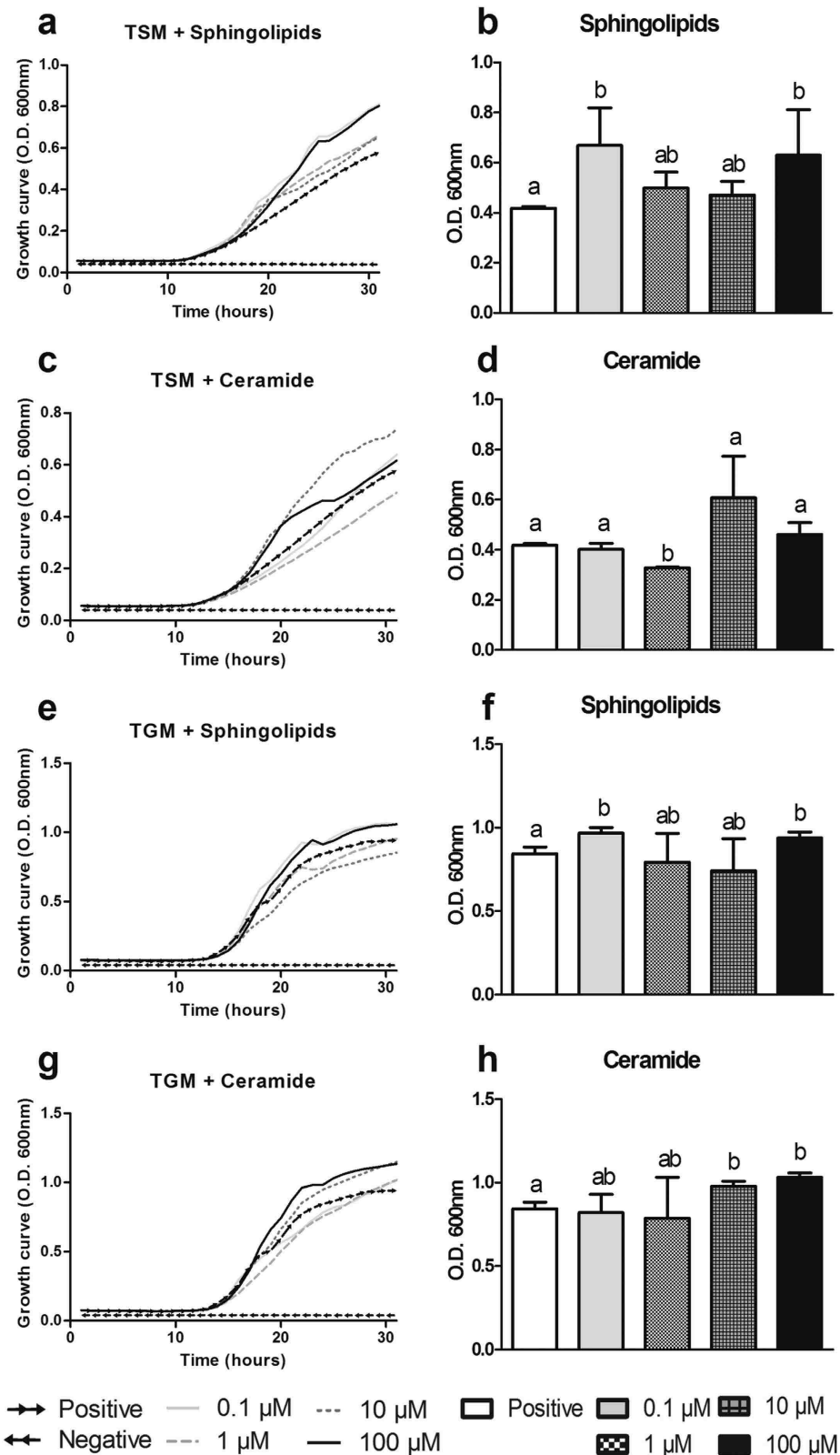


Figure 3. *F. major* sphingolipids modulate the growth of other trout bacterial symbionts. Effects of *F. major*-sphingolipids on trout total skin aerobic microbiota (TSM) growth over a 30 h period (a) or after 24 h (b). Effects of commercial ceramide on TSM growth over a 30 h period (c) or after 24 h (d). Effects of *F. major* sphingolipids on trout total gill aerobic microbiota (TGM) growth over a 30 h period (e) or after 24 h (f). Effects of commercial ceramide on TGM growth over a 30 h period (g) or after 24 h (h). Results are expressed as the mean and/or the mean ± SEM (N = 3). Different letters denote statistically significant differences among treatments (p < 0.05).

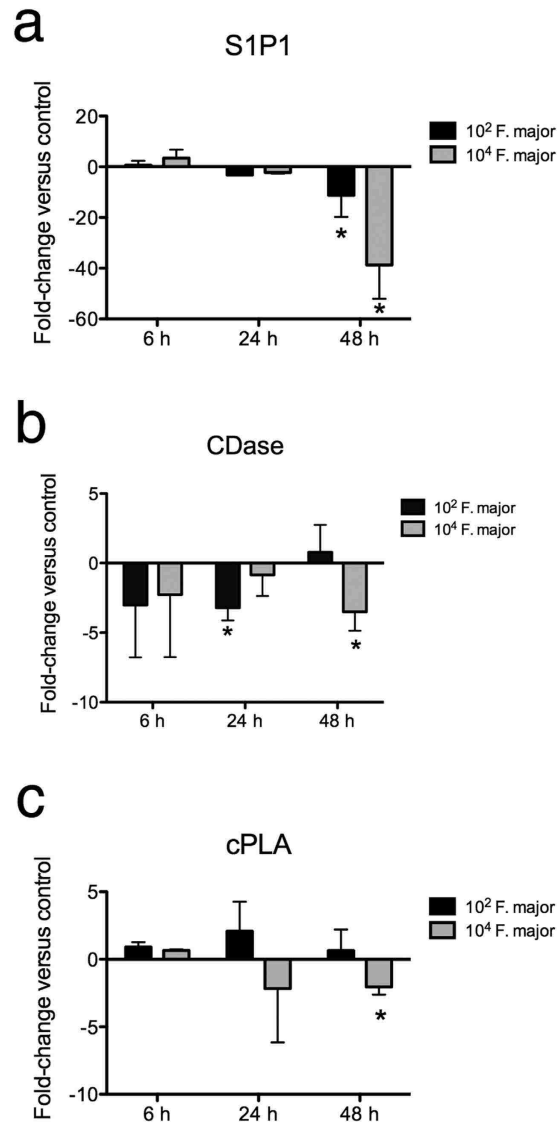


Figure 4. *F. major* regulates the expression of lipid metabolism genes in rainbow trout gill. Expression of (a) S1P1 (b) CDase and (c) cPLA in trout gill explants following incubation with 10^2 cfu/ml or 10^4 cfu/ml *F. major* for 6, 24 or 48 h. Results are expressed as the mean fold-change \pm SEM compared to unstimulated control as measured by RT-qPCR (N = 5). *Denotes statistically significant changes compared to the unstimulated control ($p < 0.05$).

***F. major* and *F. major* sphingolipids induce IgT but not IgM production in trout gills explants.** In order to investigate if *F. major* or its sphingolipids play a role in antibody production at mucosal and systemic lymphoid tissues, we performed a number of *in vitro* experiments with live *F. major* or *F. major* sphingolipids using trout tissue explants and measure antibodies by western blot. Live *F. major* cells induced increases in IgM production in gills and HK but they were not significant (Fig. 5a and Supplementary Fig. S5). A significant increase in IgT production was detected in gill explants but not HK explants exposed to live *F. major* (Fig. 5b and Supplementary Fig. S5). Moreover, *F. major* sphingolipids did not significantly stimulate IgM production in gills or HK *in vitro* (Fig. 5c and Supplementary Fig. S5). However, *F. major* sphingolipids significantly induced IgT production in gill explants but not HK explants (Fig. 5d and Supplementary Fig. S5). These results showed that the symbiont *F. major* as well as *F. major* sphingolipids modulate IgT responses at the protein level in rainbow trout gill.

***F. major* sphingolipids regulate the distribution of IgT⁺ B cells in trout lymphoid tissues.** We hypothesized that if symbiont-derived sphingolipids play a role in maintaining high IgT⁺ B cells numbers at mucosal sites, then systemic delivery of these sphingolipids would result in a change of IgT/IgM ratios in systemic lymphoid tissues. Consistent with our hypothesis, we found that in BSA treated control HKLs, ~86% of all B cells were IgM⁺ and ~14% were IgT⁺. Following i.v injection of *F. major* sphingolipids the proportions of IgM⁺ B cells and IgT⁺ B cells in the HKLs were significantly changed with IgM⁺ and IgT⁺ B cells contributing to ~78% and

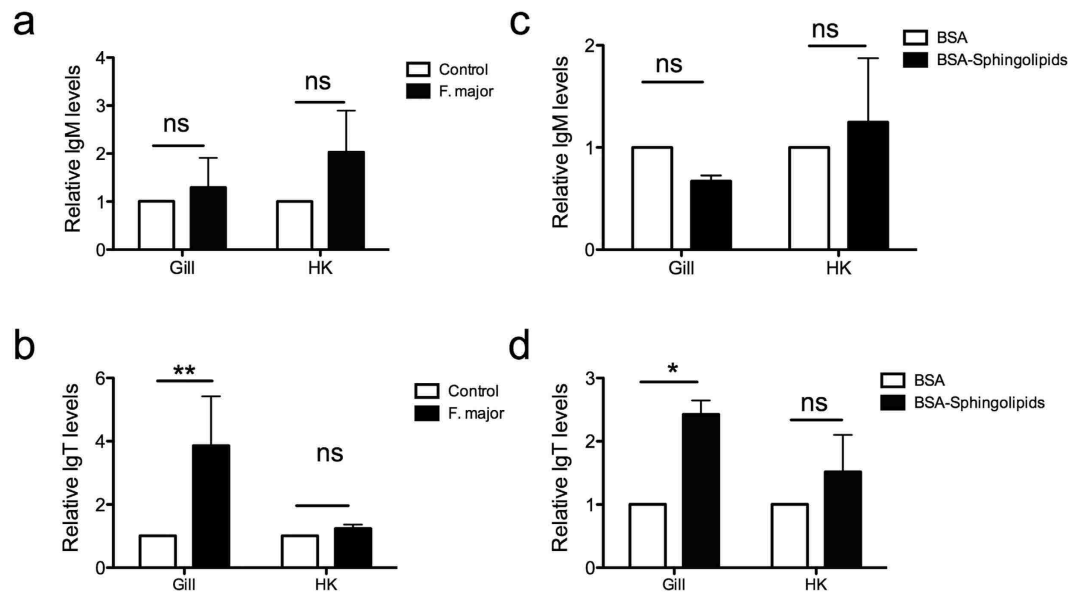


Figure 5. *F. major* and *F. major*-derived sphingolipids stimulate Ig production in trout gills *in vitro*. Rainbow trout gill and HK tissue explants (N = 5) were incubated with DMEM alone (control), live *F. major* cells, *F. major* sphingolipids conjugated with BSA or BSA alone. Explant supernatants were collected and total IgM (a,c) and total IgT (b,d) levels were measured by Western Blot. Results are expressed as the mean relative IgM or IgT protein levels \pm SEM compared to their respective controls. Results are representative of two independent experiments. *Indicates $p < 0.05$, **Indicates $p < 0.01$.

~22% of all B cells, respectively (Fig. 6a,b). Additionally, the proportion of all B cells within the lymphocyte gate in the HK significantly raised from ~30% in controls to ~45% in the sphingolipid treated group (Fig. 6c). As expected in the control group, gill B cells consisted of ~50% of IgM⁺ and ~50% IgT⁺ B cells. In response to the sphingolipid i.v injection, these proportions did not change significantly neither did the total number of B cells present in the gills (Fig. 6d–f). These results demonstrated that *F. major* sphingolipids, when delivered systemically, are able to increase the proportion of B cells within the HK and, specifically, to increase the proportion of IgT⁺ to IgM⁺ B cells in this organ.

Discussion

Vertebrate mucosal surfaces have co-evolved with symbiotic microorganisms for over 500 million years. In order to co-exist with these complex microbial communities, mucosal surfaces secrete mucosal Igs that prevent microbial colonization. Symbiotic bacteria, in turn, stimulate mucosal Ig secretion^{33,34}. Apart from Ig secretion, this intimate relationship brings vast benefits to the host including adequate development, physiology and immunity^{3,4,35,36}.

Similar to mammalian IgA, teleost IgT is produced at mucosal sites in response to parasitic or bacterial infection, whereas systemic adaptive immune responses are characterized by specific IgM production^{11,13–15}. Importantly, IgT, like IgA, keeps commensal bacteria at check through the process of immune exclusion^{11,13–15}.

Among the vast diversity of microorganisms living at vertebrate mucosal epithelia, certain species appeared to have been selected through evolution due to the specific benefits that they provide to the host. We selected the symbiont *F. major* based on previous studies performed in our laboratory that revealed the high abundance of this species in the skin and gill microbiota of hatchery rainbow trout¹². In that study, we found *F. major* as part of the microbiome of adult outbred rainbow trout and therefore different genetic background. However, whether the skin and gill microbiomes of rainbow trout from other environments is also dominated by this species is currently unknown. Here we report for the first time the presence of symbiont-specific IgT responses in mucosal secretions as well as symbiont-specific IgM responses in plasma of rainbow trout. The observed IgT and IgM antibody titres were low in all samples, suggesting that these antibodies may be natural antibodies or antibodies that are cross-reactive against a number of symbiotic species. Critically, we found *F. major*-specific titers in skin and gill mucus but not in gut mucus, indicating that Ig responses to symbionts in teleost fish, similar to mammals³⁷, are tissue specific.

Additionally, we identified differences between the skin and gill IgT *F. major*-specific antibodies. Whereas in the skin all *F. major*-specific IgT was bound to bacteria, in the gills, titers were still detected after bacterial cells had been removed. This result suggests different tissue dynamics in these two sites and can be explained by a number of scenarios. It is possible that in the skin, symbiont-specific IgT production is tightly regulated by the local bacterial communities present, with no excess IgT being produced to reach the unbound, free state. An alternative explanation is that in the gills, removal of symbionts still leaves unbound IgT in the gill mucus and these unbound antibodies have a greater cross-reactivity with *F. major* than the free IgT found in the skin.

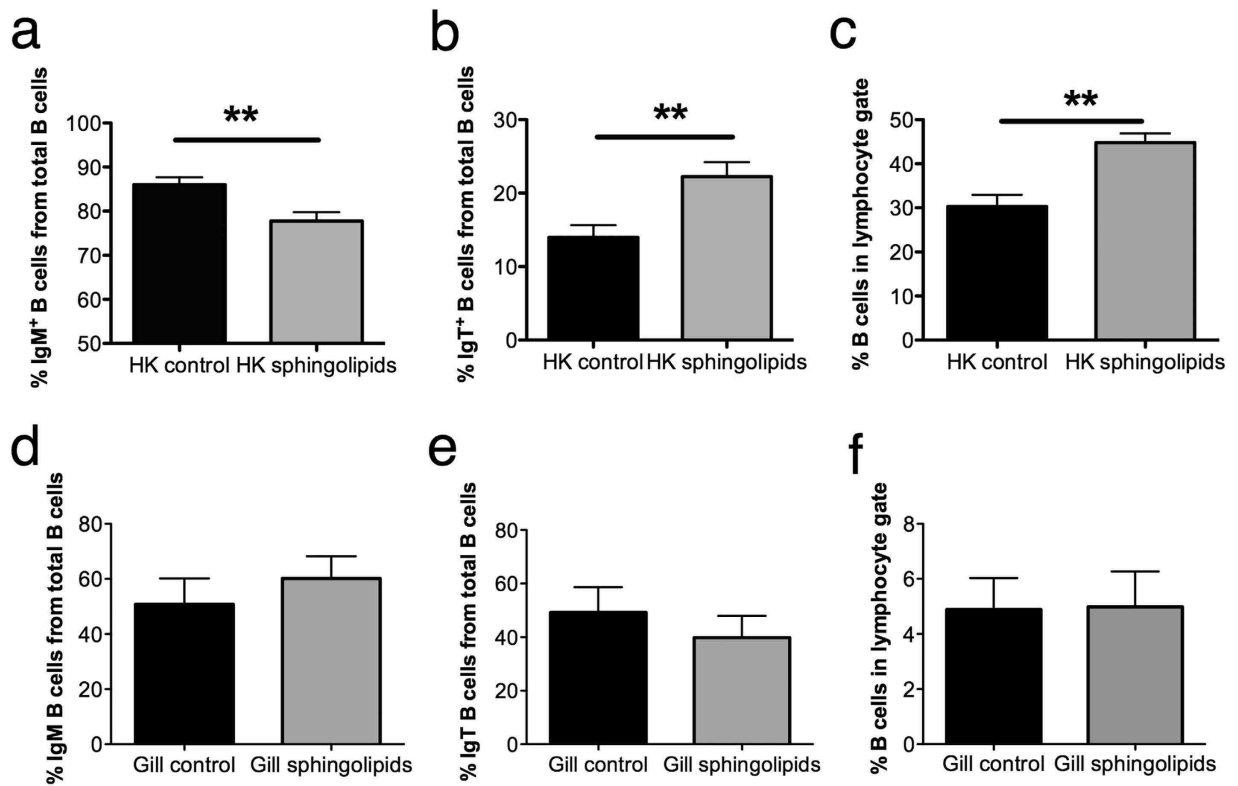


Figure 6. Systemic delivery of *F. major*-derived sphingolipids changes the proportions of B cell subsets and increase the total number of B cells in HK but not gills. Rainbow trout (N = 6) were injected i.v with *F. major* sphingolipids combined with BSA or BSA alone. Fish were sampled 60 h later and leukocytes isolated from the HK and gills. Percentages of IgM⁺ and IgT⁺ B cells were measured by flow cytometry. (a) Mean percentage of IgM⁺ cells in HK. (b) Mean percentage of IgT⁺ cells in HK. (c) Total percentage of B cells in the lymphocyte gate in HK. (d) Mean percentage of IgM⁺ cells in gills. (e) Mean percentage of IgT⁺ cells in gills. (f) Total percentage of B cells in the lymphocyte gate in gills. Results are expressed as the mean % of B cells \pm SEM. Results are representative of four independent experiments. **Denote statistically significant differences compared to the control group ($p < 0.01$).

Symbiotic bacteria regulate the host physiology via the production of different metabolites³⁸. Whereas sphingolipids are produced by most eukaryotic cells, prokaryotes rarely synthesize sphingolipids. However, a few examples of sphingolipid producing bacteria have been reported^{29,30,32}, including the mammalian gut symbiont *Bacteroides fragilis*^{27,30,39}. Symbiont-derived sphingolipids may have unique molecular structures that may confer them unique functional properties. For instance, sphingolipids from *B. fragilis* have anti-inflammatory properties and regulate iNK T cells responses in the gut of mammals³⁰. Moreover, sphingolipid production is critical for the growth of *B. fragilis*²⁷. Since *F. major* is a predominant commensal species of rainbow trout and previous reports had identified this species as a major producer of unique sphingolipids, we hypothesized that *F. major* sphingolipids play a major role in antibody and B cells responses at mucosal sites.

It is worth mentioning that our study was not performed with purified sphingolipids. The methodology used to extract *F. major* lipids has been shown to extract lipids other than sphingolipids³². These amount to approximately 11% of total polar lipids. Additionally, the preparation should also contain ~10% non-polar lipids but these should have been removed during the clean-up step. The two other polar lipids present in our preparations apart from sphingolipids are phosphatidylethanolamine and a monoglycosyldiacylglycerol³². We speculate that these two polar lipids are unlikely to stimulate the teleost immune system since phosphatidylethanolamine is common to teleost fish and monoglycosyldiacylglycerol is common to many bacteria, although further research is needed in this area. We found that *F. major* sphingolipids were able to modulate the growth of other aerobic symbionts isolated from trout skin and gills. The responses were not always dose-dependent, since intermediate concentrations (1 and 10 μ M) of the sphingolipids did not stimulate bacterial growth but low and high concentrations did. Thus, these results may suggest that different bacterial species have different capabilities to metabolize lipids; some bacteria may sense the concentration gradients of these sphingolipids as growth factors whereas others may suffer from their antimicrobial effects and therefore the combined effects on the overall growth of the microbiota may be masked under specific sphingolipid concentrations. Additionally, the total trout aerobic bacteria community measured in this study is biased by the culture conditions and does not capture the entire breadth of modulatory growth effects that this product may have in non-culturable bacterial species. This capability from a bacterial symbiont to modulate the microbiota through sphingolipid pathway is an interesting finding that deserves further investigation.

F. major was able to stimulate IgT gene expression in trout gills but not HK *in vitro* whilst IgM stimulation was modest. In support, *F. major* and *F. major* sphingolipids induced secretion of IgT but not IgM antibodies in gills but not HK *in vitro*, suggesting that they can induce differentiation of B cells into antibody secreting cells. These results also indicate the existence of unique differentiation programs of B cells into antibody secreting cells in gills compared to HK. Finally, IgT but not IgM secretion was stimulated highlighting the intimate co-evolution between symbionts and mucosal antibodies of vertebrates.

Because we found that *F. major* cells increase the expression of antibody transcripts *in vitro*, we hypothesized that sphingolipids produced by this symbiont play a role in the distribution of trout B cell populations. A number of studies have demonstrated that at mucosal sites of trout such as the gut, skin, gill and nose, the ratio of IgT to IgM B cells is 1:1^{11,13–15}. This is in sharp contrast to the preponderance of IgM B cells in systemic lymphoid tissues such as the HK, the spleen and the blood^{14,16}. However, the mechanisms contributing to this unique distribution of B cells at trout mucosal lymphoid tissues is unknown. In mammals, host-derived sphingolipids are known to control lymphocyte trafficking in and out of lymphoid tissues^{20,21,23,40–45}. Moreover, host-derived sphingolipids were shown to determine IgA B cell trafficking in mice^{23,24}. Since under natural conditions, trout skin and gill B cells may be exposed to *F. major* sphingolipids, we hypothesized that these sphingolipids may be responsible for the maintenance of IgT⁺ B cells at these two mucosal sites. In order to test this, we delivered sphingolipids systemically, expecting to shift the proportions of B cells in the HK towards a more “mucosal-like” distribution. We found that symbiont-derived sphingolipids increase the proportion of B cells in the HK. The latter may be achieved by local production of B cells or recruitment. Importantly, *F. major* sphingolipids shifted the proportion of IgT⁺ to IgM⁺ B cells, which again shows that this symbiont product preferentially recruits or stimulates production of IgT⁺ B cells over IgM⁺ cells. These data are not in line with our gene expression results *in vitro* performed with the whole *F. major* bacterium, where no significant increase in IgT expression was recorded in HK. Although both experiments are not directly comparable, this disparity may imply that effects of sphingolipids on HK B cell populations require the intact HK microenvironment for B cells to proliferate or the influx of B cells from other lymphoid organs into the HK. Both requirements are met in the *in vivo* injection experiments but not in the *in vitro* ones.

Our *in vivo* results using *F. major* sphingolipids suggested that trout B cells may have receptors that bind these sphingolipids. In mammals, S1P1 receptor binding to its ligand S1P leads to the internalization of this complex⁴⁶. The reduced S1P1 expression on the surface of lymphocytes results, in turn, in the sequestration of lymphocytes within lymphoid tissues therefore preventing them from entering in circulation^{20,21,23,40–45}. Additionally, S1P has been shown to control intestinal IgA production^{24,25}. In teleosts, S1P1 controls venous vascular integrity and development⁴⁷ but its functional role in immune cells is so far unknown. We found that *F. major* is able to reduce the expression of S1P1 in the gill of rainbow trout. This could potentially lead to the sequestration of IgT B cells produced in the HK and circulating through the gills. Future studies should address the particular S1P1 expression patterns in IgT⁺ and IgM⁺ B cells and whether mucosal versus systemic B cells display different levels of expression of this receptor.

In conclusion, the present study demonstrates the intimate relationship between the symbiont *F. major* and the immune system of rainbow trout. Our results support the idea of an ancient co-existence between symbiotic bacteria and mucosal Igs and B cells. Moreover, sensing of symbiont-derived sphingolipids by trout B cells may be a novel mechanism of symbiont regulation of the host immune system. Fish symbiont sphingolipids could have beneficial applications for the aquaculture industry due to their IgT modulatory properties.

Materials and Methods

Animals, serum and mucus sample collection. Healthy adult triploid rainbow trout (*O. mykiss*) with a mean body weight of 250 ± 20 g were obtained from Lisboa Springs Fish Hatchery (Pecos, New Mexico, USA). Fish were anesthetized with MS-222 and bled from the caudal vein with a heparinized 3 mL syringe. Plasma samples were collected and stored at –80 °C until use. Total gill, gut and skin mucus were collected with a sterile cell scraper as explained elsewhere^{13,14}. Half of the sample was used directly for antibody titer measurement (containing all Igs, bound to bacteria and not bound to bacteria) whereas the other half was subject to a series of centrifugation steps as explained elsewhere¹³. At the end of this procedure, the supernatants were filtered through a 0.2 µm filter in order to detect antibodies unbound to bacteria. The pellets were used for the growth assays described below. All animal studies were reviewed and approved by the Institutional Animal Care and Use Committee (IACUC) at the University of New Mexico, protocol number 16-200384-MC. All methods were performed in accordance with the relevant guidelines and regulations.

Bacteria culture. *F. major* was grown in the specific culture medium ATCC® 29496TM at 25 °C for 30 h in 956 *Microcycylus* medium as per manufacturer’s instructions, and adjusted to the desirable concentration in each case.

Sphingolipid extraction and purification. Five hundred ml of an *F. major* culture grown for 30 hours were centrifuged at 4000 g for 15 min. Supernatants were discarded and pellets were washed once in PBS. Pellets were left to dry in a sterile tissue culture hood for 4 h and then frozen at –20 °C until lipid extraction. Lipids were extracted as explained elsewhere³¹ and then cleaned-up using a G25 Sephadex column as explained elsewhere⁴⁸. In order to avoid toxicity to cells when used *in vitro*, purified sphingolipids and ceramide (a simple glycosphingolipid that serves as the substrate for the sphingolipid synthesis pathway), were combined with a 2 mM bovine serum albumin solution in Dulbecco’s Modified Eagle Medium (DMEM, Life Technologies).

In vitro exposure of rainbow trout gill and HK to *F. major* and *F. major* sphingolipids. After serum and mucus collection, gill tissue was excised with sterile scissors and placed in a Petri dish. Gills were rinsed until all the blood was removed by injecting sterile cold PBS into the gill arch with a 1 ml syringe. Blood-free gill samples were excised into 0.5 cm wide pieces and placed in flat bottom 24-well plates. Trout HK and HKLs were obtained as explained elsewhere¹¹ and seeded onto flat-bottom 24-well plates at 10^6 cells/well. Both gills and HK explants ($N = 5$) were cultured in 1 ml DMEM supplemented with 10% fetal bovine serum (Sigma-Aldrich) and 1% Penicillin-Streptomycin (Gibco). For gene expression studies, gill explants and single cell HKLs suspensions were incubated for 6, 24, and 48 h with 10^2 or 10^4 *F. major* cfu/ml. Wells without bacteria were used as negative control. At each time point, samples were collected and placed in 1 ml TRIzol (Life Technologies) for RNA extraction according to the manufacturer's instructions. Synthesis of cDNA was performed using 2 µg of total RNA, which was first denatured (65 °C, 5 min) in the presence of 1 µl of oligo-dT (Life Technologies), 1 µl dNTPs (10 mM each, Promega). Next, samples containing 1 µl Superscript III enzyme reverse transcriptase (Life Technologies) with 5 µl of 5x first strand buffer (Life Technologies), 1 µl of DTT 0.1 M (Life Technologies) and RNA/DNA free molecular water (Sigma-Aldrich) in a final volume of 25 µl were incubated at 55 °C for 1 h followed by 15 min at 70 °C for later qPCR analysis.

For IgT and IgM detection in supernatants, gill explants and HKLs ($N = 5$) were cultured for 5 days in 1 ml Dulbecco's Modified Eagle Medium (DMEM, Life Technologies) supplemented with 10% fetal bovine serum (Sigma-Aldrich), 1% Penicillin-Streptomycin (Gibco) and 0.5 µg/ml fungizone (Gibco). Explants were incubated for 5 days with only medium (DMEM control), live *F. major* (10^4 cfu/ml), 30 µM *F. major* sphingolipids conjugated with 2 mM BSA in DMEM; 30 µM C2-ceramide (Enzo Life Sciences) conjugated with 2 mM BSA in DMEM or 2 mM BSA alone in DMEM (BSA control). Supernatants were stored at -20 °C until use.

Effects of *F. major* sphingolipids and ceramide on the growth of total gill and skin aerobic bacteria. Total microbiota from skin and gut mucus ($N = 3$) were collected as explained elsewhere¹², washed twice in PBS and adjusted to an optical density of 0.01 in tryptic soy broth (TSB, Sigma-Aldrich). Samples were incubated with 0.1, 1, 10 and 100 µM of sphingolipids from *F. major* or commercial ceramide for 30 h and the optical density at 600 nm was measured in a plate reader (Synergy H1). Wells containing TSB only and TSB with lipids or ceramide without bacteria were used as negative controls.

ELISA. *F. major*-specific IgM and IgT titres were measured in serum, gill, gut and skin mucus from healthy control hatchery trout ($N = 10-12$) using an enzyme-linked immunosorbent assay (ELISA). Mucus samples were used in whole or as bacteria-free mucus after all symbionts were removed as explained elsewhere¹⁴. Flat-bottomed 96-well plates were coated overnight at 4 °C with 100 µl of a *F. major* culture adjusted at 10^7 cfu/ml in PBS. The plates were rinsed once with PBS before blocking for 2 h at room temperature with blocking solution containing 8% non-fat dry milk (LabScientific) in PBS containing 0.05% Tween 20 (PBS-T). After rinsing with PBS-T containing 10 mM EDTA (pH 7.2), the plates were then incubated for 90 min with 100 µl of diluted serum or mucus samples in PBS with 10 mM EDTA. After washing three times, 100 µl of either mouse anti-trout IgM antibody or rabbit anti-trout IgT were added to each well (1/500 in PBS-T) or their respective isotype controls (mouse IgG1 or rabbit prebleed). After washing, wells were incubated for 45 min with the corresponding secondary antibodies (HRP-conjugated donkey anti-mouse IgG or HRP-conjugated donkey anti-rabbit IgG, both at 1/1000 in PBS-T, Jackson ImmunoResearch). After four washes in PBS, the plates were developed using 100 µl of a 0.42 mM solution of 3,3',5,5'-tetramethylbenzidine hydrochloride (TMB, Sigma-Aldrich) prepared in water containing 0.01% H₂O₂. The reaction was stopped after 2-15 min by adding 50 µl of 2 M H₂SO₄. The plates were read at 450 nm in a plate reader (Synergy H1). Samples without bacteria and without serum/mucus were also used as negative controls. Positive titres were determined by subtracting the absorbance detected in the isotype controls from the absorbance in the sample wells.

Western blotting. Western blotting was performed as explained elsewhere¹¹. Briefly, 10 µl of each explant supernatant were mixed with 10 µl of Laemmli buffer (Bio-Rad) under non-reducing conditions. Samples were boiled for 3 min at 97 °C and resolved on 4-15% SDS-PAGE gels (Bio-Rad). Gels were run for 50 min at 120 V and transferred onto PVDF membranes (Amersham). Membranes were blocked in PBS-T containing 5% non-fat milk overnight at 4 °C. Membranes were incubated with rabbit anti-trout IgT (1:1000) for 90 min, washed three times in PBS-T and then incubated for 60 min with HRP-conjugated donkey anti-rabbit IgG (1:2500). Detection was performed using ECL Western Blotting Substrate (Pierce). Membranes were stripped for 20 min in stripping buffer (0.1 M Glycine, 0.02% NaN₃, pH = 2.5) and reprobed with mouse anti-trout IgM for 90 min followed by HRP-conjugated donkey anti-mouse IgG (1:2500) for 60 min. After washing, membranes were developed as explained before. Immunoblots were scanned using a ChemiDoc XRS+ System (Bio-Rad) and band densitometry was analysed with Image Lab Software (Bio-Rad).

RT-qPCR. cDNA synthesis was carried out using 1 µl Superscript III enzyme reverse transcriptase (Invitrogen) in the presence of 5 µl of 5x first strand buffer, 1 µl 0.1 M DTT, made up to a final volume of 25 µl with water, and incubated at 55 °C for 1 h. The resultant cDNA was stored at -20 °C. The expression of IgM, IgT, cytosolic phospholipase A2 (cPLA), ceramidase (CDase) and S1P1 was measured by RT-qPCR using specific primers (Table 2). IgM and IgT primers were designed to amplify the CH regions of the antibody molecules and therefore amplification of both functionally and non-functionally rearranged Igs was performed. The qPCR was performed using 3 µl of a diluted cDNA template as described elsewhere⁴⁹. The relative expression level of the genes was determined using the Pfaffl method⁵⁰.

Sequence analysis of salmonid S1P1. Salmonid S1P1 sequences were identified by data mining in NCBI as well as the rainbow trout and Atlantic salmon genomes. Available mammalian S1P1 sequences were blasted to

Gene symbol	Accession number	Sequence (5' → 3')
<i>Efla</i>	AF498320	F: CAACGATATCCGTCGTGGCA
		R: ACAGCGAAACGACCAAGAGG
<i>S1P1</i>	BX863528	F: AAGGGAGACCGTCGTATCCT
		R: CACACACACTTGCACACTGC
<i>CDase</i>	CX034530	F: GGTGGCATTGGATCACTT
		R: TTGGGCAGGTATCTTTTGG
<i>cPLA</i>	FP321558	F: GCAGTGCCTTCCATTCTC
		R: CCCAGGATGTGTGAGGTTT
<i>IgM</i>	OMU04616	F: AAGAAAGCCTACAAGAGGGAGA
		R: CGTCAACAAGCCAAGCCACTA
<i>IgT</i>	AY870264	F: CAGACAACGACACCTCACCTA
		R: GAGTCAATAAGAAGACACAACGA

Table 2. Primers used for RT-qPCR study.

identify teleost S1P1 molecules. We identified zebrafish (*Danio rerio*) S1P1, Nile tilapia (*Oreochromis niloticus*) S1P1 and Atlantic salmon (*Salmo salar*) S1P1. The salmon sequence was used in further searches conducted in (<http://salmobase.org/>) that identified a second molecule in this species names (CIGSSA_084099.t1) that was named salmon S1P1-like. The zebrafish S1P1 sequence was used in the rainbow trout genome browser Genoscope (<http://www.genoscope.cns.fr/blat-server/cgi-bin/trout>) using default parameters in order to find rainbow trout S1P1 sequences. In that way, we identified 4 scaffolds (6065, 406, 1988 and 2747) in the trout genome. Blast searches of each scaffold revealed that only scaffold 6065 corresponded with S1P1 whereas the other scaffolds contained S1P2 and S1P3 molecules. BlastX of scaffold 6065 identified two rainbow trout unnamed protein products, one with 100% identity with the 6065 scaffold (CDQ90261.1) and one with 97% identity (CDQ69631.1) with the 6065 scaffold. CDQ90261.1 was identical to the translated protein sequence obtained from scaffold 6065. Sequence alignments were performed in CLUSTALW and a phylogenetic Neighbor-Joining tree (10,000 bootstrap) was constructed in MEGA6. Amino acid sequence identity and similarity were determined using MatGAT. Synteny analysis was performed in Genomicus version 01.01 (<http://www.genomicus.biologie.ens.fr/genomicus-trout-01.01/cgi-bin/search.pl>).

In vivo administration of *F. major* sphingolipids. Rainbow trout (N = 6) received 50 µl of DMEM containing 1.4 µg of *F. major* sphingolipids combined with 2 nM BSA by intravenous (i.v) injection. The negative control group received the same volume of DMEM containing BSA only. Trout were sampled 60 h post-injection. The gill and HK of each fish were collected and leukocytes isolated as explained elsewhere¹⁵.

Flow cytometry. One hundred thousand gill leukocytes or HKs from each fish were stained with mouse anti-trout IgT and mouse anti-trout IgM as described elsewhere¹⁴. For secondary antibodies, a FITC-conjugated rat anti-mouse IgG2b and a Dylight 649-conjugated anti mouse IgG1 (both from Biolegend) were used. A total of 20,000 events from the lymphocyte gates were collected in an Attune Flow Cytometer (Life Technologies) and analyzed in the Attune analysis software. The total number of B cells was calculated by adding the percentage of IgM⁺ and IgT⁺ cells from the lymphocyte gate in each sample.

Statistical analysis. Results are expressed as the mean ± standard error (SE). Data analysis was performed in GraphPad Prism version 5.0. Results were analyzed by unpaired t-test, paired t-test (for IgT and IgM quantification by western blot) or ANOVA followed by post-hoc Tukey test according to each dataset to identify statistically significant differences among groups. Statistically significant differences were considered when $p < 0.05$, which were denoted with asterisks or different letters according to each dataset.

References

- Gomez, D., Sunyer, J. O. & Salinas, I. The mucosal immune system of fish: the evolution of tolerating commensals while fighting pathogens. *Fish Shellfish Immunol.* **35**, 1729–1739 (2013).
- Ivanov, I. I. & Honda, K. Intestinal commensal microbes as immune modulators. *Cell Host Microbe* **12**, 496–508 (2012).
- Hooper, L. V. & Gordon, J. I. Commensal host-bacterial relationships in the gut. *Science* **292**, 1115–1118 (2001).
- Hooper, L. V., Littman, D. R. & Macpherson, A. J. Interactions between the microbiota and the immune system. *Science* **336**, 1268–1273 (2012).
- Hooper, L. V., Midtvedt, T. & Gordon, J. I. How host-microbial interactions shape the nutrient environment of the mammalian intestine. *Annu. Rev. Nutr.* **22**, 283–307 (2002).
- Lochmiller, R. L. & Deerenberg, C. Trade-offs in evolutionary immunology: just what is the cost of immunity? *Oikos* **88**, 87–98 (2000).
- Cerf-Bensussan, N. & Gaboriau-Routhiau, V. The immune system and the gut microbiota: friends or foes? *Nat. Rev. Immunol.* **10**, 735–744 (2010).
- Feng, T. & Elson, C. O. Adaptive immunity in the host-microbiota dialog. *Mucosal Immunol.* **4**, 15–21 (2011).
- Salinas, I. The Mucosal Immune System of Teleost Fish. *Biology* **4**, 525–539 (2015).
- Sepahi, A. & Salinas, I. The evolution of nasal immune systems in vertebrates. *Mol. Immunol.* **69**, 131–138 (2016).
- Tacchi, L. *et al.* Nasal immunity is an ancient arm of the mucosal immune system of vertebrates. *Nat. Commun.* **5**, 6205 (2014).

12. Lowrey, L., Woodhams, D. C., Tacchi, L. & Salinas, I. Topographical mapping of the rainbow trout (*Oncorhynchus mykiss*) microbiome reveals a diverse bacterial community in the skin with antifungal properties. *Appl. Environ. Microbiol.* **81**, 6915–6925 (2015).
13. Xu, Z. *et al.* Teleost skin, an ancient mucosal surface that elicits gut-like immune responses. *Proc. Natl. Acad. Sci. USA* **110**, 13097–13102 (2013).
14. Zhang, Y.-A. *et al.* IgT, a primitive immunoglobulin class specialized in mucosal immunity. *Nat. Immunol.* **11**, 827–835 (2010).
15. Xu, Z. *et al.* Mucosal immunoglobulins at respiratory surfaces mark an ancient association that predates the emergence of tetrapods. *Nat. Commun.* **7** (2016).
16. Salinas, I., Zhang, Y.-A. & Sunyer, J. O. Mucosal immunoglobulins and B cells of teleost fish. *Dev. Comp. Immunol.* **35**, 1346–1365 (2011).
17. Cinque, B. *et al.* Sphingolipids and the immune system. *Pharmacol. Res.* **47**, 421–437 (2003).
18. El Alwani, M., Wu, B. X., Obeid, L. M. & Hannun, Y. A. Bioactive sphingolipids in the modulation of the inflammatory response. *Pharmacol. Ther.* **112**, 171–183 (2006).
19. Olivera, A. & Rivera, J. Sphingolipids and the balancing of immune cell function: lessons from the mast cell. *J. Immunol.* **174**, 1153–1158 (2005).
20. Cyster, J. G. Chemokines, sphingosine-1-phosphate, and cell migration in secondary lymphoid organs. *Annu. Rev. Immunol.* **23**, 127–159 (2005).
21. Cyster, J. G. & Schwab, S. R. Sphingosine-1-phosphate and lymphocyte egress from lymphoid organs. *Annu. Rev. Immunol.* **30**, 69–94 (2012).
22. Matloubian, M. *et al.* Lymphocyte egress from thymus and peripheral lymphoid organs is dependent on S1P receptor 1. *Nature* **427**, 355–360 (2004).
23. Schwab, S. R. & Cyster, J. G. Finding a way out: lymphocyte egress from lymphoid organs. *Nat. Immunol.* **8**, 1295–1301 (2007).
24. Kunisawa, J. & Kiyono, H. Immunological function of sphingosine 1-phosphate in the intestine. *Nutrients* **4**, 154–166 (2012).
25. Kunisawa, J. *et al.* Sphingosine 1-phosphate dependence in the regulation of lymphocyte trafficking to the gut epithelium. *J. Exp. Med.* **204**, 2335–2348 (2007).
26. van Meer, G. & de Kroon, A. I. Lipid map of the mammalian cell. *J. Cell Sci.* **124**, 5–8 (2011).
27. An, D., Na, C., Bielawski, J., Hannun, Y. A. & Kasper, D. L. Membrane sphingolipids as essential molecular signals for *Bacteroides* survival in the intestine. *Proc. Natl. Acad. Sci. USA* **108**, 4666–4671 (2011).
28. Kato, M., Muto, Y., Tanaka-Bandoh, K., Watanabe, K. & Ueno, K. Sphingolipid composition in *Bacteroides* species. *Anaerobe* **1**, 135–139 (1995).
29. Olsen, I. & Jantzen, E. Sphingolipids in bacteria and fungi. *Anaerobe* **7**, 103–112 (2001).
30. An, D. *et al.* Sphingolipids from a symbiotic microbe regulate homeostasis of host intestinal natural killer T cells. *Cell* **156**, 123–133 (2014).
31. Batrakov, S. G., Sheichenko, V. I. & Nikitin, D. I. A novel glycosphingolipid from Gram-negative aquatic bacteria. *Biochim. Biophys. Acta (BBA)-Molecular and Cell Biology of Lipids* **1440**, 163–175 (1999).
32. Batrakov, S. G., Mosezhnyi, A. E., Ruzhitsky, A. O., Sheichenko, V. I. & Nikitin, D. I. The polar-lipid composition of the sphingolipid-producing bacterium *Flectobacillus major*. *Biochim. Biophys. Acta* **1484**, 225–240 (2000).
33. Cerutti, A., Chen, K. & Chorny, A. Immunoglobulin responses at the mucosal interface. *Annu. Rev. Immunol.* **29**, 273 (2011).
34. Cerutti, A. & Rescigno, M. The biology of intestinal immunoglobulin A responses. *Immunity* **28**, 740–750 (2008).
35. Mazmanian, S. K., Liu, C. H., Tzianabos, A. O. & Kasper, D. L. An immunomodulatory molecule of symbiotic bacteria directs maturation of the host immune system. *Cell* **122**, 107–118 (2005).
36. Sommer, F. & Bäckhed, F. The gut microbiota—masters of host development and physiology. *Nat. Rev. Microbiol.* **11**, 227–238 (2013).
37. Macpherson, A. & Uhr, T. Compartmentalization of the mucosal immune responses to commensal intestinal bacteria. *Ann. N. Y. Acad. Sci.* **1029**, 36 (2004).
38. Brestoff, J. R. & Artis, D. Commensal bacteria at the interface of host metabolism and the immune system. *Nat. Immunol.* **14**, 676–684 (2013).
39. Brown, L. C. W. *et al.* Production of α -galactosylceramide by a prominent member of the human gut microbiota. *PLoS Biol.* **11**, e1001610 (2013).
40. Allende, M. L., Dreier, J. L., Mandala, S. & Proia, R. L. Expression of the sphingosine 1-phosphate receptor, S1P1, on T-cells controls thymic emigration. *J. Biol. Chem.* **279**, 15396–15401 (2004).
41. Chi, H. Sphingosine-1-phosphate and immune regulation: trafficking and beyond. *Trends Pharmacol. Sci.* **32**, 16–24 (2011).
42. Chiba, K. FTY720, a new class of immunomodulator, inhibits lymphocyte egress from secondary lymphoid tissues and thymus by agonistic activity at sphingosine 1-phosphate receptors. *Pharmacol. Ther.* **108**, 308–319 (2005).
43. Rivera, J., Proia, R. L. & Olivera, A. The alliance of sphingosine-1-phosphate and its receptors in immunity. *Nat. Rev. Immunol.* **8**, 753–763 (2008).
44. Spiegel, S. & Milstien, S. The outs and the ins of sphingosine-1-phosphate in immunity. *Nat. Rev. Immunol.* **11**, 403–415 (2011).
45. Takabe, K., Paugh, S. W., Milstien, S. & Spiegel, S. “Inside-out” signaling of sphingosine-1-phosphate: therapeutic targets. *Pharmacol. Rev.* **60**, 181–195 (2008).
46. Schwab, S. R. *et al.* Lymphocyte sequestration through S1P lyase inhibition and disruption of S1P gradients. *Science* **309**, 1735–1739 (2005).
47. Tobia, C. *et al.* Sphingosine-1-phosphate receptor-1 controls venous endothelial barrier integrity in zebrafish. *Arterioscler. Thromb. Vasc. Biol.* **32**, e104–e116 (2012).
48. Wuthier, R. E. Purification of lipids from nonlipid contaminants on Sephadex bead columns. *J. Lipid Res.* **7**, 558–561 (1966).
49. Tacchi, L., Larragoite, E. & Salinas, I. Discovery of J chain in African lungfish (*Protopterus dolloi*, Sarcopterygii) using high throughput transcriptome sequencing: implications in mucosal immunity. *PLoS ONE* **8**, e70650 (2013).
50. Pfaffl, M. W. A new mathematical model for relative quantification in real-time RT-PCR. *Nucleic Acids Res.* **29**, 2002–2007 (2001).

Acknowledgements

This work was funded by NIH award P20GM103452. H. Cordero thanks Spanish Ministry of Economy and Competitiveness (MINECO) for both PhD and USA stay grants (BES-2012-052742 and EEBB-I-15-09235, respectively). We thank Dr. JO Sunyer and Dr. J.D. Hansen for providing trout antibodies and Elisa Casadei and Ryan Heimroth for help with the bioinformatics analysis. We appreciate the technical help of all the staff from Lisboa Springs Fish Hatchery for kindly providing fish.

Author Contributions

A.S. and H.C. conducted all experiments and analyzed data. H.G. extracted lipids. M.A.E. wrote the manuscript. I.S. conceived the project, designed experiments and wrote the manuscript.

Additional Information

Supplementary information accompanies this paper at <http://www.nature.com/srep>

Competing financial interests: The authors declare no competing financial interests.

How to cite this article: Sepahi, A. *et al.* Symbiont-derived sphingolipids modulate mucosal homeostasis and B cells in teleost fish. *Sci. Rep.* **6**, 39054; doi: 10.1038/srep39054 (2016).

Publisher's note: Springer Nature remains neutral with regard to jurisdictional claims in published maps and institutional affiliations.



This work is licensed under a Creative Commons Attribution 4.0 International License. The images or other third party material in this article are included in the article's Creative Commons license, unless indicated otherwise in the credit line; if the material is not included under the Creative Commons license, users will need to obtain permission from the license holder to reproduce the material. To view a copy of this license, visit <http://creativecommons.org/licenses/by/4.0/>

© The Author(s) 2016

Supplementary Fig. S1: Amino acid sequence alignment of vertebrate S1P1 performed in CLUSTALW. Accession numbers used were: Hs S1P1 (AAH18650.1 Sphingosine-1-phosphate receptor 1 [Homo sapiens]); Hs S1P2 (AAH69598.1 Sphingosine-1-phosphate receptor 2 [Homo sapiens]); Mm S1P1 (AAH51023.1 Sphingosine-1-phosphate receptor 1 [Mus musculus]); Rn S1P1 (NP_058997.1 Sphingosine 1-phosphate receptor 1 [Rattus norvegicus]); Gg S1P1 (XP_422305.3 PREDICTED: sphingosine 1-phosphate receptor 1 [Gallus gallus]); Xt S1P1 (NP_001072893.1 sphingosine 1-phosphate receptor 1 [Xenopus tropicalis]); On S1P1 (XP_005475711.1 PREDICTED: sphingosine 1-phosphate receptor 1 [Oreochromis niloticus]); Dr S1P1 (AAG45430.1 sphingosine 1-phosphate receptor [Danio rerio]); Ss S1P1 (XP_014071480.1 PREDICTED: sphingosine 1-phosphate receptor 1 [Salmo salar]); Ss S1P1-like (CIGSSA_084099.t1); Om S1P1 (CDQ90261.1 and Scaffold 6065) and Om S1P1 (CDQ69631.1).

```
Om_S1P1_CDQ69631.1      -----MGDSMYSDLIARHYNFTGKLRKVEQDS-RLKADS
CIGSSA_084099.t1       -----MGDSMYSDLIARHYNFTGKLRKVEQDS-RLKADS
Om_S1P1_CDQ90261.1_Scaffold_60 -----MGDSMYSDLIARHYNFTGKLRKVEQDS-RLKADS
Ssalar_S1P1            -----MGDSMYSDLIARHYNFTGKLRKVEQDS-RLKADS
Drerio_S1P1            -----MDDL IARHYNFTGKFRKVHKDP-GLKADS
Oniloticus_S1P1       -----MEAMAEPSYSDLI AKHYNYTGKFRKTEQDS-GLKADS
Mmusculus_S1P1        -MVSTSIPEVKALRSSVSDYGNVDIIVRHYNYTGKLNIGA EKDHG IKLTS
Rnorvegicus_S1P1      MVSSTSI PVVKALRSQVSDYGNVDIIVRHYNYTGKLNIGVEKDHG IKLTS
Hsapiens_S1P1         -MGPTSVPLVK AHRSSVSDYVNYDII VRHYNYTGKLNISADKENS IKLTS
Ggallus_S1P1          --MSSGTTAPVRVVSSLTNTDVNVI KEHYNYTGKL NENADSG--IKVTS
Xtropicalis_S1P1     -----MTPTSATQRRNEYDHEIIIEHYN YTGKYKG--NLSTD I KPTS
                             :* .***:*** . . . . . :* *

Om_S1P1_CDQ69631.1    VVFII VCCFI ILENVLVLLTIWR TKKFHKPMYYFIGNLALS DLLAGVVYT
CIGSSA_084099.t1      VVFII VCCFI ILENVLVLLTIWR TKKFHKPMYYFIGNLALS DLLAGVVYT
Om_S1P1_CDQ90261.1_Scaffold_60 VVFII VCCFI ILENVLVLLTIWR TKKFHKPMYYFIGNLALS DLLAGVVYT
Ssalar_S1P1           VVFII VCCFI ILENVLVLLTIWR TKKFHKPMYYFIGNLALS DLLAGVVYT
Drerio_S1P1           VVFII VCCFI ILENVLVLLTIWR TKKFHKPMYYFIGNLALS DLLAGVVYT
Oniloticus_S1P1      VIFII VCCFI ILENILVLLTIWR TKKFHKPMYYFIGNLALS DLLAGVVYT
Mmusculus_S1P1       VVFILICCFI ILENIFVLLTIWKT KKFHRP MYYFIGNLALS DLLAGVAYT
Rnorvegicus_S1P1     VVFILICCFI ILENIFVLLTIWKT KKFHRP MYYFIGNLALS DLLAGVAYT
Hsapiens_S1P1        VVFILICCFI ILENIFVLLTIWKT KKFHRP MYYFIGNLALS DLLAGVAYT
Ggallus_S1P1         VVFII IICCFI ILENIFVLLTIWKT KKFHRP MYYFIGNLALS DLLAGVAYT
Xtropicalis_S1P1     IIFII IICCFI VLENILVLLTIWR TKKFHRP MYYFIGNLALS DLLAGTAYT
                             ::***: **:*:***:* ** **:*:****:***** ..**

Om_S1P1_CDQ69631.1    ANILLSGANTYKLTPTQWFFREGSMFVALAASVFSL LAIAIERH LTM LKM
CIGSSA_084099.t1      ANILLSGANTYKLTPTQWFFREGSMFVALAASVFSL LAIAIERH LTM LKM
Om_S1P1_CDQ90261.1_Scaffold_60 ANILLSGANTYKLTPTQWFFREGSMFVALAASVFSL LAIAIERH LTM LKM
Ssalar_S1P1           ANILLSGANTYKLTPTQWFFREGSMFVALAASVFSL LAIAIERH LTM LKM
Drerio_S1P1           ANILLSGANTYKLTPTQWFFREGSMFVALAASVFSL LAIAIERH LTM LKM
Oniloticus_S1P1      ANILLSGANTYKLTPTQWFFREGSMFVALAASVFSL LAIAIERH LTM LKM
Mmusculus_S1P1       ANLLLSGATTYKLT PAQWFLREGSMFVALSASVFSLLAIAIERYITMLKM
Rnorvegicus_S1P1     ANLLLSGATTYKLT PAQWFLREGSMFVALSASVFSLLAIAIERYITMLKM
Hsapiens_S1P1        ANLLLSGATTYKLT PAQWFLREGSMFVALSASVFSLLAIAIERYITMLKM
```

Ggallus_S1P1 ANLLLSGHKTYSLTPSQWVREGSMFVALSASVFSLLAIAIERYITMLKM
Xtropicalis_S1P1 ANILLSGPHTYKLTPEWLIRESMFMVALSASVFSVAIAIERYITMLKM
**:*:* * * * * * : * : * * * * * : * * * * * : * * * * * : * * * * *

Om_S1P1_CDQ69631.1 KLHNNNGNTRVFMFLISTVWVLI AAILGGLPIMGWNCIQSMPCSTVLP LYH
CIGSSA_084099.t1 KLHNNNGNTRVFMFLISTVWVLI AAILGGLPIMGWNCIQSMPCSTVLP LYH
Om_S1P1_CDQ90261.1_Scaffold_60 KLHNNNGNTRVFMFLISTVWVLI AAILGGLPIMGWNCIQSMPCSTVLP LYH
Ssalar_S1P1 KLHNNNGNTRVFMFLISTVWVLI AAILGGLPIMGWNCIQSMPCSTVLP LYH
Drerio_S1P1 KLHNNNGKTRVFMFLISTVWFIA AAILGGLPVMGWNCIDSINN CSTVLP LYH
Oniloticus_S1P1 KLHNNNGNTRVFMFLISTVWVMI AAVLGGLPVMGWNCIQSMTQCSTVLP LYH
Mmusculus_S1P1 KLHNGSNSSRSFLLISACWV I SLILGGLPIMGWNCISLSSCSTVLP LYH
Rnorvegicus_S1P1 KLHNGSNSSRSFLLISACWV I SLILGGLPIMGWNCISLSSCSTVLP LYH
Hsapiens_S1P1 KLHNGSNFRFLISACWV I SVILGGLPIMGWNCISLSSCSTVLP LYH
Ggallus_S1P1 KLHNGSNFRFLISACWV I SVILGGLPIMGWNCISLSSCSTVLP LYH
Xtropicalis_S1P1 KLHNGSKSSRSFLLISGCW I LSLFLGGLPIMGWNCIKQISACSTVLP LYH
***** : * * * * * * * : * : * * * * * : * * * * * : * * * * *

Om_S1P1_CDQ69631.1 KTYILFCTTVFVSVILMAIVVLYARIYALVRTRSRKMVFRKVSNGRGGGSA
CIGSSA_084099.t1 KTYILFCTTVFVSVILMAIVVLYARIYALVRTRSRKMVFRKVSNGRGGGSA
Om_S1P1_CDQ90261.1_Scaffold_60 KTYILFCTTVFVSVILMAIVVLYARIYALVRTRSRKLVFRKVSNGRGGGSA
Ssalar_S1P1 KTYILFCTTVFVSVILMAIVVLYARIYALVRTRSRKLVFRKVSNGRGGGSA
Drerio_S1P1 KAYILFCTTVFVSVILMAIVVLYARIYALVRTRSRKLVFRKVSNGRGGGSA
Oniloticus_S1P1 KAYILFCTTVFVSVILMAIVVLYARIYALVRTRSRKLVFRKVSNGRGNASA
Mmusculus_S1P1 KHYILFCTTVFTLLLSIVILYCRIYSLVRTRSRRLTFRKN-----ISK
Rnorvegicus_S1P1 KHYILFCTTVFTLLLSIVILYCRIYSLVRTRSRRLTFRKN-----ISK
Hsapiens_S1P1 KHYILFCTTVFTLLLSIVILYCRIYSLVRTRSRRLTFRKN-----ISK
Ggallus_S1P1 KHYILFCTTVFTGLLSIVVLYCRIYSMVTRSRRLTFRKN-----ITK
Xtropicalis_S1P1 KHYILFCTTVFTLLLSIVVLYCRIYSMVTRSRRLTFRKN-----LAR
* * * * * : * : * * * * * : * * * * * : * * * * *

Om_S1P1_CDQ69631.1 SSKSSEKSMALLKTVIIVLSCFIACWAPLFILLLL DVACNIRMCPILYKA
CIGSSA_084099.t1 SSKSSEKSMALLKTVIIVLSCFIACWAPLFILLLL DVACDIRMCPILYKA
Om_S1P1_CDQ90261.1_Scaffold_60 SSKSSEKSMALLKTVIIVLSCFIACWAPLFILLLL DVACDIRMCAILYKA
Ssalar_S1P1 SSKSSEKSMALLKTVIIVLSCFIACWAPLFILLLL DVACDIRMCAILYKA
Drerio_S1P1 SNKSSEKSMALLKTVIIVLSCFIACWAPLFILLLL DVACQTLTCSILYKA
Oniloticus_S1P1 NSKSSEKSMALLKTVIIVLSCFIACWAPLFILLLL DVACETLSCPILYKA
Mmusculus_S1P1 ASRSSEKSLALLKTVIIVLSVFIACWAPLFILLLL DVGCKAKTCDILYKA
Rnorvegicus_S1P1 ASRSSEKSLALLKTVIIVLSVFIACWAPLFILLLL DVGCKAKTCDILYKA
Hsapiens_S1P1 ASRSSEKSLALLKTVIIVLSVFIACWAPLFILLLL DVGCKVKTCDILFRA
Ggallus_S1P1 ATRSSEKSLALLKTVIIVLSAFIACWAPLFILLLL DVGCRVKTCPILYKA
Xtropicalis_S1P1 PSRSSEKSMALLKTVIIVLSVFIACWAPLFILLLL DFGCKVKTCPVLFKA
.:*****:***** * * * * * : * * * * * : * * * * *

Om_S1P1_CDQ69631.1 EWFLALAVLNSAMNPLIYTLTNSNEMRAFLKTLCCSVCTQSS-GKFSKP
CIGSSA_084099.t1 EWFLALAVLNSAMNPLIYTLTNSNEMRAFLKTLCCSICTRPS-GKFSQP
Om_S1P1_CDQ90261.1_Scaffold_60 EWFLALAVLNSAMNPLIYTLTNSNEMRAFLKTLCCSVCTRPS-GKFSRP
Ssalar_S1P1 EWFLALAVLNSAMNPLIYTLTNSNEMRAFLKTLCCSVCTRPS-GKFSRP
Drerio_S1P1 EWFLALAVLNSAMNPLIYTLTNSNEMRAFIKMLNCG-VCVQPS-GKFSRP
Oniloticus_S1P1 EWFLALAVLNSAMNPLIYTLTNSNEMRAFLKTLCCCTAFIRPR-TKLTGP
Mmusculus_S1P1 EYFLVLA VLNSTNPIIYTLTNKEMRAFI RIVSCCKCPNGDSAGKFKRP
Rnorvegicus_S1P1 EYFLVLA VLNSTNPIIYTLTNKEMRAFI RIVSCCKCPNGDSAGKFKRP

Hsapiens_S1P1
Ggallus_S1P1
Xtropicalis_S1P1

EYFLVLAVLNSGTNPIIYTLTNKEMRRAFIRIMSCCKCPSGDSAGKFKRP
EYFLVLAVLNSATNPIIYTLTNKEMRRAFIKILCCCKCPPTDSGTFKFRP
EYFLSLAVLNSATNPIIYTLTNREMRRAFMKMACCSHCIFGSSSKVKRP
*:** *****. **:*****..*****::: * *.. *

Om_S1P1_CDQ69631.1
CIGSSA_084099.t1
Om_S1P1_CDQ90261.1_Scaffold_60
Ssalar_S1P1
Drerio_S1P1
Oniloticus_S1P1
Mmusculus_S1P1
Rnorvegicus_S1P1
Hsapiens_S1P1
Ggallus_S1P1
Xtropicalis_S1P1

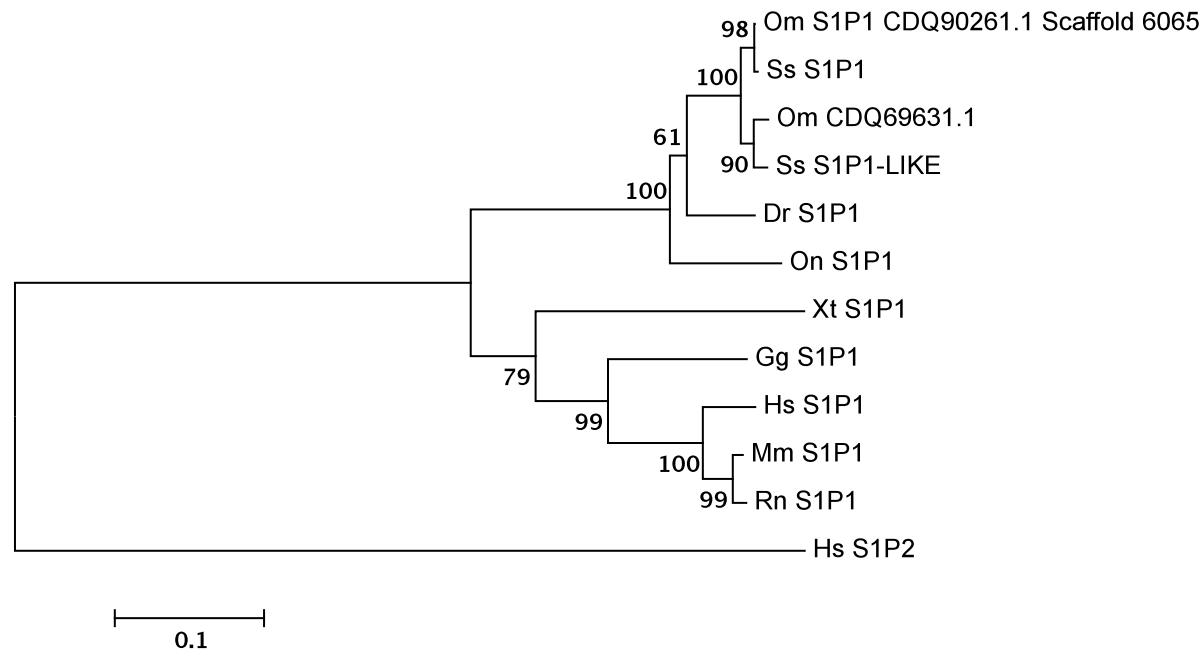
IIG-AEFSRSKSDNSSHPNKDEPEYLPRETIVSSGIITSSS-
IIG-AEFSRSKSDNSSHPNKDEPEYLPREAIVSSGNITSSS-
IMG-AEFSRSKSDNSSHPNKDEPEYSPRETVVSSGNITSSS-
IMG-AEFSRSKSDNSSHPNKDEPEYSPRETVVSSGNITSSS-
IMG-AEFSRSKSDNSSHPNKDEPEYSPRETIVSSGNITSSS-
IMG-AEFSRSKSDNSSHPNKEVEYSPRETTVVSSGNVTSSS
IIPGMEFSRSKSDNSSHPQKDDGDNP--ETIMSSGNVNSSS-
IIPGMEFSRSKSDNSSHPQKDDGDNP--ETIMSSGNVNSSS-
IAGMEFSRSKSDNSSHPQKDEGDNP--ETIMSSGNVNSSS-
IIGMEFSRSKSDNSSHPQKEGDRP--ETIMSSGNVTSSS-
IITGMEFSRSKSDNSSHPQKDEGEYP--VTLMSSGNVTSSS-
*: *****:~::~ : : * . :~**

Supplementary Fig. S2: Percentage amino acid identity and similarity among vertebrate S1P1. Accession numbers used were: Hs S1P1 (AAH18650.1 Sphingosine-1-phosphate receptor 1 [Homo sapiens]); Hs S1P2 (AAH69598.1 Sphingosine-1-phosphate receptor 2 [Homo sapiens]); Mm S1P1 (AAH51023.1 Sphingosine-1-phosphate receptor 1 [Mus musculus]); Rn S1P1 (NP_058997.1 Sphingosine 1-phosphate receptor 1 [Rattus norvegicus]); Gg S1P1 (XP_422305.3 PREDICTED: sphingosine 1-phosphate receptor 1 [Gallus gallus]); Xt S1P1 (NP_001072893.1 sphingosine 1-phosphate receptor 1 [Xenopus tropicalis]); On S1P1 (XP_005475711.1 PREDICTED: sphingosine 1-phosphate receptor 1 [Oreochromis niloticus]); Dr S1P1 (AAG45430.1 sphingosine 1-phosphate receptor [Danio rerio]); Ss S1P1 (XP_014071480.1 PREDICTED: sphingosine 1-phosphate receptor 1 [Salmo salar]); Ss S1P1-like (CIGSSA_084099.t1); Om S1P1 (CDQ90261.1 and Scaffold 6065) and Om S1P1 (CDQ69631.1).

	1	2	3	4	5	6	7	8	9	10	11
1. Om_S1P1_CDQ90261.1		97	67.8	67.2	89.2	87.5	99.7	67.6	65.9	67.8	97.6
2. Om_S1P1_CDQ69631.1	98.9		67.8	67	88.4	86.2	96.8	67.6	65.9	67.9	98.1
3. Mm_S1P1	81.4	81.2		94.2	68.4	66.5	67.9	98.4	73.3	84.8	67.5
4. Hs_S1P1	82.5	82.2	97.1		67.3	65.5	67.2	93.2	73.7	84.3	66.9
5. Dr_S1P1	93.3	92.2	81.7	81.4		84.3	89.2	68.2	66.5	68.3	88.2
6. On_S1P1	92.6	91.8	81.4	81.4	91		87.5	65.3	65.7	67.1	86.7
7. Ss_S1P1	99.7	98.7	81.4	82.5	93.3	92.3		67.8	65.6	67.9	97.3
8. Rn_S1P1	81.5	81.2	99	96.6	81.7	80.9	81.5		72.8	84.6	67.3
9. Xt_S1P1	80.7	81	84.8	85.6	79.4	80.9	80.5	84.3		73.1	65.6
10. Gg_S1P1	81	81.5	90.1	90.3	80.7	80.7	81.8	90.1	83.9		67.8
11. Ss_S1P1_LIKE	99.2	99.2	80.9	81.9	92.5	92.3	98.9	80.9	80.7	81	

identity
similarity

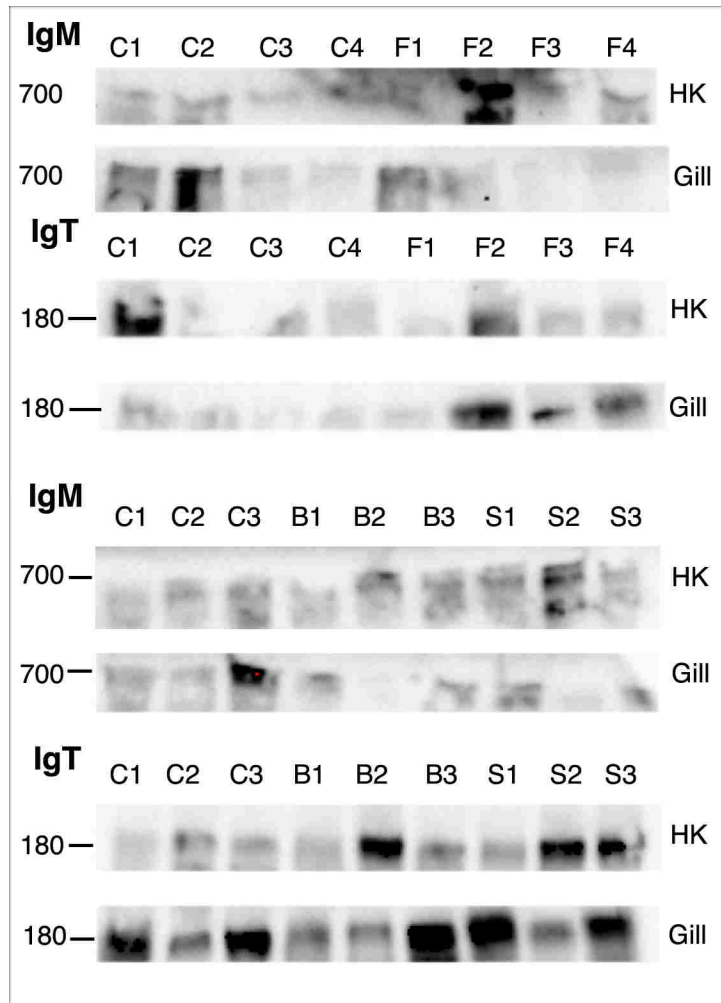
Supplementary Fig. S3: Neighbour Joining Tree of vertebrate S1P1. Phylogenetic tree was constructed using MEGA6 with 10,000 bootstrap value. Human S1P1 was used as a tree outlier. Accession numbers used were: Hs S1P1 (AAH18650.1 Sphingosine-1-phosphate receptor 1 [Homo sapiens]); Hs S1P2 (AAH69598.1 Sphingosine-1-phosphate receptor 2 [Homo sapiens]); Mm S1P1 (AAH51023.1 Sphingosine-1-phosphate receptor 1 [Mus musculus]); Rn S1P1 (NP_058997.1 Sphingosine 1-phosphate receptor 1 [Rattus norvegicus]); Gg S1P1 (XP_422305.3 PREDICTED: sphingosine 1-phosphate receptor 1 [Gallus gallus]); Xt S1P1 (NP_001072893.1 sphingosine 1-phosphate receptor 1 [Xenopus tropicalis]); On S1P1 (XP_005475711.1 PREDICTED: sphingosine 1-phosphate receptor 1 [Oreochromis niloticus]); Dr S1P1 (AAG45430.1 sphingosine 1-phosphate receptor [Danio rerio]); Ss S1P1 (XP_014071480.1 PREDICTED: sphingosine 1-phosphate receptor 1 [Salmo salar]); Ss S1P1-like (CIGSSA_084099.t1); Om S1P1 (CDQ90261.1 and Scaffold 6065) and Om S1P1 (CDQ69631.1).



Supplementary Fig. S4: Conserved synteny of vertebrate S1P1 genes generated by Genomicus. Rainbow trout scaffold 6065 is not shown due to lack of the complete annotation of the scaffold. The central vertical line indicates the position of S1P1. From that line moving left, we found DPH5 homolog (*S. cerevisiae*) [Source:ZFIN;Acc:ZDB-GENE-041114-85], solute carrier family 30 (zinc transporter), member 7 [Source:ZFIN;Acc:ZDB-GENE-030131-5650], vascular cell adhesion molecule 1 [Source:ZFIN;Acc:ZDB-GENE-070209-238], G protein-coupled receptor 88 [Source:HGNC Symbol;Acc:4539], CDC14 cell division cycle 14 homolog A, b [Source:ZFIN;Acc:ZDB-GENE-070705-309], RNA terminal phosphate cyclase domain 1 [Source:ZFIN;Acc:ZDB-GENE-030131-9687], dihydrolipoamide branched chain transacylase E2 [Source:ZFIN;Acc:ZDB-GENE-050320-85], leucine rich repeat containing 39 [Source:ZFIN;Acc:ZDB-GENE-050417-279] and coiled-coil domain containing 76 [Source:ZFIN;Acc:ZDB-GENE-050327-19].



Supplementary Fig. S5: Immunoblots detecting IgM or IgT in supernatants obtained from rainbow trout HK and gill explants incubated for 5 days with control DMEM medium (C), 10^4 cfu/ml *F. major* (F), BSA (B) or *F. major* sphingolipids conjugated with BSA (S). Relative IgM and IgT levels were quantified by densitometry. Images show three different fish samples that are representative of two independent experiments with N=5 in each experiment.



Appendix B

Sanchez, Mariah, Ali Sepahi, Elisa Casadei, and Irene Salinas. "Symbiont-derived sphingolipids regulate inflammatory responses in rainbow trout (Oncorhynchus mykiss)." Aquaculture (2018).



Symbiont-derived sphingolipids regulate inflammatory responses in rainbow trout (*Oncorhynchus mykiss*)



Mariah Sanchez, Ali Sepahi, Elisa Casadei, Irene Salinas*

Department of Biology, Center for Evolutionary and Theoretical Immunology, University of New Mexico, Albuquerque, NM 87131-0001, USA

ABSTRACT

Farmed fish live in association with diverse bacterial communities that produce wide arrays of metabolites. In rainbow trout, the skin and the gills are colonized by *Flectobacillus major*, a bacterium known to produce sphingolipids (SLs). The goal of this study is to evaluate the ability of *F. major* SLs to regulate rainbow trout inflammatory responses. *F. major* SLs were delivered by themselves or in combination with Freund's Complete Adjuvant (FCA), an oil-based adjuvant known to cause severe abdominal inflammation when injected to fish. Trout injected with SL + FCA showed decreased severity of FCA toxic effects including necrosis, granuloma formation and presence of oil droplets. However, inclusion of SLs in the FCA preparation did not decrease infiltration of immune cells intramuscularly at the site of injection. Intraperitoneal or intravenous delivery of *F. major* SLs resulted in increased expression of IgT, IgM and TGF β transcripts in the gills but not the head-kidney and had no effects on IL-10 expression. These results indicate the *F. major* SLs regulate rainbow trout inflammatory responses and indicate that this compound can have important applications in farmed fish health management.

1. Introduction

Farmed fish suffer from a number of inflammatory diseases that can hamper their welfare, growth and market value. For example, soybean meal-induced enteritis (SBMIE) is a disease that causes severe inflammation in the intestine of salmonids (Booman et al., 2018; Sahlmann et al., 2013; Urán et al., 2008; Urán et al., 2009). Examples of inflammation caused by disease agents include heart and skeletal muscle inflammation (HSMI) disease in salmon (Kongtorp et al., 2004) or *Flavobacterium psychrophylum* infections in salmonids (Nematollahi et al., 2003).

Vaccination is the most effective way to prevent disease outbreaks in finfish farming. Although some vaccines elicit strong immune responses by themselves, several studies have shown that vaccine efficacy in teleost fish is improved by using adjuvants in the vaccine preparation (Siwicki et al., 1998; Tafalla et al., 2013; Thim et al., 2014). The most studied and potent adjuvants in fish are oil-based adjuvants. However, oil-based adjuvants are not approved for use in aquaculture due to the detrimental side effects they cause to fish, including lesions, adhesions, granulomas and inflammation (Bricknell and Dalmo, 2005; Noia et al., 2014; Vazirzadeh et al., 2008). Thus, finding alternative adjuvants or reducing the inflammatory side effects induced by oil-based adjuvants, such as Freund's adjuvant, would increase the sustainability of the fish

farming industry.

Commensal bacteria bring many benefits to the host (Gomez et al., 2013; Hooper et al., 2012; Kelly and Salinas, 2017; Sepahi and Salinas, 2016) and can produce metabolites with potent biological properties (Arpaia and Rudensky, 2014; Gomez et al., 2013; Hooper et al., 2012; Levy et al., 2016; Sharon et al., 2014). Teleost fish live in symbiosis with large and diverse communities of microorganisms. In rainbow trout (*Oncorhynchus mykiss*), one of the most abundant commensal species residing in the skin and gills is *Flectobacillus major* (Lowrey et al., 2015; Sepahi et al., 2016), a bacterium that has the unique ability to synthesize glycosphingolipids (Batrakov et al., 2000; Batrakov et al., 1999). Recent studies in the mammalian gastrointestinal tract suggest that dietary sphingolipids or sphingolipids produced by bacteria can be absorbed by enterocytes in a number of ways including fusion of outer-membrane vesicles with host cell membranes (Heaver et al., 2018). Absorbed sphingolipids are then mostly converted to free fatty acids and incorporated into triglycerides that enter the bloodstream in the form of chylomicrons (Heaver et al., 2018) allowing for effects at distal sites. Uptake mechanisms at other tissue barriers such as the gills or skin have not been investigated, but sphingolipid-derived metabolites such as ceramide and S1P can be taken up by cells by different mechanisms including binding to G-protein coupled receptors (Blah and Hla, 2014). Thus, although yet to be investigated, epithelial cells in the

* Corresponding author.

E-mail address: isalin@unm.edu (I. Salinas).

gills and skin of teleosts may uptake sphingolipids or their metabolites which could then enter the bloodstream eliciting local and distant effects.

Our laboratory has recently demonstrated that *F. major*-derived sphingolipids are key modulators of mucosal B cells in rainbow trout and that they can stimulate secretion of IgT and modulate the proportions of IgM and IgT B cells in lymphoid organs (Sepahi et al., 2016). Yet, other biological functions of *F. major* sphingolipids remain unknown.

Previous work in mice has shown that sphingolipids produced by the intestinal bacterium *Bacteroides fragilis* have anti-inflammatory functions and regulate iNK T cells (An et al., 2014). Thus, we hypothesized that *F. major*-derived sphingolipids may have important anti-inflammatory properties in rainbow trout and therefore can be used in aquaculture to ameliorate inflammatory processes. The aim of this study was to determine the ability of *F. major*-derived sphingolipids to induce anti-inflammatory cytokine responses and to test this compound in an adjuvant-model of inflammation in rainbow trout. Our results show that *F. major*-derived sphingolipids have both anti- and pro-inflammatory functions and that they are able to ameliorate side-effects caused by oil adjuvant injection in rainbow trout.

2. Material and methods

2.1. Animals

Healthy adult rainbow trout (with mean body weight of 250 ± 20 g) were obtained from Lisboa Springs Fish Hatchery (Pecos, New Mexico, USA) and maintained at the University of New Mexico Biology Animal Research Facility. Fish were acclimatized for two weeks prior to conducting any experiments. Fish were kept in a recirculation system with a 12-hour photoperiod and fed commercial pellets (Rangen, Inc.) *ad libitum*. Prior to sampling, fish were anesthetized with MS-222 and bled from the caudal vein with a heparinized 3 ml syringe. All animal studies were reviewed and approved by the Institutional Animal Care and Use Committee (IACUC) at the University of New Mexico, protocol number 16-200384-MC.

2.2. Bacterial growth and sphingolipid extractions and purification

F. major was grown in the specific culture medium ATCC® 29,496™ at 25 °C for 30 h in 956 Microcyclus medium. *F. major* sphingolipids were extracted using chloroform-methanol mixtures as explained in (Batra et al., 2000). Non-lipid contents were then removed by chromatography on a Sephadex G-25 column (GE Healthcare) as described by (Wuthier, 1966). The cleaned fraction was resuspended in Dulbecco's Modified Eagle Medium (DMEM, Life Technologies) containing 2 nM bovine serum albumin (BSA).

2.3. In vivo administration of *F. major* sphingolipids

Rainbow trout were divided into four experimental groups, sphingolipids alone (SL), Freund's complete adjuvant (FCA, Sigma Aldrich, USA) alone, FCA + sphingolipid (FCA + SL) and DMEM-BSA alone (N = 4). The SL and FCA + SL groups received a total of 1.4 µg of *F. major* sphingolipids in 50 µl. FCA was first emulsified in DMEM/BSA and then mixed 1:1 vol/vol with SL to make the FCA + SL emulsion. Trout were injected intraperitoneally (i.p) with 50 µl of each solution and were sampled 3 weeks later for gross morphology, examination of internal organs, and histology of the abdominal wall tissue. This experiment was repeated two-independent times.

For gene expression analysis, two independent experiments were conducted separately from the adjuvant experiments. The first experiment consisted of two groups (N = 6) injected with either 50 µl of DMEM containing 1.4 µg of *F. major* sphingolipids combined with 2 nM BSA or DMEM containing 2 nM BSA (control) i.p. The second

Table 1
Gross morphology scoring system (arbitrary units).

Damage	Score
Reddening: no superficial reddening Inflammation: no inflammation Necrosis: no visible necrosis Adhesions: no adhesions of peritoneum to abdominal wall or visceral organs	0
Reddening: minor superficial reddening Inflammation: minor inflammation (only visible superficially) Necrosis: minor reddening and inflammation within affected tissue Adhesions: minor adhesions of peritoneum to abdominal wall (not affecting visceral organs)	1
Reddening: moderate superficial reddening Inflammation: moderate deep and superficial inflammation Necrosis: moderate reddening and inflammation within affected tissue Adhesions: moderate adhesions of peritoneum to abdominal wall/visceral organs	2
Reddening: severe superficial reddening Inflammation: severe deep and superficial inflammation Necrosis: severe reddening and discoloration around affected tissue Adhesions: severe adhesions of peritoneum spanning entire abdominal wall or adhering to visceral organs	3

experiment contained the exact same experimental groups (N = 6) but received an intravenous (i.v) injection instead of i.p. We had previously delivered the *F. major* sphingolipid preparation by i.v injection and observed changes in immune cell populations (Sepahi et al., 2016). Thus, we used this route as a positive control. For applied purposes, however, or in adjuvant formulations, the i.p is more relevant and therefore we used both routes. Fish were sampled 60 h post-injection. A piece of the head kidney (HK) and gill tissue (from the center region of the second gill arch) were collected from each fish and placed in TRIZol for RNA extraction.

2.4. Gross morphology scoring

Overall gross morphology of the abdominal wall and internal visceral organs was scored using four parameters: reddening, inflammation, necrosis and adhesions. Each parameter was scored on a scale of 0–3 as explained in Table 1. Total gross morphology score was calculated by adding the individual scores from each of the four parameters for each fish.

2.5. Histology and light microscopy analyses

Eight abdominal wall samples per group were collected and fixed in 4% paraformaldehyde for 3 days at 4 °C. After transferring samples to 70% ethanol, samples were processed and embedded in paraffin using routine histological procedures. Five µm-thick paraffin sections were stained with hematoxylin-eosin. Ten random fields were observed per samples and scored on a 0–3 scale for the presence of necrosis, granulomas, empty vesicles, oil masses and immune cell infiltration. A granuloma was defined as nodular structure composed of granulomatous cells surrounding an oil core. No attempt to identify the cellular composition of the granuloma was made. A score of 0 represents absence of observation whereas a score of 3 represents high abundance/presence of a particular feature. Light micrographs were observed under a Zeiss AxioSkop using the AxioVision software by two independent researchers.

2.6. RT-qPCR

Tissues were homogenized in 1 ml TRIZol (Invitrogen) using tungsten carbide beads (3 mm, Qiagen) and shaking (300 times per min) as per the manufacturer's instructions for RNA extraction. The RNA pellet was washed in 80% ethanol, air-dried and resuspended in RNase-free

Table 2
Primers used for RT-qPCR study.

Gene symbol	Accession number	Sequence (5' → 3')
Ef1a	AF498320	F: CAACGATATCCGTCGTGGCA R: ACAGCGAAACGACCAAGAGG
IgM	OMU04616	F: AAGAAAGCCTACAAGGGGAGA R: CGTCAACAAGCCAAGCCACTA
IgT	AY870264	F: CAGACAACAGCACCTCACCTA R: GAGTCAATAAGAAGACACAACGA
IL-10	NM_001245099.1	F: CTGCTGGACGAAGGATTCTAC R: GGCCTTTATCCTGCATCTTCTC
IL-1β	AJ223954	F: ACATTGCCAACCTCATCATCG R: TTGAGCAGGTCTTGTCTCTTG
TGFβ-1a	AJ007836	F: CTCACATTTTACTGATGTCACTTCTGT R: GGACAACCTGCCACCTTGTG
TGFβ-1b	FN822750	F: CATGTCCATCCCCAGAACT R: GGACAACCTGTTCCACCTGTGTT
TNF-α	AJ277604	F: GGGGACAAACTGTGGACTGA R: GAAGTTCITGCCCTGCTCTG

H₂O. The RNA concentration was measured by spectrophotometry (Nanodrop ND1000, LabTech) and RNA integrity determined by electrophoresis (Agilent Bioanalyser, 2100). cDNA synthesis was performed using 500 ng of total RNA, which was denatured (65 °C, 5 min) in the presence of 1 µl of oligo-dT17, 1 µl dNTP (deoxynucleoside triphosphate mix 10 mM each Promega) and RNA/DNA free water (Sigma) in a volume of 13 µl. Synthesis was carried out using 1 µl Superscript III enzyme reverse transcriptase (Invitrogen) in the presence of 5 µl of 5 × first strand buffer, 1 µl 0.1 M DTT, made up to a final volume of 25 µl with water and incubated at 55 °C for 1 h. The resultant cDNA was stored at -20 °C. The expression of IgM, IgT, IL-10, IL-1β, TGFβ-1a, TGFβ-1b and TNF-α was measured by RT-qPCR using specific primers (Table 2). qPCR was performed using 3 µl cDNA template using specific primers as explained elsewhere (Sepahi et al., 2017). Analysis was performed using the Pfaffl method (Pfaffl, 2001).

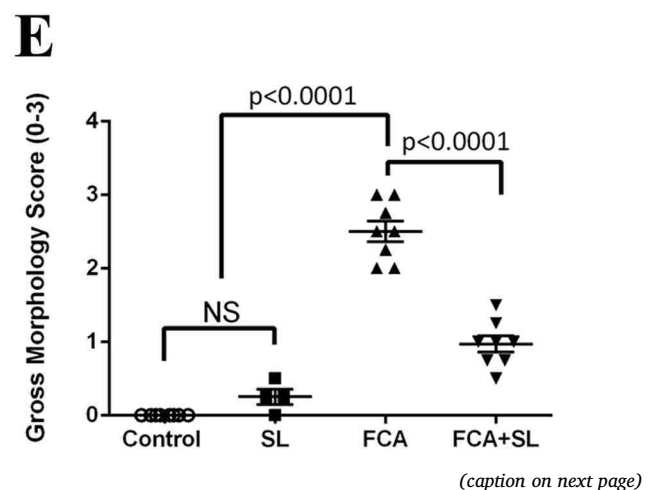
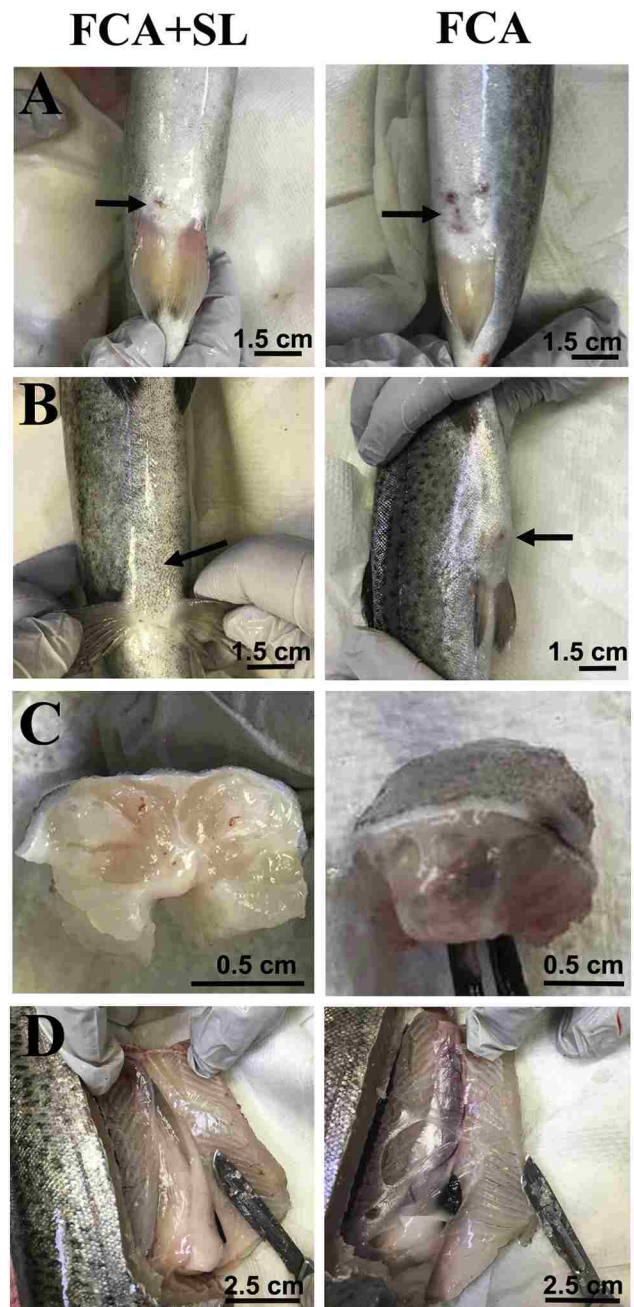
2.7. Statistical analysis

Data are expressed as the mean ± sem. Gene expression data was analyzed by *t*-test to identify statistically significant differences between groups. Data analysis was performed in GraphPad Prism version 5.0. One-way ANOVA and a Tukey *post hoc* analysis test were performed to identify statistically significant differences among groups. P values < 0.05 were considered statistically significant.

3. Results

3.1. Combination of FCA with *F. major* sphingolipids ameliorates gross morphology of adjuvant-derived tissue damage

The abdominal wall and visceral organs were inspected for inflammation, reddening, necrosis and adhesions (Fig. 1A–D). Substantially more reddening at and around the injection site was observed in FCA group, as compared to FCA + SL (Fig. 1A). Inflammation of the abdominal wall was also observed in both FCA and FCA + SL groups, but was greater in the FCA group compared to the FCA + SL group (Fig. 1B). The muscle tissue of the abdominal wall surrounding the site of injection showed signs of necrosis in both groups but was significantly more extensive in the FCA group compared to the FCA + SL treatment (Fig. 1C). As expected, FCA *i.p* injection resulted in presence of adhesions throughout the entire abdominal cavity (Fig. 1D). Small adhesions of the peritoneum to the abdominal wall were observed in FCA + SL group. Injection of SL alone resulted in a mean score of 0.25 ± 0.17 (Fig. 1E and Table 3). The DMEM-BSA group (negative control) showed no signs of damage around the site of injection (0.00 ± 0.00). Reddening, inflammation, necrosis and adhesions were lower in FCA + SL group (0.97 ± 0.58) compared to FCA alone



(caption on next page)

Fig. 1. Gross morphology of rainbow trout abdomen 3 weeks post injection (i.p) of Freund's Complete Adjuvant combined with *F. major* sphingolipids (FCA + SL) or Freund's Complete Adjuvant alone (FCA). Pictures are representative of four different fish per group. (A) reddening of the skin at the site of injection (black arrow), (B) inflammation at the site of injection (black arrow) and (C) necrosis of abdominal tissue and (D) adhesions of the peritoneum to the abdominal wall. Total average score (arbitrary units) of all four parameters (reddening, inflammation, necrosis and adhesions) for each of the four experimental groups are plotted in (E). Results are representative of two independent experiments.

Table 3

Tabulated mean and standard deviation for each parameter.

Groups	Damage	Mean	Standard deviation
DMEM/BSA	Reddening	0.00	0.00
	Inflammation	0.00	0.00
	Necrosis	0.00	0.00
	Adhesions	0.00	0.00
SL only	Reddening	0.00	0.00
	Inflammation	0.25	0.43
	Necrosis	0.75	0.43
	Adhesions	0.00	0.00
FCA + SL	Reddening	0.50	0.50
	Inflammation	1.25	0.33
	Necrosis	1.25	0.43
	Adhesions	1.00	0.71
FCA only	Reddening	2.37	2.37
	Inflammation	2.50	0.50
	Necrosis	3.50	0.50
	Adhesions	3.62	0.62

(2.5 ± 0.61) (Fig. 1E). These results indicate the *F. major* sphingolipids ameliorate gross damage caused by FCA injection.

3.2. Combination of FCA with *F. major* sphingolipids ameliorates adjuvant-derived tissue damage but causes intramuscular immune cell infiltration

Histological observation of the skeletal muscle tissue at the site of injection showed no damage or immune cell infiltration in DMEM-BSA controls (Fig. 2A). As expected, infiltrates of immune cells were observed among skeletal muscle fibers in the FCA only group (Fig. 2B).

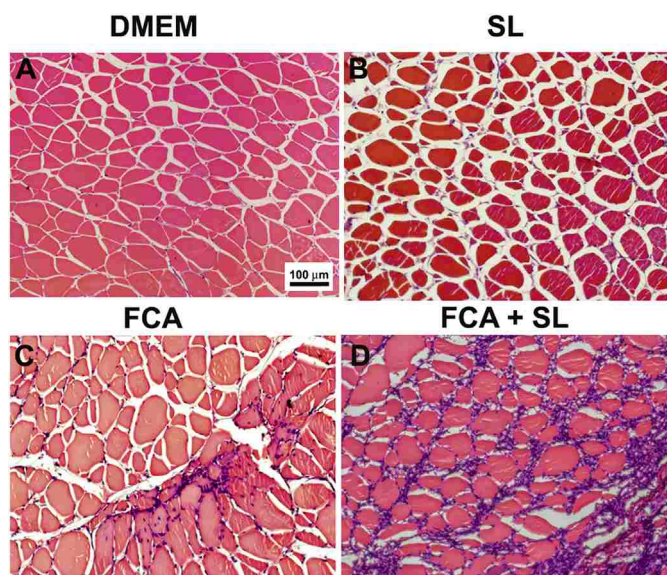


Fig. 2. Hematoxylin and eosin staining of abdominal wall muscle tissue from rainbow trout injected i.p. with DMEM (control), Freund's Complete Adjuvant (FCA), *F. major* sphingolipids alone (SL), or Freund's Complete Adjuvant containing sphingolipids (FCA + SL) and sampled 3 weeks later.

Surprisingly, the FCA + SL group showed a higher degree of immune cell infiltration compared to the FCA only (Fig. 2C). Extensive areas of necrosis were observed in the FCA only but was far less frequently observed in the SL and FCA + SL groups (Fig. 3A). Granulomas were observed most frequently and extensively in FCA group with only one granuloma observed in the FCA + SL group and no granulomas in the DMEM-BSA or SL only groups (Fig. 3B). In agreement with previous study (Noia et al., 2014), large empty vacuoles were observed in both FCA and FCA + SL groups (Fig. 3C). The vacuoles that were observed in FCA only group were larger and surrounded by few cells. In contrast, the FCA + SL group contained smaller vacuoles that were surrounded by several cells (not shown). Within the abdominal wall section, oil masses were observed only in FCA only and FCA + SL groups, appearing to be far larger and more prevalent in FCA only group (Fig. 3D). Finally, increased deposits of melanin were only observed in the FCA group around the site of injection (not shown). Combined, these results indicate that *F. major* sphingolipids reduce the side effects caused by FCA injection, but they also stimulate infiltration of immune cells intramuscularly.

3.3. In vivo delivery of *F. major* sphingolipids induces changes in IgM, IgT and cytokine expression in HK and gills

I.p injection of SL resulted in a significant up-regulation of both IgM (3-fold) and IgT (5-fold) gene expression in the gills. In the HK, i.p delivery of SLs resulted in a down-regulation in IgM and IgT expression, 2-fold and 4-fold, respectively (Fig. 4A, B). Pro-inflammatory cytokine IL-1 β expression was down-regulated 2-fold in the HK but did not change significantly in gill (Fig. 4C). TNF α expression was up-regulated 1.6-fold in the gills but not in the HK of i.p SL injected group (Fig. 4D). The expression of anti-inflammatory cytokine TGF β -1b was upregulated in the gills and remained unchanged in the HK (Fig. 4F). No significant changes in expression were observed for IL-10 or TGF β -1a (Fig. 4E, G) in response to i.p administration of SL.

IgM and IL10 expression remained unchanged in both HK and gills in response to i.v SL delivery (Fig. 5A, G). I.v delivery of SLs caused an up-regulation of IgT expression in the gill (Fig. 5B) but not in the HK. IL-1 β expression was significantly upregulated in the gill but not HK in response to i.v SL delivery (Fig. 5C). The expression of the pro-inflammatory cytokine TNF α was up-regulated in the HK but not the gill (Fig. 5D) Finally, anti-inflammatory cytokines TGF β -1a and TGF β -1b were both significantly up-regulated in the gill but not in the HK (Fig. 5E, F).

These results indicate that, at mucosal surfaces such as the gills, *F. major* sphingolipids stimulate IgT as well as pro-inflammatory and anti-inflammatory cytokine expression but that these effects are less pronounced systemic lymphoid tissues such as the HK compared to mucosal sites such as the gills.

4. Discussion

Host biological processes can be influenced by commensal-derived metabolites (Gomez et al., 2013; Hooper et al., 2012; Kelly and Salinas, 2017; Sepahi and Salinas, 2016). Host immunological responses can be directed by commensals in a variety of ways, including the induction or suppression of inflammation (An et al., 2014; Hooper et al., 2012). Thus far, the functions of commensal-derived metabolites such as lipids have not been exploited in the context of aquaculture. In this particular study, we evaluated the ability of *F. major*-derived sphingolipids to regulate inflammatory responses in rainbow trout.

We focused on sphingolipids derived from *F. major* since this is a prevalent commensal of the skin and gills of trout (Lowrey et al., 2015) and we recently showed that sphingolipids isolated from this bacterium modulate rainbow trout immunoglobulin and B cell responses (Sepahi et al., 2016). To investigate the effects of the *F. major*-derived sphingolipids in trout inflammatory responses, we paired it with the

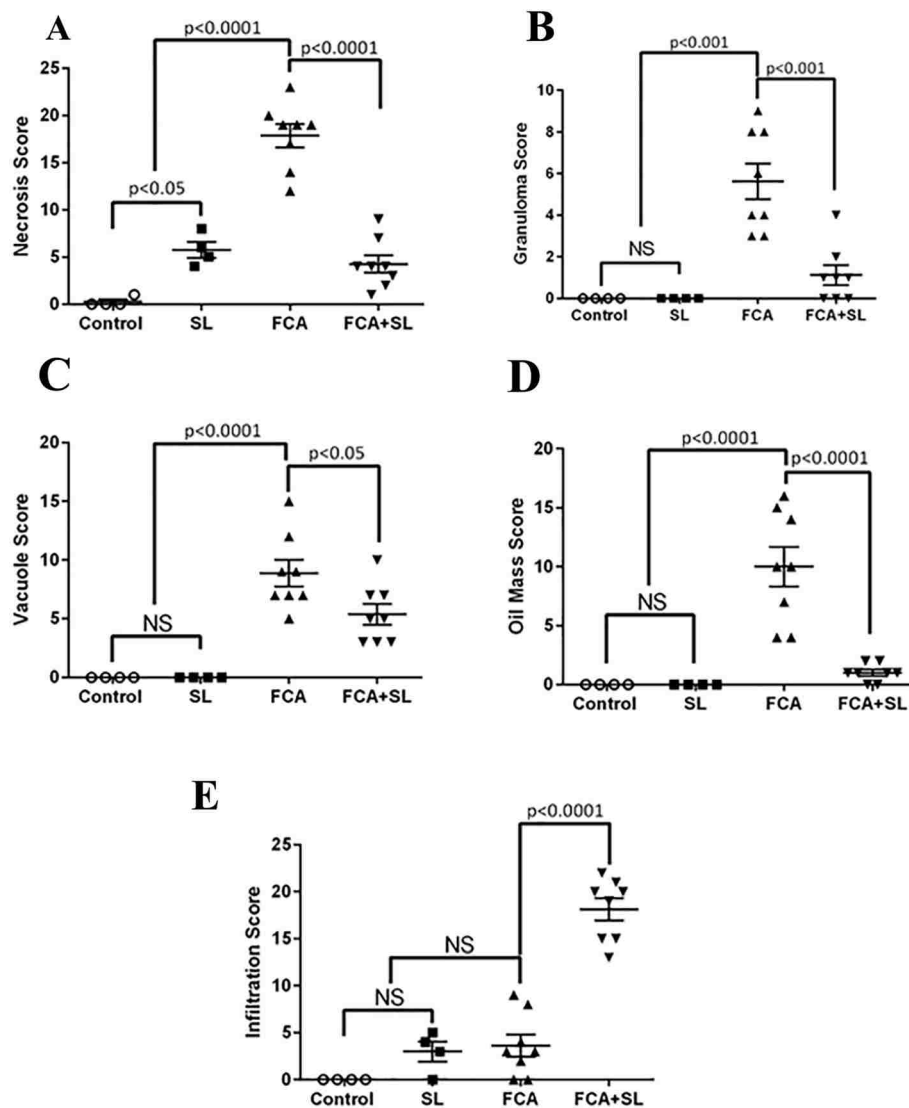


Fig. 3. Pathology scores based on histological observation (Fig. 2) of rainbow trout (N = 4) injected i.p with DMEM (control), Freund's Complete Adjuvant (FCA), *F. major* sphingolipids alone (SL), or Freund's Complete Adjuvant containing *F. major* sphingolipids (FCA + SL) and sampled 3 weeks later and sections were stained with hematoxylin-eosin. Ten random sections from each sample were scored by two independent researchers using scores of 0, 1, 2 or 3 for (A) cellular necrosis; (B) granulomas; (C) vacuoles; (D) oil masses; and (E) immune cell infiltration. Results are representative of two independent experiments.

commonly used oil-based adjuvant, Freund's Adjuvant. Oil-based adjuvants paired with vaccines are widely used to help elicit effective immunological responses but are often accompanied by several adverse side effects in fish (Tafalla et al., 2013). Specifically, Freund's Adjuvant has been shown to induce inflammation, adhesions and granulomatous lesions at the injection site and visceral organs, and has also been shown to deposit droplets of the emulsified adjuvant within the abdominal cavity (Gjessing et al., 2012; Noia et al., 2014; Villumsen et al., 2015). Thus, there is a current need to develop new adjuvants or, as proposed in this study, combine FCA with other compounds that decrease its toxicity. Our findings indicate that commensal-derived sphingolipids like the one tested here are an inexpensive and promising tool to regulate inflammatory diseases in farmed fish. Injection of *F. major* sphingolipids alone did not result in leucocyte infiltration at the site of injection 3 weeks later. It is possible that leucocytes infiltrated the injection site at earlier time points and it deserves further investigation. Based on our observations, however, it is possible that the leucocyte influx elicited by FCA delivery acquires an anti-inflammatory phenotype when FCA + SL are present. A final point to consider is that vaccines formulated with sphingolipids should afford equal or better protection than the vaccine formulation without the sphingolipids.

Thus, future studies will evaluate the effects of incorporating *F. major* sphingolipids with FCA in a vaccine preparation with regards to vaccine immunogenicity, levels of protection and types of specific adaptive immune responses.

Previous studies with *F. major* sphingolipids have demonstrated the ability to stimulate secretion of IgT and modulate the proportions of IgM and IgT B cells via i.v. injection in rainbow trout (Sepahi et al., 2016). IgT is an immunoglobulin isotype specialized in mucosal immunity in teleost fish (Salinas et al., 2011; Tacchi et al., 2014; Xu et al., 2016; Xu et al., 2013; Zhang et al., 2010). Thus, we expected to observe greater modulation of IgT expression compared to IgM expression in our present study. In accord, we were able to demonstrate that *F. major* sphingolipids mostly stimulated IgT expression and to a lesser extent IgM expression in a mucosal tissue, the gills. Interestingly, these effects occurred in parallel to a decrease in IgT and IgM expression in systemic lymphoid tissues (HK). Given that we have previously shown that *F. major* sphingolipids orchestrate the distribution of B cells in mucosal and systemic organs, we speculate that the changes in gene expression here recorded may be due to redistribution of B cells exiting the HK and reaching the gills in response to sphingolipid treatment. Further studies will address the mechanisms by which *F. major* sphingolipids is able to

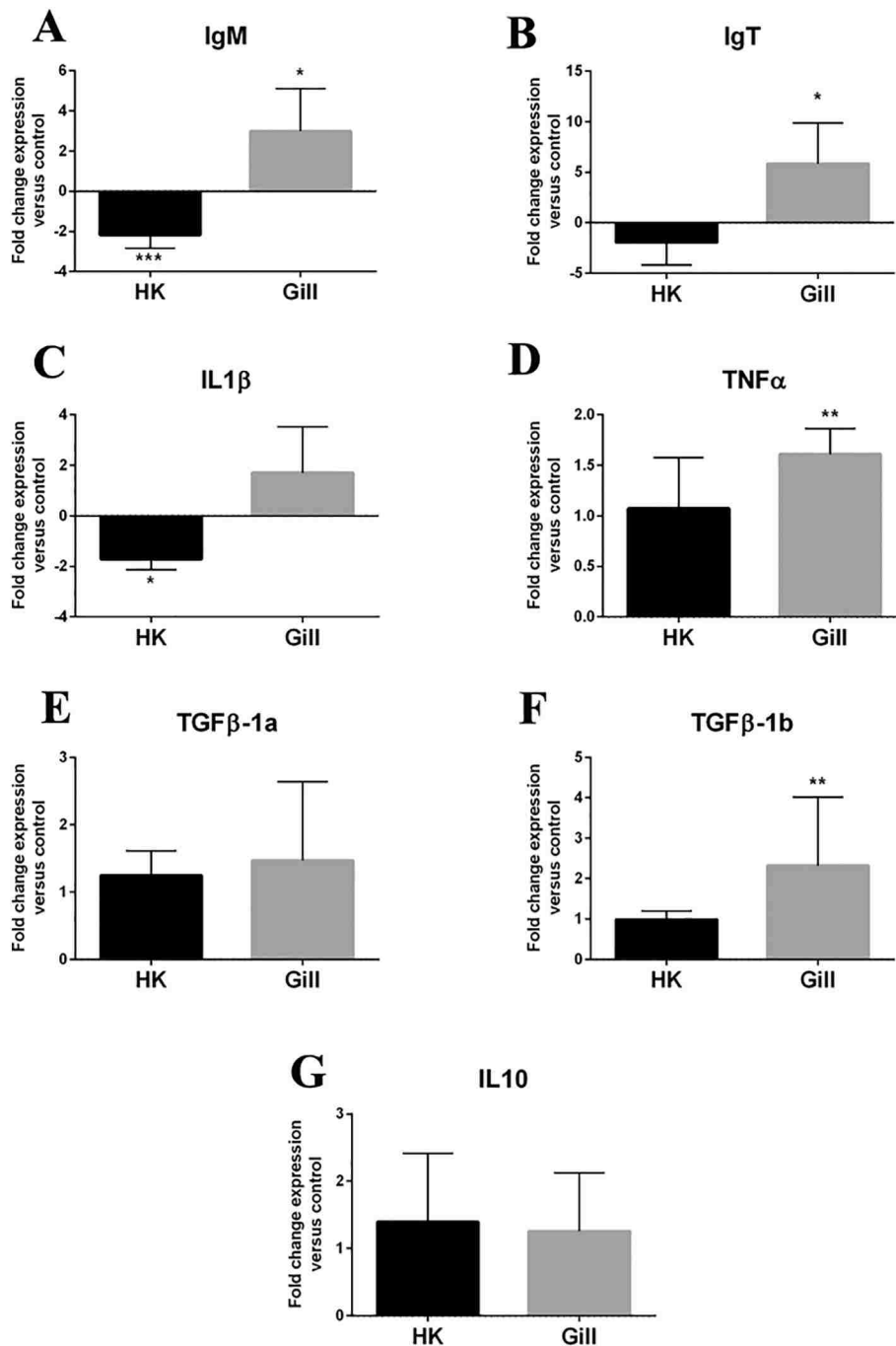


Fig. 4. Rainbow trout (N = 6) were injected i.p with *F. major* SLs combined with BSA in DMEM or BSA in DMEM alone. Fold-change expression of (A) IgM; (B) IgT; (C) IL-1β; (D) TNFα; (E) TGFβ-1a; (F) TGFβ-1b; (G) IL-10 were measured in the Head Kidney (HK) and gills 60 h post-treatment by RT-qPCR. Bars represent mean fold change \pm standard error. Asterisks denote statistically significant differences (*p < 0.05, **p < 0.01).

regulate Ig transcript expression.

Commensals are known to influence host transcriptional programs (Brestoff and Artis, 2013; Meireles-Filho and Deplancke, 2017; Meisel et al., 2018). Commensals, compared to pathogens, are known to induce anti-inflammatory responses in the mucosal environment (Round and Mazmanian, 2010; Sokol et al., 2008; Tlaskalová-Hogenová et al., 2011). Previous studies in mammals using *Bacteroides fragilis* sphingolipids identified anti-inflammatory roles for this compound. The present study tested a crude preparation of *F. major* sphingolipids that likely contains mixtures of phosphatidylethanolamine, a common molecule in teleost fish, and monoglycosyldiacylglycerol, a common molecule in most bacteria. Thus, delivery of *F. major* sphingolipids resulted in mixed

pro-inflammatory and anti-inflammatory cytokine expression responses in trout. We observed different gene expression responses depending on the route of delivery (i.p or i.v). I.p injection of sphingolipids resulted in significant up-regulation of IgM, IgT, TNFα and TGFβ-1b expression in the gills but down-regulation of IgM and IL-1β in the HK. I.v delivery, in turn, stimulated a significant upregulation of TNFα in the HK and IgT, IL-1β, TGFβ-1a and TGFβ-1b in the gills. We previously reported that i.v injection of *F. major* sphingolipids results in lower IgT proportions in the gills and higher IgT proportions in the HK compared to control trout (Sepahi et al., 2016). Thus, the changes in cytokine gene expression observed in the i.v group may reflect the effects that sphingolipids have on B cells populations. Alternatively, effects on other cells types cannot

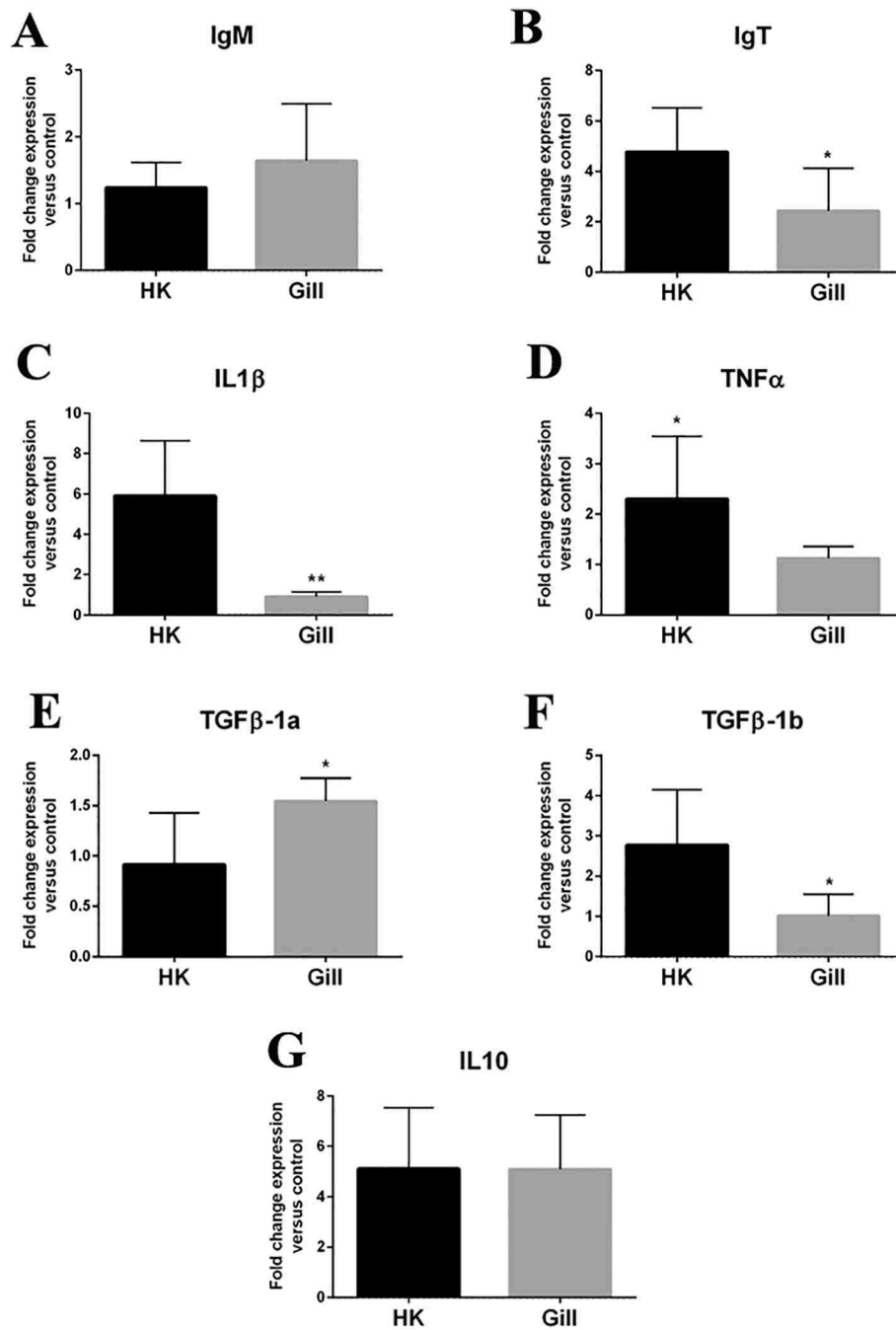


Fig. 5. Rainbow trout (N = 6) were injected i.v with *F. major* SLs combined with BSA in DMEM or BSA in DMEM alone. Fold-change expression of (A) IgM; (B) IgT; (C) IL-1 β ; (D) TNF α ; (E) TGF β -1a; and (F) TGF β -1b; (G) IL-10 were measured in the Head Kidney (HK) and gills 60 h post-treatment by RT-qPCR. Bars represent mean fold change \pm standard error. Asterisks denote statistically significant differences (* p < 0.05, ** p < 0.01).

be ruled out. Overall, our results highlight the potential for application of *F. major* sphingolipids in a variety of diseases and disorders in rainbow trout farming. Since we used a mixture of phosphatidylethanolamine and monoglycosyldiacylglycerol, future studies using purified fractions from this preparation should be conducted in order to identify the specific compounds that trigger anti-inflammatory versus pro-inflammatory responses in fish.

Our studies have thus far only evaluated effects of *F. major* sphingolipids by injection. However, mucosal delivery of this compound either in the water or incorporated into the feed should be tested in order to facilitate larger scale applications of our results. Additionally, we did not quantify whether sphingolipid administration exerted long-lasting effects on the local and systemic trout immune system. Future studies

will address these key aspects of sphingolipid administration.

In conclusion, we have demonstrated the immunological functions of a commensal derived sphingolipid in rainbow trout. The diverse and potent effects that *F. major* sphingolipids have on rainbow trout immune and inflammatory responses suggest that this compound can have important applications in aquaculture.

Acknowledgments

Authors wish to thank Lisboa Springs for supplying the animals used in this work and Dr. H. Goldfine for performing the lipid extraction. Mariah Sanchez was funded by the IMSD program at UNM. This work was partially funded by National Institutes of Health award P20-

GM103452.

References

- An, D., Oh, S.F., Olszak, T., Neves, J.F., Avci, F.Y., Erturk-Hasdemir, D., Lu, X., Zeissig, S., Blumberg, R.S., Kasper, D.L., 2014. Sphingolipids from a symbiotic microbe regulate homeostasis of host intestinal natural killer T cells. *Cell* 156, 123–133.
- Arpaia, N., Rudensky, A.Y., 2014. Microbial metabolites control gut inflammatory responses. *Proc. Natl. Acad. Sci. U. S. A.* 111, 2058–2059.
- Batrakov, S.G., Sheichenko, V.I., Nikitin, D.I., 1999. A novel glycosphingolipid from Gram-negative aquatic bacteria. *BBA Mol. Cell Biol. Lipids* 1440, 163–175.
- Batrakov, S., Mosezhnyi, A., Ruzhitsky, A., Sheichenko, V., Nikitin, D., 2000. The polar-lipid composition of the sphingolipid-producing bacterium *Flectobacillus major*. *Biochim. Biophys. Acta* 1484, 225.
- Blaho, V.A., Hla, T., 2014. An update on the biology of sphingosine 1-phosphate receptors. *J. Lipid Res.* 55, 1596–1608.
- Booman, M., Forster, I., Vederas, J.C., Groman, D.B., Jones, S.R., 2018. Soybean meal-induced enteritis in Atlantic salmon (*Salmo salar*) and Chinook salmon (*Oncorhynchus tshawytscha*) but not in pink salmon (*O. gorbuscha*). *Aquaculture* 483, 238–243.
- Brestoff, J.R., Artis, D., 2013. Commensal bacteria at the interface of host metabolism and the immune system. *Nat. Immunol.* 14, 676–684.
- Bricknell, I., Dalmo, R.A., 2005. The use of immunostimulants in fish larval aquaculture. *Fish Shellfish Immunol.* 19, 457–472.
- Gjessing, M.C., Falk, K., Weli, S.C., Koppang, E.O., Kvellestad, A., 2012. A sequential study of incomplete Freund's adjuvant-induced peritonitis in Atlantic cod. *Fish Shellfish Immunol.* 32, 141–150.
- Gomez, D., Sunyer, J.O., Salinas, I., 2013. The mucosal immune system of fish: the evolution of tolerating commensals while fighting pathogens. *Fish Shellfish Immunol.* 35, 1729–1739.
- Heaver, S.L., Johnson, E.L., Ley, R.E., 2018. Sphingolipids in host–microbial interactions. *Curr. Opin. Microbiol.* 43, 92–99.
- Hooper, L.V., Littman, D.R., Macpherson, A.J., 2012. Interactions between the microbiota and the immune system. *Science* 336, 1268–1273.
- Kelly, C., Salinas, I., 2017. Under pressure: interactions between commensal microbiota and the teleost immune system. *Front. Immunol.* 8, 559.
- Kongtorp, R., Taksdal, T., Lyngøy, A., 2004. Pathology of heart and skeletal muscle inflammation (HSMI) in farmed Atlantic salmon *Salmo salar*. *Dis. Aquat. Org.* 59, 217–224.
- Levy, M., Thaiss, C.A., Elinav, E., 2016. Metabolites: messengers between the microbiota and the immune system. *Genes Dev.* 30, 1589–1597.
- Lowrey, L., Woodhams, D.C., Tacchi, L., Salinas, I., 2015. Topographical mapping of the rainbow trout (*Oncorhynchus mykiss*) microbiome reveals a diverse bacterial community in the skin with antifungal properties. *Appl. Environ. Microbiol.* 81 (19), 6915–6925.
- Meireles-Filho, A.C., Deplancke, B., 2017. Gene regulatory mechanisms underlying the intestinal innate immune response. *Curr. Opin. Genet. Dev.* 43, 46–52.
- Meisel, J.S., Sfyroera, G., Bartow-McKenney, C., Gimblet, C., Bugayev, J., Horwinski, J., Kim, B., Brestoff, J.R., Tyldsley, A.S., Zheng, Q., 2018. Commensal microbiota modulate gene expression in the skin. *Microbiome* 6, 20.
- Nematollahi, A., Decostere, A., Pasmans, F., Haesebrouck, F., 2003. Flavobacterium psychrophilum infections in salmonid fish. *J. Fish Dis.* 26, 563–574.
- Noia, M., Domínguez, B., Leiro, J., Blanco-Méndez, J., Luzardo-Álvarez, A., Lamas, J., 2014. Inflammatory responses and side effects generated by several adjuvant-containing vaccines in turbot. *Fish Shellfish Immunol.* 38, 244–254.
- Pfaffl, M.W., 2001. A new mathematical model for relative quantification in real-time RT-PCR. *Nucleic Acids Res.* 29, 2002–2007.
- Round, J.L., Mazmanian, S.K., 2010. Inducible Foxp3+ regulatory T-cell development by a commensal bacterium of the intestinal microbiota. *Proc. Natl. Acad. Sci. U. S. A.* 107, 12204–12209.
- Sahlmann, C., Sutherland, B.J., Kortner, T.M., Koop, B.F., Krogdahl, Å., Bakke, A.M., 2013. Early response of gene expression in the distal intestine of Atlantic salmon (*Salmo salar* L.) during the development of soybean meal induced enteritis. *Fish Shellfish Immunol.* 34, 599–609.
- Salinas, I., Zhang, Y.-A., Sunyer, J.O., 2011. Mucosal immunoglobulins and B cells of teleost fish. *Dev. Comp. Immunol.* 35, 1346–1365.
- Sepahi, A., Salinas, I., 2016. The evolution of nasal immune systems in vertebrates. *Mol. Immunol.* 69, 131–138.
- Sepahi, A., Cordero, H., Goldfine, H., Esteban, M.Á., Salinas, I., 2016. Symbiont-derived sphingolipids modulate mucosal homeostasis and B cells in teleost fish. *Sci. Rep.* 6, 39054.
- Sepahi, A., Tacchi, L., Casadei, E., Takizawa, F., LaPatra, S.E., Salinas, I., 2017. CK12a, a CCL19-like chemokine that orchestrates both nasal and systemic antiviral immune responses in rainbow trout. *J. Immunol.* 199, 3900–3913.
- Sharon, G., Garg, N., Debelius, J., Knight, R., Dorrestein, P.C., Mazmanian, S.K., 2014. Specialized metabolites from the microbiome in health and disease. *Cell Metab.* 20, 719–730.
- Siwicki, A., Morand, M., Terech-Majewska, E., Niemczuk, W., Kuzu, K., Glabski, E., 1998. Influence of immunostimulants on the effectiveness of vaccines in fish: in vitro and in vivo study. *J. Appl. Ichthyol.* 14, 225–227.
- Sokol, H., Pigneur, B., Watterlot, L., Lakhdari, O., Bermúdez-Humarán, L.G., Gratadoux, J.-J., Blugeon, S., Bridonneau, C., Furet, J.-P., Corthier, G., 2008. Faecalibacterium prausnitzii is an anti-inflammatory commensal bacterium identified by gut microbiota analysis of Crohn disease patients. *Proc. Natl. Acad. Sci. U. S. A.* 105, 16731–16736.
- Tacchi, L., Musharrafieh, R., Larragoite, E.T., Crossey, K., Erhardt, E.B., Martin, S.A., LaPatra, S.E., Salinas, I., 2014. Nasal immunity is an ancient arm of the mucosal immune system of vertebrates. *Nat. Commun.* 5, 6205.
- Tafalla, C., Bogwald, J., Dalmo, R.A., 2013. Adjuvants and immunostimulants in fish vaccines: current knowledge and future perspectives. *Fish Shellfish Immunol.* 35, 1740–1750.
- Thim, H.L., Villoing, S., McLoughlin, M., Christie, K.E., Grove, S., Frost, P., Jørgensen, J.B., 2014. Vaccine adjuvants in fish vaccines make a difference: comparing three adjuvants (Montanide ISA763A oil, CpG/poly I: C combo and VHSV glycoprotein) alone or in combination formulated with an inactivated whole salmonid alphavirus antigen. *Vaccine* 2, 228–251.
- Tlaskalová-Hogenová, H., Štěpánková, R., Kozáková, H., Hudcovic, T., Vannucci, L., Tučková, L., Rossmann, P., Hrnčíř, T., Kverka, M., Zákostelská, Z., 2011. The role of gut microbiota (commensal bacteria) and the mucosal barrier in the pathogenesis of inflammatory and autoimmune diseases and cancer: contribution of germ-free and gnotobiotic animal models of human diseases. *Cell. Mol. Immunol.* 8, 110–120.
- Urán, P., Gonçalves, A., Taverne-Thiele, J., Schrama, J., Verreth, J., Rombout, J., 2008. Soybean meal induces intestinal inflammation in common carp (*Cyprinus carpio* L.). *Fish Shellfish Immunol.* 25, 751–760.
- Urán, P., Schrama, J., Rombout, J., Taverne-Thiele, J., Obach, A., Koppe, W., Verreth, J., 2009. Time-related changes of the intestinal morphology of Atlantic salmon, *Salmo salar* L., at two different soybean meal inclusion levels. *J. Fish Dis.* 32, 733–744.
- Vazirzadeh, A., Hajimoradloo, A., Esmaili, H.R., Akhlaghi, M., 2008. Effects of emulsified versus saline administration of GnRH α on induction of ovulation in rainbow trout, *Oncorhynchus mykiss*. *Aquaculture* 280, 267–269.
- Villumsen, K.R., Koppang, E.O., Raida, M.K., 2015. Adverse and long-term protective effects following oil-adjuvanted vaccination against *Aeromonas salmonicida* in rainbow trout. *Fish Shellfish Immunol.* 42, 193–203.
- Wuthier, R.E., 1966. Purification of lipids from nonlipid contaminants on Sephadex bead columns. *J. Lipid Res.* 7, 558–561.
- Xu, Z., Parra, D., Gómez, D., Salinas, I., Zhang, Y.-A., von Gersdorff Jørgensen, L., Heinecke, R.D., Buchmann, K., LaPatra, S., Sunyer, J.O., 2013. Teleost skin, an ancient mucosal surface that elicits gut-like immune responses. *Proc. Natl. Acad. Sci. U. S. A.* 110, 13097–13102.
- Xu, Z., Takizawa, F., Parra, D., Gómez, D., von Gersdorff Jørgensen, L., LaPatra, S.E., Sunyer, J.O., 2016. Mucosal immunoglobulins at respiratory surfaces mark an ancient association that predates the emergence of tetrapods. *Nat. Commun.* 7, 10728.
- Zhang, Y.-A., Salinas, I., Li, J., Parra, D., Bjork, S., Xu, Z., LaPatra, S.E., Bartholomew, J., Sunyer, J.O., 2010. IgT, a primitive immunoglobulin class specialized in mucosal immunity. *Nat. Immunol.* 11, 827–835.

Appendix C

Author contributions

1. Sepahi, A., & Salinas, I. (2016). *The evolution of nasal immune systems in vertebrates*. Molecular immunology, 69, 131-138.

Authorship status	First
Designed research	Yes
Perform research	Yes
Analyzed data	Yes
Designed figures	Yes
Wrote paper	Yes

2. Sepahi, A., Tacchi, L., Casadei, E., Takizawa, F., LaPatra, S. E., & Salinas, I. (2017). *CK12a, a CCL19-like chemokine that orchestrates both nasal and systemic antiviral immune responses in Rainbow trout*. The Journal of Immunology, 199(11), 3900-3913.

Authorship status	First
Designed research	Yes
Perform research	Yes
Analyzed data	Yes
Designed figures	Yes
Wrote paper	Yes

3. Sepahi, A., Casadei, E., Tacchi, L., Muñoz, P., LaPatra, S. E., & Salinas, I. (2016). *Tissue microenvironments in the nasal epithelium of rainbow trout (*Oncorhynchus mykiss*) define two distinct CD8 α ⁺ cell populations and establish regional immunity*. The Journal of Immunology, 197(11), 4453-4463.

Authorship status	First
Designed research	Yes
Perform research	Yes
Analyzed data	Yes
Designed figures	Yes
Wrote paper	Yes

4. Sepahi, A., Kraus, A., Johnston, C., Galindo-Villegas, J., Kelly, C., Garcia-Moreno, D., Muñoz, P., Mulero, V., Huertas, M & Salinas, I. *Olfactory sensory neurons mediate ultra-rapid antiviral immune responses in teleosts in a TrkA-dependent manner*. Immunity (Under review).

Authorship status	First
Designed research	Yes
Perform research	Yes
Analyzed data	Yes
Designed figures	Yes
Wrote paper	Yes

5. Sepahi, A., Cordero, H., Goldfine, H., Esteban, M. Á., & Salinas, I. (2016). *Symbiont-derived sphingolipids modulate mucosal homeostasis and B cells in teleost fish*. Scientific reports, 6, 39054.

Authorship status	First
Designed research	Yes
Perform research	Yes
Analyzed data	Yes
Designed figures	Yes
Wrote paper	Yes

6. Sanchez, Mariah, Ali Sepahi, Elisa Casadei, and Irene Salinas. "Symbiont-derived sphingolipids regulate inflammatory responses in rainbow trout (*Oncorhynchus mykiss*)."
Aquaculture (2018).

Authorship status	Second
Designed research	No
Perform research	Yes
Analyzed data	Yes
Designed figures	Yes
Wrote paper	Yes



Editor-in-Chief

Pamela J. Fink, Ph.D.

**Executive Director
and Executive Editor**

M. Michele Hogan, Ph.D.

Director of Publications

Todd D. Reitzel

**Chair, Publications
Committee**

Brian D. Evavold, Ph.D.

May 16, 2018

Ali Sepahi

The University of New Mexico

230 Castetter Hall MSC03-2020 1 University of New

Albuquerque, NM, 87131

Email: sepahi@unm.edu

Dear Dr. Sepahi:

The American Association of Immunologists, Inc., grants permission to use the entire article, “CK12a, a CCL19-like Chemokine That Orchestrates both Nasal and Systemic Antiviral Immune Responses in Rainbow Trout” published in *The Journal of Immunology*, vol. 199, pp. 3900-3913, 2017, in your Ph.D. thesis, contingent on the following conditions:

1. That you give proper credit to the authors and to *The Journal of Immunology*, including in your citation the volume, date, and page numbers.
2. That you include the statement:

Copyright 2017. The American Association of Immunologists, Inc.

3. That permission is granted for one-time use only for print and electronic format. Permission must be requested separately for future editions, revisions, derivative works, and promotional pieces. Reproduction of any content, other than Figures and Figure Legends, from *The Journal of Immunology* is permitted in English only.

Thank you for your interest in *The Journal of Immunology*.

Sincerely,

Todd D. Reitzel

Director of Publications

The Journal of Immunology

THE AMERICAN ASSOCIATION OF IMMUNOLOGISTS



The Journal of
Immunology

Editor-in-Chief

Pamela J. Fink, Ph.D.

**Executive Director
and Executive Editor**

M. Michele Hogan, Ph.D.

Director of Publications

Todd D. Reitzel

**Chair, Publications
Committee**

Brian D. Evavold, Ph.D.

May 16, 2018

Ali Sepahi

The University of New Mexico

230 Castetter Hall MSC03-2020 1 University of New

Albuquerque, NM, 87131

Email: sepahi@unm.edu

Dear Dr. Sepahi:

The American Association of Immunologists, Inc., grants permission to use the entire article, “Tissue Microenvironments in the Nasal Epithelium of Rainbow Trout (*Oncorhynchus mykiss*) Define Two Distinct CD8a+ Cell Populations and Establish Regional Immunity” published in *The Journal of Immunology*, vol. 197, pp. 4453-4463, 2016, in your *Ph.D.* thesis, contingent on the following conditions:

1. That you give proper credit to the authors and to *The Journal of Immunology*, including in your citation the volume, date, and page numbers.
2. That you include the statement:

Copyright 2016. The American Association of Immunologists, Inc.

3. That permission is granted for one-time use only for print and electronic format. Permission must be requested separately for future editions, revisions, derivative works, and promotional pieces. Reproduction of any content, other than Figures and Figure Legends, from *The Journal of Immunology* is permitted in English only.

Thank you for your interest in *The Journal of Immunology*.

Sincerely,

Todd D. Reitzel

Director of Publications

The Journal of Immunology

THE AMERICAN ASSOCIATION OF IMMUNOLOGISTS